

**UNIVERSITÀ DEGLI STUDI DI NAPOLI  
FEDERICO II  
SCUOLA DI MEDICINA E CHIRURGIA**



DEPARTMENT OF PHARMACY

*PhD in Pharmaceutical Science- XXXIII cycle*

**DESIGN & SYNTHESIS OF PEPTIDOMIMETICS  
AS TOOLBOX TO PROBE EMERGING  
ANTIMICROBIAL AND ANTICANCER  
STRATEGIES**

PhD Coordinator:  
Chiar.ma Prof.ssa  
MARIA VALERIA D'AURIA

Tutor:  
Chiar.mo Prof.  
PAOLO GRIECO

Candidate:  
ROSA BELLAVITA

## LIST OF PUBLICATIONS

**Bellavita R**, Falanga A, Buommino E, Merlino F, Casciaro B, Cappiello F, Mangoni ML, Novellino E, Catania MR, Paolillo R, Grieco P, Galdiero S. Novel temporin L antimicrobial peptides: promoting self-assembling by lipidic tags to tackle superbugs. *Journal of Enzyme Inhibition Medicinal Chemistry*. 2020, 35, 1751–1764.

**Bellavita R**, Vollaro A, Catania MR, Merlino F, De Martino L, Nocera FP, Della Greca M, Lembo F, Grieco P, Buommino E. Novel antimicrobial peptide from Temporin L in the treatment of *Staphylococcus pseudintermedius* and *Malassezia pachydermatis* in polymicrobial inter-Kingdom infection. *Antibiotics (Basel)*. 2020, 9:530.

**Bellavita R**, Raucci F, Merlino F, Piccolo ML, Ferraro MG, Irace C, Santamaria R, Iqbal AJ, Novellino E, Grieco P, Mascolo N, Maione F. Temporin L-derived peptide as a regulator of the acute inflammatory response in zymosan-induced peritonitis. *Biomedicine and Pharmacotherapy*. 2019, 123:109788.

Buommino E, Carotenuto A, Antignano I, **Bellavita R**, Casciaro B, Loffredo MR, Merlino F, Novellino E, Mangoni ML, Nocera FP, Brancaccio D, Punzi P, Roversi D, Ingenito R, Bianchi E, Grieco P. The Outcomes of Decorated Prolines in the Discovery of Antimicrobial Peptides from Temporin-L. *Chem Med Chem*. 2019, 14, 1283–1290.

Merlino F, Billard E, Yousif AM, Di Maro S, Brancaccio D, Abate L, Carotenuto A, **Bellavita R**, D'Emmanuele di Villa Bianca R, Santicioli P, Marinelli L, Novellino E, Hebert T, Lubell WD, Chatenet D, Grieco P. Functional selectivity revealed by *N*-methylation scanning of human Urotensin II and related peptides. *Journal of Medicinal Chemistry*. 2019, 62, 1455–1467.

Yousif AM, Ingangi V, Merlino F, Brancaccio D, Monopoly M, **Bellavita R**, Novellino E, Carriero MV, Carotenuto A, Grieco P. Urokinase receptor derived peptides as potent inhibitors of the Formyl Peptide Receptor type 1-triggered cell migration. *European of Journal Medicinal Chemistry*. 2018, 143, 348–360.

### **PATENT PENDING**

**Inventors:** Mascolo Nicola, Maione Francesco, Carotenuto Alfonso, Novellino Ettore, Merlino Francesco, **Bellavita Rosa**, Buommino Elisabetta, Grieco Paolo.

**Title:** “Temporin L Analogues with anti-inflammatory and antimicrobial activity”.

**Application:** P021300IT-01/lm. **Date:** 19/06/2019.

# Table Of Contents

<b>LIST OF ABBREVIATIONS</b> .....	1
<b>SUMMARY</b> .....	4
<b>PART 1-ANTIMICROBIAL PEPTIDOMIMETICS</b> .....	6
ABSTRACT .....	7
<b>CHAPTER 1. INTRODUCTION</b> .....	8
1.1 Antibiotic history at a glance .....	9
1.2 Antibiotic resistance .....	10
1.3 The antimicrobial peptides (AMPs) .....	12
1.4 Temporins .....	15
1.5 References .....	20
<b>CHAPTER 2. CHEMICAL DECORATION OF PROLINE</b> .....	24
2.1 Targeting ESKAPE Pathogens .....	25
2.2 Results and Discussions .....	27
2.2.1. Design .....	27
2.2.2. Biological activity against ESKAPE .....	28
2.2.3. Structural studies .....	33
2.3 Conclusions .....	39
2.4 Experimental Section .....	39
2.4.1. Chemistry .....	39
2.4.2. Biology .....	41
2.4.3. Conformational analysis .....	42
2.5 References .....	43
<b>CHAPTER 3. PROMOTING SELF-ASSEMBLING BY LIPIDIC TAGS</b> .....	46
3.1 Peptide self-assembling .....	47
3.2 Results and Discussions .....	49
3.2.1. Design .....	49
3.2.2. Effect of self-assembling on antibacterial activity .....	50

3.2.3. Long lipidic tails increase the cytotoxicity .....	52
3.2.4. Aggregation studies.....	54
3.2.5. Oligomerization in bacterial membrane.....	56
3.2.6. Lipopeptides influences membrane fluidity .....	57
3.2.7. Liposomes leakage by lipopeptides .....	58
3.2.8. Helical aggregates in bacterial membrane .....	59
3.2.9. Self-assembling improves proteolytic stability .....	61
3.3 Conclusions .....	62
3.4 Experimental Section .....	63
3.4.1. Chemistry .....	63
3.4.2. Biology .....	68
3.4.3. Critical aggregation concentration determination .....	70
3.4.4. Liposome preparation .....	71
3.4.5. ANT/DPX leakage assay .....	72
3.4.6. Laurdan assay.....	73
3.4.7. Peptide aggregation.....	73
3.4.8. CD spectroscopy .....	74
3.5 References .....	74
<b>CHAPTER 4. TEMPORIN L ANALOGUES WITH DUAL ACTIVITY IN</b>	
<b>POLYMICROBIAL INFECTIONS .....</b>	<b>78</b>
4.1 Polymicrobial infections .....	79
4.2 Results and Discussions .....	81
4.2.2. Design .....	81
4.2.2. Biological studies on <i>M. Pachydermatis</i> and <i>S. Pseudintermedius</i> .....	82
4.2.3. <i>In vitro</i> and <i>in vivo</i> anti-inflammatory studies .....	89
4.3 Conclusions .....	96
4.4 Experimental Section .....	96
4.4.1. Chemistry .....	96
4.4.2. Biology .....	97
4.4.3. <i>In Vitro</i> assays .....	102

4.4.4. <i>In Vivo</i> study .....	103
4.5 References .....	104
<b>CHAPTER 5. CONSTRAINING <math>\alpha</math>-HELICAL CONTENT BY CYCLIZATION STRATEGIES</b> .....	109
5.1 Macrocyclization Strategies .....	110
5.2 Results and discussions .....	112
5.2.1. Design of stapled $\alpha$ -helical peptides .....	112
5.2.2. Helical stabilization versus biological activity .....	115
5.2.3. Measurement of helicity by circular dichroism .....	119
5.2.4. Mode of action studies .....	123
5.2.5. Lactamization improves proteolytic stability .....	127
5.3 Conclusions .....	128
5.4 Future Perspectives .....	129
5.5 Experimental Section .....	130
5.5.1. Chemistry .....	130
5.5.2. Biology .....	137
5.5.3. Laurdan and Thioflavin T assays .....	138
5.5.4. Conformational analysis .....	138
5.6 References .....	139
<b>PART 2-ANTICANCER PEPTIDOMIMETICS</b> .....	143
ABSTRACT .....	144
<b>CHAPTER 1. INTRODUCTION</b> .....	145
1.1 Protein-protein interactions .....	146
1.2 Wnt/ $\beta$ -catenin signaling .....	147
1.3 Direct targeting of $\beta$ -catenin .....	149
1.4 References .....	151
<b>CHAPTER 2. BICYCLIC STAPLED PEPTIDES INHIBITORS OF <math>\beta</math>-CATENIN</b> .....	155
2.1 Targeting $\beta$ -catenin/E-Cadherin interaction .....	156
2.2 Results and discussions .....	158
2.2.1. Design of stapled bicyclics .....	158

2.2.2. St-3 binds $\beta$ -catenin .....	160
2.3 Conclusions & future perspectives .....	162
2.4 Experimental section .....	162
2.4.1. Chemistry .....	162
2.4.2. Binding assay .....	169
2.5 References .....	169
<b>CHAPTER 3. BIVALENT PEPTIDE INHIBITOR OF <math>\beta</math>-CATENIN AND TCF</b>	
<b>INTERACTIONS .....</b>	<b>171</b>
3.1 Bioorthogonal reactions .....	172
3.2 Results and discussions .....	173
3.2.1. Design .....	173
3.2.2. Lima binds $\beta$ -catenin .....	175
3.2.3. Synthesis of click handle-containing peptides .....	177
3.2.4. Bivalent inhibitor of $\beta$ -catenin .....	178
3.2.5. Preliminary kinetic studies .....	181
3.3 Conclusions .....	184
3.4 Experimental section .....	184
3.4.1. Chemistry .....	184
3.4.2. Binding assay .....	191
3.5 References .....	193

## LIST OF ABBREVIATIONS

<b>AMPs</b>	Antimicrobial peptides
<b>ANTS</b>	8-Aminonaphthalene-1,3,6-trisulfonic acid, disodium salt
<b>Ac<sub>2</sub>O</b>	Acetic anhydride
<b>Alloc</b>	Allyloxycarbonyl group
<b>CD</b>	Circular dichroism
<b>CAC</b>	Critical Aggregation Concentration
<b>CL</b>	Cardiolipin
<b>CuAAC</b>	Copper-catalyzed azide-alkyne cycloadditions
<b>DCM</b>	Dichloromethane
<b>DMF</b>	Dimethylformamide
<b>DIC</b>	<i>N-N'</i> -Diisopropylcarbodiimide
<b>DPC</b>	Dodecylphosphocholine
<b>DCE</b>	1,2-Dichloroethane
<b>DIEA</b>	Diisopropylethyl amine
<b>DPX</b>	<i>p</i> -Xylene-bis-pyridinium bromide
<b>DOPG</b>	1,2-Dioleoyl-sn glycerol-3-phospho-(1'-rac-glycerol) sodium salt
<b>DOPE</b>	1,2-Dioleoyl-sn-glycerol-3-phosphoethanolamine
<b>DBCO</b>	Dibenzocyclooctyne
<b>Dex</b>	Dexamethasone
<b>Fam</b>	Carboxyfluorescein
<b>FITC</b>	Fluorescein isothiocyanate
<b>FP</b>	Fluorescence polarization
<b>FIC</b>	Fractional inhibitory concentration
<b>GP</b>	Generalized Polarization



<b>HOA</b>	1-Hydroxy-7-azabenzotriazole
<b>HATU</b>	2-(7-Aza-1H-benzotriazole-1-yl)-1,1,3,3-tetramethyluronium hexafluorophosphate
<b>HBTU</b>	2-(1H-Benzotriazole-1-yl)-1,1,3,3-tetramethyluronium hexafluorophosphate
<b>HOBt</b>	1-Hydroxybenzotriazole
<b>HPLC</b>	High-Performance Liquid Chromatography
<b>HRMS</b>	High resolution mass spectrometry
<b>IC50</b>	Median inhibition concentration
<b>LC</b>	Liquid Chromatography
<b>Laurdan</b>	6-Dodecanoyl- <i>N,N</i> -dimethyl-2-naphthylamine
<b>LUVs</b>	Large unilamellar vesicles
<b>MS</b>	Mass spectrometry
<b>MTBE</b>	Tert-butyl methyl ether
<b>MTT</b>	3-(4,5-dimethylthiazol-2-yl)-2,5-Diphenyltetrazolium bromide
<b>MMC</b>	Minimum mycoidal concentration
<b>MIC</b>	Minimum inhibitory concentration
<b>MBC</b>	Minimum bactericidal concentration
<b>MeCN</b>	Acetonitrile
<b>NCS</b>	<i>N</i> -Chlorosuccinimide
<b>NMR</b>	Nuclear Magnetic Resonance
<b>RCM</b>	Ring-closing metathesis
<b>SDS</b>	Sodium dodecyl sulfate
<b>SAR</b>	Structure-activity relationship
<b>SPPS</b>	Standard solid-phase peptide synthesis
<b>SUVs</b>	Small unilamellar vesicles
<b>SPAAC</b>	Strain-promoted click reaction

<b>TL</b>	Temporin L
<b>TA</b>	Temporin A
<b>TB</b>	Temporin B
<b>TFE</b>	2,2,2-Trifluoroethanol
<b>TEA</b>	Triethylamine
<b>THF</b>	Tetrahydrofuran
<b>TFA</b>	Trifluoroacetic acid
<b>TIS</b>	Triisopropylsilane
<b>ThT</b>	Thioflavin T
<b>TCF</b>	T cell factor protein
<b>UHPLC</b>	Ultra-high Performance Liquid Chromatography
<b>UV-Vis</b>	Ultraviolet-visible
<b>XTT</b>	2,3-Bis(2-methoxy-4-nitro-5-sulfophenyl)-2H-tetrazolium-5-carboxanilide

## SUMMARY

Peptides are biological polymers that perform many hormonal and vital functions in humans. In the field of medicinal chemistry, peptides are recognized for being highly efficacious, relatively safe and well tolerated, but, suffering from pharmacokinetic drawbacks, they are mainly engaged as models. In the light of advances in the peptide-based drug discovery field, peptidomimetics are rather considered more drug-like molecules, endowed with improved pharmacokinetic properties and widely employed as powerful tools to probe the biological mechanism of several diseases and emerging therapeutic strategies.

This Ph.D. thesis, divided into two parts, **Part 1** and **Part 2**, describes the development of peptidomimetics toolbox designed *ad hoc* and synthesized to challenge antibiotic resistance and Wnt/ $\beta$ -catenin pathway involved in several types of cancer. Nowadays, these phenomena are the leading causes of increase in mortality rates worldwide, hence scientific research constantly works in order to progress the treatment strategies.

In particular, the studies disclosed in the **Part 1** were aimed at investigating the following issues:

- development of novel antimicrobial Temporin L analogues by means of innovative chemical modifications for tackling ESKAPE infections (**Chapter 2, 3, 5**).
- investigation of antimicrobial and anti-inflammatory activities of selected Temporin L derivatives in polymicrobial infections (**Chapter 4**).

In **Chapters 2** and **4**, the Ph.D. thesis will focus on the design and synthesis of antimicrobial peptidomimetics by applying local modifications consisting in the incorporation of non-native amino acids such as decorated prolines and D-amino acids, in order to improve SAR knowledge about antimicrobial behavior. **Chapter 3** describes a lipidation strategy by the conjugation of saturated fatty acids with

different carbon chain length in both N- and C-termini. The library of lipidated peptidomimetics was used to probe the self-assembling process, as boosting the interaction with the bacterial membranes, and fine-tune a more potent and broad-spectrum antimicrobial activity. **Chapter 5** focuses on the introduction of chemical restrictions to generate conformationally-reduced peptidomimetics that delineates the correlation between bioactivity and amphipathic  $\alpha$ -helix structure of temporins. In the **Part 2**, the studies reported have been addressed to develop peptidomimetics acting as inhibitors of  $\beta$ -catenin implicated in oncogenic activation of Wnt/ $\beta$ -catenin pathway. In **Chapter 2**, the Ph.D. thesis will focus on the design and synthesis of a library of stapled bicyclic peptidomimetics by using the hydrocarbon stapling chemistry and the head-to-tail cyclization, to induce conformational constrictions and increase the binding activity towards  $\beta$ -catenin. Finally, in **Chapter 3**, the strain-promoted click reaction was exploited as strategy to tether two inhibitors of  $\beta$ -catenin and increase the potency and selectivity of  $\beta$ -catenin inhibition.

# **PART I**

---

## *Antimicrobial Peptidomimetics*

## ABSTRACT

Infections caused by ESKAPE pathogens are a huge challenge in both human and veterinary medicine. Among the antimicrobial peptides (AMPs), temporins represent encouraging candidates since they act through a different mode of action from conventional antibiotics. Despite the strong antimicrobial activity, the native Temporin L has not considered an efficacious alternative due to its cytotoxicity. In this scenario, our efforts have been addressed to the improvement of drug-like features of some Temporin L analogues, applying several synthetic approaches spanning from local modification and conformational constraints. Specifically, we performed local modifications consisting of the incorporation of D-amino acids or “decorated prolines” featured by appropriate functional groups (polar-, positively charged-, aliphatic- and aromatic groups) and lipidation strategy in order to improve antimicrobial activity and to preserve low cytotoxicity. In addition, we probed the correlation between  $\alpha$ -helix secondary structure and antimicrobial activity using different side-chain to side-chain cyclization strategies. In particular, lactamization, the formation of disulfide bridge between cysteines, triazole formation by CuAAC click chemistry reaction, and ring closing metathesis were used to stabilize  $\alpha$ -helical conformation and to increase the biological activity. Thanks to the application of these several synthetic strategies, we discovered novel Temporin L analogues with a high therapeutic index that have shown characteristics desired to be good candidates in the development of novel antimicrobial agents for topical applications.

# **CHAPTER 1**

## **INTRODUCTION**

## 1.1. ANTIBIOTICS HISTORY AT A GLANCE

The prompt emergence of resistant bacteria is endangering the efficacy of traditional antibiotics, which have always been considered a blessing to human civilization to their power to eradicate most of the bacterial infections, saving millions of people.<sup>[1,2]</sup> The beginning of the “modern antibiotic era” was associated with the names of Paul Ehrlich and Alexander Fleming.<sup>[3]</sup> In 1911, Paul Ehrlich discovered the synthetic pro-drugs Salvarsan for the treatment of *Treponema pallidum*, the agent of syphilis.<sup>[4,5]</sup> Salvarsan became the cornerstone for the discovery of sulfa drugs by Gerhard Domagk, but they were largely superseded by penicillin discovered by Alexander Fleming in 1928.<sup>[6,7]</sup> However, the high production of  $\beta$ -lactamase enzyme in bacteria led to rapid destruction of penicillin, making it totally ineffective and developing the phenomena of penicillin resistance.<sup>[8]</sup> Thus, the period from the 1950s and 1960s was named the “golden era” for the discovery of several antibiotics able to bypass penicillin resistance.<sup>[9]</sup> During this “golden era”, many academic institutions and major pharmaceutical companies in the United States and other countries were involved in the research of about 20 classes of antibiotics (Figure 1), like aminoglycosides (1940s), tetracyclines (1940s), macrolides (1950s), glycopeptides (1950s), cephalosporins (1960s), quinolones (1960s) and carbapenems (1980s).<sup>[10]</sup> Unfortunately, the resistance to these new classes of antibiotics spread very fast in this golden age (Figure 1). Despite recent commercialization for some of them, the last classes of antibiotics discovered are from the 1980s. Indeed, the last antibiotic discovered was daptomycin in 1986 and it was only approved by the US Food and Drug Administration in 2003.<sup>[11]</sup> This detail confirms that any new classes have been found after about 50 years. In fact, antibiotic therapy for the treatment of many bacterial infections currently consists of associations or improvements of existing molecules. For example, molecules recently discovered belong to already known classes, as tedizolid (oxazolidinones), dalbavancin (lipoglycopeptides), ceftaroline and ceftobiprole (cephalosporins).<sup>[12,13]</sup> Instead, examples of combinations of existing



molecules recently commercialized are ceftolozane/tazobactam or ceftazidime/avibactam.<sup>[14]</sup> The rapid rise of antibiotic resistance due to overuse and incorrectly prescribing of antibiotics has led to pharmaceutical industries to gradually leave the field altogether.<sup>[15]</sup> As a result, the rhythm of antibiotic discovery has slowed down and there is always an urgent need to identify novel molecules that potentially could combat the “bacteria killer” and eradicate hard-to-treat infections.

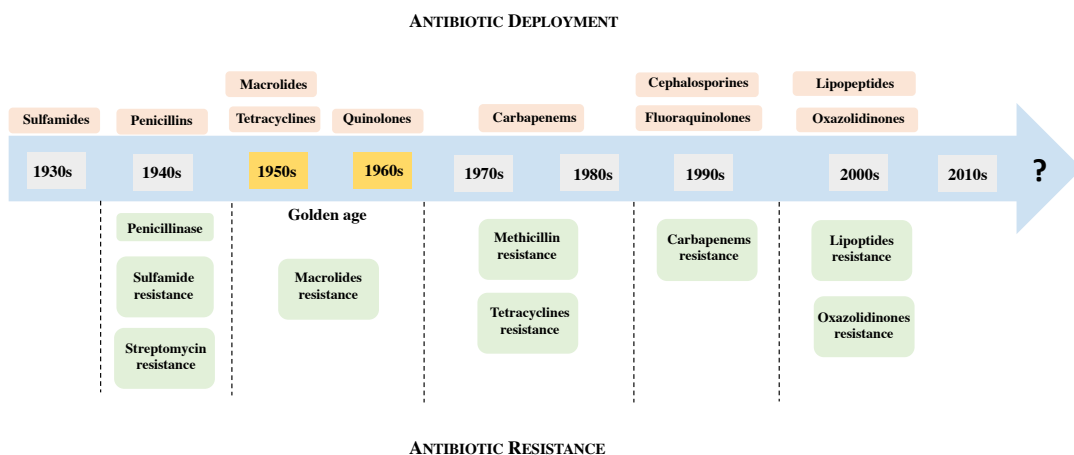


**Figure 1.** Developing antibiotic resistance: a timeline of key events.

## 1.2. ANTIBIOTIC RESISTANCE

As reported by the World Health Organization (WHO), in Europe every year an estimated 25000 patients die due to antibiotic resistance occurring in hospitals, in the community and through the food chain in Europe.<sup>[16,17]</sup> In the global priority pathogens list of antibiotic-resistant bacteria established by WHO, are included *Enterococcus faecium*, *Staphylococcus aureus*, *Klebsiella pneumoniae*, *Acinetobacter baumannii*, *Pseudomonas aeruginosa*, and *Enterobacter* species, referred to as “ESKAPE group”.<sup>[18,19]</sup> The ESKAPE bugs have developed resistance against oxazolidinones, lipopeptides, macrolides, fluoroquinolones, tetracyclines,  $\beta$ -lactams and antibiotics that are the last line of defense, including carbapenems and

glycopeptides.<sup>[20]</sup> In general, bacteria may adapt to “antibiotic attack” through two major genetic mechanisms: *i*) mutations in chromosomal genes often associated with the mechanism of action of antibiotic; *ii*) acquisition of foreign DNA coding for resistance determinants by horizontal gene transfer (HGT).<sup>[21]</sup> The horizontal evolution can occur by a conjugation, a transduction or a transformation mechanism. Conjugation consists of a transfer of resistance plasmids containing resistance genes between bacteria by a conjugative pilus; transduction includes a transmission of DNA bacterial by a viral vector; while transformation involves an incorporation of exogenous DNA in bacterial genome.<sup>[22]</sup> These genetic resistance mechanisms include modification of target protein by disabling the antibiotic-binding but leaving intact the cellular functionality of target;<sup>[23]</sup> an inactivation of antibiotic by chemical covalent modifications;<sup>[24]</sup> an antibiotic efflux via pump that secrete antibiotic from the cell; a target bypass involving a formation of additional antibiotic targets or subunits that are not susceptible to binding of the antibiotic (Figure 2).<sup>[25]</sup> In addition, bacteria can protect themselves by self-assembling in biofilms, which are hydrated matrices composed of eDNA, proteins, and polysaccharides, in which bacterial cells are embedded and an exchange of genetic material between cells occurs very easily.<sup>[26]</sup> In biofilm communities, a slow or incomplete penetration of antibiotic and the transformation of bacterial cells in dormant cells which are less susceptible to antibiotics,<sup>[27]</sup> contribute to antibiotic resistance. Advances in genomics, system biology and structural biology have provided a lot of information related to events underpinning resistance, since a detailed understanding of resistance mechanisms could be the key to identify novel antibacterial agents, enable countering the resistance threat.

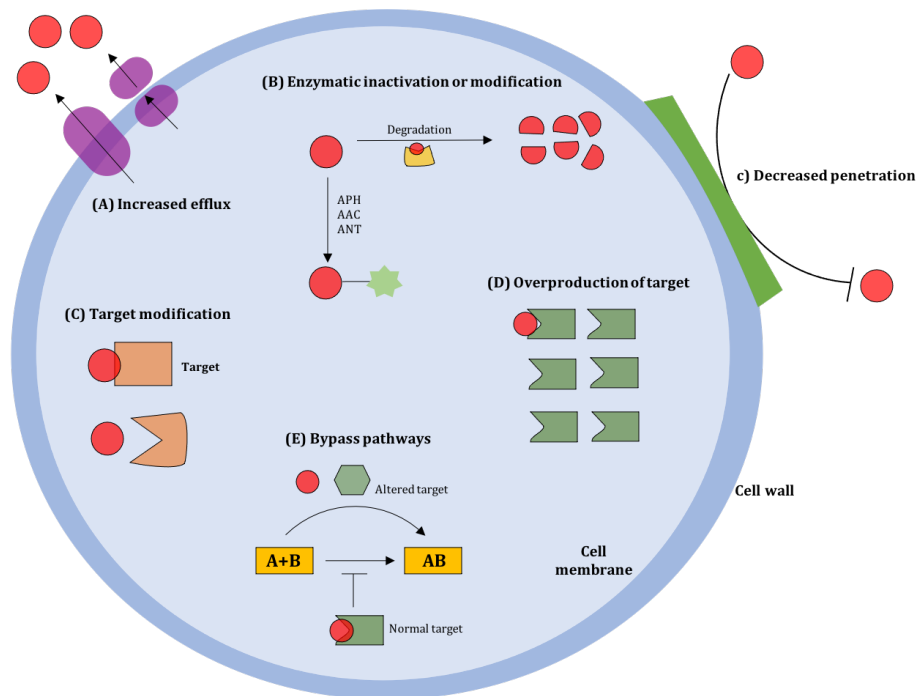


**Figure 2.** Mechanism of antibiotic resistance: **A)** Antibiotic efflux pumps remove the antibiotic from the cell before it can reach its target site. **B)** Antibiotic modification involving the addition of acetyl, phosphate, or adeny groups to aminoglycosides by N-acetyl transferases (AAC), O-phosphotransferases (APH), and O-adenyltransferases (ANT). Antibiotic degradation involving a hydrolysis by  $\beta$ -lactamases. **C)** Target modification such as 23S rRNA or 16S rRNA methylation. **D)** Target bypass involves the generation of additional antibiotic targets or subunits that are not susceptible to binding of the antibiotic. **E)** Overproduction of target.<sup>[15,25]</sup>

### 1.3. THE ANTIMICROBIAL PEPTIDES (AMPs)

The speedy growth of bacterial resistance to conventional antibiotics has caused an inefficiency of traditional approaches for eradicating infections and in addition the lack of choice of antimicrobials for their treatment, emphasizes the urgent need to discover novel antibacterial strategies.<sup>[28]</sup> Antimicrobial peptides (AMPs) appear as a valid therapeutic option for the development of novel antibiotics classes.<sup>[29]</sup> AMPs are an abundant and varied group of molecules produced by many tissues and cell types in a variety of invertebrate, plant and animal species.<sup>[30]</sup> They can be divided in gene-encoded ribosomally synthesized peptides present in all organisms and in non-ribosomally synthesized peptide antibiotics produced by bacteria and fungi.<sup>[31,32]</sup> Some non-ribosomally peptide antibiotics were clinically approved and widely used,

such as bacitracin, gramicidin S, polymyxin B, streptogramins as well as the two glycopeptide antibiotics vancomycin and teicoplanin.<sup>[33]</sup> Regarding ribosomally synthesized peptides are furtherly subdivided in eukaryotic AMPs and in defence peptides and proteins derived from bacteria, called bacteriocins.<sup>[34,35]</sup> In mammals, AMPs are an essential component of the innate immune system and represent the first line of immune biological defense.<sup>[36]</sup> In fact, they are also considered as effectors and regulators of the innate immune system, modulating profoundly the immune response through several mechanisms, for example, increasing the chemokine production and release by immune and epithelial cells and/or having an adjuvant activity in promoting adaptive immunity.<sup>[37]</sup>

Host-defense (antimicrobial) peptides (HDP) produced mostly by amphibian skin, derive from precursor peptides subjected to proteolytic activation steps.<sup>[38]</sup> They are typically amphipathic small peptides composed of 10–50 amino acids, have an overall net positive charge of +2 to +9 at physiological pH due to the presence of Lys and/or Arg residues, and have a substantial proportion ( $\geq 30\%$ ) of hydrophobic residues.<sup>[39]</sup> On the basis of their conformation, HDP are classified in four broad structural groups: *i*)  $\alpha$ -helical peptides free of cysteine residues (*e.g.* magainins);  $\beta$ -sheet peptides stabilized by two to four disulfide bridges (*e.g.* human  $\alpha$ - and  $\beta$ -defensins); loop peptides with one disulfide bridge (*e.g.* bactenecin); peptides characterized by extended structures rich in glycine, proline, tryptophan, arginine and/or histidine (*e.g.* indolicidin).<sup>[40]</sup> The main target for most HDP is bacterial membrane and their cationicity and amphiphilic nature are correlated to their activity.<sup>[40]</sup> The positively charged residues of AMPs determinate an accumulation at polyanionic microbial cell surfaces featured by lipopolysaccharide and teichoic acids in Gram-negative and Gram-positive bacteria, respectively. After crossing the outer membrane via self-promoted uptake, AMPs interact with acidic phospholipids (phosphatidylglycerol, phosphatidylethanolamine and cardiolipin) of the monolayer of cell membrane of both types of bacteria. The insertion of peptides into cell

membrane can cause a disruption of the physical integrity of bilayers by three different models, that is the barrel- stave, carpet and toroidal pore models.<sup>[41]</sup> In the carpet model, peptides interact with anionic phospholipid head groups and cover the membrane surface in a carpet-like manner.<sup>[42]</sup> When a critical threshold concentration is reached, peptides form toroidal transient holes in the membrane and the membrane ruptures in a detergent-like manner, resulting in micelle formation.<sup>[41,42]</sup> In the barrel stave model, hydrophobic peptide regions align with the lipid core region of bilayer and the hydrophilic peptide regions form the inner surface of pore channel.<sup>[43]</sup> Instead, in the toroidal-pore model, peptides aggregate and induce the lipid monolayers to bend incessantly through the pore, so that the water core is lined by both the inserted peptides and the lipid head groups.<sup>[43]</sup>

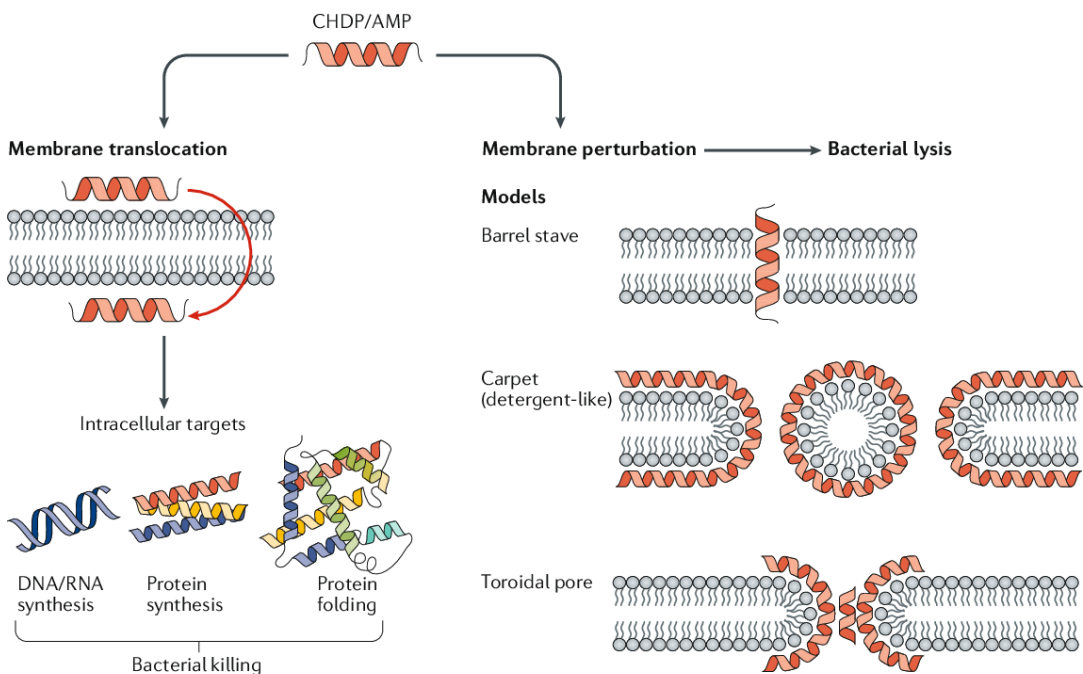


**Figure 3.** Models of mechanisms of antimicrobial host defence peptides.<sup>[46]</sup>

These two pore models differs from each other, because the pore is partly lined by lipid in toroidal model, while a cylindrical pore is completely lined by peptides in

barrel stave model,<sup>[44]</sup> but what drives the preference of AMPs for a certain models is not yet fully understood. In addition, a further mode of action of AMPs consists in crossing the bacterial membrane and binding to intracellular targets such as nucleic acids and/or proteins, killing bacteria by an arrest of cell processes such as replication, transcription or cell wall synthesis.<sup>[45]</sup> Exploiting this different mode of action of AMPs, an alternative route for the successful AMPs introduction may be their use in combination with conventional antibiotics in a synergistic mode of action. In a combined therapy, the disintegration of the bacterial membrane by AMP allows the antibiotic to enter the bacterial cell at higher concentrations and to interact with its specific intracellular targets, inducing bacterial cell death.<sup>[46]</sup>

Despite the mode of action of AMPs does not involve a specific target and so it is almost unlikely that bacteria can develop resistance, cases of AMP resistance have been reported anyway. Bacterial strategies which induce resistance to AMPs include bacterial cell envelope change as modifications in the polysaccharide layer and teichoic acid;<sup>[47]</sup> a production of bacterial proteins that can degrade or sequester peptides,<sup>[48]</sup> a removal of AMPs by an efflux system; and the formation of capsular polysaccharides hamper that capture the peptides.<sup>[49]</sup> Overall, unlike antibiotic resistance, the emergence of AMPs resistance is less recurrent and also less worrying, due to the lack of horizontal transmissions of resistance genes.

## **1.4. TEMPORINS**

The amphibian skin is one of the richest source of ribosomally synthesized antimicrobial peptides (AMPs), especially the skin of the *Rana* genus which includes more than 250 species around the world.<sup>[50]</sup> Temporins, first isolated from the skin of the Asian frog *Rana erythraea*,<sup>[51]</sup> are known as vespa-like peptides because their sequence is similar to chemotactic peptides isolated from the venom of wasps of genus *Vespa*.<sup>[52]</sup> In 1996, a family of 10 temporins (from A to L) were identified from skin secretions of the European red frog *Rana Temporaria*, through a mild electrical

stimulation.<sup>[53]</sup> By a screening of a cDNA library prepared from the skin of *Rana temporaria* using the precursor of esculentin from *Rana esculenta* as probe, the biosynthetic precursor of temporins was identified.<sup>[51,53]</sup> This large peptide precursor made of 22 residues, contains a cysteine residue in position 22 representing the site of cleavage of the signal peptide in the pre-protemporins. The pro-sequence contains at the C-terminus an acidic propiece ending with the pair Lys-Arg, which represents a processing site for prohormone convertases for generating the mature sequence. The glycine residue flanking the carboxyl-terminus of the mature peptide, is recognized by peptidylglycine  $\alpha$ -amidating monooxygenase for the formation of C-terminal amides.<sup>[54]</sup> Temporins are among the shortest amphipathic  $\alpha$ -helical AMPs (10 to 14 amino acids) found in nature to date. Their derived composite consensus sequence is FLP(I/L)IASLL(S/G)KLL-NH<sub>2</sub> and their general amino acid type sequence is X<sub>1</sub>X<sub>2</sub>X<sub>3</sub>X<sub>4</sub>X<sub>5</sub>X<sub>6</sub>Y<sub>7</sub>X<sub>8</sub>X<sub>9</sub>Y<sub>10</sub>Y<sub>11</sub><sup>+</sup>X<sub>12</sub>X<sub>13</sub>-NH<sub>2</sub>, where X and Y indicate hydrophobic and hydrophilic residues, respectively, whereas Y<sup>+</sup> denotes charged amino acids.<sup>[55]</sup> X<sub>2</sub>, X<sub>3</sub>, X<sub>9</sub> and X<sub>13</sub> are highly conserved amino acids and, since leucine is the most abundant amino acid in temporins, hydrophobic residues (Y) represent about 70% of the peptide sequence.<sup>[54,55]</sup> Temporins are C-terminally  $\alpha$ -amidated, have a low net positive charge (from 0 to +3 at physiological pH) due to the presence of Lys and Arg residues in their sequence and adopt an  $\alpha$ -helical conformation in a hydrophobic environment.<sup>[56]</sup> Temporins A (TA), B (TB), and L (TL) are the most studied among members of the temporin family. TA (Phe-Leu-Pro-Leu-Ile-Gly-Arg-Val-Leu-Ser-Gly-Ile-Leu-NH<sub>2</sub>) and TB (Leu-Leu-Pro-Ile-Val-Gly-Asn-Leu-Leu-Lys-Ser-Leu-Leu-NH<sub>2</sub>) show greater potencies against Gram-positive bacteria, including clinically isolated methicillin-resistant *Staphylococcus aureus*, vancomycin-resistant *Enterococcus faecium* and *E. faecalis* (with a minimal inhibitory concentration ranging from 2.5 to 20  $\mu$ M) than against Gram-negative bacterial strains. These isoforms have also a strong activity against the human parasitic protozoan *Leishmania*, inducing severe damage to the plasma

membrane.<sup>[56]</sup> Differently, Temporin L (Phe-Val-Gln-Trp-Phe-Ser-Lys-Phe-Leu-Gly-Arg-Ile-Leu- NH<sub>2</sub>) displays the strongest activity against fungi, yeasts, Gram-positive and is noticeably potent against Gram-negative species such as *Escherichia coli* D21 and *Pseudomonas aeruginosa* ATCC 15692, with a lethal concentration of 1.5 and 3.6  $\mu$ M, respectively.<sup>[57,58]</sup> The hydrophobic residues, in particular the phenylalanine zipper motif made of Phe1, Phe5, Phe8 in TL, are involved in the initial binding to the Gram-positive membrane and the stabilization of peptide aggregates in the membrane, leading to the formation of large pores and consequential cell death. The killing activity of TL against Gram-negative bacteria is due to its strong affinity toward the lipopolysaccharide LPS, a component of the outer membrane.<sup>[59]</sup> Neutralizing the toxic effect of LPS during a Gram-negative infection may help to eradicate the risk of sepsis, which can lead to mortality. LPS is made of a variable and polyanionic polysaccharide portion and lipid A consisting of a disaccharide of phosphorylated glucosamines; both are involved in the interaction with TL through a mixture of hydrophobic and ionic bonds.<sup>[55,59]</sup> According to “self-promoted uptake model”, these interactions permit TL to anchorage to the outer membrane, a loss of membrane integrity and a following increased permeability of peptide itself, reaching the cytoplasmic membrane.<sup>[60]</sup> A recent study using *E.coli* cells has showed that TL binds through a competitive inhibition mechanism the GTP binding site of FtsZ protein, involved in the first step of cell division process.<sup>[72]</sup> A high binding affinity was detected for TL toward FtsZ with a  $K_D$  value of  $17.4 \pm 0.8$  nM. A morphologic investigation by a TEM analysis has displayed that in presence of TL, *E. coli* cells form elongated “necklace-like” structures absent in untreated cells, which are originated by a multitude of bacterial cells unable to divide. Instead, the weak activity of TA and TB against Gram-negative bacteria may be due to their oligomerization process in presence of the LPS, because oligomers have a large size and cannot diffuse efficiently through the cell wall; in contrast, TL is completely aggregated in aqueous solution adopting an  $\alpha$ -





assumes a similar behavior but its  $\alpha$ -helix extends along 3–11 residues and its N-terminus has a higher propensity to form helical structures (Figure 4).<sup>[63,64]</sup>

Both temporins exhibited a “dynamic peptide-lipid supramolecular pore” model in SDS micelles, consisting in binding to negatively charged phospholipids membrane surface and when a local high concentration of a peptide was reached, transient aqueous pores of variable sizes are formed. The considerable difference in hemolytic activity of TA and TL is correlated to their diverse conformational propensities in DPC micelles. TL assumes an  $\alpha$ -helix conformation along its entire sequence, which allows the peptide to insert in a perpendicular orientation into micelle surface with its N-terminus located within the hydrophobic core, forming the staves of a barrel-like channel, as described in “barrel stave” model. Instead, the loss of  $\alpha$ -helical structure along the entire sequence of TA in DPC, explains its inability to deeply insert into the hydrophobic core of micelles and to form barrel-like channel. This could be the reason why the lytic effect of TA on red blood cells is weaker in comparison to TL.<sup>[63,64]</sup> The proline residue in TA is responsible to the substantial difference observed between TL and TA secondary structures, since proline is well-known as a  $\alpha$ -helix breaking amino acid and a  $\beta$ -turn inducer. In this context, a TL analogue, in which Gln<sup>3</sup> was replaced by Pro residue showed a hemolytic effect 2- to 5- fold lower than that of the native TL (at the 3-12  $\mu$ M concentration range), since a breaking of  $\alpha$ -helix and a  $\beta$ -turn centered on Pro<sup>3</sup> in N-terminal has conferred a high flexibility at N-terminus, which prevents to act via “barrel stave” mechanism in DPC micelles.<sup>[64]</sup> Therefore, TL cannot be considered as an efficacious alternative to traditional antibiotics because of its biological profile, but modifications of its chemical structure could contribute to challenge its drawbacks and to discover novel antibacterial agents with a high therapeutic index, referred to as the ratio between the concentration of hemolytic activity and antimicrobial activity.

## 1.5. REFERENCES

- [1] S.B. Zaman, M.A. Hussain, R. Nye, V. Mehta, K.T. Mamun, N. Hossain. A Review on antibiotic resistance: alarm bells are ringing. *Cureus*. 2017, 9:e1403.
- [2] S.B. Levy SB. From tragedy the antibiotic age is born . *The Antibiotic Paradox*. Springer, Boston, MA. 1992, pp 1–12.
- [3] R.I. Aminov. A brief history of the antibiotic era: lessons learned and challenges for the future. *Front. Microbiol*. 2010, 1:134.
- [4] M.I. Hutchings, A.W. Truman, B. Wilkinson. Antibiotics: past, present and future. *Curr. Opin. Microbiol*. 2019, 51, 72–80.
- [5] P. Ehrlich, S. Hata. *Die Experimentelle Chemotherapie der Spirilosien*. Berlin: Julius Springer. 1910, pp 1–85.
- [6] C.L. Ventola. The Antibiotic Resistance Crisis, Part 1: Causes and Threats. *P T*. 2015, 40, 277–283.
- [7] J. Mahoney, R. Arnold, A. Harris. Penicillin treatment of early syphilis. A preliminary report. *Verer. Dis. Inform*. 1943, 24, 355–357.
- [8] E.P. Abraham, E. Chain. An enzyme from bacteria able to destroy penicillin. *Nature*. 1940, 146:837.
- [9] I. Chopra, L. Hesse, A. O’Neill. Discovery and development of new antibacterial drugs,” in *Pharmacochemistry Library*, Vol. 32, Trends in Drug Research III, ed. H. van der Goot (Amsterdam: Elsevier). 2002, pp 213–225.
- [10] E. Peterson, P. Kaur. Antibiotic resistance mechanisms in bacteria: relationships between resistance determinants of antibiotic producers, environmental bacteria, and clinical pathogens. *Front. Microbiol*. 2018, 9:2928.
- [11] G. A. Durand, D. Raoult, G. Dubourg. Antibiotic discovery: history, methods and perspectives. *Int. J. of Antimicrob. Agents*. 2019, 53, 371–382.
- [12] H.W. Boucher, G.H. Talbot, J.S. Bradley, J.E. Edwards , D. Gilbert, L.B. Rice, M. Scheld, B. Spellberg, J. Bartlett. Bad bugs, no drugs: no ESKAPE! An update from the Infectious Diseases Society of America. *Clin. Infect. Dis*. 2009, 48, 1–12.
- [13] A.M. Slee, M.A. Wuonola, R.J. McRipley, I. Zajac, M.J. Zawada, P.T. Bartholomew, W.A. Gregory, M. Forbes. Oxazolidinones, a new class of synthetic antibacterial agents: in vitro and in vivo activities of DuP 105 and DuP 721. *Antimicrob. Agents Chemother*. 1987, 31, 1791-1797.
- [14] D. Cluck, P. Lewis, B. Stayer, J. Spivey, J. Moorman. Ceftolozane-tazobactam: A new-generation cephalosporin. *Am. J. Health Syst. Pharm*. 2015, 72, 2135–2146.
- [15] K. Lewis. Platforms for antibiotic discovery. *Nat. Rev. Drug Discov*. 2013, 12, 371–387.
- [16] <https://www.euro.who.int>.
- [17] G.M. Rossolini, F. Arena, P. Pecile, S. Pollini. Update on the antibiotic resistance crisis. *Curr. Opin. Pharmacol*. 2014, 18, 56–60.
- [19] Global priority list of antibiotic-resistant bacteria to guide research, discovery, and development of new antibiotics. <https://www.who.int>.

- [20] L.B. Rice. Federal funding for the study of antimicrobial resistance in nosocomial pathogens: no ESKAPE. *J. Infect. Dis.* 2008, 197:1079–1081.
- [21] D.M.P. De Oliveira, B.M. Forde, T.J. Kidd, P.N.A. Harris, M.A. Schembri, S.A. Beatson, D.L. Paterson, M.J. Walker. Antimicrobial resistance in ESKAPE pathogens. *Clin. Microbiol. Rev.* 2020, 33:e00181-19.
- [22] J.M. Blair, M.A. Webber, A.J. Baylay, D.O. Ogbolu, L.J. Piddock. Molecular mechanisms of antibiotic resistance. *Nat. Rev. Microbiol.* 2015, 13, 42–51.
- [23] A.J. Alanis. Resistance to antibiotics: are we in the post-antibiotic era?. *Arch. Med. Res.* 2005, 36, 697–705.
- [24] J.M. Munita, C.A. Arias. Mechanisms of antibiotic resistance. *Microbiol. Spectr.* 2016 4:10.1128.
- [25] M. Laws, A. Shaaban, K.M. Rahman. Antibiotic resistance breakers: current approaches and future directions. *FEMS Microbiol. Rev.* 2019, 43, 490-516.
- [26] H.K. Allen, J. Donato, H.H. Wang, K.A. Cloud-Hansen, J. Davies, J. Handelsman. Call of the wild: antibiotic resistance genes in natural environments. *Nat. Rev. Microbiol.* 2010, 8, 251-259.
- [27] R.M. Donlan. Biofilms: microbial life on surfaces. *Emerg. Infect. Dis.* 2002, 8, 881–890.
- [28] T.K. Wood, S.J. Knabel, B.W. Kwan. Bacterial persister cell formation and dormancy. *Appl. Environ. Microbiol.* 2013, 79, 7116–7121.
- [29] M.S. Zharkova, D.S. Orlov, O.Y. Golubeva, O.B. Chakchir, I.E. Eliseev, T.M. Grinchuk, O.V. Shamova. Application of antimicrobial peptides of the innate immune system in combination with conventional antibiotics—a novel way to combat antibiotic resistance?. *Front. Cell. Infect. Microbiol.* 2019, 9:128.
- [30] K.A. Brogden. Antimicrobial peptides: pore formers or metabolic inhibitors in bacteria?. *Nat. Rev. Microbiol.* 2005, 3, 238-250.
- [31] J. Wiesner, A. Vilcinskas. Antimicrobial peptides: the ancient arm of the human immune system. *Virulence.* 2010, 1, 440–464.
- [32] E. Guaní-Guerra, T. Santos-Mendoza, S.O. Lugo-Reyes, L.M. Terán. Antimicrobial peptides: general overview and clinical implications in human health and disease. *Clin. Immunol.* 2010, 135, 1–11.
- [33] W. Wohlleben, Y. Mast, E. Stegmann, N. Ziemert. Antibiotic drug discovery. *Microb. Biotechnol.* 2016, 9, 541-548.
- [34] M. Papagianni. Ribosomally synthesized peptides with antimicrobial properties: biosynthesis, structure, function, and applications. *Biotechnol. Adv.* 2003, 21, 465-499.
- [35] B.P. Cammue, M.F. De Bolle, H.M. Schoofs, F.R. Terras, K. Thevissen, R.W. Osborn, S.B. Rees, W.F. Broekaert. Gene encoded antimicrobial peptides from plants. *Ciba Found Symp.* 1994, 186, 91-101.
- [36] H.G. Boman. Peptide antibiotics and their role in innate immunity. *Annu. Rev. Immunol.* 1995, 12, 61–92.

- [37] R.E.W. Hancock, H.G. Sahl. Antimicrobial and host defense peptides as new anti-infective therapeutic strategies. *Nature Biotech.* 2006, 24, 1551–1557.
- [38] M. Zasloff. Magainins, a class of antimicrobial peptides from *Xenopus* skin: isolation, characterization of two active forms, and partial cDNA sequence of a precursor. *Proc. Natl. Acad. Sci. U S A.* 1987, 84, 5449–5453.
- [39] M. Zasloff. Antimicrobial peptides of multicellular organisms. *Nature.* 2002, 415, 389–395.
- [40] N. Mookherjee, M.A. Anderson, H.P. Haagsman, D.J. Davidson. Antimicrobial host defence peptides: functions and clinical potential. *Nat. Rev. Drug. Discov.* 2020, 19, 311–332.
- [41] R.M. Epanand, C. Walker, R.F. Epanand, N.A. Magarvey. Molecular mechanisms of membrane targeting antibiotics. *Biochim. Biophys. Acta.* 2016, 1858, 980–987.
- [42] Y. Pouny, D. Rapaport, A. Mor, P. Nicolas, Y. Shai. Interaction of antimicrobial dermaseptin and its fluorescently labeled analogues with phospholipid membranes. *Biochemistry.* 1992, 31, 12416–12423.
- [43] L. Yang, T.A. Harroun, T.M. Weiss, L. Ding, H.W. Huang. Barrel-stave model or toroidal model? A case study on melittin pores. *Biophys. J.* 2001, 81, 1475–1485.
- [44] M. Mihajlovic, T. Lazaridis. Charge distribution and imperfect amphipathicity affect pore formation by antimicrobial peptides. *Biochim. Biophys. Acta.* 2012, 1818, 1274–1283.
- [45] J. Wang, X. Dou, J. Song, Y. Lyu, X. Zhu, L. Xu, W. Li, A. Shan. Antimicrobial peptides: Promising alternatives in the post feeding antibiotic era. *Med. Res. Rev.* 2019, 39, 831–859.
- [46] H. Jenssen, P. Hamill, R.E. Hancock. Peptide antimicrobial agents. *Clin. Microbiol. Rev.* 2006, 19, 491–511.
- [47] A. Hollmann, M. Martinez, P. Maturana, L.C. Semorile, P.C. Maffia. Antimicrobial peptides: interaction with model and biological membranes and synergism with chemical antibiotics. *Front. Chem.* 2018, 6:204.
- [48] S.A Loutet, R.S. Flannagan, C. Kooi, P.A. Sokol, M.A. Valvano. A complete lipopolysaccharide inner core oligosaccharide is required for resistance of *Burkholderia cenocepacia* to antimicrobial peptides and bacterial survival in vivo. *J. Bacteriol.* 2006, 188, 2073–2080.
- [49] D.C. Nelson, J. Garbe, M. Collin. Cysteine proteinase SpeB from *Streptococcus pyogenes*—a potent modifier of immunologically important host and bacterial proteins. *Biol. Chem.* 2011, 392, 1077–1088.
- [50] C.Y. Okumura, V. Nizet. Subterfuge and sabotage: evasion of host innate defenses by invasive gram-positive bacterial pathogens. *Annu. Rev. Microbiol.* 2014, 68, 439–458.
- [51] J.M. Conlon, J. Kolodziejek, N. Nowotny. Antimicrobial peptides from ranid frogs: taxonomic and phylogenetic markers and a potential source of new therapeutic agents. *Biochim. Biophys. Acta.* 2004, 1696, 1–14.

- [52] M. Simmaco, D. De Biase, C. Severini, M. Aita, G.F. Erspamer, D. Barra, F. Bossa. Purification and characterization of bioactive peptides from skin extracts of *Rana esculenta*. *Biochim. Biophys. Acta*. 1990, 1033, 318–323.
- [53] M.L. Mangoni. Temporins, anti-infective peptides with expanding properties. *Cell. Mol. Life Sci*. 2006, 63, 1060–1069.
- [54] M. Simmaco, G. Mignogna, S. Canofeni, R. Miele, M.L. Mangoni, D. Barra. Temporins, antimicrobial peptides from the European red frog *Rana temporaria*. *Eur. J. Biochem*. 1996, 242, 788–792.
- [55] M.L. Mangoni, A.D. Grazia, F. Cappiello, B. Casciaro, V. Luca. Naturally occurring peptides from *Rana temporaria*: antimicrobial properties and more. *Curr. Top. Med. Chem*. 2016, 16, 54–64.
- [56] M.L. Mangoni, Y. Shai. Temporins and their synergism against Gram-negative bacteria and in lipopolysaccharide detoxification. *Biochim. Biophys. Acta*. 2009, 1788, 1610–1619.
- [57] S.M. Romero, A.B. Cardillo, M.C. Martínez Ceron, S.A. Camperi, S.L. Giudicessi. Temporins: an approach of potential pharmaceutical candidates. *Surg. Infect. (Larchmt)*. 2020, 21, 309–322.
- [58] A.K. Mahalka, P.K. Kinnunen. Binding of amphipathic  $\alpha$ -helical antimicrobial peptides to lipid membranes: lessons from temporins B and L. *Biochim. Biophys. Acta*. 2009, 1788, 1600–1609.
- [60] A.C. Rinaldi, M.L. Mangoni, A. Rufo, C. Luzi, D. Barra, H. Zhao, P.K. Kinnunen, A. Bozzi, A. Di Giulio, M. Simmaco. Temporin L: antimicrobial, haemolytic and cytotoxic activities, and effects on membrane permeabilization in lipid vesicles. *Biochem. J*. 2002, 368, 91–100.
- [61] A. Giacometti, O. Cirioni, R. Ghiselli, F. Mocchegiani, F. Orlando, C. Silvestri, A. Bozzi, A. Di Giulio, C. Luzi, M.L. Mangoni, D. Barra, V. Saba, G. Scalise, A.C. Rinaldi. Interaction of antimicrobial peptide Temporin L with lipopolysaccharide *in vitro* and in experimental rat models of septic shock caused by Gram-Negative bacteria. *Antimicrob. Agents Chemother*. 2006, 50, 2478–2486.
- [62] Y. Rosenfeld, D. Barra, M. Simmaco, Y. Shai, M.L. Mangoni. A synergism between temporins toward Gram-negative bacteria overcomes resistance imposed by the lipopolysaccharide protective layer. *J. Biol. Chem*. 2006, 281, 28565–28574.
- [63] A. Di Somma, C. Avitabile, A. Cirillo, A. Moretta, A. Merlino, L. Paduano, A. Duilio, A. Romanelli. The antimicrobial peptide Temporin L impairs *E. coli* cell division by interacting with FtsZ and the divisome complex. *Biochim. Biophys. Acta Gen. Subj*. 2020, 1864:129606.
- [64] A. Carotenuto, S. Malfi, M.R. Saviello, P. Campiglia, I. Gomez-Monterrey, M.L. Mangoni, L.M. Gaddi, E. Novellino, P. Grieco. A different molecular mechanism underlying antimicrobial and hemolytic actions of Temporins A and L. *J. Med. Chem*. 2008, 51, 2354–2362.

# CHAPTER 2

## CHEMICAL DECORATION OF PROLINE

This chapter is published in:

Buommino, E., Carotenuto, A., Antignano, E., **Bellavita, R.**, Casciaro, B., Loffredo, M.R., Merlino, F., Novellino, E., Mangoni, M.L., Nocera, F.P., Brancaccio, D., Punzi, P., Roversi, D., Ingenito, R., Bianchi, E., Grieco, P. The outcomes of decorated prolines in discovering novel antimicrobial peptides from Temporin-L. *ChemMedChem*. 14, 1283–1290 (2019).

**CONTRIBUTIONS:** Peptide synthesis.

## 2.1. TARGETING ESKAPE PATHOGENS

The uncontrollable growth of antibiotic resistance by superbugs, including the ESKAPE pathogens (*Enterococcus faecium*, *Staphylococcus aureus*, *Klebsiella pneumoniae*, *Acinetobacter baumannii*, *Pseudomonas aeruginosa*, and *Escherichia coli*), is the second cause of human mortality worldwide.<sup>[1,2]</sup> These resistant ESKAPE pathogens cause infectious diseases above all in hospitals, since their spread is very quickly in immune compromised-patients.<sup>[3]</sup> Among them, methicillin-resistant *Staphylococcus aureus* (MRSA) has become the leading pathogen in hospitals worldwide.<sup>[4]</sup> Vancomycin has long been considered the privileged drug for the treatment of MRSA infections, which can cause pneumonia and sepsis.<sup>[4]</sup> The methicillin resistance is conferred by expression of *mecA* gene encoding an altered penicillin binding protein PBP2a, which has a low affinity for all  $\beta$ -lactam antibiotics and enables the bacteria to synthesize cell-wall and to survive.<sup>[5]</sup> *Staphylococcus* strains isolated mainly from skin and mucosa of dogs is *Staphylococcus pseudointermedius*, which can cause skin infections and otitis externa along with *M. pachydermatis* yeast.<sup>[6]</sup> Methicillin-resistant *S. pseudointermedius* (MRSP) and MRSA infections are a huge challenge in veterinary medicine.<sup>[7]</sup> The close contact between household pets and their owners facilitates the transmission of MRSA and MRSP infections from household pets to owners and vice versa.<sup>[7]</sup> The presence of MRSP in food producing animals and in people working with food animals is considered a risk factor for human health, increasing the mortality rate in population.<sup>[8]</sup> In addition, antibiotic resistance developed by Gram-negative strains represents a demanding issue, since no novel class of drugs against Gram-negative strains has been introduced during the last four decades.<sup>[9,10]</sup> For example, *Escherichia coli* poses a large number of resistance genes that are the principal cause of treatment failures in both human and veterinary medicine.<sup>[11-13]</sup> The emergence of infections by ESKAPE pathogens (*e.g.* MRSA, MRSP, *E. coli*, *P. aeruginosa*) and the failure of antibiotics in their treatment has rung alarm bell in field of research,



leading to the discovery of novel antimicrobial agents such as antimicrobial peptides (AMPs). Among AMPs, temporins might represent an alternative to traditional antibiotics since act with a different mode of action from conventional antibiotics.<sup>[14]</sup> Herein, we performed a structure-activity relationship (SAR) study on interesting Temporin L (TL) analogue,<sup>[15]</sup> named [Pro<sup>3</sup>]TL, with the aim to discover novel promising anti-infective agents in both human and veterinary medicine. Proline residue, existing in the majority of naturally occurring membrane-acting peptides, has a crucial role in their structures being a potent  $\alpha$ -helix breaking amino acid and influences their biological activity.<sup>[16]</sup> The incorporation of a Pro residue may reduce the hemolytic activity, but may also facilitate membrane insertion as in antimicrobial peptide maculatin 1.1,<sup>[17]</sup> or may improve the antimicrobial activity as in AMP gaegurin peptide.<sup>[18]</sup> In the case of [Pro<sup>3</sup>]TL, the replacement of glutamine in position 3 with the proline has induced a  $\beta$ -turn structure in N-terminal centered on Pro<sup>3</sup> (Figure 1), which has caused a drastic reduction in the hemolytic activity in comparison to TL.<sup>[19,20]</sup>

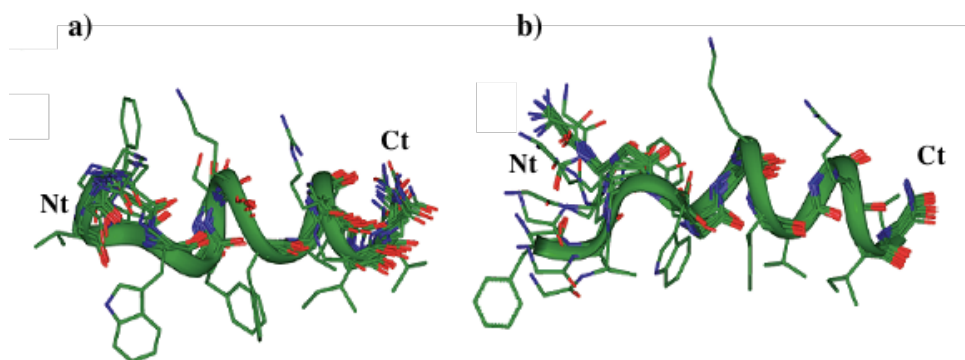


**Figure 1.** Superposition of the 20 lowest-energy conformers of Pro<sup>3</sup>-TL in SDS (a), and Pro<sup>3</sup>-TL in DPC (b). In SDS (a), Pro<sup>3</sup>-TL showed an  $\alpha$ -helix along residues 6–11 and a  $\beta$ -turn centered on Pro<sup>3</sup>. In DPC (b), Pro<sup>3</sup>-TL showed an  $\alpha$ -helix along residues 6–13 and a  $\beta$ -turn centered on 3–5 residues in N-terminal. Heavy atoms are shown with different colors (carbon, green; nitrogen, blue; oxygen, red).<sup>[19]</sup>

Preserving the low toxicity of [Pro<sup>3</sup>]TL, we performed a chemical decoration of proline residue using various chemical functionalities in position 4 of the ring,

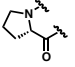
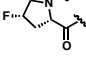
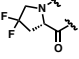
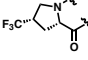
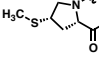
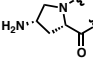
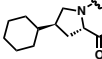
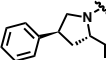
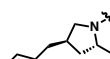
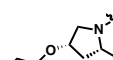
modifying the physicochemical properties of [Pro<sup>3</sup>]TL peptide and consequently its broad-spectrum antimicrobial activity. The antimicrobial activity of peptides **3–11** was evaluated both on human bacterial strains and on some veterinary bacterial strains. The hemolytic activity was investigated only for the most promising peptides. Conformational analysis by CD spectroscopy was performed for all compounds, while the NMR spectroscopy was carried out only for selected analogues.

## **2.2. RESULTS AND DISCUSSIONS**

### **2.2.1. DESIGN**

A previous SAR study on TL has led to the promising [Pro<sup>3</sup>]TL analogue featuring a low hemolytic activity and a satisfactory antimicrobial activity.<sup>[15,19]</sup> In this study, we selected appropriate functional groups to perform a chemical decoration of proline residue in [Pro<sup>3</sup>]TL analogue. Polar electronwithdrawing (fluoro, trifluoromethyl), apolar (methylthio), positively charged (amino), aliphatic (cyclohexyl), or aromatic (phenyl and benzyl) groups were chosen to yield peptides **3–11** (Table 1). A “chemical decoration” of Pro<sup>3</sup> with appropriate functional groups may cause an alteration of physicochemical properties such as hydrophilicity and hydrophobicity, affecting peptide interaction with bacterial membrane. For instance, the incorporation of aliphatic, apolar, and aromatic groups increases peptide hydrophobicity,<sup>[21]</sup> in contrast an amino group enhances peptide cationicity. In both cases, peptide-membrane interaction may be altered.<sup>[22,23]</sup> While a high net positive charge could reinforce peptide-membrane interaction, an excessive hydrophobicity could favor peptide aggregation with resultant reduced activity. Besides, an increase of hydrophobicity could promote the binding to mammalian membranes and reduce easily cell selectivity.<sup>[21]</sup> Therefore, our purpose was to perform a chemical decoration of [Pro<sup>3</sup>]TL analogue to improve its broad-spectrum antimicrobial activity, but conserving simultaneously its low hemolytic activity.

**Table 1.** Antimicrobial activity of designed compounds **3–11**.

Peptides	decorated Pro <sup>3</sup> residue	Sequence
1	-	F V Q W F S K F L G R I L
2		F V <b>Pro</b> W F S K F L G R I L
3		F V ( <i>cis</i> - <b>4F-Pro</b> ) W F S K F L G R I L
4		F V ( <b>4,4diF-Pro</b> ) W F S K F L G R I L
5		F V ( <i>cis</i> - <b>4CF<sub>3</sub>-Pro</b> ) W F S K F L G R I L
6		F V ( <i>cis</i> - <b>4MeS-Pro</b> ) W F S K F L G R I L
7		F V ( <i>cis</i> - <b>4NH<sub>2</sub>-Pro</b> ) W F S K F L G R I L
8		F V ( <i>trans</i> - <b>4Chx-Pro</b> ) W F S K F L G R I L
9		F V ( <i>trans</i> - <b>4Ph-Pro</b> ) W F S K F L G R I L
10		F V ( <i>trans</i> - <b>4Bn-Pro</b> ) W F S K F L G R I L
11		F V ( <i>cis</i> - <b>4PhO-Pro</b> ) W F S K F L G R I L

## 2.2.2. BIOLOGICAL ACTIVITY

**Antibacterial activity on human strains.** The antimicrobial activity of designed peptides **3–11** was evaluated against some reference bacterial and *Candida* strains in the broth microdilution assay to determine their MIC (Table 2).<sup>[24]</sup> All synthesized compounds displayed a good antimicrobial activity towards Gram-positive bacterial strains (*B. megaterium* BM11 and *S. epidermidis* ATCC 12228) with MICs values comparable to those of **1** and **2**. Notably, almost all compounds displayed a similar efficacy against *Candida albicans* ATCC 24433, as compound **2**. Peptide **3**, in which

the residue of Pro<sup>3</sup> was replaced with *cis*-4-fluoro-proline, showed a similar antibacterial activity as the parent peptide **2**, on both Gram-negative and Gram-positive bacterial strains. In addition, the activity towards *C. albicans* resulted to be 2-fold lower respect to TL. Peptides **4** and **5**, featuring by 4,4-difluoro-Pro and *cis*-trifluoromethyl-Pro, respectively, had the same behavior on both Gram-positive and Gram-negative strains. Their antimicrobial activity did not increase on Gram-positive strains in comparison to TL, but they resulted to be 2-fold less active than TL toward *P. aeruginosa* ATCC 27853, and their activity on *E. coli* ATCC 25922 was unchanged. Peptide **6**, characterized by the apolar methylthio group on Pro<sup>3</sup>, conserved the same activity of peptides **4** and **5** on both Gram-negative and Gram-positive bacteria, but its activity towards *C. albicans* resulted to slightly improved respect to parent [Pro<sup>3</sup>]TL (**2**). Surprisingly, by replacing the Pro<sup>3</sup> with its *trans*-4-cyclohexyl-Pro derivative, the resulting peptide **8** showed a dramatic reduction in activity on *E. coli* ATCC 25922 and lost effect on *P. aeruginosa* ATCC 27853. In addition, the activity towards *C. albicans* resulted to be 2-fold lower than the parent peptide **2**. Finally, analogues **9–11**, all characterized by an aromatic-containing functionality in position 4 of the pyrrolidine ring, *trans*-4-phenyl-Pro (**9**), *trans*-4-benzyl-Pro (**10**), *cis*-4-phenoxy-Pro (**11**), respectively, resulted to be poorly active on *P. aeruginosa* ATCC 27853 (MIC 50 µM), while the activity on *E. coli* ATCC 25922 was 2-fold lower for compounds **10** and **11**, compared to both reference peptides TL (**1**) and [Pro<sup>3</sup>]TL (**2**). However, the anticandidal activity remained almost unchanged with respect to **2**, except for compound **10**, showing a MIC of 25 µM. The one exception of enhancement of activity against Gram-negative was highlighted by a decoration of Pro<sup>3</sup> residue with a positively charged amino group in peptide **7**. In fact, peptide **7** displayed a significant lower MIC (3.12 µM) on *E. coli* ATCC 25922, while conserved a similar activity against *P. aeruginosa* ATCC 27853 in comparison to TL. Furthermore, the anticandidal activity was slightly decreased with respect to **1**.

**Table 2.** Antimicrobial activity of designed compounds **3–11**.

MIC values ( $\mu\text{M}$ ) <sup>a</sup>					
Peptides	<i>E. coli</i> ATCC 25922	<i>P. aeruginosa</i> ATCC 27853	<i>B. megaterium</i> BM11	<i>S. epidermidis</i> ATCC 12228	<i>C. albicans</i> ATCC 24433
<b>1</b>	12.5	12.5	3.12	3.12	6.25
<b>2</b>	12.5	25.0	3.12	6.25	12.5
<b>3</b>	12.5	12.5	3.12	6.25	12.5
<b>4</b>	12.5	25.0	3.12	3.12	12.5
<b>5</b>	12.5	25.0	3.12	3.12	12.5
<b>6</b>	12.5	25.0	3.12	3.12	6.25
<b>7</b>	3.12	12.5	3.12	3.12	12.5
<b>8</b>	50.0	100	3.12	3.12	12.5
<b>9</b>	12.5	50.0	3.12	3.12	12.5
<b>10</b>	25.0	50.0	3.12	3.12	25.0
<b>11</b>	25.0	50.0	3.12	3.12	12.5

On the basis of these results, the net charge positive seemed to be crucial for the activity toward Gram-negative. In fact, the introduction of an amino group on Pro<sup>3</sup> conferred to peptide **7** a net positive charge of +4 in contrast to other peptides (+3), which promoted an increase of its activity on *E. coli* ATCC 25922 compared to native TL and lead compound [Pro<sup>3</sup>]TL. Instead, the net positive charge did not affect the activity on Gram-positive bacteria, since all peptides showed a good activity towards Gram-positive strains.

**Antimicrobial activity on veterinary bacterial strains.** The activity of peptides **3–11** was evaluated on veterinary bacterial strains, such as *E. coli* and *P. mirabilis* (Gram-negative), *S. pseudintermedius* (Gram-positive), *M. pachydermatis* (yeast). The veterinary clinical isolates were first analyzed by disc diffusion test for the occurrence of antibiotic resistance, demonstrating a strong resistance to most common antibiotics used in the therapy of pet animals (data not shown).

**Table 3.** Antimicrobial activity of designed compounds **3–11** on veterinary strains.

MIC values ( $\mu\text{M}$ )					
Peptides	<i>E. coli</i>	<i>Proteus mirabilis</i>	MSSP	MRSP	<i>M. pachydermatis</i>
<b>1</b>	12.5	>100	3.12	3.12	25
<b>2</b>	12.5	>100	3.12	3.12	25
<b>3</b>	>100	>100	1.56	1.56	25
<b>4</b>	12.5	25.0	3.12	3.12	12.5
<b>5</b>	>100	>100	>100	>100	25
<b>6</b>	12.5	>100	3.12	3.12	12.5
<b>7</b>	3.12	>100	6.25	6.25	25
<b>8</b>	>100	>100	3.12	3.12	25
<b>9</b>	>100	>100	3.12	6.25	12.5
<b>10</b>	>100	>100	3.12	3.12	25.0
<b>11</b>	>100	>100	1.56	1.56	12.5

Regarding the activity on Gram-negative strains, only compounds **6** and **7** were active on *E. coli*, in particular, compound **7** resulted in the most potent one with a MIC of 3.12  $\mu\text{M}$ . On the contrary, all other synthesized compounds were inactive against *P. mirabilis* (MIC >100 $\mu\text{M}$ ). Further interesting results were obtained on *S. pseudintermedius* all peptides, except for peptides **4** and **5**, showed a good activity as parent Pro<sup>3</sup>TL (**2**). Specifically, compounds **3** and **11** displayed a strong activity against both MSSP and MRSP with a MIC of 1.56  $\mu\text{M}$ . Additionally, the compounds were tested on the yeast *M. pachydermatis*. Good activity was shown for all compounds, especially for **6**, **9**, and **11** with a MIC of 12.5  $\mu\text{M}$ . Overall, compound **11** showed the best activity on both *M. pachydermatis* and *S. pseudintermedius*. Because both strains can be etiological agents in canine pyoderma and otitis, compound **11** may be considered a potential lead compound for combined therapy in the care of pet animals. Taking into account the antimicrobial activity against reference strains and clinical isolates, the compounds **6**, **7**, and **11** showed a better

activity than compound **2** and for this reason they were selected for further characterization in the hemolysis assay.

**Hemolytic activity versus human erythrocytes.** The compounds with the best antimicrobial activity (**6**, **7** and **11**) were tested for their effect on circulating blood cells (*i.e.* erythrocytes) and the percentages of hemolysis are reported in Figure 2 and compared to those of the parent peptide (**2**).

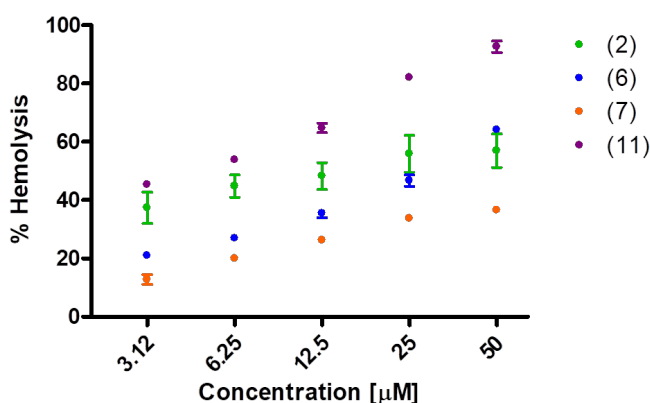


**Figure 2.** Hemolytic activity of compounds **6**, **7** and **11** compared to the parent peptide **2**. Percentages of hemolysis  $\pm$  SEM were calculated with respect to the complete lysis of erythrocytes in distilled water.

Compound **11**, characterized by *cis*-4-phenoxy-Pro, showed a potent hemolytic effect even at low concentrations ( $> 40\%$  at 3.12 or 6.25  $\mu\text{M}$ ), probably due to its high hydrophobic content that creates strong interactions with eukaryotic membranes. In comparison, compound **6** was found to be less hemolytic than compounds **11** and **2** at a concentration range from 3.12 to 25  $\mu\text{M}$ , but more active than the parent peptide **2** at the highest concentration (*i.e.* 50  $\mu\text{M}$ ). Interestingly, compound **7** was less toxic than compound **2** ( $p < 0.01$ ) and all the other tested analogs at all concentrations tested. This makes peptide **7** the compound with the best biological profile.

### 2.2.3. STRUCTURAL STUDIES

**CD analysis.** To explore the conformational changes of TL analogues synthesized in this study, we performed CD spectroscopy studies in phosphate buffer (PB, pH 7.4), sodium dodecylsulphate (SDS), dodecylphosphocholine (DPC), and DPC/SDS 9:1 micelle solutions (Figure 3). These micelles were used as mimetics of bacterial, mammalian, and yeast membranes, respectively.<sup>[26,27]</sup>

Secondary structure content (Table 4) was evaluated from CD spectra by the Bestsel method.<sup>[28]</sup> CD spectra in PB revealed the prevalence of disordered conformers for all compounds characterized by a minimum close to 200 nm (Figure 3a and Table 4). For some analogues (**8**, **10**, and **11**) a relatively intense minimum at 228 and maximum at 190 nm were observed. These spectral features were associated by Bestsel prediction to an increase of the  $\beta$ -sheet and/or  $\beta$ -turn structures content (Table 4). In SDS, DPC, and DPC/SDS 9:1 membrane mimetic solutions, CD spectra indicated more structured peptides (Figures 3b–d).

In all cases, two minima close to 208 and 222 nm were obtained, indicating helical propensity (Table 4). Indeed, helical percentage of the peptides varied from 21 to 52% in SDS and from 24 to 60% in DPC/SDS according to Bestsel prediction (Table 4). Nonetheless, antibacterial activity on Gram-positive strains and antifungal activity were almost identical regardless of helical content. For example, peptides **7** (42.7% helix in SDS) and **8** (21.3% helix in SDS) had the same activity on both *B. megaterium* and *S. epidermidis* (Table 2). The relationships between the conformations of the synthesized peptides and the antibacterial activity on Gram-negative bacteria is more intriguing.



**Table 4.** Secondary structure\* percentages of TL analogues.

Pept	PB solution				DPC solution				SDS solution				DPC/SDS Solution			
	<i>h</i>	<i>b</i>	<i>t</i>	<i>r</i>	<i>h</i>	<i>b</i>	<i>t</i>	<i>r</i>	<i>h</i>	<i>b</i>	<i>t</i>	<i>r</i>	<i>h</i>	<i>b</i>	<i>t</i>	<i>r</i>
1	12.7	31.5	14.2	41.5	62.2	2.0	9.5	26.4	47.7	8.7	11.0	32.6	60.5	3.7	11.1	24.7
2	9.6	19.1	18.7	52.7	42.8	16.2	11.2	29.8	45.6	3.4	15.0	36.0	43.2	14.5	12.7	29.5
3	11.9	25.1	16.3	46.7	42.2	9.9	12.8	35.2	42.0	10.9	14.3	32.8	43.5	8.4	13.8	34.3
4	12.3	26.9	16.2	44.5	40.2	17.1	11.0	31.7	43.5	5.9	12.0	38.6	41.0	16.5	11.2	31.3
5	15.3	17.9	14.8	51.9	39.5	13.4	11.3	35.9	51.7	2.8	12.4	33.1	40.9	14.5	11.9	32.7
6	0.0	51.7	13.1	35.2	42.6	8.1	12.4	36.9	44.1	2.3	16.1	37.5	45.3	5.1	13.0	36.7
7	14.9	14.5	16.1	54.5	44.3	16.1	12.0	27.5	42.7	9.4	12.8	35.2	45.1	15.2	11.5	28.2
8	6.1	36.7	16.1	41.0	25.0	13.4	13.5	48.2	21.3	15.8	13.6	49.3	24.4	21.2	12.3	42.1
9	13.3	31.0	16.1	39.7	28.8	17.9	13.4	39.9	32.3	6.7	14.7	46.3	26.5	15.2	16.6	41.7
10	4.8	35.8	18.0	41.3	39.4	6.1	12.9	41.6	30.9	4.2	14.3	50.6	35.8	12.5	12.4	39.3
11	5.5	22.1	27.6	44.8	51.8	6.8	10.8	30.6	48.4	4.2	12.7	34.8	49.9	8.0	13.9	28.2

\*h helix,  $\beta$  beta-sheet, t turn, r random coil. Peptide **8** in LPS: h 1.6,  $\beta$  41.3, t 13.9, r 43.2.

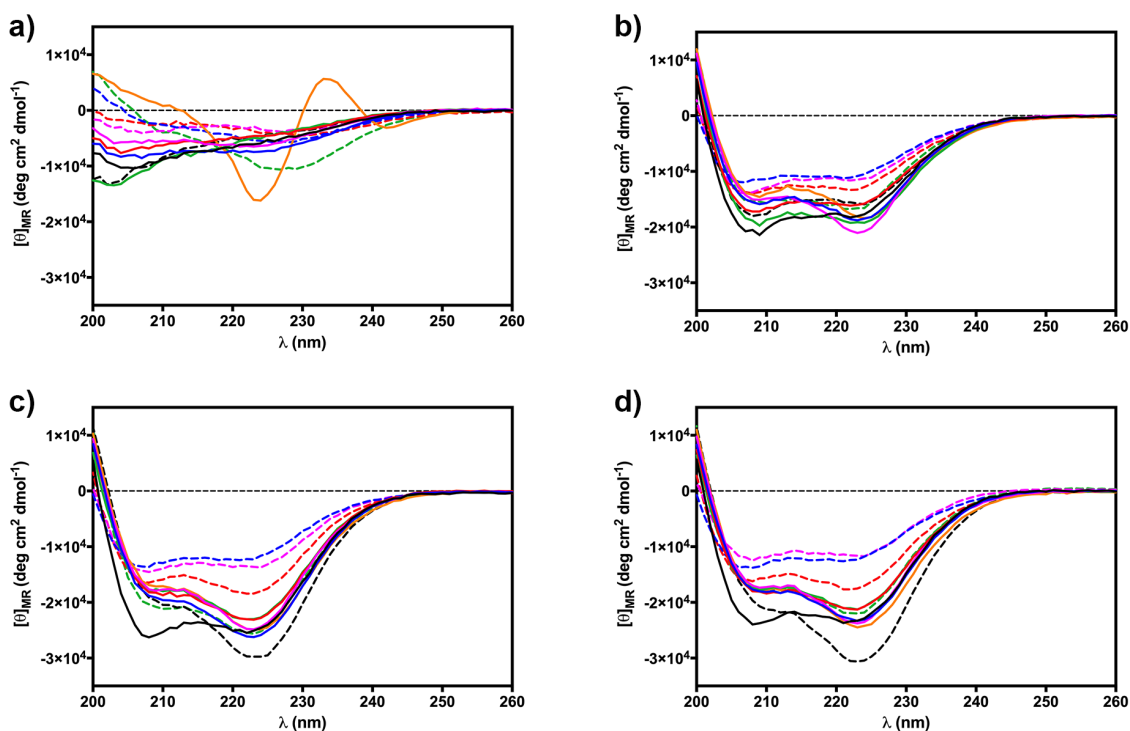


**Figure 3.** CD spectra of peptide **1** and its analogues **2-11** in PB a), SDS b), DPC c), and DPC/SDS 9:1 micelle solutions d). (**1**, black solid line; **2**, blue solid line; **3**, magenta solid line; **4**, red solid line; **5**, green solid line; **6**, orange solid line; **7**, black dashed line; **8**, blue dashed line; **9**, magenta dashed line; **10**, red dashed line; **11**, green dashed line).

Three peptides (**8**, **10**, and **11**) showed lower activity than the parent **2** against both the human Gram-negative bacteria tested (Table 2). Those peptides had different degrees of helical content in SDS (from 21 to 48%), hence, there is not a clear correlation between antibacterial activity and helical content. Interestingly enough, peptides **8**, **10**, and **11** showed a relatively high propensity to the  $\beta$ -sheet or turn formation in PB solution, which could indicate their tendency to aggregate in amyloid-like structures. It has been hypothesized that this aggregation tendency increased in contact with the external membrane of the Gram-negative bacteria, in particular, in the presence of lipopolysaccharides (LPS). This possibility was tested by acquiring the CD spectrum of peptide **8**, which was almost inactive against Gram-negative bacteria, in the presence of LPS micelles (Figure 4).

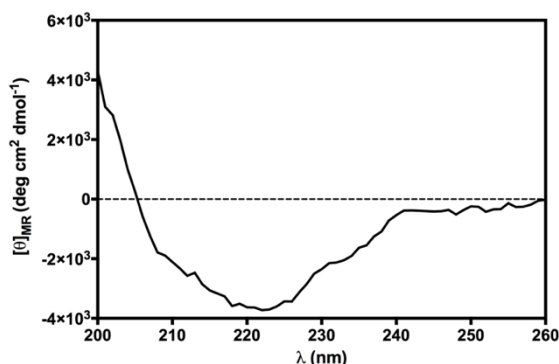


Figure 4. CD spectrum of peptide **8** (25  $\mu$ M) in a 100  $\mu$ M LPS solution.

The spectrum displayed a minimum at 220 nm and a maximum at 196 nm, and its deconvolution by Bestsel algorithm gave a  $\beta$ -sheet content higher than 40%, a situation often associated with amyloid-like peptide oligomers.<sup>[14]</sup> Therefore, peptide **8** inactivity against Gram-negative bacteria could be due to its oligomeric state induced by contact with LPS. The large size of the oligomer makes it more difficult for the peptide to diffuse through the cell wall into the target cytoplasmic membrane.<sup>[30]</sup> Notably, TL, in contrast to peptide **8**, was active against Gram-negative bacteria differently, because it showed a high helical propensity and disassembles in contact with LPS.<sup>[31]</sup> Compound **7** showed very high activity against

*E. coli*, being 4-fold higher than both its parent **2** and the native TL (**1**). Notably, the activity of peptide **7** against *E. coli* was also confirmed on the veterinary strain (Table 3). Considering the effect of the conformational propensities of the peptides on their hemolytic effect, peptide **11** showed the highest hemolytic effect (Figure 2) and also the highest helical content (Table 4) in the eukaryotic mimetic DPC solution. This result was in accordance with our previous result correlating peptide helicity in DPC with its hemolytic effect.<sup>[14]</sup> Peptides **2**, **6**, and **7** displayed similar helical content (Table 4). The lower hemolytic potency of peptide **7** could be tentatively explained by considering our previous result on the mechanism of the hemolytic action of TL (**1**) and its derivatives. In fact, studying the interaction between **1** and zwitterionic DPC micelles by NMR and MD simulations,<sup>[15,19]</sup> we found that **1** inserts into the micelle, perpendicular to the membrane, with the N terminus deeply buried in the micelle hydrophobic core, thus unveiling the barrel-stave mechanism.<sup>[19]</sup> The presence of a hydrophilic group on Pro<sup>3</sup> within the N-terminal region, such as in peptide **7**, probably prevented the peptide from exerting the above-described mechanism, thus explaining its low toxicity.

***NMR analysis of peptides 7 and 8.*** Considering the very interesting antimicrobial activity of compound **7**, in particular against Gram-negative bacteria, and its low hemolytic effect, it was also investigated by NMR spectroscopy. Moreover, peptide **8**, which was almost inactive against Gram-negative, was also investigated by NMR for comparison. NMR spectroscopy was performed in SDS micellar solution. Complete <sup>1</sup>H NMR chemical shift assignments were effectively achieved for both peptides according to the Wüthrich procedure.<sup>[32]</sup> Peptide **7** in SDS solution exhibited NMR spectral features pointing to helical propensity. Structure calculation gave an ensemble of 20 structures (Figure 5a) satisfying the NMR-derived constraints (violations smaller than 0.10 Å). Backbone is well defined, with a RMDS = 0.34 Å. An inverse  $\gamma$ -turn centered on the amino-Pro<sup>3</sup> can be observed at the N-terminus followed by an  $\alpha$ -helix from Trp<sup>4</sup> to Leu<sup>13</sup> (Figure 5a). Interestingly, the peptide

assumes an amphipathic structure with a positive side (Figure 5a) and a hydrophobic side (lower side in Figure 5b). In particular, the *cis*-4-amino group on Pro<sup>3</sup> points towards the other positively charged groups (Lys<sup>7</sup> amino and Arg<sup>11</sup> guanidinium groups) enlarging the charged peptide surface. Diagnostic NMR parameters observed for **8** also indicated conformational propensity toward helical or turn structures but with higher flexibility. Calculated structures, shown in Figure 5b, were less defined than those obtained for **7** (backbone heavy atoms RMSD=0.72 Å), which was in accordance with the CD result indicating a minor content of helix structure compared to **1**, **2**, and **7** (Table 4). A helix structure was observable from residue 5 to 12 in many structures of the ensemble (18/20), while the N-terminal region was in extended conformation. Notably, the cyclohexyl group was positioned near the phenyl rings of Phe<sup>1</sup> and Phe<sup>5</sup> forming a hydrophobic cluster. The overall structure was amphipathic with the cyclohexyl cluster oriented on the same side of Phe<sup>8</sup>, Leu<sup>9</sup>, and Ile<sup>12</sup> (Figure 5b). However, the loss of the N-terminal helical segment, observed in **7** and **8**, did not affect the antimicrobial activity of the TL derivatives, as already demonstrated for peptide **2**.<sup>[15,19]</sup> In fact, the high flexibility of the N-terminal region of these peptides allowed an optimal orientation of the additional group on the proline for membrane interactions.

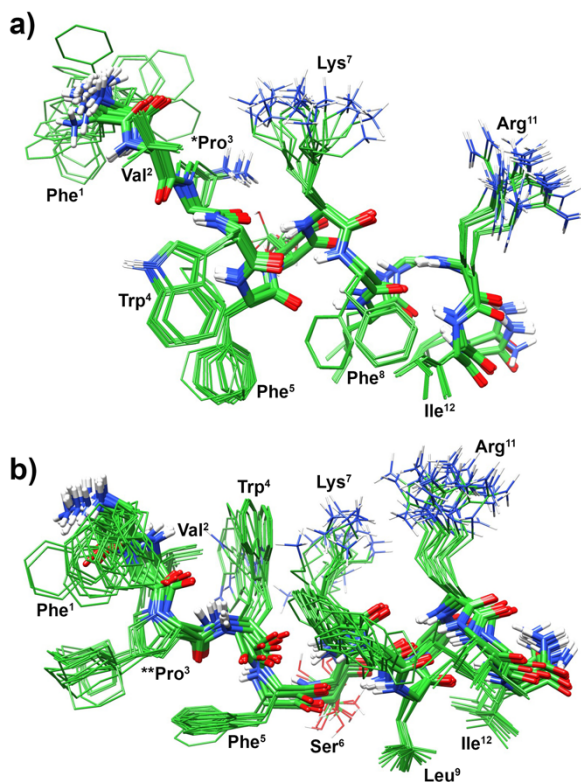


**Figure 5.** Superposition of the 20 lowest energy conformers of **7** (a, PDB ID code: 6QXB) and **8** (b, PDB ID code: 6QXC) in SDS. Structures were superimposed using the backbone heavy atoms. Only heavy backbone atoms are shown for clarity. Backbone atoms were evidenced as a ribbon. Heavy atoms are shown with different colors (carbon, green; nitrogen, blue; oxygen, red). \*Pro: *cis*-4-amino proline. \*\*Pro: *trans*-4-cyclohexyl proline.

This could explain the high activity against Gram-positive bacteria and good activity against fungi observed for all peptides (Table 2). In the same way, an optimal orientation of the positively charged amino group of **7** could explain its increased activity against many Gram-negative strains. In the same way, this flexibility at N-terminus of peptide **7** could also explain its increased activity against many Gram-negative strains. On the other hand, the reduction or loss of activity against Gram-negative bacteria observed in some of the novel peptides was likely due to peptide aggregation as stated above. In fact, the hydrophobic cluster found in the structure of peptide **8** (Figure 5b), but also predictable in other peptides such as **10** and **11**, could work as an aggregation point leading to oligomerization.

## 2.3. CONCLUSIONS

TL (**1**) has unique anti-yeast and anti-Gram-negative activity among the temporins. These activities were maintained by its analogue [Pro<sup>3</sup>]TL (**2**), which also showed a reduced cytotoxicity against red blood cells. By decorating the Pro residue with several chemical functionalities (fluoro, trifluoromethyl, amino, cyclohexyl, phenyl and benzyl groups) in [Pro<sup>3</sup>]TL (**2**), we have obtained interesting candidates for antimicrobial clinical studies. In particular, peptide **7** characterized by a *cis*-4-amino-Pro residue, showed an improved activity than the parent peptide **2** against human and veterinary Gram-negative bacterial strains. At the same time, it conserved the activity of **2** on Gram-positive bacteria and yeasts and a low toxicity on red blood cells. Peptide **11** was also interesting due to its activity against veterinary strains but, because of its toxicity, it could be considered as a starting point for further chemical modifications. More generally, we demonstrated that the decoration of Pro<sup>3</sup> on peptide **2** is a successful strategy to obtain active antimicrobial peptides, since the flexibility of the N-terminal peptide region allows an optimal orientation of additional group to establish strong membrane interactions and increase antimicrobial activity.

## 2.4. EXPERIMENTAL SECTION

### 2.4.1. CHEMISTRY

**Materials.** All N<sup>α</sup>-Fmoc-protected amino acids were purchased from NovaBiochem. Other non-natural N<sup>α</sup>-Fmoc-amino acids, namely Fmoc-l-Pro(4,4-diF<sub>2</sub>), Fmoc-l-Pro(*cis*-4-F), Fmoc-l-Pro(*cis*-4-CF<sub>3</sub>), Fmoc-l-Pro(*cis*-4-OPh), Fmoc-l-Pro(*trans*-4-Bz), Fmoc-l-Pro(*trans*-4-Ph), Fmoc-l-Pro(*trans*-4-Chx), and Fmoc-l-Pro(*cis*-4-SMe), were purchased from Polypeptide Laboratories. Fmoc-l-Pro(*cis*-4-NHBoc) was purchased from 3B Scientific Corp. The Rink amide resin was purchased from

Chem-Impex. Coupling reagents were purchased as follows: N,N'-diisopropylcarbodiimide (DIC) from Sigma-Aldrich, ethyl cyano(hydroxyimino)acetate (Oxyma Pure) from Chem-Impex, 1-hydroxy-7-azabenzotriazole (HOAt) from CreoSalus. All were reagent grade acquired from commercial sources and used without further purification.

**Peptide synthesis.** The synthesis of peptides **1–11** was performed by solid-phase peptide synthesis (SPPS) using Fmoc/tBu chemistry. All peptides were assembled on a Rink amide PS resin 100–200 mesh, (0.2 mmol scale with 0.47 mmol  $\times$  g<sup>-1</sup> of loading). The synthesis of peptides **1** and **2** was performed manually using a Microwave CEM Accent instrument. Amino acids (3 equiv) were acylated using equimolar amounts of DIC and Oxyma as activators. Double coupling conditions: 75°C, 170 W, 15 min, then 90°C, 30 W, 110 min, were used for all amino acids. The synthesis of all other peptides was performed on a Liberty Blue microwave synthesizer (CEM corporation) using a 5-fold excess of amino acids and equimolar amounts of DIC and Oxyma. The synthesis proceeded on the synthesizer up to Trp<sup>4</sup>, followed by acylation with the different pyrrolidine analogues for each sequence by manual synthesis using 3 equivalents of each amino acid and equimolar amounts of activators DIC and HOAt in DMF. The last two residues Val<sup>2</sup> and Phe<sup>1</sup> were acylated by double acylation with DIC and HOAt as activators. The final peptide resins were washed and dried with CH<sub>2</sub>Cl<sub>2</sub>, MeOH, and Et<sub>2</sub>O. Peptide **1** and its analogues **2–11** were cleaved from the resin using a solution of TFA/TIS/phenol/H<sub>2</sub>O (87:3:5:5, v/v/v) for 2 h. The resins were filtered, and peptide solutions were precipitated with MTBE. The peptide precipitates were centrifuged and washed with fresh MTBE. The peptide pellets were dried dissolved in 50:50 H<sub>2</sub>O/CH<sub>3</sub>CN and lyophilized. Purification of peptides was performed by preparative reversed phase chromatography on a Waters 2545 HPLC system equipped with a 2489 UV detector on a Waters XBridge™ C18 preparative column (130 Å, 5µm, 150  $\times$  50 mm) using

as eluents (A) 0.1% TFA in water and (B) 0.1% TFA in CH<sub>3</sub>CN. All fractions with the highest purity were collected and lyophilized, obtaining peptides with a purity >95%. Purified peptides were characterized on an Acquity UPLC Waters chromatograph, using a Waters BEH130 C18 Acquity column (2.1 × 100 mm, 1.7 μm, at 45°C) for compounds **1–6** and an Aeris PEPTIDE XB-C18 100 Å column (2.1 × 100 mm, 2.6 μm, at 45°C) for compounds **7–11**, using as eluents (A) 0.1% TFA in water and (B) 0.1% TFA in CH<sub>3</sub>CN, and by ESI on an Acquity SQ2 Mass Detector (Table 5).

**Table 5.** Analytical data of compounds **1–11**.

Cmpd#	R <sub>t</sub> (min)	MW	MW
		calcd	found
<b>1</b>	3.15	1640.01	1641.2
<b>2</b>	3.34	1609.00	1610.2
<b>3</b>	3.47	1626.99	1628.2
<b>4</b>	3.51	1644.98	1646.3
<b>5</b>	3.74	1677.00	1678.0
<b>6</b>	3.61	1655.09	1655.9
<b>7</b>	3.64	1624.02	1625.5
<b>8</b>	3.69	1691.15	1692.6
<b>9</b>	3.08	1685.10	1686.6
<b>10</b>	3.20	1699.13	1700.2
<b>11</b>	3.25	1702.10	1702.5

## 2.4.2. BIOLOGY

**Antimicrobial assay.** The MIC values were obtained by adapting the microbroth dilution method outlined by the Clinical and Laboratory Standards Institute, using sterile 96-well plates (Falcon NJ, USA). Aliquots (50 μL) of bacteria in mid-log phase at a concentration of 2×10<sup>6</sup> colony-forming units (CFU) per mL (5×10<sup>4</sup> CFU mL<sup>-1</sup> for *C. albicans*) in culture medium (Mueller–Hinton, MH or Winge broth, WB, for *C. albicans*, and Sabouraud broth for *M. pachydermatis*) were added to 50 μL of MH/WB containing the peptide in serial 2-fold dilutions in water.<sup>[29]</sup> Peptide dilutions ranged from 0.1 to 100 μM. MICs were considered as



the peptide concentration at which 100% inhibition of microbial growth is visually observed after 18–20 h of incubation at 37°C (30°C for yeasts). Each MIC value is the average of at least three independent experiments.

**Hemolytic assay.** The hemolytic activity was measured on sheep red blood cells (OXOID, SR0051D).<sup>[20]</sup> Briefly, aliquots of erythrocyte suspension ( $1 \times 10^8$  cells mL<sup>-1</sup>) in 0.9% (w/v) NaCl were incubated with serial 2-fold dilutions of the peptides in water for 40 min at 37°C with gentle shaking. The samples were then centrifuged for 5 min at 900×g and the absorbance of the supernatant was measured at 415 nm using a microplate reader (Infinite M200; Tecan, Salzburg, Austria). The complete lysis of red blood cells was measured by suspending erythrocytes in distilled water.

### 2.4.3. CONFORMATIONAL ANALYSIS

**Circular dichroism spectroscopy.** Circular dichroism spectra were recorded at 25°C using quartz cells of 0.1 cm path length with a JASCO J-710 CD spectropolarimeter (JASCO International Co. Ltd.). Measurements were run in the 260–185 nm spectral range, 1 nm bandwidth, 16 s response time, and 2 nm min<sup>-1</sup> scanning speed. The concentration of peptides was 100 μM in 10 mM, sodium phosphate buffer (pH 7.4), SDS (20 mM), DPC (20 mM), or DPC/SDS (18/2 mM) micellar solutions.<sup>[29]</sup> The Bestsel algorithm was used to extract secondary structure content. A CD spectrum of peptide **8** was also acquired in LPS 100 μM.

**NMR spectroscopy.** The samples for NMR spectroscopy were prepared by dissolving the appropriate amount of peptides in 0.55 mL of 1H<sub>2</sub>O, 0.05 mL of 2H<sub>2</sub>O to obtain a concentration of 1–2 mM peptides and 200 mM [D<sub>25</sub>]SDS.<sup>[32]</sup> The NMR experiments were performed at pH 5.0. NMR spectra were recorded on a Varian Unity INOVA 700 MHz spectrometer equipped with a z-gradient 5

mm triple-resonance probe head. All spectra were recorded at a temperature of 25°C. One-dimensional (1D) NMR spectra were recorded in the Fourier mode with quadrature detection. Two-dimensional (2D) DQF-COSY, TOCSY, and NOESY spectra were recorded in the phase-sensitive mode using the method from States *et al.* Data block sizes were 2048 addresses in  $t_2$  and 512 equidistant  $t_1$  values. A mixing time of 80 ms was used for the TOCSY experiments. NOESY experiments were run with mixing times in the range of 100–200 ms. The qualitative and quantitative analysis of DQF-COSY, TOCSY, and NOESY spectra were obtained using the interactive program package XEASY.

The structure was determined by NOESY spectra that were collected with a mixing time of 100 ms. The NOE cross-peaks were integrated with the XEASY program and were converted into upper distance bounds using the CALIBA program incorporated into the program package CYANA. For each examined peptide, an ensemble of 200 structures was generated with the simulated annealing of the program CYANA.

## 2.5. REFERENCES

- [1] J. Davies, D. Davies. Origins and evolution of antibiotic resistance. *Microbiol. Mol. Biol. Rev.* 2010, 74, 417–433.
- [2] S.C. Davies, T. Fowler, J. Watson, D.M. Livermore, D. Walker. Annual report of the chief medical officer: infection and the rise of antimicrobial resistance. *Lancet.* 2013, 381, 1606–1609.
- [3] S. Maria-Neto, K.C. de Almeida, M.L. Macedo, O.L. Franco. Understanding bacterial resistance to antimicrobial peptides: from the surface to deep inside. *Biochim. Biophys. Acta.* 2015, 1848, 3078–3088.
- [4] Y. Guo<sup>1</sup>, G. Song, M. Sun, J. Wang, Y. Wang. Prevalence and therapies of antibiotic-resistance in *Staphylococcus aureus*. *Front. Cell. Infect. Mi.* 2020, 10, 107.
- [5] H.F. Chambers, F.R. DeLeo. Waves of resistance: *Staphylococcus aureus* in the antibiotic era. *Nat. Rev. Microbiol.* 2009, 7, 629–641.
- [6] W. Kmiecik, E.M. Szewczyk. Are zoonotic *Staphylococcus pseudintermedius* strains a growing threat for humans?. *Folia Microbiol (Praha).* 2018, 63, 743–747.

- [7] M.G. Papich. Antibiotic treatment of resistant infections in small animals. *Vet. Clin. North Am. Small Anim. Pract.* 2013, 43, 1091–1107.
- [8] J.S. Weese, E. van Duijkeren. Methicillin-resistant *Staphylococcus aureus* and *Staphylococcus pseudintermedius* in veterinary medicine. *Vet. Microbiol.* 2010, 27, 418–429.
- [9] R.J. Fair, Y. Tor. Antibiotics and bacterial resistance in the 21st century. *Perspect. Medicin. Chem.* 2014, 6, 25–64.
- [10] R. Maviglia, R. Nestorini, M. Pennisi. Role of old antibiotics in multidrug resistant bacterial infections. *Curr. Drug. Targets.* 2009, 10, 895–905.
- [11] K. Sen, T. Berglund, M.A. Soares, B. Taheri, Y. Ma, L. Khalil, M. Fridge, J. Lu, R.J. Turner. Antibiotic resistance of *E. coli* isolated from a constructed wetland dominated by a crow roost, with emphasis on ESBL and AmpC containing *E. coli*. *Front. Microbiol.* 2019, 10:1034.
- [12] Y. Sàenz, L. Brinas, E. Domínguez, J. Ruiz, M. Zarazaga, J. Vila, C. Torres. Mechanisms of resistance in multiple-antibiotic-resistant *Escherichia coli* strains of human, animal, and food origins. *Antimicrob. Agents. Chemiother.* 2004, 48, 3996–4001.
- [13] L. Poirel, J.Y. Madec, A. Lupo, A.K. Schink, N. Kieffer, P. Nordmann, S. Schwarz. Antimicrobial resistance in *Escherichia coli*. *Microbiol. Spectr.* 2018, 6.
- [14] M.L. Mangoni, A.C. Rinaldi, A. Di Giulio, G. Mignogna, A. Bozzi, D. Barra, M. Simmaco. Structure-function relationships of temporins, small antimicrobial peptides from amphibian skin. *Eur. J. Biochem.* 2000, 267, 1447–1454.
- [15] A. Carotenuto, S. Malfi, M.R. Saviello, P. Campiglia, I. Gomez-Monterrey, M.L. Mangoni, L.M. Gaddi, E. Novellino, P. Grieco. A different molecular mechanism underlying antimicrobial and hemolytic actions of temporins A and L. *J. Med. Chem.* 2008, 51, 2354–2362.
- [16] E. Azuma, N. Choda, M. Odaki, Y. Yano, K. Matsuzaki. Improvement of therapeutic index by the combination of enhanced peptide cationicity and proline introduction. *ACS Infect. Dis.* 2020, 6, 2271–2278.
- [17] D. I. Fernandez, T.H. Lee, M.A. Sani, M.I. Aguilar, F. Separovic. Proline facilitates membrane insertion of the antimicrobial peptide maculatin 1.1 via surface indentation and subsequent lipid disordering. *Biophys. J.* 2013, 104, 1495–1507.
- [18] J.Y. Suh, Y.T. Lee, C.B. Park, K.H. Lee, S.C. Kim, B.S. Choi. Structural and functional implications of a proline residue in the antimicrobial peptide gaegurin. *Eur. J. Biochem.* 1999, 266, 665–674.
- [19] M.R. Saviello, S. Malfi, P. Campiglia, A. Cavalli, P. Grieco, E. Novellino, A. Carotenuto. New insight into the mechanism of action of the temporin antimicrobial peptides. *Biochemistry.* 2010, 49, 1477–1485.
- [20] M.L. Mangoni, A. Carotenuto, L. Auriemma, M.R. Saviello, P. Campiglia, I. Gomez-Monterrey, S. Malfi, L. Marcellini, D. Barra, E. Novellino, P. Grieco.

Structure-activity relationship, conformational and biological studies of temporin L analogues. *J. Med. Chem.* 2011, 54, 1298–1307.

[21] Y. Chen, M.T. Guarnieri, A.I. Vasil, M.L. Vasil, C.T. Mant, R.S. Hodges. Role of peptide hydrophobicity in the mechanism of action of  $\alpha$ -helical antimicrobial peptides. *Antimicrob. Agents Chemother.* 2007, 51, 1398–1406.

[22] M. Stark, L. Liu, C.M. Deber. Cationic hydrophobic peptides with antimicrobial activity. *Antimicrob. Agents Chemother.* 2002, 46, 3585–3590.

[23] M. Mahlapuu, J. Hakansson, L. Ringstad, C. Bjorn. Antimicrobial peptides: an emerging category of therapeutic agents. *Front. Cell. Infect. Microbiol.* 2016, 6, 194.

[24] F. Merlino, A. Carotenuto, B. Casciaro, F. Martora, M.R. Loffredo, R. Di Grazia, A.M. Yousif, D. Brancaccio, L. Palomba, E. Novellino, M. Galdiero, M.R. Iovene, M.L. Mangoni, P. Grieco. Glycine-replaced derivatives of [Pro3, DLeu9] TL, a temporin L analogue: evaluation of antimicrobial, cytotoxic and hemolytic activities. *Eur. J. Med. Chem.* 2017, 139, 750–761.

[25] E.C. Ledbetter, J.K. Starr. *Malassezia pachydermatis* keratomycosis in a dog. *Med. Mycol. Case Rep.* 2015, 10, 24–26.

[26] P. Grieco, A. Carotenuto, L. Auriemma, A. Limatola, S. Di Maro, F. Merlino, M.L. Mangoni, V. Luca, A. Di Grazia, S. Gatti, P. Campiglia, I. Gomez-Monterrey, E. Novellino, A. Catania. Novel  $\alpha$ -MSH peptide analogues with broad spectrum antimicrobial activity. *PLoS One.* 2013, 8.

[27] P. Grieco, V. Luca, L. Auriemma, A. Carotenuto, M.R. Saviello, P. Campiglia, D. Barra, E. Novellino, M.L. Mangoni. Alanine scanning analysis and structure–function relationships of the frog-skin antimicrobial peptide temporin-1Ta. *J. Pept. Sci.* 2011, 17, 358–365.

[28] A. Micsonai, F. Wien, L. Kernya, Y.H. Lee, Y. Goto, M. Refrégiers, J. Kardos. Accurate secondary structure prediction and fold recognition for circular dichroism spectroscopy. *Proc. Natl. Acad. Sci. U S A.* 2015, 112, 3095–3103.

[29] P. Grieco, A. Carotenuto, L. Auriemma, M.R. Saviello, P. Campiglia, I. Gomez-Monterrey, L. Marcellini, V. Luca, D. Barra, E. Novellino, M.L. Mangoni, *Biochim.* The effect of d-amino acid substitution on the selectivity of temporin L towards target cells: identification of a potent anti-*Candida* peptide. *Biophys. Acta.* 2013, 1828, 652–660.

[30] M. Lindberg, J. Jarvet, U. Langel, A. Gräslund. Secondary Structure and Position of the Cell-Penetrating Peptide Transportan in SDS Micelles As Determined by NMR. *Biochemistry.* 2001, 10, 3141–3149.

[31] Y. Rosenfeld, D. Barra, M. Simmaco, Y. Shai, M.L. Mangoni. A synergism between temporins toward Gram-negative bacteria overcomes resistance imposed by the lipopolysaccharide protective layer. *J. Biol. Chem.* 2006, 281, 28565–28574.

[32] K. Wütrich in *NMR of Proteins and Nucleic Acids*, John Wiley & Sons, Inc, New York, 1986.

# CHAPTER 3

## PROMOTING SELF-ASSEMBLING BY LIPIDIC TAGS

This chapter is published in:

**Bellavita, R.**, Falanga, A., Buommino, E., Merlino, F., Casciaro, B., Cappiello, F., Mangoni, M.L., Novellino, E., Catania, M.R., Paolillo, R., Grieco, P., Galdiero, S. Novel Temporin L antimicrobial peptides: promoting self-assembling by lipidic tags to tackle superbugs. *Journal of Enzyme Inhibition and Medicinal Chemistry*. 35, 1751–1764 (2020).

**CONTRIBUTIONS:** Peptide synthesis; fluorescence assays (Laurdan, Thioflavin T and ANTS/DPX assay); circular dichroism; protease stability assay.

### 3.1. PEPTIDE SELF-ASSEMBLING

Peptide self-assembly is driven by intra- and intermolecular interactions, involving hydrophobic, charged and aromatic residues for the organization in supramolecular structures.<sup>[1]</sup> The formation of highly stable assemblies is mainly driven by non-covalent interactions, although are known as weak interactions (2–250 kJ mol<sup>-1</sup>).<sup>[2]</sup> Biomimetic peptide-based motifs, such as peptide amphiphiles and lipopeptides, are examples of molecules that can readily self-assemble without losing their activity, but interacting effectively with their biological target.<sup>[3]</sup> The self-assembling of amphipathic AMPs depends strongly on their amphiphilicity and their secondary structures. Generally, in water solution, AMPs could self-organize in aggregate with polar residues located on the surface of aggregate, while the apolar residues are localized in the core;<sup>[4]</sup> instead they can self-assemble smoothly in fibrillar amyloid-like nanostructure or helical bundles in membrane environments. This self-assembly might alter the interaction between AMPs and cell membranes and thus their activity could change.<sup>[4]</sup> However, the self-assembly confers some marked features,<sup>[5]</sup> such as cell selectivity towards bacterial membranes and not mammalian cells,<sup>[6]</sup> and high proteolytic stability because self-assembly protects their cleavage sites to proteases, increasing *in vivo* half-life.<sup>[2,5]</sup> Lipopeptides are a class of amphiphilic AMPs showing a strong self-assembly behavior.<sup>[7]</sup> They are composed of a hydrophobic moiety covalently attached, *e.g.* fatty acid or a sterol group, which acts as the driving force of the self-assembling process. Among AMPs, temporins have a strong tendency to aggregate in water; in fact temporin L (TL) has higher propensity to aggregate in water, forming a single aggregate as shown in a MD simulation.<sup>[9]</sup> In addition, an *in silico* study focused on the mechanism of action of TL, have shown that hydrophobic residues, in particular the phenylalanine zipper motif (Phe<sup>1</sup>, Phe<sup>5</sup>, Phe<sup>8</sup>), are involved in the initial peptide binding to the Gram-positive cytoplasmic membrane and in the stabilization of peptide aggregates as tetramers inside the membrane, leading to the formation of large pores and consequential cell death.<sup>[10]</sup>

This phenylalanine zipper motif mediates also the TL self-assembling in monomer, dimer and trimer aggregates in Gram-negative bacterial membrane, but its mechanism does not seem to be membranolytic as for Gram-positive bacteria.<sup>[10]</sup> Unfortunately, TL also kills human erythrocytes at its antimicrobial concentration, and earlier structure-activity relationship studies (SAR) showed that this drawback is correlated to its  $\alpha$ -helical content.<sup>[11–13]</sup> By previous SAR studies on TL, two analogue devoid of toxicity to human erythrocytes, [Pro<sup>3</sup>,DLeu<sup>9</sup>] and [Pro<sup>3</sup>,DLeu<sup>9</sup>,DLys<sup>10</sup>],<sup>[14,15]</sup> were identified, but both compounds did not show an improved antimicrobial activity in comparison to TL. In our study, considering the intrinsic ability of TL to aggregate both in water and in inside the bacterial membrane, we designed a library of lipopeptides by addition of saturated fatty acids with different carbon chain length at N- or C-terminus of [Pro<sup>3</sup>,DLeu<sup>9</sup>] and [Pro<sup>3</sup>,DLeu<sup>9</sup>,DLys<sup>10</sup>], in order to induce the self-assembling state to boost membrane binding and increase their antimicrobial activity, but preserving simultaneously their low cytotoxic activity. The increased hydrophobicity induced by fatty acids may facilitate the incorporation into lipid bilayers<sup>[16–18]</sup> and induce self-organization into micelles in the bacterial membrane.<sup>[19,20]</sup> Altogether these effects determine fluidization of bilayer and deformation of packing of the phospholipid acyl chain, causing typically large channel formation and cell death.<sup>[21]</sup> It is well-known that a too high hydrophobicity may cause cytotoxicity due to a robust binding to eukaryotic cell membranes, hence it is crucial to conserve an accurate hydrophilic/hydrophobic balance, in order that selectivity and specificity of self-assembled AMPs can be finely adjusted.<sup>[20]</sup> Moreover, the addition of long hydrophobic lipid tails confers the peptides self-organization that makes them also less sensitive to enzymatic degradation.<sup>[22]</sup> The designed compounds were characterized by means of antimicrobial assays against ATCC reference strains of *S. aureus*, *K. pneumoniae* and *P. aeruginosa* and cytotoxicity assay. The mechanism of action of the most promising peptides was studied by fluorescence assays such as Laurdan, Thioflavin T and leakage assays.

Their self-assembling in aqueous solution was calculated by critical aggregation concentration (CAC) and their conformational analysis was performed by CD spectroscopy. Additionally, the most active peptide was preliminarily evaluated for its activity against clinically isolated *S. aureus*, *K. pneumoniae* and *P. aeruginosa* strains, and finally, its biostability in human serum was assessed.

## **3.2. RESULTS AND DISCUSSIONS**

### **3.2.1. DESIGN**

In order to induce self-assembling properties to improve membrane binding and broad-spectrum antimicrobial activity, herein, we designed a library of lipopeptides by the addition of fatty acids of variable length at the N- and C-termini of peptides **1A** and **1B**. Valeric, heptanoic, undecanoic and tridecanoic acids were linked at the N-terminus of **1A** and **1B** (Table 1), to obtain, respectively, peptides **2A–5A** and **2B–5B**. After the first screening of biological activity, we designed peptide **C** featured by pentyl chain in para position of the Phe<sup>1</sup> aromatic ring preserving the net positive charge of +4 as the peptide **1B**, in order to investigate the activity towards Gram-negative strains. Besides, we investigated the effects of C-5 and C-7 hydrophobic lipid tails attached to the side chain of the ornithine residue at C-terminus of peptide **1B**, achieving peptides **D** and **E**.



**Table 1.** Lipopeptide sequences of [Pro<sup>3</sup>,DLeu<sup>9</sup>,DLys<sup>10</sup>]TL (**1B**) and its reference peptide [Pro<sup>3</sup>,DLeu<sup>9</sup>] (**1A**).

Peptides	Lipidic tag (- R <sub>1</sub> )	Sequence
<b>1A</b>	-	F V P W F S K F dL G R I L
<b>2A</b>	CH <sub>3</sub> (CH <sub>2</sub> ) <sub>3</sub> CO-	R <sub>1</sub> -F V P W F S K F dL G R I L
<b>3A</b>	CH <sub>3</sub> (CH <sub>2</sub> ) <sub>5</sub> CO-	R <sub>1</sub> -F V P W F S K F dL G R I L
<b>4A</b>	CH <sub>3</sub> (CH <sub>2</sub> ) <sub>9</sub> CO-	R <sub>1</sub> -F V P W F S K F dL G R I L
<b>5A</b>	CH <sub>3</sub> (CH <sub>2</sub> ) <sub>11</sub> CO-	R <sub>1</sub> -F V P W F S K F dL G R I L
<b>1B</b>	-	F V P W F S K F dL dK R I L
<b>2B</b>	CH <sub>3</sub> (CH <sub>2</sub> ) <sub>3</sub> CO-	R <sub>1</sub> -F V P W F S K F dL dK R I L
<b>3B</b>	CH <sub>3</sub> (CH <sub>2</sub> ) <sub>5</sub> CO-	R <sub>1</sub> -F V P W F S K F dL dK R I L
<b>4B</b>	CH <sub>3</sub> (CH <sub>2</sub> ) <sub>9</sub> CO-	R <sub>1</sub> -F V P W F S K F dL dK R I L
<b>5B</b>	CH <sub>3</sub> (CH <sub>2</sub> ) <sub>11</sub> CO-	R <sub>1</sub> -F V P W F S K F dL dK R I L
<b>C</b>	[CH <sub>3</sub> (CH <sub>2</sub> ) <sub>5</sub> CO]-	F[ R <sub>1</sub> ] V P W F S K F dL dK R I L
<b>D</b>	-[NHCO(CH <sub>2</sub> ) <sub>3</sub> CH <sub>3</sub> ]	F V P W F S K F dL dK R I L Orn[ R <sub>1</sub> ]
<b>E</b>	-[NHCO(CH <sub>2</sub> ) <sub>5</sub> CH <sub>3</sub> ]	F V P W F S K F dL dK R I L Orn[ R <sub>1</sub> ]

### 3.2.2. EFFECT OF SELF-ASSEMBLING ON ANTIBACTERIAL ACTIVITY

The antimicrobial activity of lipopeptides (**1A–5A**, **1B–5B** and **C**, **D**, **E**) was initially assessed against the reference bacterial strains of *P. aeruginosa* ATCC 27853, *K. pneumoniae* ATCC BAA-1705 and *S. aureus* ATCC 25923 by evaluating their minimal growth inhibitory concentration (MIC). The MIC values are shown in Table 2. Peptide **1A** was active against all tested microorganisms with a stronger efficacy towards *S. aureus* (MIC of 6.25 μM), compared to 50 μM for both *P. aeruginosa* and *K. pneumoniae*. Peptide **1B** resulted to be active against all tested microorganisms with a stronger efficacy towards *S. aureus* (MIC of 6.25 μM), compared to 12.5 μM for *P. aeruginosa* and *K. pneumoniae*. Peptides **4A**, **5A**, **4B** and **5B** did not show any antimicrobial effect up to 100 μM, probably due to a reduction of positive charge from +3 to +2 in comparison to their parent peptide **1A**. The peptide **3B** featuring by

the heptyl chain showed the best activity on *S. aureus* (MIC of 3.12  $\mu\text{M}$ ), but displayed a weak activity on Gram-negative strains.

Instead, the peptide **2B** characterized by a pentyl chain has lost activity on Gram negative bacteria (50  $\mu\text{M}$ ), while a discrete activity was reported on *S. aureus* (12.5  $\mu\text{M}$ ). This reduction of activity of peptides **2B** and **3B** was probably due to a reduction of positive charge from +4 to +3 in comparison to their parent peptide **1B**.

**Table 2.** *In vitro* antimicrobial activity of compounds **1A-5A**, **1B-5B**, **C**, **D**, **E**

Peptides	MIC values ( $\mu\text{M}$ ) <sup>a</sup>		
	<i>P. aeruginosa</i> ATCC 27853	<i>K. pneumoniae</i> ATCC BAA-1705	<i>S. aureus</i> ATCC 25923
<b>1A</b>	50	50	6.25
<b>2A</b>	>100	>100	12.5
<b>3A</b>	>100	>100	12.5
<b>4A</b>	>100	>100	>100
<b>5A</b>	>100	>100	>100
<b>1B</b>	12.5	12.5	6.25
<b>2B</b>	50	50	12.5
<b>3B</b>	25	50	3.12
<b>4B</b>	>100	>100	>100
<b>5B</b>	>100	>100	>100
<b>C</b>	25	6.25	6.25
<b>D</b>	>100	50	25
<b>E</b>	>100	50	25
<b>Gentamicin</b>	4	4	1
<b>Imipenem</b>	4	>8	0.5
<b>Tobramycin</b>	4	>4	1
<b>Vancomycin</b>	NA	NA	2

In fact, peptide **C** characterized by pentyl chain in *para* position of the Phe<sup>1</sup> aromatic ring and by a net positive charge of +4 as peptide parent **1B**, was able to preserve the same activity (6.25  $\mu\text{M}$ ) of **1B** on *S. aureus* and on *K. pneumoniae*. This means that the net positive charge of +4 plays a crucial role in maintaining a right

hydrophilic/hydrophobic balance to preserve the antimicrobial activity both against Gram-positive and Gram-negative strains. Peptides **D** and **E**, designed to investigate the effects of C5 and C7 hydrophobic lipids at C-terminus, respectively, were not effective against *P. aeruginosa* and have weak activity against *K. pneumoniae* (50  $\mu$ M) and *S. aureus* (25  $\mu$ M).

**Table 3.** In vitro antibacterial activity of peptides 1B and C against multidrug resistant clinical isolates. For the antibiotic, MIC values are expressed as  $\mu$ g/ml; NA, not applicable

MIC values ( $\mu$ M) <sup>a</sup>									
Peptides	<i>Pa1</i>	<i>Pa2</i>	<i>Pa3</i>	<i>KpCR1</i>	<i>KpCR2</i>	<i>KpCR3</i>	<i>Sa1</i>	<i>Sa2</i>	<i>Sa3</i>
<b>1B</b>	12.5	12.5	12.5	12.5	12.5	12.5	12.5	12.5	6.25
<b>C</b>	25	25	25	12.5	12.5	12.5	12.5	12.5	12.5
<b>Gentamicin</b>	>4	>4	>4	1	>8	1	<1	<1	<1
<b>Imipenem</b>	>4	>4	>4	>8	>8	>8	8	>8	>8
<b>Tobramycin</b>	4	4	4	2	2	>4	1	<1	1
<b>Vancomycin</b>	NA	NA	NA	NA	NA	NA	2	1	2

By considering these biological results, the peptides **1B** and **C** were selected as the best and were further assessed against clinical strains of against carbapenem-, fluoroquinolones-, and gentamicin- resistant *P. aeruginosa*, carbapenemase resistant *K. pneumoniae* and methicillin resistant *S. aureus* (MRSA) clinical strains. As reported in Table 3 both peptides **1B** and **C** were able to efficiently inhibit the growth of all the tested clinical strains, with MIC values very close to those reported for reference strains.

### 3.2.3. LONG LIPIDIC TAILS INCREASE THE CYTOTOXICITY

The cytotoxic effect of the active compounds, **1B**, **2B**, **3B**, and **C**, was evaluated at the short-term against mammalian red blood cells after 40 min treatment at different concentrations. As reported in Figure 1A, peptides **1B**, **2B** and **C** showed a weak

hemolytic activity (lower than 20%) at 3.12 and 6.25  $\mu\text{M}$ . Peptide **3B** showed the highest hemolytic potency (over 50%), especially at the highest concentrations used. It is clear that long hydrophobic tails as in peptide **3B** cause non-selective binding to the cell membrane and consequently stronger hemolytic activity. Interestingly, compounds **1B** and **C** had a similar hemolytic profile, with a percentage of lysed cells of about 30% at the highest concentrations tested (12.5 and 25  $\mu\text{M}$ ).

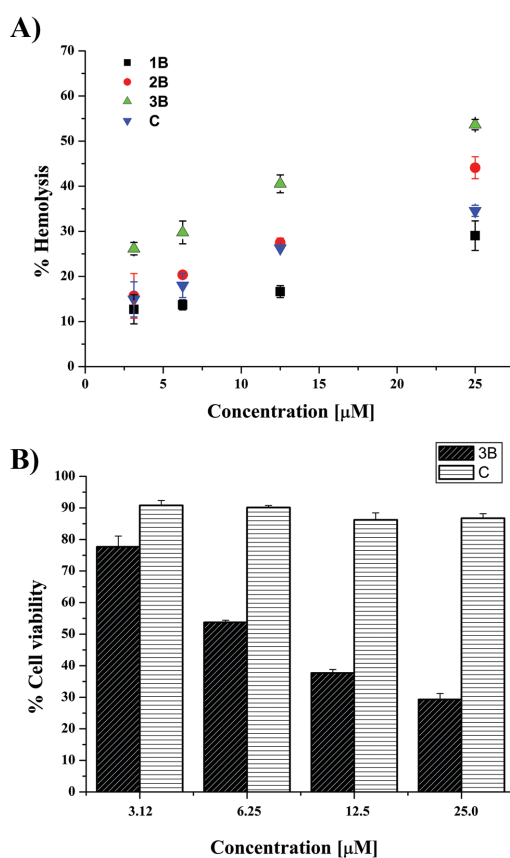


**Figure 1.** Panel A reports the effect of peptides **1B**, **3B**, **2B** and **C** at different concentrations on hemoglobin release from mammalian red blood cells after 40 minutes treatment. All data are expressed as a percentage with respect to the controls (erythrocytes treated with vehicle) and are the mean of three independent experiments  $\pm$  standard error of the mean (SEM). Panel B reports the viability of peptide-treated HaCaT cells evaluated by MTT assay at 24h. All data are expressed as a percentage with respect to the untreated control cells and are the mean of three independent experiments  $\pm$  standard error of the mean (SEM).

For long-term treatment (24 h), the cytotoxic effect of peptides **3B** and **C** was further investigated by the 3-(4,5-dimethylthiazol-2-yl)-2,5-diphenyltetrazolium bromide (MTT) assay on human keratinocytes (HaCaT cells) (Figure 1B). Compound **3B** was confirmed to be harmful causing a strong reduction in cell viability, about 50% already at 6.25  $\mu\text{M}$ . However, note that peptide **C** showed a negligible cytotoxic effect even at the highest tested concentration (25.0  $\mu\text{M}$ ), resulting even less toxic than peptide **1B**, already shown in Merlino et al. (13.29% cytotoxicity for peptide **C** vs 28.22% for peptide **1B**, at 25.0  $\mu\text{M}$ ).<sup>[15]</sup>

### 3.2.4. AGGREGATION STUDIES

*Critical Aggregation Concentration (CAC)*. The tendency to aggregate in water usually determines a significant reduction in antibacterial activity, which may be attributed to a reduced diffusion of the aggregates through the cell wall, due to their large size in comparison to the corresponding monomers as was previously demonstrated for other peptide sequences.<sup>[16,17]</sup> Nile red was used as a fluorescent probe to determine the ability of the designed peptides to self-assemble in the aqueous solution. The poor solubility of Nile red is responsible to its preference for hydrophobic binding sites and thus to a blue shift and hyperchromic effect. The change in the emission signal allows to ascertain the formation of the aggregates as well as to determine the concentration at which the aggregate forms (CAC).

In Figure 2 (panels A–D), the experiments performed at pH 7 (physiological condition) for all peptides are reported. In particular, the wavelength of Nile red maximum fluorescence emission is reported as a function of the concentration of single peptides.

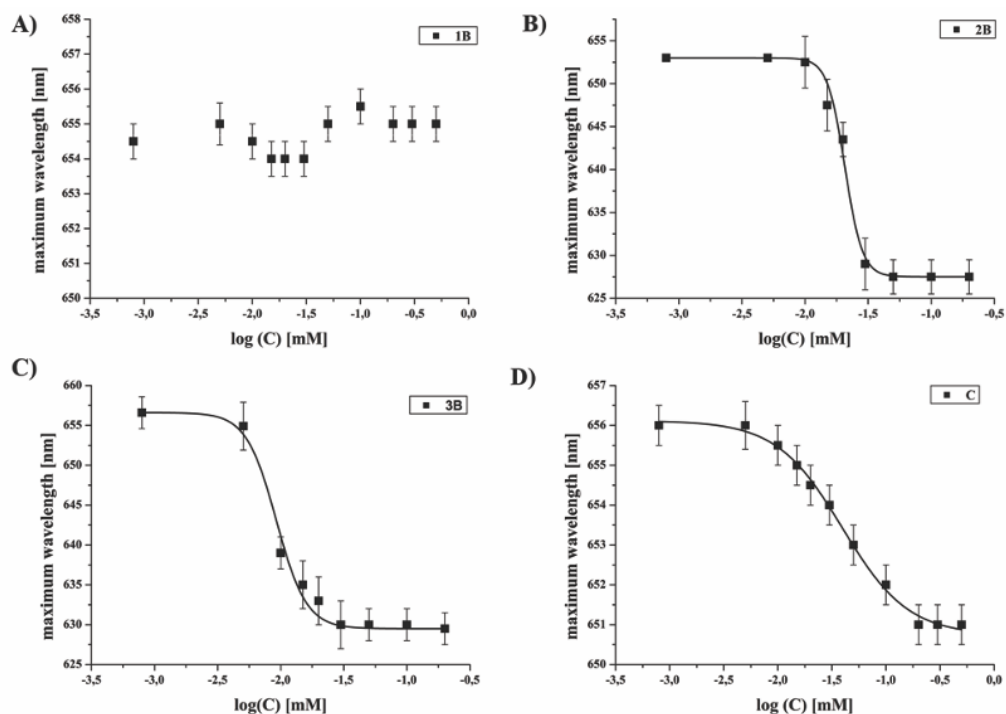


**Figure 2.** Wavelength corresponding to the maximum fluorescence emission of Nile red was plotted as a function of concentration of: **1B** (panel A), **3B** (panel B), **2B** (panel C), **C** (panel D) to determine their CAC. The measurements were repeated in triplicate.

For peptide **1B**, we were unable to observe any blue shift, indicating that this peptide is unable to aggregate under the range of concentrations investigated. On the contrary, the presence of lipids was sufficient to confer the hydrophobic driving force to promote peptide aggregation. The modified sequences containing the valeric (**2B**) and heptanoic (**3B**) acids at the N-terminus showed a significant ability to aggregate with a CAC, respectively, of 20.9 and 9.33  $\mu\text{M}$ . That means that both peptides are active because are not aggregated at tested concentrations. Instead, probably, the peptides characterized by C11 or C13 hydrophobic lipid tails (**4A-5A**, **5A-5B**) are so completely aggregated in aqueous solution that were resulted to be not active at tested concentrations. Regarding the compound **C** has a high CAC (39.5  $\mu\text{M}$ ) indicating that the peptide is still able to aggregate and the presence of the positive charge on the N-terminal amino group reduced its aggregating ability.

### 3.2.5. OLIGOMERIZATION IN BACTERIAL MEMBRANE

The ability of designed peptides to oligomerize inside the membrane was investigated using Thioflavin T (ThT) as fluorescent probe (Figure 3).<sup>[18]</sup> The peptide aggregation was studied using liposomes (LUVs) mimicking the Gram-positive DOPG/CL (58/42) and Gram-negative membranes DOPG/DOPE/CL (63/23/12). We observed a dramatic increase of fluorescence as a function of concentration for all peptides, indicating a progressive phenomenon of aggregation in LUVs. In particular, at low peptide/lipid ratios, peptides **1B** and **C** produced a drastic increase of fluorescence, indicating that both peptides oligomerize significantly in liposomes. In fact, both peptides are able to oligomerize in the membrane monomeric at lower peptide/lipid ratios, but are monomeric in aqueous solution at the same condition of peptide/lipid ratios.

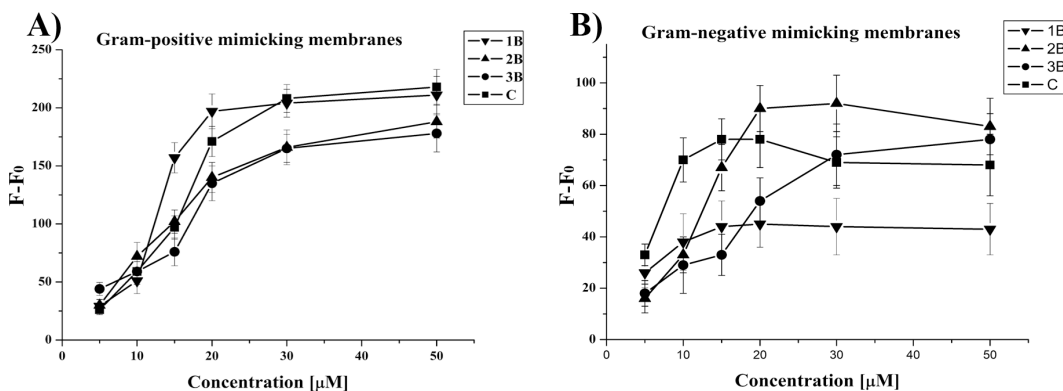


**Figure 3.** ThT aggregation as a function of the peptide/lipid ratio of **1B**, **3B**, **2B**, **C** in liposomes mimicking Gram-positive (A) and Gram-negative (B) membranes. The difference between the value of fluorescence after peptide addition (F) and the initial fluorescence in the absence of peptide (F<sub>0</sub>) was reported on the x-axis.

Peptides **3B** and **2B** showed a lower aggregation at low peptide/lipid ratio while enhanced aggregation was observed at higher ratios as revealed by an increased fluorescence. These results are in agreement with those obtained in the other experiments; in fact, **2B** and **3B** are already aggregated in aqueous solution and thus they aggregate in membranes at a higher concentration as it is likely that they need first to disaggregate in the move between the two environments.

### 3.2.6. LIPOPEPTIDES INFLUENCES MEMBRANE FLUIDITY

The effect of the peptides **1B**, **2B**, **3B**, **C** on the fluidity of the bilayer was analyzed below and above the CAC using the fluorescent probe Laurdan.<sup>[19]</sup> Laurdan changes its emission when inserted in the gel phase membranes (440 nm) or in the liquid phase membranes (490 nm). The Generalized Polarization (GP) parameter, which is commonly used to quantify the change in the lipid fluidity, can be calculated from the emissions at 440 and 490 nm. LUVs mimicking Gram positive and Gram negative bacterial membranes were used. The emission spectra clearly indicated the presence of more fluid membranes at 25 °C; the reproducibility of the spectra after 24 h (data not shown) further supported that LUVs were stable and not leaky in the condition used for the experiments. The GP parameter allowed to quantify the effect of the peptide (Table 4).

**Table. 4.** Membrane fluidity evaluation using the generalized polarization (GP) value calculate as  $GP = (I_{440} - I_{490}) / (I_{440} + I_{490})$ .

<i>Gram negative mimicking membranes</i>			
Compound	Unloaded LUVs	LUVs + 5 µM Cmpd	LUVs + 30 µM Cmpd
<b>1B</b>	-0.07	0.09	0.11
<b>2B</b>	-0.07	-0.05	0.03
<b>3B</b>	-0.07	-0.07	0.07
<b>C</b>	-0.03	0.07	0.15
<i>Gram positive mimicking membranes</i>			
Compound	Unloaded LUVs	LUVs + 5 µM Cmpd	LUVs + 30 µM Cmpd
<b>1B</b>	-0.18	-0.06	0.26
<b>2B</b>	-0.18	-0.14	-0.02
<b>3B</b>	-0.18	-0.18	-0.11
<b>C</b>	-0.23	-0.14	0.18

The GP parameter of the membranes mimicking Gram positive bacteria at 25 °C increased significantly for all tested peptides at 30 µM, indicating a shift towards



more ordered membranes. Interestingly, **1B** and **C** provided the highest increase. The fluidity of the membranes in the presence of peptides at 5  $\mu\text{M}$  was not modified significantly, except for peptide **C**. For the Gram- negative mimicking membranes, we observe the same trend although we obtain fewer modifications.

### **3.2.7. LIPOSOMES LEAKAGE BY LIPOPEPTIDES**

Since the mode of action of AMPs involves mostly a membrane disintegration induced by a formation of large pores, the ANTS/DPX assay was exploited to determine eventual leakage of liposomes mimicking Gram-positive and Gram-negative membranes in presence of the peptides **1B**, **2B**, **3B**, **C**.<sup>[19]</sup> In both tested conditions, we observed a significant leakage with all peptides, supporting pore formation as the primary mechanism of toxicity against bacteria (Figure 4). In particular, we observe higher leakage in presence of Gram-positive membranes; thus, membrane leakage resulted to be strongly dependent on the content of negatively charged lipids. This is in line with the biological data showing a greater activity against *S. aureus* (Figure 4). These data indicate that leakage is involved in the antimicrobial mechanism of these molecules. Leakage events are typical of AMPs; nonetheless, in order to have promising molecules to be developed for further applications it is important to have membrane perturbation not accompanied by hemolysis. The peptides **2B** and **3B** showed the highest leakage ability but also the highest hemolysis. They have lower CACs and are likely already aggregated when they induce the leakage of the membrane. On the contrary, **1B** presents the lowest leakage ability and its percentage of hemolysis is similar to **C**. This latter presents an intermediate ability to produce leakage of both Gram-positive and Gram-negative membranes and low hemolysis up to 25  $\mu\text{M}$ . At this concentration, it is also below the CAC, indicating that it is not already aggregated when in contact with the membranes.

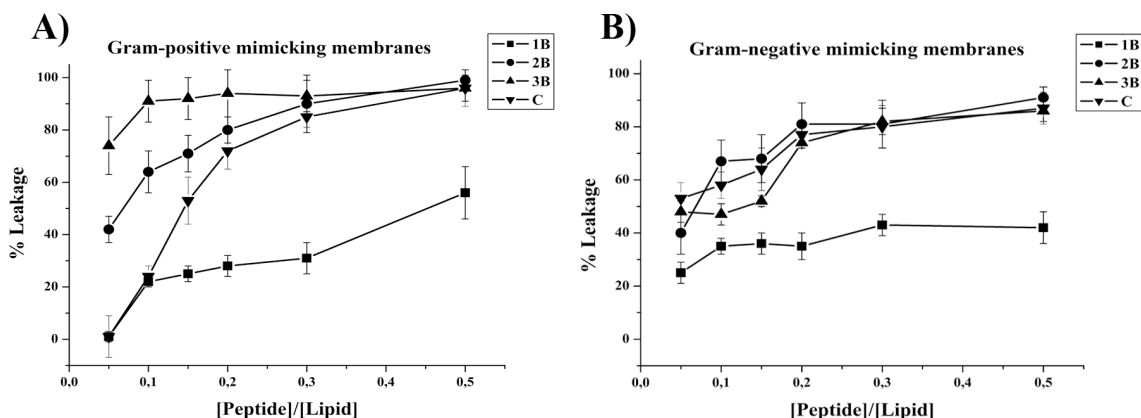


**Figure 4.** Peptide-promoted membrane leakage of compounds **1B**, **3B**, **2B**, **C** in LUVs mimicking Gram-positive (panel A) and Gram-negative (panel B) membranes. Percentage of leakage is reported as a function of the peptide/lipid ratio and each trace represents an average of three independent experiments.

### 3.2.8. HELICAL AGGREGATION IN BACTERIAL MEMBRANE

The molecular conformation of the peptides was investigated by far-UV CD spectroscopy, which is widely exploited for the determination of the secondary structure and for studying the formation of peptide assemblies in solution (Figure 5 panels A, B). In fact, changes in secondary structures compared to monomers often characterize self-assembly processes. We here determined the secondary structure in liposomes mimicking the Gram-positive and Gram-negative membranes at a concentration below the CAC obtained in aqueous solution, in order to better understand if peptides that were not aggregated in water solution could self-aggregate when in membrane environment. The data obtained clearly demonstrate that the peptides were monomeric with a random coil conformation in aqueous solution (data not shown). Moreover, they showed a significant ability to aggregate in membrane mimetic environments with a high tendency to give helical aggregates in both Gram-positive and Gram-negative membranes. In fact, we observe a helical conformation in Gram-positive membranes with two negative bands at about 208 and 222 nm.

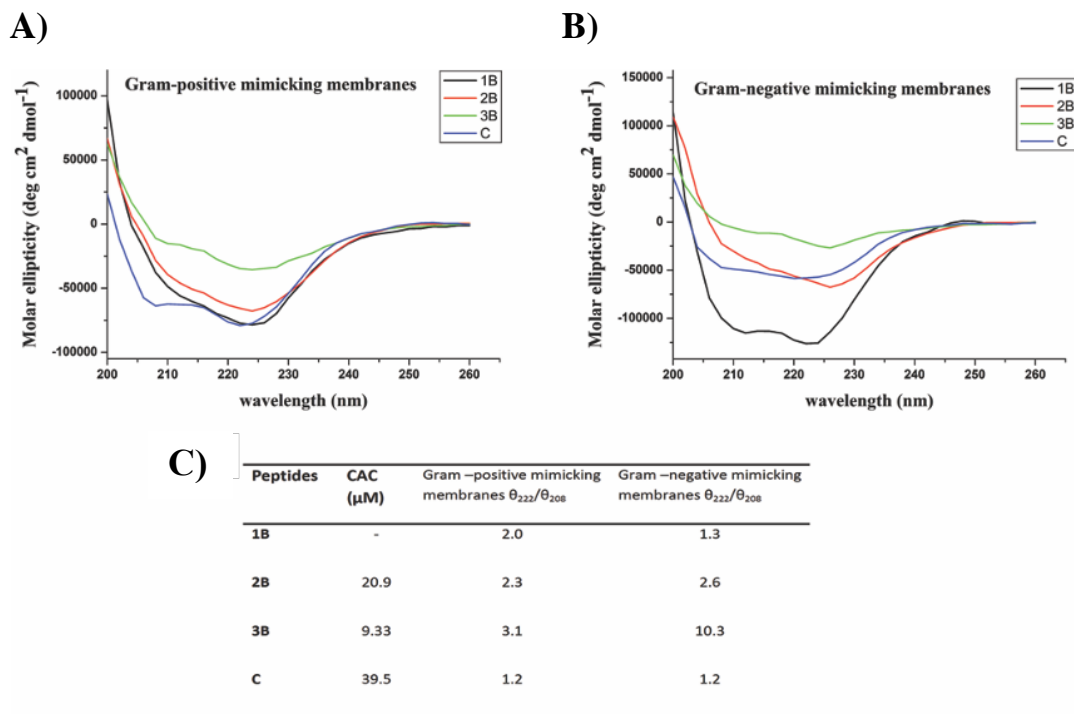


**Figure 5.** Conformational characterization of the four peptides by CD spectroscopy in membranes mimicking Gram-positive (panel A) and Gram-negative (panel B) membranes. Panel C reports the critical aggregation concentration (CAC) calculated by a fluorescence assay with the fluorophore Nile red and the ratio of the ellipticities at 222 and 208 nm, which discriminates between monomeric and oligomeric states of helices for peptides **1B**, **2B**, **3B** and **C**.

The visual analysis of the spectra clearly indicates the presence of aggregates. To establish whether we were observing oligomerization processes which likely occur through self-assembly in the experimental condition used for our assays we determined the ratio of the ellipticities at 222 and 208 nm (Figure 5, panel C), which helps in discriminating between monomeric and oligomeric states of helices.<sup>[20]</sup> In our spectra, the ratio  $\theta_{222}/\theta_{208}$  is always greater than 1.0, indicating a  $\alpha$ -helical conformation in its oligomeric state; for a monomeric state the ratio  $\theta_{222}/\theta_{208}$  would have been lower than 0.8.<sup>[21]</sup> Moreover, we performed experiments after centrifugation of the samples to get rid from solution of eventually precipitated peptides and as expected we did not observe any effect on the spectra. One of the

main features of peptides able to enter the bilayer is the change of conformation from random to helical.<sup>[22]</sup>

### **3.2.9. SELF-ASSEMBLING IMPROVES PROTEOLYTIC STABILITY**

Peptide aggregation or ordered self-assembly might positively effect both on pharmacokinetic and pharmacodynamic proprieties of AMPs; in fact, it might reduce effectively their susceptibility to proteolytic degradation, increasing their half-life.<sup>[23]</sup> In this context, we probed the proteolytic human serum stability upon peptide incubation with 90% fresh human serum at  $37 \pm 1$  °C within 120 min and the percentage of intact peptide was calculated by the peak area of the RP-HPLC performed on a Phenomenex Kinetex column (4.6 mm x 150 mm, 5  $\mu$ m, C18) chromatograms using a linear gradient from 10 to 90% MeCN (0.1% TFA) in water (0.1% TFA) over 20 min (flow rate of 1 mL/min, and absorbance detection at 220 nm). Figure 6 reports the data obtained for peptide **1B** and **C**. As expected, peptide **1B**, our starting sequence is rapidly degraded and cleaved in fragments, notwithstanding the presence of D-amino acids. Chemical modifications in the sequence and formation of the self-assembled structures can significantly modify enzymatic degradation rates. As a matter of fact, we observed that peptide **C** is stable up to 1 h (Figure 6); while we observed partial degradation starting from 80 min even though a significant part of the active peptide is present. Clearly, the further addition of the hydrophobic tail in **C** and the formation of supramolecular assemblies can be used as a viable strategy to reduce protease susceptibilities of AMPs.

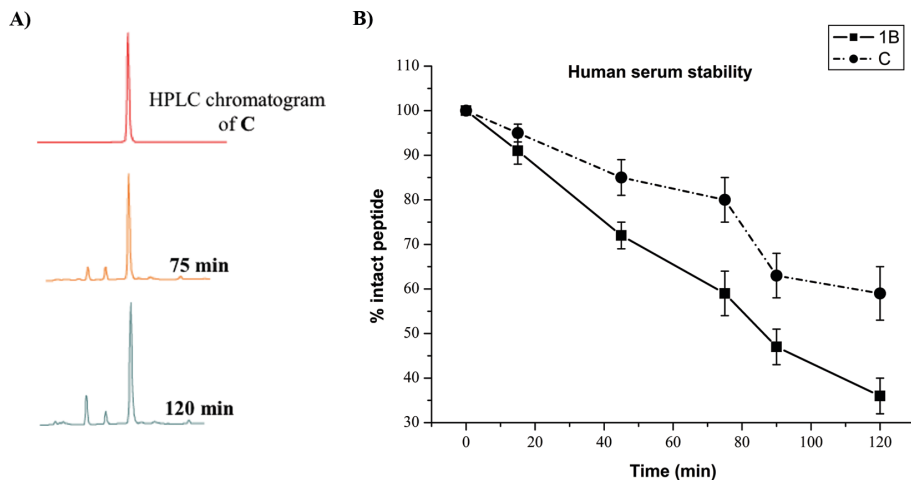


**Figure 6.** (Panel A) RP-HPLC analysis of peptide **C** in 90% human serum at 37 °C at different times (X, 75 and 120 min). The HPLC profile shows the results of one representative experiment out of at least three independent ones. (Panel B) Percentage of intact peptides **1B** and **C** detected at different time intervals after incubation in 90% fresh human serum (200  $\mu$ M) at 37  $\pm$  1 °C.

### 3.3. CONCLUSIONS

The obtained results clearly show that modification in the hydrophobicity and hydrophilicity may influence the self-aggregation in both water solution and in the bilayer. The most active peptide is monomeric in aqueous solution but is able to form molecular helical aggregates in the membrane environment of Gram-positive bacteria (Figure 7). In addition, it is also able to boost the membrane modifications which certainly are correlated to the affinity for the membrane and formation of pores. The hydrophilic/hydrophobic balance also helps to reduce hemolysis and toxicity. Interestingly, the same peptide (**C**) is the only one to show a higher activity against *K. pneumoniae*, conserving a good activity against *S. aureus*. The analysis of the data showed that also from a biophysical point of view the interaction of **C** with membrane mimicking Gram-negative bacteria is stronger compared to the other peptides. Nonetheless, it is interesting to note that the interaction is very different because the aggregation is less evident but the fluidity of the membrane changes more. The conformational change inside the membrane is clearly involving the presence of  $\beta$ -structures compared to helical aggregates in Gram-positive

membranes. We may hypothesize that the mechanism of interaction with Gram-positive and negative bacteria is completely different, involving different secondary structures although both leading to leakage of the membranes. Biological data on clinical strains further support the possible application of TL analogues as novel AMPs able to help in the fight against antibiotic resistant bacteria.

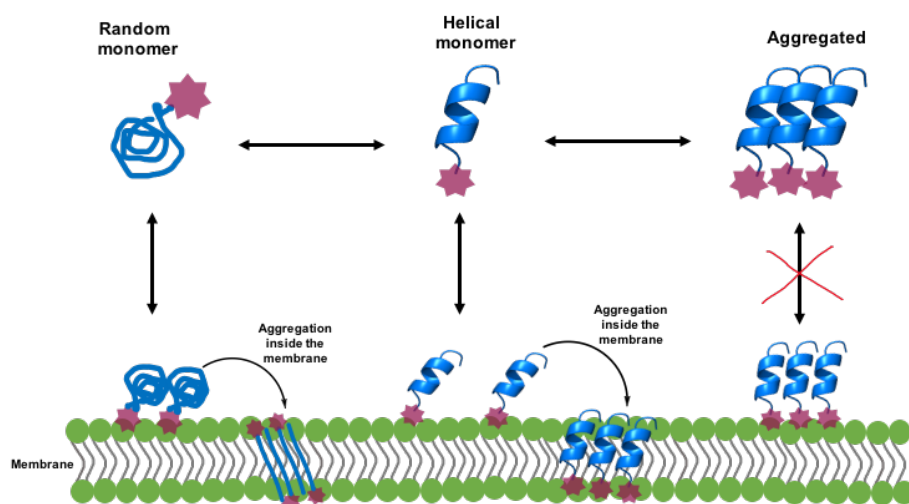


**Figure 7.** Schematic description of the hypothetical mechanisms involved in Temporin L coupled to lipid tags. Monomeric structures are involved in the membrane attachment, while self-aggregated peptides are present inside the membrane and both steps are influenced by the presence of lipid tags.

### 3.4. EXPERIMENTAL SECTION

#### 3.4.1. CHEMISTRY

**Materials.**  $N^\alpha$ -Fmoc-protected amino acids used were purchased from GL Biochem Ltd (Shanghai, China). Fatty acids used, such as tridecanoic, undecanoic, heptanoic, and valeric acids, were purchased by Sigma-Aldrich/Merck. Anhydrous solvents [*N,N*-dimethylformamide (DMF) and dichloromethane (DCM)], Rink amide resin, 1,3-dimethylbarbituric acid, tetrakis(triphenylphosphine)palladium(0) [ $\text{Pd}(\text{PPh}_3)_4$ ], tin(II)chloride [ $\text{SnCl}_2$ ], 2,2,2-trifluoroethanol (TFE) were purchased from Sigma-

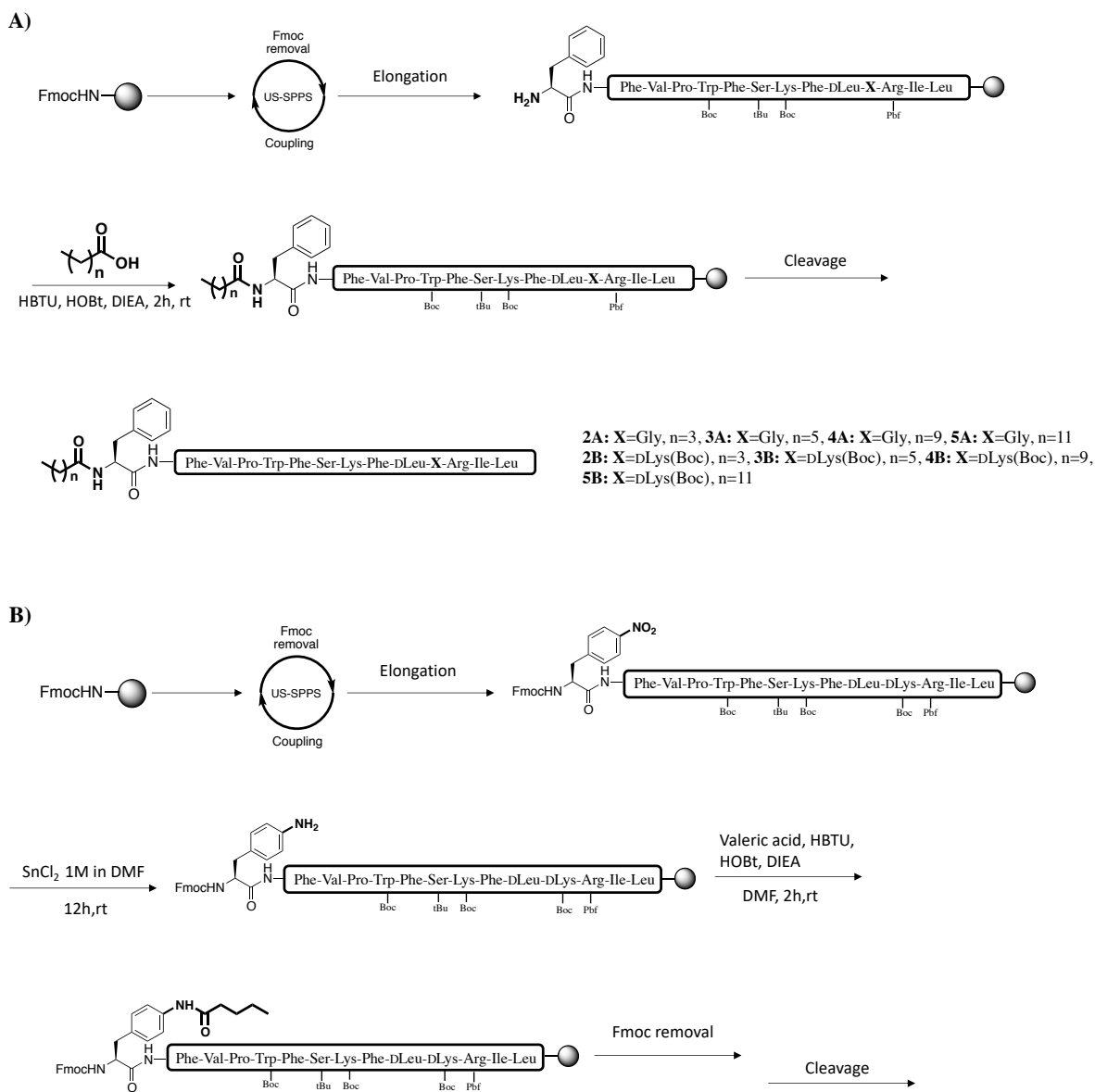
Aldrich/Merck. Fmoc-Orn(Alloc)-OH, *N,N*-diisopropylethylamine (DIEA), piperidine, and trifluoroacetic acid (TFA) were purchased from Iris-Biotech GMBH. Phospholipids: 1,2-dioleoyl-sn-glycero-3-phosphoethanolamine (DOPE), 1,2-dioleoyl-sn-glycero-3-phospho-(1'-rac-glycerol) sodium salt (DOPG), and cardiolipin (CL) sodium salt (Heart, Bovine) were purchased from Avanti Polar Lipids (Birmingham, AL, USA), Phosphate-buffered saline (PBS) tablets were bought by Life Technologies Corporation. 8-aminonaphthalene-1,3,6-trisulfonic acid, disodium salt (ANTS) and *p*-xylene-bis-pyridinium bromide (DPX) were purchased from Molecular Probes. Triton X-100 and the fluorescent probes Nile red, Thioflavin T and 6-dodecanoyl-*N,N*-dimethyl-2-naphthylamine (Laurdan) were purchased by Sigma-Aldrich-Merck. 3-(4,5-dimethylthiazol-2-yl)-2,5-diphenyltetrazolium bromide (MTT) and human serum from human male AB plasma, USA origin, sterile-filtered was obtained by Sigma-Aldrich-Merck.

***Peptide Synthesis by US-SPPS.*** The synthesis of peptides **1A–5A, 1B–5B, C, D, E** was performed by using the ultrasound-assisted solid-phase peptide synthesis (US-SPPS) integrated with the Fmoc/*t*Bu orthogonal protection strategy.<sup>[24]</sup> Each peptide was assembled on a Rink amide resin (0.1 mmol from 0.72 mmol/g as loading substitution) as solid support in order to obtain amidated C-termini. In particular, the resin was first placed into a 10 mL plastic syringe tube equipped with Teflon filter, stopper and stopcock, and swollen in DMF on an automated shaker for 30 min at rt. Then, the Fmoc group of the rink amide linker was removed by treatment with 20% piperidine in DMF solution (0.5 + 1 min) by ultrasonic irradiation. The first coupling was carried out by adding a solution of *N*<sup>α</sup>-Fmoc-amino acid, HBTU, HOBt (3-fold excess), and DIEA (6-fold excess) in DMF to the resin, thus the resulting suspension was irradiated by ultrasound waves for 5 min. After each coupling and Fmoc-deprotection reaction the resin was washed with DMF (3 × 2 mL) and DCM (3 × 2 mL) and Kaiser or Chloranil tests were employed as colorimetric assays to monitor

the progress of the synthesis, used for the detection of solid-phase bound primary and secondary amine, respectively. Subsequent Fmoc-deprotection and coupling steps were performed following the same procedures described above.

The introduction of lipid amidated tails for peptides **2A–5A**, **2B–5B** was accomplished by reacting the released primary amine in *N*-terminal region with 3 equiv of valeric (**2A** and **2B**), heptanoic (**3A** and **3B**), undecanoic (**4A** and **4B**), tridecanoic (**5A** and **5B**), acids, respectively, HBTU/HOBt (3 equiv) as coupling/additive reagents, in presence of DIEA (6 equiv) in DMF/DCM (1:1 v/v), by ultrasonic irradiation for 15 min (Scheme 1A). Upon filtering and washings (3×2 mL of DMF; 3×2 mL of DCM) of the resin, the lipidation was ascertained by Kaiser test. Thus, peptides **2A–5A**, **2B–5B** were released from the resin and simultaneously cleaved by their protecting groups by using a cocktail of TFA/TIS/H<sub>2</sub>O (95:2.5:2.5 v/v/v) at rt for 3 h. Finally, the resins were removed by filtration and crudes were recovered by precipitation with cool anhydrous Et<sub>2</sub>O as amorphous solids. As for the synthesis of peptide **C**, the Fmoc-Phe(4-NO<sub>2</sub>) reagent was used in replacement of Fmoc-Phe residue in order to give the valeric acid amide in *para* position of the aromatic ring of the Phe<sup>1</sup> in *N*-terminal. More specifically, after the elongation of peptide sequence, the resin-bound peptide sequence carrying the Phe(4-NO<sub>2</sub>) was treated with a 1M solution of SnCl<sub>2</sub> in DMF and the resulting suspension was gently shaken at rt for 12 h (Scheme 1B).<sup>[25]</sup> Such reaction was monitored by LC-MS analysis of the residue obtained from the cleavage of an aliquot of resin [5 mg treated with 1 mL of TFA/TIS/H<sub>2</sub>O (95:2.5:2.5, v/v/v)], and by chloranil test, as colorimetric assay used to reveal resin-bound aromatic primary amines. Once the reduction of aromatic nitro group was ascertained, the coupling with valeric acid (3 equiv) was performed by adding HBTU (3 equiv), HOBt (3 equiv), and DIEA (6 equiv) to the resin, and the mixture was therefore stirred on automated shaker at rt for 2 h. The LC-MS analysis and chloranil test were repeated to confirm coupling had achieved >80% conversion.

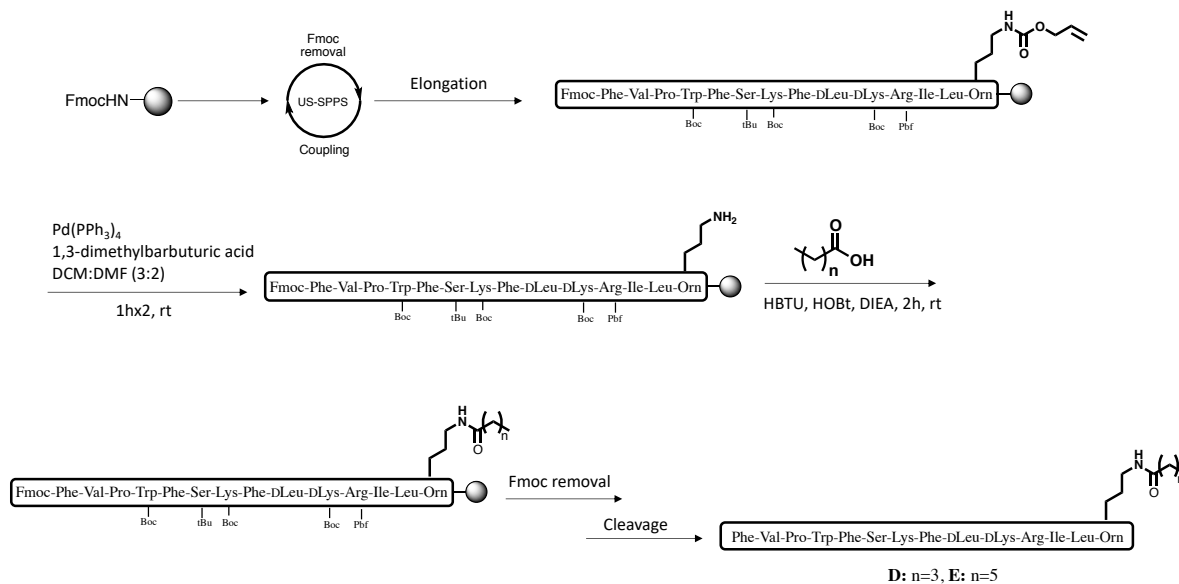




**Scheme 1.** (A) Synthesis of lipopeptides **2A–5A**, **2B–5B**. (B): Synthesis of lipopeptide **C**.

Peptides **D** and **E** were otherwise obtained by the introduction of Orn(Alloc) residue at C-terminal. The ornithine allyl protecting group was removed in orthogonal condition with respect to the Fmoc/*t*Bu.<sup>[26]</sup> Specifically, the resin was treated with a

suspension of Pd(PPh<sub>3</sub>)<sub>4</sub> (0.15 equiv) and 1,3-dimethylbarbituric acid (3 equiv) in DCM/DMF (3:2 v/v) and gently shaken for 1 h under argon (Scheme 2).



**Scheme 2.** Synthesis of lipopeptides **D** and **E**.

The resin was filtered and washed with DMF (3×2 mL) and DCM (3×2 mL), and the Alloc-deprotection procedure was repeated. After the complete removal was ascertained by Kaiser test and LC-MS, the heptanoic (3 equiv) or valeric (3 equiv) acids were coupled to the  $\delta$ -amine group of Orn by following the same coupling procedure by ultrasonic irradiation as described above. The resin was filtered and washed with DMF (3×2 mL) and DCM (3×2 mL) and the lipidation was monitored by Kaiser test. Finally, the N-terminal Fmoc group was removed and the peptides were treated with a cleavage cocktail, consisting of TFA/TIS/H<sub>2</sub>O (95:2.5:2.5 v/v/v), at rt for 3 h, to be released from the resin and cleaved by their protecting groups.

Analytical UHPLC (Shimadzu Nexera Liquid Chromatograph LC-30AD) analyses to assess critical synthetic steps as well as the purity of final compounds **1A–5A**, **1B–5B**, **C**, **D**, **E** were performed on a Phenomenex Kinetex reverse-phase column (C18, 5  $\mu$ m, 100 Å, 150 × 4.6 mm) with a flow rate of 1 mL/min using a gradient of

MeCN (0.1% TFA) in water (0.1% TFA), from 10 to 90% over 20 min, and UV detection at 220 and 254 nm. Purification of peptides **1A–5A**, **1B–5B**, **C**, **D**, **E** was performed by RP-HPLC (Shimadzu Preparative Liquid Chromatograph LC-8A) equipped with a preparative column (Phenomenex Kinetex C18 column, 5  $\mu$ m, 100 Å, 150 x 21.2 mm) using linear gradients of MeCN (0.1% TFA) in water (0.1% TFA), from 10 to 90% over 30 min, with a flow rate of 10 mL/min and UV detection at 220 nm. Final products were obtained by lyophilization of the appropriate fractions after removal of the MeCN by rotary evaporation. All compounds examined for biological activity were purified to >96%, and the correct molecular ions were confirmed by high-resolution mass spectrometry (HRMS) (Table 5).

**Table 5.** HRMS calculated and observed for peptides **2A–5A**, **2B–5B**, **C**, **D**, **E**.

Peptides	R <sub>t</sub> (min)	m/z calcd	m/z found
<b>2A</b>	13.4	1694.0027	[M+H/2] <sup>+</sup> =847.5036
<b>3A</b>	13.9	1722.0340	[M+H/2] <sup>+</sup> =861.5185
<b>4A</b>	15.8	1778.0966	[M+H/2] <sup>+</sup> = 889.551
<b>5A</b>	15.2	1806.1279	[M+H/2] <sup>+</sup> =903.5670
<b>2B</b>	12.7	1765.0762	[M+2H/2] <sup>+</sup> =883.0450
<b>3B</b>	13.1	1793.1075	[M+2H/2] <sup>+</sup> =897.0603
<b>4B</b>	14.9	1849.1701	[M+H/2] <sup>+</sup> =925.0869
<b>5B</b>	14.3	1877.2014	[M+2H/2] <sup>+</sup> =939.1046
<b>C</b>	12.6	1780.0871	[M+H/2] <sup>+</sup> =890.5464
<b>D</b>	12.4	1879.1555	[M+2H/2] <sup>+</sup> =940.0730
<b>E</b>	11.8	1907.1868	[M+2H/2] <sup>+</sup> =954.0976

### 3.4.2. BIOLOGY

**Bacterial strains and culture.** *Staphylococcus aureus* ATCC 25923, *Pseudomonas aeruginosa* ATCC 27853 and *Klebsiella pneumoniae* ATCC BAA-1705 (carbapenemase producer) were obtained from the American Type Culture Collection (Rockville, MD). Clinical strains of *P. aeruginosa* (*Pa1*, *Pa2* and *Pa3*), *K. pneumoniae* (*KpCR1*, *KpCR2* and *KpCR3*), and *S. aureus* (*Sa1*, *Sa2* and *Sa3*) were isolated from bloodstream or pulmonary infections, and belong to a collection of bacterial strains established between 2010 and 2018 at the Department of

Molecular Medicine and Medical Biotechnologies (University Federico II, Naples) for research use. *Pa1*, *Pa2* and *Pa3* resulted resistant to carbapenems, fluoroquinolones, and gentamicin; *KpCR1*, *KpCR2* and *KpCR3* were carbapenem-resistant since KPC carbapenemase producers; *Sa1*, *Sa2* and *Sa3* resulted MRSA strains. The antimicrobial susceptibility testing of all isolates was determined using Vitek II system and results were interpreted according to European Committee on Antimicrobial Susceptibility Testing (EUCAST version 9.0, 2019).

***Antimicrobial susceptibility testing.*** Minimal inhibitory concentrations (MIC) of all the peptides were determined in Mueller–Hinton medium by the broth microdilution assay as described in Chapter 2.<sup>[27]</sup>

***Cytotoxicity assay.*** The hemolytic assay was carried out following the procedures described in Chapter 2. The colorimetric MTT assay was performed to measure cellular metabolic activity in terms of cell viability.<sup>[27,28]</sup> Viable cells are able to reduce, by active mitochondrial dehydrogenases, the yellow salt MTT to purple formazan crystals. Briefly,  $4 \times 10^4$  HaCaT cells, suspended in DMEMg supplemented with 2% FBS, were plated in each well of a 96-well microtiter plate. After overnight incubation, at 37 °C in a 5% CO<sub>2</sub> atmosphere, keratinocytes were treated for 24 h with fresh serum free medium containing the peptides **3B** and **C** at concentrations ranging from  $3.12 \times \mu\text{M}$  to  $25 \mu\text{M}$ . Afterward, the culture medium was replaced with Hank's buffer supplemented with 0.5 mg/mL MTT and the plate was incubated at 37°C and 5% CO<sub>2</sub> for 4 h. At the end, acidified isopropanol was employed to dissolve the formazan crystals. Cell viability was calculated, with respect to cells not treated with peptide, by absorbance measurements at 570nm using a microplate reader (Infinite M200; Tecan, Salzburg, Austria).<sup>[28]</sup> Colour solution changes are directly related to the number of viable, metabolically active cells.

**Plasma stability assay.** Human serum from human male AB plasma was acquired by Sigma-Aldrich-Merck. Water and MeCN were obtained from commercial suppliers and used without further purification. Analytical RP-UHPLC was performed on a Shimadzu Nexera equipped with a Phenomenex Kinetex column (C<sub>18</sub>, 4.6 mm x 150 mm, 5 mm) and H<sub>2</sub>O (0.1% TFA) and MeCN (0.1% TFA) as eluents. Serum stability was evaluated by modification of elsewhere described methods.<sup>[15,29]</sup> In particular, the human serum was allocated into a 1.5 mL eppendorf tube and temperature equilibrated at 37 ± 1 °C for 15 min. Peptides **1B, C** were dissolved in sterile water to prepare a stock solution of 2 mM and then mixed with the human serum to make a final concentration of 0.2 mM (90% serum). The resulting reaction solution was incubated at 37 ± 1 °C. Aliquots of the reaction solutions were taken at known time intervals (0 min, 15 min, 45 min, 75 min, 90 min, 120 min), subjected to serum proteins precipitation by addition of MeCN (double volume respect to the aliquot). The cloudy reaction sample was cooled (4 °C) for 15 min and then spun at 13000 rpm for 10 min to pellet the precipitated serum proteins. The supernatant was then analyzed by RP-UHPLC by using a linear elution gradient from 10 to 90% MeCN (0.1% TFA) in water (0.1% TFA) over 20 min. A flow rate of 1 mL/min was used, absorbance was detected at 220 nm, and the analysis was performed at room temperature.

### **3.4.3. CRITICAL AGGREGATION CONCENTRATION DETERMINATION**

The solvatochromic fluorescent probe Nile red is widely used to determine the critical aggregation concentration (CAC) of self-assembling peptides. Nile red shows a blue shift with decreasing solvent polarity. Since Nile red is poorly soluble in water, there is a large preference to partition aggregates, which offer hydrophobic binding sites. Initially, 1 mM methanolic Nile red was prepared. Then, the methanolic Nile red was diluted with water in order to have a final concentration of 500 nM (solution A). The peptides **1B, 2B, 3B, C**, were prepared as follows:<sup>[30]</sup> peptide stock solutions

(0.4 mM) were prepared by dissolving the single peptides in water (**1B**, **C**) or tetrahydrofuran (**3B**, **2B**) and sonicating for 15 min. Different aliquots were taken to prepare solutions of each peptide at different concentrations (1, 5, 10, 15, 20, 30, 50, 100 and 200  $\mu\text{M}$ ). Then, all solutions were diluted with water, sonicated for 15 min and freeze-dried. Finally, the peptide powders were dissolved with the right volume of solution A and allowed to stand in the dark place for 1 h before measurement. Emission spectra for each solution were measured by a Cary Eclipse Varian spectrometer. Spectra were taken between 570 and 700 nm at a slit width of 5 nm, using an excitation wavelength of 550 nm and a 10 nm slit width. The measurements were performed in triplicate. The data were analyzed by plotting the maximum emission fluorescence corresponding wavelength ( $y$ ) as a function of peptide concentration ( $x$ ) and fitting with the sigmoidal Boltzmann equation:

$$y = \frac{A_1 + A_2}{1 + e^{\left(x - \frac{x_0}{\Delta x}\right)}} + A_2$$

where the variables  $A_1$  and  $A_2$  correspond to the upper and lower limits of the sigmoid,  $x_0$  is the inflection point of the sigmoid and  $\Delta x$  is the parameter, which characterizes the steepness of the function. The sigmoidal plot allows calculating the CAC value at  $x_0$ .

#### **3.4.4. LIPOSOME PREPARATION**

Large unilamellar vesicles (LUVs) and small unilamellar vesicles (SUVs) consisting of DOPG/CL (58/42 ratio in moles) and DOPG/DOPE/CL (63/23/12 ratio in moles), which mimic the Gram-positive membrane and Gram-negative membrane, respectively. LUVs were prepared using the extrusion method.<sup>[31]</sup> First, lipid films were prepared by dissolving an appropriate amount of lipids in chloroform and fluorescent probes was added when necessary, then dried under a nitrogen gas stream

and freeze-dried overnight. In all experiments, we used a final lipid concentration of 0.1 mM. For fluorescence experiments, buffer was added to dry lipid films and vortexed for 1 h; then the lipid suspension was freeze-thawed 6 times and extruded 10 times through polycarbonate membranes with 0.1  $\mu\text{m}$  diameter pores to obtain LUVs. For circular dichroism measurements, peptide samples in SUVs were prepared.<sup>[32]</sup> Lipids were dissolved in chloroform and added to an equal volume of peptide solution dissolved in TFE containing appropriate peptide concentration. The samples were vortexed and lyophilized overnight. The dry samples were rehydrated with phosphate buffer 5mM, pH 7.4 for 1 h and sonicated for 30 min.

### **3.4.5. ANTS/DPX LEAKAGE ASSAY**

The ANTS/DPX leakage assay was used to measure the ability of peptide to permeabilize and induce leakage of encapsulated dyes. After lipid films were prepared as previously described, ANTS (12.5 mM) and DPX (45 mM) were dissolved in 2mL water, were added to lipid films and then lyophilized overnight. The lipid films with encapsulated ANTS and DPX were hydrated with PBS 1X buffer, vortexed for 1h and then treated to obtain LUVs. The not encapsulated ANTS and DPX were removed by gel filtration using a Sephadex G-50 column (1.5 cm x 10 cm) at room temperature.<sup>[33]</sup> To start up the leakage experiment, a 2 mM peptide stock solution was prepared and LUVs were titrated with the peptide. Samples were excited at 385 nm (slit width, 5 nm) and fluorescence emission was recorded at 512 nm (slit width, 5 nm). After the addition of peptide, we evaluated leakage of encapsulated ANTS through a change in fluorescence spectra of ANTS and DPX. In particular, leakage is associated to an increase in ANTS fluorescence at 512 nm. Complete release of ANTS was obtained by using 0.1% Triton X, which caused total destruction of liposomes. The percentage of leakage was calculated as % leakage =  $(F_i - F_0) / (F_t - F_0)$ , where  $F_0$  represents the fluorescence of intact LUVs before the

addition of peptide, and  $F_i$  and  $F_t$  denote the intensities of the fluorescence achieved after peptide and Triton-X treatment, respectively.

### 3.4.6. LAURDAN ASSAY

Membrane fluidity was determined using LUVs containing the fluorescent probe Laurdan.<sup>[19]</sup> Laurdan was encapsulated into lipid films (0.1 mM) at a concentration of 0.001 mM. After lipid films with Laurdan were lyophilized, hydrated with PBS 1X buffer, pH= 7.4, and vortexed for 1h, they were freeze-thawed 6 times and extruded 10 times through polycarbonate membranes with 0.1  $\mu\text{m}$  diameter pores, obtaining LUVs. The variation of fluidity membrane in presence of peptide was evaluated at 5 and 30  $\mu\text{M}$ , under and above the CAC. The peptide, dissolved in water (2 mM peptide stock solution), was added to LUVs at specific P/L molar ratio and after 10 min the fluorescence spectra were recorded using a 1 cm path length quartz cell, thermostated at 25 °C. Spectra were corrected for the baseline signal. Laurdan emission spectra were recorded from 400 to 550 nm with  $\lambda_{\text{ex}}$  365 nm in the absence or presence of peptide. Laurdan emission can shift from 440 nm, in the ordered phase, to 490 nm in the disordered phase. The Generalized Polarization (GP) is a parameter commonly used to quantify the change in the lipid fluidity. It was calculated as  $\text{GP} = (I_{440} - I_{490}) / (I_{440} + I_{490})$ , where  $I_{440}$  and  $I_{490}$  are the fluorescence intensities at the maximum emission wavelength in the ordered ( $\lambda_{\text{em}}$  440 nm) and disordered ( $\lambda_{\text{em}}$  490 nm) phases.<sup>[19]</sup>

### 3.4.7. PEPTIDE AGGREGATION

Peptide aggregation in bacterial membrane was assayed using fluorescent probe Thioflavin T (ThT). ThT associates rapidly with aggregated peptides giving rise to a new excitation maximum at 450 nm and an enhanced emission at 482 nm.<sup>[33]</sup> Lipid films were hydrated with 100 mM NaCl, 10 mM Tris-HCl, 25  $\mu\text{M}$  Tht buffer, pH= 7.4 and then treated as described above to obtain LUVs. Each peptide was dissolved



in sterile water to prepare a 2 mM peptide stock solution and LUVs were titrated with a peptide concentration of 5, 10, 15, 20, 30, 50  $\mu\text{M}$ . Fluorescence was measured before and after the addition of peptide into the cuvette using a Varian Cary Eclipse fluorescence spectrometer at 25 °C. Samples were excited at 450 nm (slit width, 10 nm) and fluorescence emission was recorded at 482 nm (slit width, 5 nm). Aggregation was quantified according to the equation,  $\%A = (F_f - F_0)/(F_{\text{max}} - F_0) \times 100$ , where  $F_f$  is the value of fluorescence after peptide addition,  $F_0$  the initial fluorescence in the absence of peptide and  $F_{\text{max}}$  is the fluorescence maximum obtained immediately after peptide addition.

### 3.4.8. CD SPECTROSCOPY

CD spectra were recorded at room temperature on a Jasco J-715 spectropolarimeter in a 1 cm quartz cell under a constant flow of nitrogen gas. The spectra are an average of 3 consecutive scans from 260 to 190 nm, recorded with a band width of 3 nm, a time constant of 16 s, and a scan rate of 10 nm/min. Spectra were recorded and corrected for the blank. A solution of 8  $\mu\text{M}$  of peptide with SUVs consisting of DOPG/CL (58/42 ratio in moles) was prepared, as reported above, and then hydrated with phosphate buffer 5 mM.<sup>[20]</sup> Instead, a solution of 8  $\mu\text{M}$  of peptide with SUVs consisting of DOPG/DOPE/CL (63/23/12 ratio in moles) was prepared and hydrated with phosphate buffer 5 mM. Each spectrum was converted the signal to mean molar ellipticity.

### 3.5. REFERENCES

- [1] A.W. Simonson, M.R. Aronson, S.H. Medina. Supramolecular peptide assemblies as antimicrobial scaffolds. *Molecules*. 2020, 25:2751.
- [2] L. Lombardi, A. Falanga, V. Del Genio, S. Galdiero. New hope: self-assembling peptides with antimicrobial activity. *Pharmaceutics*. 2019, 4:166.
- [3] A. Levin, T.A. Hakala, L. Schnaider, G.J.L. Bernardes, E. Gazit, T.P.J. Knowles. Biomimetic peptide self-assembly for functional materials. *Nat. Rev.Chem.* 2020, 4, 615–634.

- [4] S.M. Häffner, M. Malmsten. Influence of self-assembly on the performance of antimicrobial peptides. *Curr. Opin. Colloid Interface Sci.* 2018, 38, 56–79.
- [5] F. Sun, X.R. Zhou, S.Z. Luo, L. Chen. Role of peptide self-assembly in antimicrobial peptides. *J. Pept. Sci.* 2015, 21, 530–539.
- [6] R.N. Mitra, A. Shome, P. Paul, P.K. Das. Antimicrobial activity, biocompatibility and hydrogelation ability of dipeptide-based amphiphiles. *Org. Biomol. Chem.* 2009, 7, 94–102.
- [7] A. Makovitzki, D. Avrahami, Y. Shai. Ultrashort antibacterial and antifungal lipopeptides. *Proc. Natl. Acad. Sci. U.S.A.* 2006, 103, 15997–6002.
- [8] Y. Hu, M.N. Amin, S. Padhee, R.E. Wang, Q. Qiao, G. Bai, Y. Li, A. Mathew, C. Cao, J. Cai. Lipidated peptidomimetics with improved antimicrobial activity. *ACS Med. Chem. Lett.* 2012, 3, 683–686.
- [9] A. Farrotti, P. Conflitti, S. Srivastava, J. Kanti Ghosh, A. Palleschi, L. Stella, G. Bocchini. Molecular dynamics simulations of the host defense peptide temporin L and its Q3K derivative: an atomic level view from aggregation in water to bilayer perturbation. *Molecules.* 2017, 22: 1235.
- [10] G. Manzo, P.M. Ferguson, C.K. Hind, M. Clifford, V.B. Gustilo, H. Ali, S.S. Bansal, T.T. Bui, A.F. Drake, R.A. Atkinson, J.M. Sutton, C.D. Lorenz, D.A. Phoenix, A.J. Mason. Temporin L and aurein 2.5 have identical conformations but subtly distinct membrane and antibacterial activities. *Sci Rep.* 2019, 9: 10934.
- [11] Mangoni ML, Carotenuto A, Auriemma L, M.R. Saviello, P. Campiglia, I. Gomez-Monterrey, S. Malfi, L. Marcellini, D. Barra, E. Novellino, P. Grieco. Structure–activity relationship, conformational and biological studies of Temporin L analogues. *J. Med. Chem.* 2011, 54, 1298–1307.
- [12] Saviello MR, Malfi S, Campiglia P, M.R. Saviello, S. Malfi, P. Campiglia, A. Cavalli, P. Grieco, E. Novellino, A. Carotenuto. New insight into the mechanism of action of the temporin antimicrobial peptides. *Biochemistry.* 2010, 49, 1477–1485.
- [13] A. Carotenuto, S. Malfi, M.R. Saviello, P. Campiglia, I. Gomez-Monterrey, M.L. Mangoni, L. M. Gaddi, E. Novellino, P. Grieco. A different molecular mechanism underlying antimicrobial and hemolytic actions of temporins A and L. *J. Med. Chem.* 2008, 51, 2354–2362.
- [14] P. Grieco, A. Carotenuto, L. Auriemma, M.R. Saviello, P. Campiglia, I. Gomez-Monterrey, L. Marcellini, V. Luca, D. Barra, E. Novellino, M.L. Mangoni. The effect of d-amino acid substitution on the selectivity of temporin L towards target cells: identification of a potent anti-Candida peptide. *Biochim Biophys Acta.* 2013, 1828, 652–660.
- [15] Merlino F, Carotenuto A, Casciaro B, F. Martora, M.R. Loffredo, A. Di Grazia, A.M. Yousif, D. Brancaccio, L. Palomba, E. Novellino, M. Galdiero, M.R. Iovene, M.L. Mangoni, P. Grieco. Glycine-replaced derivatives of [Pro<sup>3</sup>,DLeu<sup>9</sup>]TL, a temporin L analogue: evaluation of antimicrobial, cytotoxic and hemolytic activities. *Eur. J. Med. Chem.* 2017, 139, 750–761.

- [16] S.Y. Lau, A.K. Taneja, R.S Hodges. Synthesis of a model protein of defined secondary and quaternary structure. Effect of chain length on the stabilization and formation of two-stranded alpha-helical coiled-coils. *J. Biol. Chem.* 1984, 259, 13253–13261.
- [17] A. Makovitzki, J. Baram, Y. Shai. Antimicrobial lipopolypeptides composed of palmitoyl Di- and tricationic peptides: *in vitro* and *in vivo* activities, self-assembly to nanostructures, and a plausible mode of action. *Biochemistry.* 2008, 47, 10630–10636.
- [18] A. Falanga, R. Tarallo, G. Vitiello, M. Vitiello, E. Perillo, M. Cantisani, G. D’Errico, M. Galdiero, S. Galdiero. Biophysical characterization and membrane interaction of the two fusion loops of glycoprotein B from herpes simplex type I virus. *PLoS One.* 2012, 7:e32186.
- [19] M. Amaro, F. Reina, M. Hof, C. Eggeling, E. Sezgin. Laurdan and Di-4-ANEPPDHQ probe different properties of the membrane. *J. Phys. D. Appl. Phys.* 2017, 50, 134004–134004.
- [20] S.Y. Lau, A.K. Taneja, R.S Hodges. Synthesis of a model protein of defined secondary and quaternary structure. Effect of chain length on the stabilization and formation of two-stranded alpha-helical coiled-coils. *J. Biol. Chem.* 1984, 259, 13253–13261.
- [21] A. Hollmann, M. Martínez, M.E. Noguera, M.T. Augusto, A. Disalvo, N. C. Santos, L. Semorile, P.C. Maffía. Role of amphipathicity and hydrophobicity in the balance between hemolysis and peptide–membrane interactions of three related antimicrobial peptides. *Colloids Surf. B. Biointerfaces.* 2016, 141, 528–536.
- [22] J.M.A Blair, M.A Webber, A.J. Baylay, D.O. Ogbolu, L.J.V. Piddock. Molecular mechanisms of antibiotic resistance. *Nat. Rev. Microbiol.* 2015, 13, 42–51.
- [23] E. Grimsey, D.W.P. Collis, R. Mikut, K. Hilpert. The effect of lipidation and glycosylation on short cationic antimicrobial peptides. *Biochim. Biophys. Acta Biomembr.* 2020, 1862:183195.
- [24] F. Merlino, S. Tomassi, A.M. Yousif, A. Messere, L. Marinelli, P. Grieco, E. Novellino, S. Cosconati, S. Di Maro. Boosting Fmoc solid phase peptide synthesis by ultrasonication. *Org. Lett.* 2019, 21, 6378–6382.
- [26] R.A. Scheuerman, D. Tumelty. The reduction of aromatic nitro groups on solid supports using sodium hydrosulfite ( $\text{Na}_2\text{S}_2\text{O}_4$ ). *Tetrahedron Lett.* 2000, 41, 6531–6535.
- [26] F. Merlino, Y. Zhou, M. Cai, A. Carotenuto, A.M. Yousif, D. Brancaccio, S. Di Maro, S. Zappavigna, A. Limatola, E. Novellino, P. Grieco, V.J. Hruby. Development of macrocyclic peptidomimetics containing constrained  $\alpha,\alpha$ -dialkylated amino acids with potent and selective activity at human melanocortin receptors. *J. Med. Chem.* 2018, 61, 4263–4269.
- [27] A. Di Grazia, F. Cappiello, A. Imanishi, A. Mastrofrancesco, M. Picardo, R. Paus, M.L. Mangoni. The frog skin derived antimicrobial peptide esculentin-1a(1-

- 21)NH2 promotes the migration of human HaCaT keratinocytes in an EGF receptor-dependent manner: a novel promoter of human skin wound healing?. *PLoS One*. 2015, 10:e0128663.
- [28] E. Buommino, A. Carotenuto, I. Antignano, R. Bellavita, B. Casciaro, M.R. Loffredo, F. Merlino, E. Novellino, M.L. Mangoni, F.P. Nocera, D. Brancaccio, P. Punzi, D. Roversi, R. Ingenito, E. Bianchi, P. Grieco. The outcomes of decorated prolines in the discovery of antimicrobial peptides from Temporin-L. *Chem. Med. Chem.* 2019, 14, 1283–1290.
- [29] M.E. Mercurio, S. Tomassi, M. Gaglione, R. Russo, A. Chambery, S. Lama, P. Stiuso, S. Cosconati, E. Novellino, S. Di Maro, A. Messere. Switchable protecting strategy for solid phase synthesis of DNA and RNA interacting nucleopeptides. *J. Org. Chem.* 2016, 81, 11612–11625.
- [30] L. Lombardi, Y. Shi, A. Falanga, E. Galdiero, E. de Alteriis, G. Franci, I. Chourpa, H.S. Azeyedo, S. Galdiero. Enhancing the potency of antimicrobial peptides through molecular engineering and self-assembly. *Biomacromolecules*. 2019, 20, 1362–1374.
- [31] M.J. Hope, M.B. Bally, G. Webb, P.R. Cullis. Production of large unilamellar vesicles by a rapid extrusion procedure. Characterization of size distribution, trapped volume and ability to maintain a membrane potential. *Biochim. Biophys. Acta*. 1985, 812, 55–65.
- [32] R.A. Parente, S. Nir, F.C. Jr. Szoka. Mechanism of leakage of phospholipid vesicle contents induced by the peptide GALA. *Biochemistry*. 1990, 29, 8720–8728.
- [33] A. Falanga, R. Tarallo, G. Vitiello, M. Vitiello, E. Perillo, M. Cantisani, G. D’Errico, M. Galdiero, S. Galdiero. Biophysical characterization and membrane interaction of the two fusion loops of glycoprotein B from herpes simplex type I virus. *PLoS One*. 2012, 7:e32186.

# CHAPTER 4

## TEMPORIN L ANALOGUES WITH DUAL ACTIVITY IN POLYMICROBIAL INFECTIONS

This chapter is published in:

**1. Bellavita, R.**, Raucci, F., Merlino, F., Piccolo, M., Ferraro, M.G., Irace, C., Santamaria, R., Iqbal, A.J., Novellino, E., Grieco, P., Mascolo, N., Maione, F. Temporin L-derived peptide as a regulator of the acute inflammatory response in zymosan-induced peritonitis. *Biomedicine and Pharmacotherapy*. 123, 109788 (2020).

**2. Bellavita, R.**, Vollaro, A., Catania, M.R., Merlino, F., De Martino, L., Nocera, F.P., Della Greca, M., Lembo, F., Grieco, P., Buommino, E. Novel antimicrobial peptide from Temporin L in the treatment of *Staphylococcus pseudintermedius* and *Malassezia pachydermatis* in polymicrobial inter-kingdom infection. *Antibiotics*. 9, 530 (2020).

### 3. PATENT PENDING

**Inventors:** Mascolo Nicola, Maione Francesco, Carotenuto Alfonso, Novellino Ettore, Merlino Francesco, **Bellavita Rosa**, Buommino Elisabetta, Grieco Paolo. **Title:** Temporin L analogues with anti-inflammatory and antimicrobial activity. **Application:** P021300IT-01/lm. **Date:** 19/06/2019.

**CONTRIBUTIONS:** Peptide synthesis.

## 4.1. POLYMICROBIAL INFECTIONS

Polymicrobial diseases are acute and chronic diseases caused by interactions between pathogens, including bacteria, viruses, fungi and parasites.<sup>[1]</sup> These physical interactions depend on several factors, such as range of environmental, pathogen and host factors. In polymicrobial infections, one microorganism could generate a niche, which favours the infection and colonisation of other pathogens and consequently the genesis of infection.<sup>[2]</sup> A polymicrobial infection associated to a bacterial-fungal interaction could be triggered by a reduction of fungal viability due to a transfer of bacterial secretions with a fungicide activity in the local environment, or by a transmission of toxins directly into fungal cell.<sup>[2]</sup> The interaction between *Staphylococcus pseudintermedius* and *Malassezia pachydermatis* are an example of bacteria-fungal interaction implicated in zoonotic diseases (e.g. otitis externa) easily transmitted from dogs to their owners.<sup>[3,4]</sup> *S. pseudintermedius* is not a common zoonotic pathogen in humans, but an opportunistic pathogen typically involved in skin and ear infections in dogs and cats.<sup>[5]</sup> The *M. pachydermatis* yeast inhabits prevalently the skin mycobiota of dogs and normally behave as “good citizen” in dogs, but can become a highly troublesome pathogen provoking ceruminous otitis externa and a “seborrhoeic” dermatitis.<sup>[6]</sup>

Today, over 60% of western families possess a pet, in most of cases a dog. A pet has a precious role in human life, because can increase the physical activity of owners reducing cardiovascular events and can help to owners suffering depression and mental stress.<sup>[7]</sup> Despite there are numerous benefits on psychosocial and physical health of their owners, many zoonotic pathogens are transmitted by dogs. Immunocompromised individuals and children are main individuals at risk in getting zoonoses infections. Generally, otitis caused by *Malassezia* is normally treated with topical or systemic azole therapy, often with miconazole—chlorhexidine shampoos or oral itraconazole or ketoconazole.<sup>[8]</sup> Recently, the emergence of azole resistance and the high toxicity of some antifungal drugs after a long treatment, have prompted

an increased interest in alternative topical antifungal drugs.<sup>[9,10]</sup> A promising alternative might be antimicrobial peptides (AMPs) such as temporins, since they have a considerable antimicrobial activity, especially towards fungal pathogens and Gram-positive bacteria.<sup>[11–13]</sup> Previously, an encouraging temporin L analogue, named [Pro<sup>3</sup>,DLeu<sup>9</sup>] (**1**), endowed with an efficient antifungal activity against *Candida albicans* and devoid of cytolytic effects *in vitro*, was identified.<sup>[14]</sup> This TL analogue was considered as a lead for our structure-activity relationship (SAR) study, in which the role of Gly in position 10 was explored by replacement with different amino acids, yielding peptides **2–11**.<sup>[15]</sup> On the basis of preliminary outcomes related their activity on Gram-positive and Gram-negative strains,<sup>[15]</sup> herein, the antifungal activity of peptides **2–11** was tested on *M. pachydermatis*. After a first screening of all compounds, only the most interesting was further evaluated for its antimicrobial activity on *S. pseudintermedius*, with the aim to discover novel agents effective against polymicrobial infections. The treatment of *S. pseudintermedius*–*M. pachydermatis* polymicrobial infection requires generally a therapy of antibacterial agents and anti-inflammatory drugs due to inflammatory process associated with it. In this regard, our aim was to get a novel molecule with a dual activity capable to eradicate successfully both polymicrobial infection and inflammation correlated to it. In view of the capacity of temporins to inhibit inflammatory process interfering with the expression of IL-6 controlling the level of pro-inflammatory cytokines (TNF- $\alpha$  and INF- $\gamma$ ),<sup>[16–18]</sup> we investigated a potential anti-inflammatory effect of the most potent peptide on both *M. pachydermatis* and *S. pseudintermedius*. In this study, we used an *in vivo* model of inflammation caused by intraperitoneal sub-lethal dose of zymosan and we elucidated the cellular and molecular profiles responsible for the mode of action.

## 4.2. RESULTS AND DISCUSSIONS

### 4.2.1 DESIGN

To understand the influence of cationic and hydrophobic residues on biological activity of native TL, a SAR study was previously performed by my research group. By the replacement of Gln<sup>3</sup> with a proline and Leu<sup>9</sup> with its D-enantiomer, analogue [Pro<sup>3</sup>,DLeu<sup>9</sup>] (**1**) endowed with an effective antimicrobial activity and devoid of cytotoxicity, was identified.<sup>[12]</sup> In our study, [Pro<sup>3</sup>,DLeu<sup>9</sup>] (**1**) was used as template for better understanding the role of Gly in position 10 by modifying the helical conformation at C-terminal region. In the past,<sup>[19]</sup> taking into consideration the high helical propensity of a leucine residue,<sup>[19]</sup> the Gly<sup>10</sup> switching was already investigated by a Leu scanning. TL analogue with a leucine in position 10, had completely lost its antimicrobial efficacy and in addition had a strong hemolytic activity.<sup>[20]</sup> In the light of this result, we designed a library of peptides (**2–11**) in which the Gly<sup>10</sup> was replaced by amino acid with different chemical properties (Table 1). Amino acids as proline, hydroxyproline (Hyp) and 2-aminoindane-2-carboxylic acid (Aic) were chosen to evaluate the impact of a  $\alpha$ -helix breaker in C-terminal on antimicrobial activity, while the influence of Gly<sup>10</sup> replacement on membrane interactions was investigated by amino acids containing a positive charge and an indole ring in their side chain (Lys and Trp, respectively) and a hydrophobic side chain such as norleucine. Additionally, L and D isomers were used to all amino acids, except for the non-chiral Aic. Preliminary results showed that most of compounds **2–12** showed a good activity towards Gram-positive and Gram-negative strains and all compounds were endowed with high anticandidal activity (Table 1).<sup>[15]</sup> Additionally, only peptides **9** and **10** showed a negligible toxicity against keratinocytes, in particular the data revealed a reduction in cell viability of about 30% versus 57% of **1** at a high concentration of 25  $\mu$ M.<sup>[15]</sup>



**Table 1.** Preliminary results on some Gram-positive (*S. aureus* and *S. epidermidis*) and Gram-negative (*E. coli* and *P. aeruginosa*) strains.<sup>[15]</sup>

Peptides	Sequence	MIC values (μM) <sup>a</sup>				
		<i>E. coli</i> D 21	<i>P. aeruginosa</i> ATCC 27853	<i>S. aureus</i> Cowan I	<i>S. epidermidis</i> ATCC 12228	<i>C. albicans</i> ATCC 10231
<b>1</b>	F V P W F S K F <sub>D</sub> L Gly <sup>10</sup> R I L	12.5	50	12.5	6.25	3.12
<b>2</b>	F V P W F S K F <sub>D</sub> L Pro <sup>10</sup> R I L	25	50	3.12	3.12	1.56
<b>3</b>	F V P W F S K F <sub>D</sub> L dPro <sup>10</sup> R I L	50	>50	>50	25	3.12
<b>4</b>	F V P W F S K F <sub>D</sub> L Hyp <sup>10</sup> R I L	25	50	6.25	6.25	3.12
<b>5</b>	F V P W F S K F <sub>D</sub> L dHyp <sup>10</sup> R I L	25	>50	>50	50	3.12
<b>6</b>	F V P W F S K F <sub>D</sub> L Nle <sup>10</sup> R I L	25	50	3.12	3.12	3.12
<b>7</b>	F V P W F S K F <sub>D</sub> L dNle <sup>10</sup> R I L	25	50	3.12	3.12	3.12
<b>8</b>	F V P W F S K F <sub>D</sub> L Lys <sup>10</sup> R I L	12.5	12.5	6.25	3.12	1.56
<b>9</b>	F V P W F S K F <sub>D</sub> L dLys <sup>10</sup> R I L	12.5	12.5	12.5	3.12	1.56
<b>10</b>	F V P W F S K F <sub>D</sub> L Trp <sup>10</sup> R I L	25	>50	3.12	1.56	3.12
<b>11</b>	F V P W F S K F <sub>D</sub> L dTrp <sup>10</sup> R I L	25	50	3.12	1.56	3.12
<b>12</b>	F V P W F S K F <sub>D</sub> L Aic <sup>10</sup> R I L	>50	>50	1.56	1.56	6.25

In the light of these promising results, we explored the effectiveness of all compounds **2–12** in the treatment of polymicrobial infection caused by an *M. pachydermatis*–*S. pseudintermedius* interaction and in inflammation associated with it. In our design, we considered the opportunity to gain a molecule with a dual activity, that is capable to act on two different targets and eradicate simultaneously two different infectious processes.

#### **4.2.2. BIOLOGICAL STUDIES ON *M. PACHYDERMATIS* AND *S. PSEUDINTERMEDIUS***

**Antimicrobial Susceptibility of *M. Pachydermatis*.** The minimum inhibitory concentration (MIC) values of tested compounds against *M. pachydermatis* are reported in Table 2. Peptide **9** showed the highest inhibitory properties with a MIC value of 6.25 μM. Peptides **8** and **11** inhibited the yeast growth at a MIC value of

12.5  $\mu\text{M}$ , while the other compounds were not as effective. The minimum mycocidal concentration (MMC) of peptide **9** causing  $\geq 3\log_{10}$  reduction in colony count from the starting inoculum, was 6.25  $\mu\text{M}$ . The MMC/MIC ratio of 1 indicated a mycocidal activity of peptide **9**.

**Table 2.** In vitro antifungal activity. Minimum inhibitory concentration (MIC), minimum mycocidal concentration (MMC) and MMC/MIC ratios for peptides evaluated against *M. pachydermatis*.

Peptides	Sequence	MIC Values ( $\mu\text{M}$ )	MMC Values ( $\mu\text{M}$ )	MMC/MIC Ratio
<b>1</b>	F V P W F S K F dL Gly <sup>10</sup> R I L	25	100	4
<b>2</b>	F V P W F S K F dL Pro <sup>10</sup> R I L	25	100	4
<b>3</b>	F V P W F S K F dL dPro <sup>10</sup> R I L	25	100	4
<b>4</b>	F V P W F S K F dL Hyp <sup>10</sup> R I L	25	100	4
<b>5</b>	F V P W F S K F dL dHyp <sup>10</sup> R I L	25	100	4
<b>6</b>	F V P W F S K F dL Nle <sup>10</sup> R I L	25	100	4
<b>7</b>	F V P W F S K F dL dNle <sup>10</sup> R I L	25	100	4
<b>8</b>	F V P W F S K F dL Lys <sup>10</sup> R I L	12.5	25	2
<b>9</b>	F V P W F S K F dL dLys <sup>10</sup> R I L	6.25	6.25	1
<b>10</b>	F V P W F S K F dL Trp <sup>10</sup> R I L	25	100	4
<b>11</b>	F V P W F S K F dL dTrp <sup>10</sup> R I L	12.5	25	2
<b>12</b>	F V P W F S K F dL Aic <sup>10</sup> R I L	25	100	4

**Resistance acquisition test.** To evaluate if the yeast acquired resistance to peptide **9** after a prolonged treatment, *M. pachydermatis* was subcultured through serial passaging in the presence of a sublethal peptide **9** concentration (3.12  $\mu\text{M}$ ). After 1 generation subculture, peptide **9** reduced cell growth, affecting only in part yeast cell vitality (Table 3); however, after 15 yeast subcultures (about 2 months treatment), *M. pachydermatis* was no more able to replicate in the presence of peptide **9**.

**Table 3.** Resistance acquisition tests to 3.12  $\mu\text{M}$  of peptide **9**. Each experiment is the result of three independent experiments performed in triplicate.

Strains	Log <sub>10</sub> CFU/mL After 1 Generation Subculture Including Pept <b>9</b>	Log <sub>10</sub> CFU/mL After 15 Generation Subcultures Including Pept <b>9</b>
<i>M. Pachydermatis</i> Untreated	8.10 $\pm$ 0.21	8.26 $\pm$ 0.29
<i>M. Pachydermatis</i> + Pept <b>9</b>	5.80 $\pm$ 0.25	2.10 $\pm$ 0.12

**Antimicrobial susceptibility of *S. pseudintermedius*.** To investigate the efficacy of peptide **9** in the treatment of *S. pseudintermedius*–*M. pachydermatis* polymicrobial infection, two strains of *S. pseudintermedius*, isolated from auricular swabs of dogs suffering from otitis externa, were used. The strains were characterized for their pattern of antibiotic susceptibility as previously reported.<sup>[20]</sup> One strain resulted in oxacillin resistant (MRSP) and the other oxacillin susceptible (MSSP).

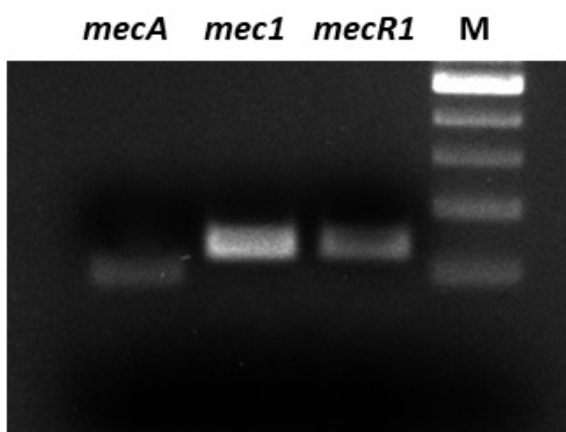


**Figure 1.** Detection of genes from *mec* operon in methicillin-resistant *S. pseudintermedius* (MRSP) strain. M: 100bp ladder marker (BiotechRabbit).

Both the MSSP and the MRSP strains were screened for the presence of *mecA*, *mec1*, *mecR1* genes by PCR. The results showed in Figure 1 are relative to MRSP strain, the only one that demonstrated to possess the *mecA* operon. The antimicrobial activity of peptide **9** against MRSP and MSSP strains is shown in Table 4. Peptide **9** exhibited a significant MIC value at 1.56  $\mu\text{M}$  for MSSP and 6.25  $\mu\text{M}$  for MRSP. As expected, oxacillin treated MRSP showed a MIC value four times higher than MSSP strain. Minimum bactericidal concentration (MBC) was also calculated and resulted in 3.12  $\mu\text{M}$  for MSSP and 12.5  $\mu\text{M}$  for MRSP. The MBC/MIC ratio values are reported in Table 4.

**Table 4.** MIC, minimum bactericidal concentration (MBC), MBC/MIC ratio, and FIC<sub>index</sub> values ( $\mu\text{M}$ ) of peptide **9** on selected bacterial strains. N.d.= not determined. Each experiment is the result of three independent experiments performed in triplicate.

Strains	MIC	MBC	Oxacillin	Vancomycin	MBC/MIC Ratio	FIC <sub>index</sub>
MSSP	1.56	3.12	<5	<1.4	2	n.d.
MRSP	6.25	12.5	25	<1.4	2	0.37

To confirm the bactericidal or bacteriostatic activity of peptide **9** we performed the time kill assay at the MIC value (Table 5). Peptide **9** inhibited bacterial growth already at 1 h. After 6h treatment, a dramatic decrease in cell growth was observed. However, the number of both MSSP and MRSP cells increased 24h after peptide **9** treatment. These results supported a bacteriostatic activity of peptide **9**, because it is likely that a critical bactericidal concentration is not reached on all cell membranes, causing the death of some bacteria (highest cell membrane accumulation) and only cell growth arrest of others (low accumulation).<sup>[21]</sup>

***Influence of Peptide 9 on mecA Gene Expression.*** Quantification data obtained by RT-PCR were normalized to the reference gene for 16S rRNA. The results showed that the mode of action of peptide **9** was not implicate in a regulation of mecA gene expression, but in a membranolytic process involving a membrane interaction, followed by an aggregation in membrane and then a disintegration of membrane by pore formation as shown in Bellavita et al.<sup>[22]</sup> On the basis of this study on membrane interaction, we hypothesize a similar mechanism of action of peptide **9** on MSSP and MRSP.

***Synergistic study between peptide 9 and oxacillin.*** The synergism between peptide **9** and oxacillin was determined using the checkerboard technique. Oxacillin and peptide **9** were used alone and in combination against MRSP planktonic cells. Oxacillin and peptide **9** MICs value were 25  $\mu\text{M}$  and 6.25  $\mu\text{M}$ , respectively. The highest synergistic interaction against MRSP was obtained in the wells with the best

combination values of 1.56  $\mu\text{M}$  peptide **9** (1/4 MIC) and 3.1  $\mu\text{M}$  oxacillin (1/8 MIC). The FIC index, equal to 0.37, confirmed the synergistic effect of peptide **9** and oxacillin (Table 4). This enhanced susceptibility of MRSP to oxacillin by peptide **9** is correlated to its capacity to induce membrane leakage, consisting in a pore formation and resultant penetration of oxacillin in bacterial cell.<sup>[22]</sup>

**Table 5.** Time-kill assay of peptide **9** against methicillin-susceptible *S. pseudintermedius* (MSSP) and MRSP. Each experiment is the result of three independent experiments performed in triplicate.

Strains	Log <sub>10</sub> CFU/mL					
	0 h	1 h	2 h	4 h	6 h	24 h
<b>MSSP untreated</b>	5.50 ± 0.21	5.74 ± 0.21	5.80 ± 0.25	5.87 ± 0.19	7.10 ± 0.31	9.8 ± 0.31
<b>MSSP + cmpd 9</b>	5.45 ± 0.25	0.60 ± 0.12	0.58 ± 0.32	0.89 ± 0.15	0.46 ± 0.15	4.97 ± 0.30
<b>MRSP untreated</b>	5.30 ± 0.21	5.37 ± 0.32	5.84 ± 0.28	5.91 ± 0.29	6.85 ± 0.25	9.36 ± 0.25
<b>MRSP+ cmpd 9</b>	5.30 ± 0.18	2.47 ± 0.18	2.38 ± 0.19	1.30 ± 0.21	0.77 ± 0.12	4.86 ± 0.28

**Peptide 9 reduces MSSP and MRSP biofilm viability.** Biofilm formation, well-known as the main virulence factor in staphylococcal skin infections, can be divided into five stages: initial reversible attachment (**1**), irreversible attachment (**2-3**), maturation (**4**) and dispersion. In a recent study, TL (precursor of peptide **1**) proved to be an effective agent able to affect *P. aeruginosa* PAO1 and methicillin-resistant *S.aureus* (MRSA) biofilms, inhibiting the biofilm attachment stage.<sup>[23]</sup> In this context, we investigated the capacity of peptide **9** to inhibit MSSP and MRSP biofilm formation in initial reversible attachment, using crystal violet (CV) assay. Peptide **9** was tested at sub-MIC concentrations ranging from 0.095 to 0.78  $\mu\text{M}$  for 24h. The max concentration used (0.78  $\mu\text{M}$ ) did not affect planktonic growth, which represents first stage of the biofilm reversible attachment. Quantification of crystal violet staining by measurement of OD595 showed the ineffectiveness of peptide **9** on MSSP and MRSP biofilm formation at each tested concentration (Figure 2).

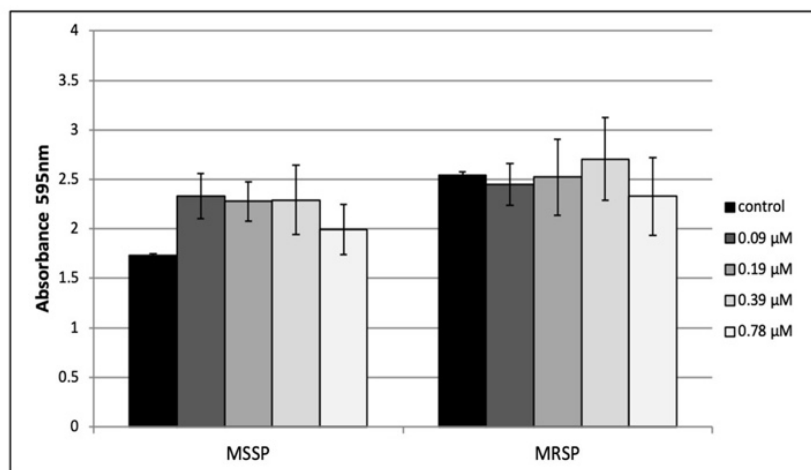


**Figure 2.** Effect of sub-MIC peptide **9** concentrations on MSSP and MRSP biofilm formation assessed by crystal violet assay. Experiments were performed in triplicate in three independent experiments.

In addition, mature biofilm displays antimicrobial resistance offering a favorable living environment for the growth of resistant bacteria. In this context, the activity of peptide **9** was also evaluated on biofilm maturation. One-day-old-biofilms of both MSSP and MRSP strains were incubated with peptide **9** at a concentration of 4X MIC, 2X MIC and 1X MIC for 24 h. Crystal violet results revealed that peptide **9** did not affect the biomass of both treated biofilms at concentrations up to 25  $\mu\text{M}$  (Figure 3, upper panel). On the contrary, XTT assay clearly demonstrated that peptide **9** caused a significant decrease of both MSSP and MSRP biofilm viability compared to the corresponding untreated control (Figure 3, bottom panel). It was able to reduce biofilm viability of MRSP at 6.25 and 12.5  $\mu\text{M}$ , by 38% and 52%, respectively, and 38% for MSSP at 12.5  $\mu\text{M}$ .

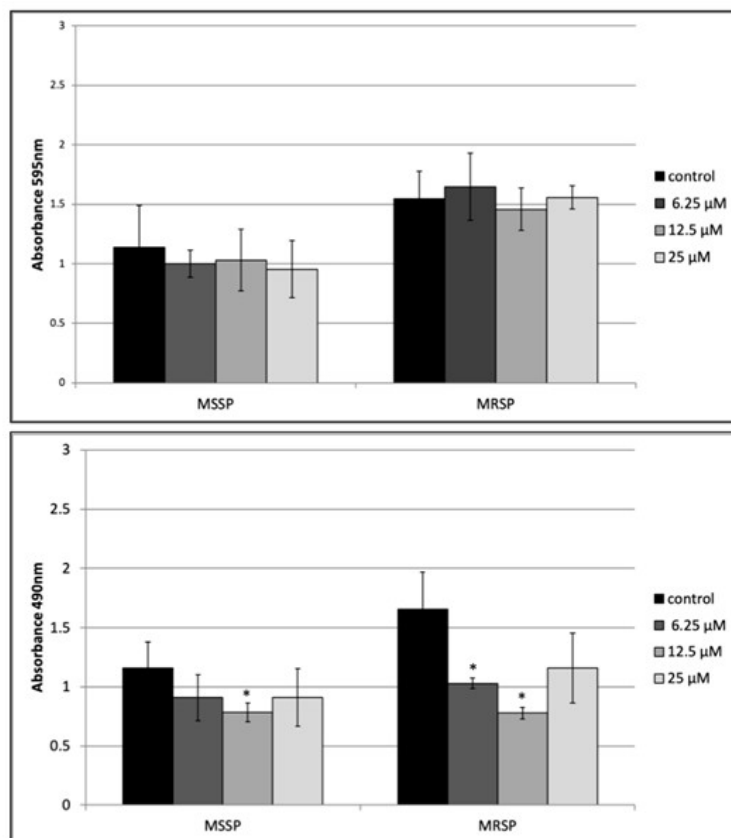


**Figure 3.** Peptide **9** activity on MSSP and MRSP mature biofilm assessed by crystal violet assay (upper panel) and XTT assay (bottom panel). Experiments were performed in triplicate in three independent experiments.

Additionally, the effect of peptide **9** on the mature biofilm of MRSP was observed by confocal microscopy at 12.5 μM, the dose at which we observed the maximal eradicating effect. Images of treated biofilm showed some red zone representing cells within biofilm that were killed or damaged by peptide **9** (Figure 4). Similarly to TL, peptide **9** can interact with the extracellular matrix of biofilm by its positive charges distributed in the peptide sequence, facilitating transition through this environment and improving its antimicrobial activity.<sup>[23]</sup>

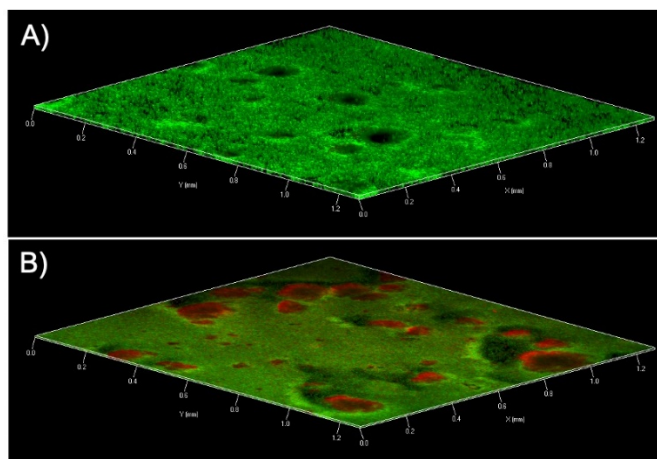


**Figure 4.** Peptide **9** effects on MRSP mature biofilm assessed by Confocal laser microscopy. (A) Untreated biofilm; (B) treated biofilm (12  $\mu\text{M}$ ).

### 4.2.3. *IN VITRO* AND *IN VIVO* ANTI-INFLAMMATORY STUDIES

With the discovery of the effectiveness of peptide **9** in the treatment of *S. pseudintermedius*–*M. pachydermatis* polymicrobial infection, we investigated a potential anti-inflammatory activity of peptide **9** to eradicate simultaneously polymicrobial infection and inflammation generally associated with it.

**Macrophages biological response to treatments *in vitro*.** First, we evaluated the activity of peptide **9** and its parent peptide (**1**) on the growth and proliferation of macrophages J774 *in vitro* to identify the lower micromolar range to allow a safe animal experimentation. As reported in Figure 5, the concentration effect curves did not show interference with cell growth and proliferation up to the concentration of 20  $\mu\text{M}$  after 4 (A) and 24 h (B) of treatment with both peptides and anti-inflammatory reference drugs, *i.e.* Diclofenac and Betamethasone. However, at 25  $\mu\text{M}$  a slight interference with cell viability was found for both peptides. Indeed, the calculated  $\text{IC}_{50}$  values of both peptides were higher than 80  $\mu\text{M}$  after 4 h and 24 h of treatment. These values were similar to those measured for betamethasone and diclofenac ( $\sim 85$  and  $\sim 200$   $\mu\text{M}$  respectively), herein used as reference drugs.



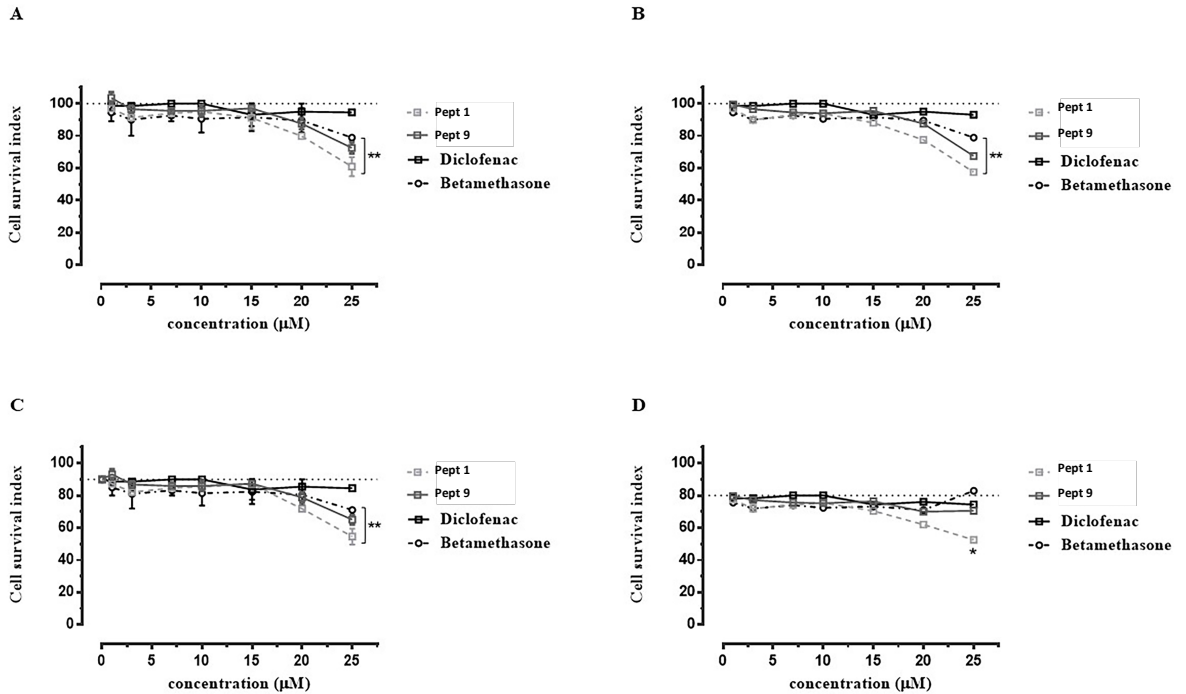


**Figure 5.** Bioactivity profile of peptides in J774 macrophages. Cell survival index, evaluated by MTT assay, on murine macrophage cell line, following 4 (A) and 24 h (B) of treatment with selected concentrations (1→25  $\mu\text{M}$ ) of peptide **1** and **9**. Anti-inflammatory positive control incubations were carried out by equivalent concentrations of Diclofenac and Betamethasone. Data are expressed as percentage of untreated control cells and are reported as mean of five independent experiments  $\pm$  S.E.M. \* $P \leq 0.05$ , \*\* $P \leq 0.01$ , vs. control cells.

In another set of experiments cells were pretreated with zymosan (100 ng/ml) followed by peptide **1** and **9** for 4 (Figure 5C) and 24 h (Figure 5D), with the same range of concentrations. Although we observed a small reduction in cell vitality after zymosan treatment, the effect of both peptides was similar to that observed in “non-stimulated” conditions.

**Anti-inflammatory effect of peptides 1 and 9 in zymosan-induced peritonitis in mice.** In light of the safety of peptide **1** and **9** evidenced through *in vitro* evaluations on J774 macrophages, we investigated the role of both peptides in an *in vivo* model of inflammation that allowed for the characterization of leukocyte recruitment and local inflammatory mediator production. Mice were subjected to i.p. injection of 500

mg/kg zymosan, in the presence or absence of peptide **1** and **9** (1–10 mg/kg dissolved in PBS).

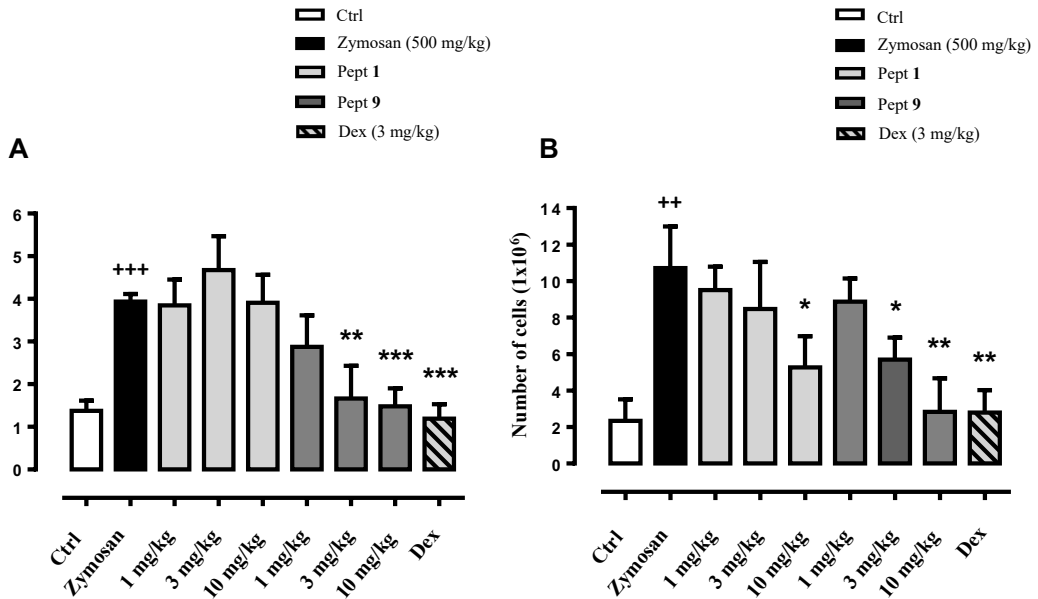


**Figure 6.** Anti-inflammatory effect of temporin-derived peptides in zymosan-induced peritonitis in mice. Mice (n=7) were injected intraperitoneally with 500 mg/kg zymosan, with 500 mg/kg zymosan and 1–10 mg/kg of peptides **1** and **9** or 500 mg/kg zymosan and 3 mg/kg of dexamethasone (Dex). At 4 (A) and 24 h (B) after zymosan injection, peritoneal exudate from each mouse was recovered and total cell number (expressed as  $1 \times 10^6$  and normalized to exudate levels) was evaluated. Results are expressed as mean  $\pm$  S.E.M. ++ $P \leq 0.01$ , +++ $P \leq 0.005$  vs. ctrl group, \* $P \leq 0.05$ , \*\* $P \leq 0.01$  and \*\*\* $P \leq 0.005$  compared to zymosan-treated mice.

As internal control, i.p injection of PBS alone without zymosan and i.p. injection of Dex (3 mg/kg) post zymosan administration were also assessed. As shown in Fig. 6A, zymosan injection elicited a strong leucocyte recruitment at 4h ( $\sim 4.5 \times 10^6$ ) which was significantly reduced after peptide **9** administration at a dose of 10 mg/kg ( $P \leq 0.05$ ). At this time-point the effect of peptide **1** (1–10 mg/kg) was not significant compared to mice injected with peptide **9** and Dex ( $P \leq 0.005$ ).

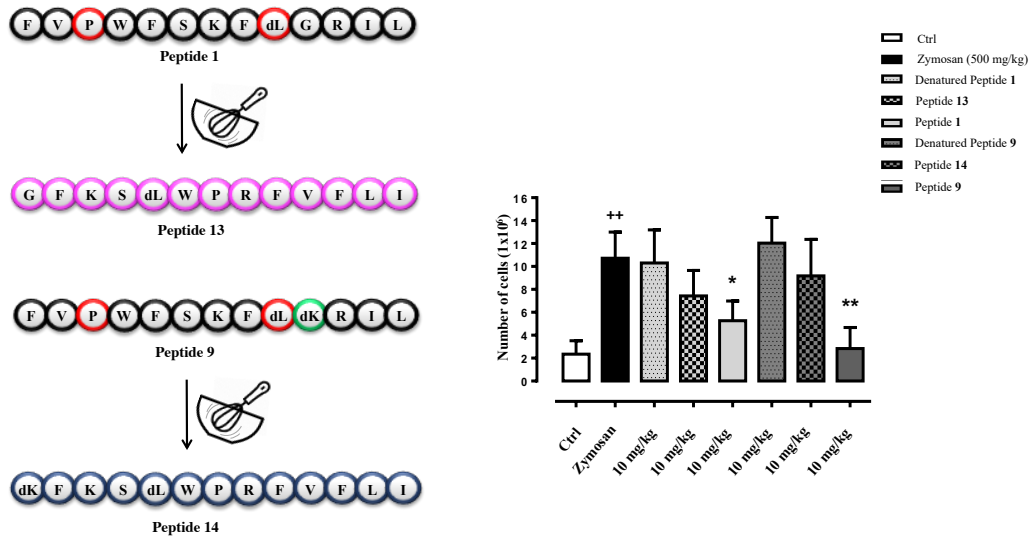


**Figure 7.** A) Peptide 13 and 14 represent scrambled sequence of peptide 1 and 9, respectively. B) Effect of denatured and scrambled temporin-derived peptides in zymosan-induced peritonitis in mice. Mice (n=7) were injected intraperitoneally with 500 mg/kg zymosan, with 500 mg/kg zymosan and 10 mg/kg of peptides 1 and 9 or 500 mg/kg zymosan and peptides (1 and 9) denatured and scrambled (peptides 13 and 14) (10 mg/kg). At 24 h post injection, peritoneal exudate from each mouse was recovered and total cell number (expressed as  $1 \times 10^6$  and normalized to exudate levels) was evaluated. Results are expressed as mean  $\pm$  S.E.M. ++ $P \leq 0.01$  compared vs. ctrl group, \* $P \leq 0.05$  and \*\* $P \leq 0.01$  vs. zymosan treated mice.

Conversely, after 24 h both peptides at 10 mg/kg significantly reduced ( $P \leq 0.05$  and  $P \leq 0.01$  respectively for peptide 1 and 9) leukocyte infiltration ( $\sim 11 \times 10^6$  after zymosan injection) with a profile, for peptide 9, comparable to Dex ( $P \leq 0.01$ ). Interestingly, peptide 9 also displayed significant effects at a lower dose of 3 mg/kg ( $P \leq 0.05$ ) (Fig. 6B). Other experimental groups also included mice that received zymosan with peptide 1 and 9 at the highest dose (10 mg/kg) inactivated by denaturation or peptides 13 and 14 with scrambled aminoacidic assembly (Figure 7). As shown in Figure 7B, both peptides at 24 h did not display any significant inhibitory effects on leukocyte recruitment, highlighting the hypothesis that only “selected peptides sequence” elicited observed anti-inflammatory effects.

**Modulation of cellular inflammatory infiltrates.** Zymosan, a polysaccharide cell wall component derived from *Saccharomyces cerevisiae*,<sup>[24]</sup> has been reported to elicit a multiple organ failure and a massive recruitment of innate immunity cells in

the peritoneal cavity, mainly characterized by neutrophils and monocytes.<sup>[25]</sup> The production of pro-inflammatory cytokines, such as IL-1, IL-6, TNF- $\alpha$ ,<sup>[26,27]</sup> and of prostaglandin metabolites<sup>[28]</sup> is high in the pathophysiology of zymosan-induced shock. TNF- $\alpha$  plays a pivotal role characterized by the release of IL-1 and IL-6 that orchestrate neutrophil, macrophage, and fibroblast accumulation to the site of inflammation.<sup>[29,30]</sup> This scenario is supported by the CC chemokine MCP-1, as one of the most potent chemotactic factors for monocyte migration to the site of tissue injury.<sup>[31]</sup> On the other hand, IL-10 is an anti-inflammatory cytokine that mainly suppresses inflammatory response by increasing anti-inflammatory factors and inhibiting the activation and function of T cells and monocytes.<sup>[32]</sup>

To test the effects of an acute systemic administration of peptide **1** and **9**, we administered these peptides with the same dose (10 mg/kg) that evoked the optimal inhibition of leukocyte recruitment to the peritoneum. A single administration of zymosan into the peritoneal cavity causes a transient infiltration of leukocytes that becomes evident between 4–24 h and declines by 48h. All mice were sacrificed 24 h after zymosan administration. A single injection of zymosan (500 mg/kg) i.p caused a significant increase of the levels of TNF- $\alpha$ , IL-6, IL-10 and MCP-1 after 24h, compared to the control group (Fig. 8A, B, C and D respectively). Interestingly, peptide **1** at 10 mg/kg significantly ( $p \leq 0.05$ ) reduced the levels of TNF- $\alpha$  (Fig. 8A) and IL-6 (Fig. 8B). The levels of IL-10 (Fig. 8C) and MCP-1 (Fig. 8D) remained unaffected. Similarly, peptide **9**, at the same dose, also reduced ( $p \leq 0.01$ ) the levels of TNF- $\alpha$  (Fig. 8A) and IL-6 (Fig. 8B), but a reduction was also observed in ( $p \leq 0.05$ ) MCP-1 (Fig. 8D). Injection of the positive control Dex (3 mg/kg) decreased the values of mentioned cyto-chemokines (Fig. 8A, B, C and D) with a profile comparable to peptide **9**.

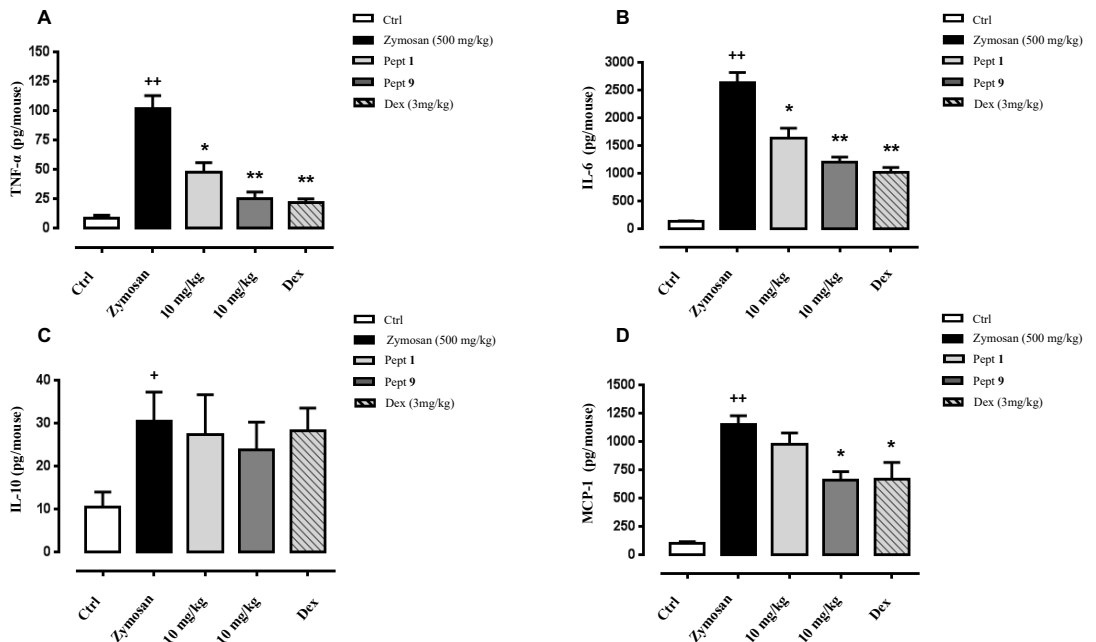


**Figure 8.** Cyto-chemokines analysis of collected peritoneal exudates. Analysis of collected peritoneal exudates identified heightened levels of the classical pro-inflammatory cyto-chemokines TNF- $\alpha$  (A), IL-6 (B), IL-10 (C), and MCP-1 (D) in the peritoneal cavity of mice from zymosan groups (n=7). Significant differences were found in relative levels after peptides **1** and **9** administration (n=7). Results (normalized to exudate levels) are expressed as mean  $\pm$  S.E.M. +P $\leq$ 0.05 and ++P $\leq$ 0.01 vs. ctrl group, \*P $\leq$ 0.05 and \*\*P $\leq$ 0.01 vs. zymosan-treated mice.

Based on these results, we selected the most active temporin L-derived peptide (peptide **9**) to investigate the phenotype of inflammatory leukocytes recruited to the peritoneal cavity. Leucocytes collected at 24h time-point post zymosan injection were stained with an anti-B220, anti-F480, anti-GR1, anti-CD115 antibodies and then analyzed by flow cytometry. We did not observe any significant difference in terms of neutrophils (GR1+ cells) and macrophages (F4/80+ cells) reduction after peptide **9** treatment (data not shown). However, to identify potential differences in monocyte subpopulations, total cells were gated on their totality (Fig. 9A, gate R1) and singlet (Fig. 9B, gate R2) for the identification of B220- population (Fig. 9C, gate R3) followed by GR1 and F480 expression (Fig. 9D–F). Double high positive population for these markers (Gate R4,  $9.05 \pm 0.32$ ,  $41.20 \pm 2.78$  and  $31.70 \pm 2.55$  of double high positive population respectively for Ctrl, zymosan and zymosan+

peptide **9**; Figure 9J) were then further interrogated for CD115 (Figure 9G–I) as its expression level is commonly correlated with the degree of maturation of inflammatory monocytes. Our results show that in zymosan-injected mice, most cells recovered were B220–/GR1hi-F480hi/CD115+ ( $10.70 \pm 1.14$  compared to  $2.70 \pm 0.24$  of Ctrl) with a significant lower expression in peptide **9**-treated group ( $3.24 \pm 1.41$ ) (Figure 10K). These values were strengthened by a low percentage of positive cells found in the staining for the isotype control antibodies.

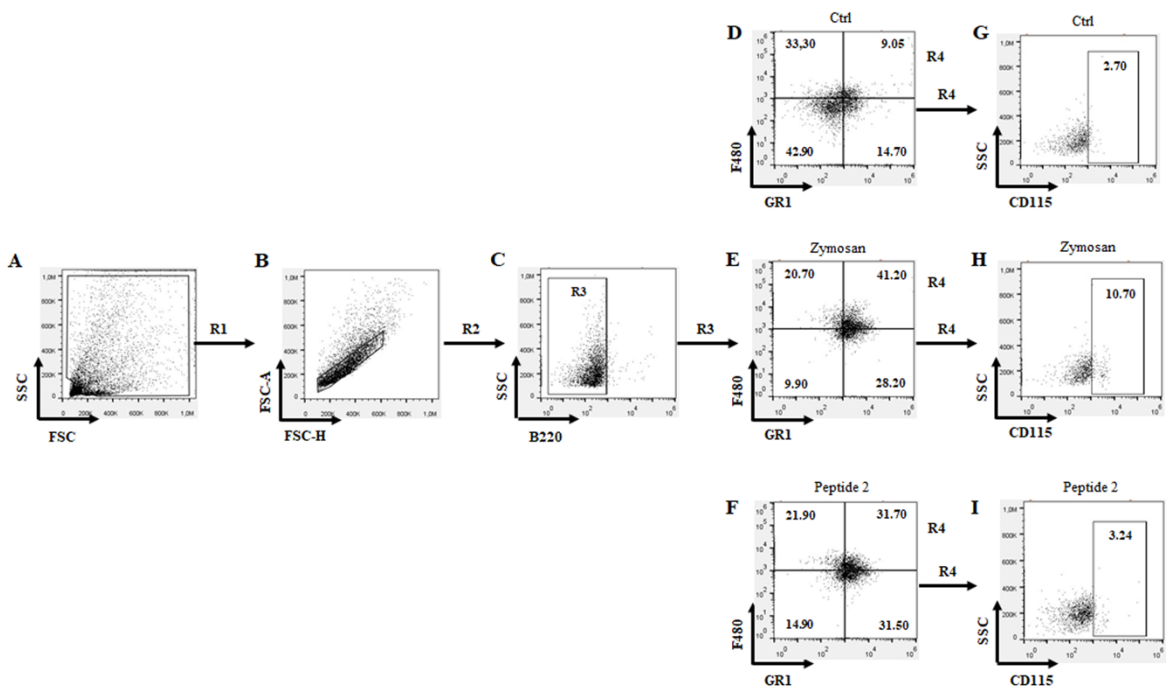


**Figure 9.** Flow cytometry strategy applied to identify the modulation of inflammatory monocytes in zymosan and zymosan+peptide **9**-treated group. Cells obtained at 24 h time-point post zymosan injection in all experimental conditions were washed and stained with the following panel of antibodies: anti-B220, anti-F480, anti-GR1 and anti-CD115. Specifically, to identify potential differences in monocyte subpopulations, total cells were gated for their totality (A, gate R1) and singlet (B, gate R2) to identify B220– population (C, gate R3) followed by GR1 and F480 expression (D-F). Double high positive population for these markers (gate R4) was then further interrogated for CD115 (G-I) The numbers in the dot plots indicated the percentage of positively stained cells after gating strategy. FACS plots are representative of seven samples with similar results. Results (normalized to exudate levels) are presented as mean  $\pm$  S.E.M (J and K) of  $n=7$  mice per group. +++ $P \leq 0.001$  vs. ctrl group, \* $P \leq 0.05$  and \*\* $P \leq 0.01$  vs. zymosan-treated mice.

### 4.3. CONCLUSIONS

In conclusion, we discovered, for the first time, an analogue of TL native with a dual activity that is capable to wipe up inter-kingdom infection caused by *S. pseudintermedius* and *M. pachydermatis* interaction and inflammatory process associated to it. Peptide **9** contrasted the growth of both *S. pseudintermedius* and *M. pachydermatis*, it did not cause yeast drug resistance and increased the susceptibility of oxacillin against MRSP, not inhibiting the *mecA* gene expression but inducing a membrane disintegration. The use of peptide **9** may provide novel avenues of possible therapeutic strategies to combat inter-kingdom infections and inflammation, since it showed a notable anti-inflammatory activity *in vivo* in response to zymosan-induced peritonitis, modulating the recruitment of inflammatory monocytes. Therefore, the topical treatment using peptide **9** as drugs in otitis externa in dogs and in wound infections in humans caused by zoonotic microorganisms, might be a valid alternative to traditional therapies.

### 4.4. EXPERIMENTAL SECTION

#### 4.4.1. CHEMISTRY

**Peptides synthesis by US-SPPS.** The synthesis of peptides was performed by using the ultrasound-assisted solid-phase peptide strategy (US-SPPS) combined with the orthogonal Fmoc/tBu chemistry, as described in Chapter 3.<sup>[33]</sup> Each peptide was assembled on a Rink amide resin (0.1 mmol from 0.64 mmol/g of loading substitution), as solid support. First, Fmoc group was deprotected by treatment with a solution of 20% piperidine in DMF (0.5 + 1 min) and the coupling reactions were performed using Fmoc-amino acid (3 equiv.), HBTU (3 equiv), HOBt (3 equiv) and DIEA (6 equiv), 5 min. Finally, peptides were purified and characterized by RP-HPLC using linear gradients of MeCN (0.1% TFA) in water (0.1% TFA), from 10 to 90% over 20 min (Table 6). All compounds examined for biological activity were purified to >96%.

**Table 6.** Analytical data of peptides 2–14.

Peptides	Sequence	R <sub>t</sub> (min)	MS Found	MS Calcd
2	F V P W F S K F dL <b>Pro</b> <sup>10</sup> R I L	13.28	1649.25	1649.03
3	F V P W F S K F dL <b>DPro</b> <sup>10</sup> R I L	12.81	1648.82	1649.03
4	F V P W F S K F dL <b>Hyp</b> <sup>10</sup> R I L	12.98	1664.97	1665.03
5	F V P W F S K F dL <b>DHyp</b> <sup>10</sup> R I L	12.61	1665.13	1665.03
6	F V P W F S K F dL <b>Nle</b> <sup>10</sup> R I L	13.41	1665.72	1665.03
7	F V P W F S K F dL <b>DNle</b> <sup>10</sup> R I L	13.49	1665.66	1665.03
8	F V P W F S K F dL <b>Lys</b> <sup>10</sup> R I L	12.52	1680.54	1680.09
9	F V P W F S K F dL <b>DLys</b> <sup>10</sup> R I L	12.52	1680.41	1680.09
10	F V P W F S K F dL <b>Trp</b> <sup>10</sup> R I L	13.49	1738.85	1738.13
11	F V P W F S K F dL <b>DTrp</b> <sup>10</sup> R I L	13.60	1737.98	1738.13
12	F V P W F S K F dL <b>Aic</b> <sup>10</sup> R I L	14.19	1711.51	1711.10
13	G F K S dL W P R F V F L I	12.72	1608.42	1607.93
14	dK F K S dL W P R F L I	11.41	1680.41	1681.02

#### 4.4.2 BIOLOGY

**Microbial Strains and Culture.** *M. pachydermatis* was cultured onto Sabouraud dextrose agar with chloramphenicol (Oxoid Ltd, London, UK) at 30 °C.<sup>[34]</sup> Veterinary clinical strains of *S. pseudintermedius* were isolated from auricular swabs of dogs suffering from otitis externa and processed at the Microbiology Laboratory of the Department of Veterinary Medicine and Animal Production, University of Naples “Federico II” (Italy). *S. pseudintermedius* strains were plated on blood agar base supplemented with 5% sheep blood and on mannitol-salt agar, and incubated aerobically at 37 °C for 24–48 h.<sup>[35]</sup>

**Molecular Analysis.** Genomic DNA extraction was performed by using GenUp Bacteria gDNA kit (BiotechRabbit, Berlin, Germany) according to the manufacturer’s instructions. All the isolates were tested for genes of the *mec* operon using the polymerase chain reaction (PCR).<sup>[ref]</sup>

**Resistance Acquisition Tests .** To evaluate if the yeast acquired resistance to the drug, after a continued treatment, *M. pachydermatis* was subcultured with a sub lethal concentration of peptide **9** (1/2 MIC). Briefly, a final 3.12 µM peptide **9**



concentration was added to yeast inoculum suspension equivalent to  $1-3 \times 10^6$  CFU/mL in Sabouraud dextrose broth (SB) and incubated 72 h at 30 °C (inoculum 1). After this period, optical density was measured and a new yeast subculture with 3.12  $\mu$ M of peptide **9** was prepared starting from inoculum 1 (inoculum 2). Three days after, optical density was again recorded and a new inoculum in presence of peptide **9** prepared. This was repeated until evident yeast death was observed.

**Antimicrobial Activity Assay.** MIC of all compounds was determined in Sabouraud Dextrose broth with 1% tween 80 (SB) medium, for *M. pachydermatis*, and Mueller–Hinton broth (MH), for *S. pseudintermedius*, by the broth microdilution assay (BMD) in 96-well microtiter plates, as previously reported.<sup>[36]</sup>

**Killing Rate.** Bacterial suspension ( $10^5$  CFU/mL) was added to microplates along with peptide **9** at 6.25  $\mu$ M MIC concentration.<sup>[37]</sup> Plates were incubated at 37 °C on an orbital shaker at 120 rpm. Viability assessments were performed at 0, 2, 4, 6 and 24 h by plating 0.01 mL undiluted and 10-fold serially diluted samples onto Mueller–Hinton plates in triplicate. After overnight incubation at 37 °C, bacterial colonies were counted and compared with counts from control cultures.

**Checkerboard Method.** The interaction between peptide **9** and oxacillin against MRSP was evaluated by the checkerboard method. Briefly, twofold serial dilutions of oxacillin distributed in horizontal rows of 96-well microtiter plate were cross-diluted vertically by twofold serial dilutions of peptide **9** to at least double the MIC. The peptide **9** tested concentration ranging from 0.19 to 12.5  $\mu$ M and Oxacillin from 1.25 to 25  $\mu$ M (0.5 to 10  $\mu$ g/mL). Microtiter plates were inoculated with bacteria at an approximate concentration of  $10^5 \times$  CFU/mL and incubated at 37 °C for 24 h. MIC values of the combinations were determined as the lowest concentrations that completely inhibited bacterial growth, recorded as optical density at 595 nm. To evaluate the effect of the combination treatment, the fractional inhibitory

concentration (FIC) index for each combination was calculated as follows: FIC index = FIC of peptide **9** + FIC of oxacillin, where FIC of peptide **9** (or oxacillin) was defined as the ratio of MIC of peptide **9** (or oxacillin) in combination and MIC of peptide **9** (or oxacillin) alone. The FIC index values were interpreted as follows:  $\leq 0.5$ , synergistic;  $>0.5$  to  $\leq 1.0$ , additive;  $>1.0$  to  $\leq 2.0$ , indifferent; and  $>2.0$ , antagonistic effects.<sup>[38]</sup>

**Biofilm study.** Anti-biofilm activity of peptide **9** was examined by the crystal violet assay previously described with minor modifications.<sup>[39]</sup> Microtiter plates were inoculated with bacteria at a final density of  $10^6$  CFU/mL and treated with peptide **9** ranging from 0.095 to 0.78  $\mu$ M. Control cells were grown in the absence of peptide **9**. After 24 h incubation at 37° C, the amount of biofilm formed in the wells was measured by crystal violet staining and the absorbance of the solution was measured at 595 nm. Biofilms were allowed to form in each well of a 96-well microtiter plate, as described by Stepanovic.<sup>[40]</sup> Cells biofilms were exposed to 200  $\mu$ l of peptide **9** at the final concentration ranging from 6.25 to 25  $\mu$ M and the plate was further incubated for 24 h at 37 °C. At the end of the experiment crystal violet-staining was performed to assess biofilm mass.

**Quantitation of Metabolic Activity of Mature Biofilm by XTT Assay.** The metabolic activity of MSSP and MRSP mature biofilms was quantified by the XTT [2,3-bis(2-methoxy-4-nitro-5-sulphophenyl)-2H-tetrazolium-5-carboxanilide] (Roche Diagnostics, Germany) reduction assay. The assay was conducted as previously described with some modifications.<sup>[41]</sup> XTT (150  $\mu$ L) was added to biofilms in each well and the plates were incubated for 40 min at 37 °C in the dark. The reduction of the tetrazolium salt by cellular dehydrogenase into orange formazan dye was photometrically measured at 490 nm. The medium was set as negative control. Viability values for each well were compared to controls.

**Confocal Laser Scanning Microscopy (CLSM).** CLSM was used to confirm the effect of peptide **9** on mature biofilm respect the controls. MSRP were grown in chambered cover glass ( $\mu$  Slide 4 well; ibidi GmbH, Germany) in a static condition for 24 h. Peptide **9** was added on a 1-day-old biofilm at 12.5  $\mu$ M. After 24 h, biofilms were rinsed with PBS and stained by using a LIVE/DEAD<sup>®</sup> BacLight Bacteria Viability stains (Life Technologies, Italy). After the staining, the images were observed using a LSM 700 inverted confocal laser-scanning microscope (Zeiss, Italy).

#### **4.4.3. IN VITRO ASSAYS**

**Cell viability.** Murine macrophage cell line, J774, was cultured in Dulbecco's modified Eagle's medium supplemented with 10 % fetal bovine serum (FBS, Cambrex, Verviers, Belgium), L-glutamine (2 mM, Sigma, Milan, Italy), penicillin (100 units/ml, Sigma) and streptomycin (100  $\mu$ g/ml, Sigma), and cultured in a humidified 5 % carbon dioxide atmosphere at 37 °C. The cells were treated for 4 and 24 h, with a range of concentrations (1  $\rightarrow$  25  $\mu$ M) of peptide **1** and **9**. Positive control incubations were carried out by equivalent concentrations of Diclofenac and Betamethasone. In another set of experiments cell were pre-treated with zymosan (100 ng/ml) followed by peptide **1** and **9** for 4 and 24 h, with the same range of concentrations. Biological activity of peptides was investigated by the estimation of a "cell survival index", arising from the combination of cell viability evaluation with cell counting. Cell viability was evaluated using MTT assay, which measures the level of mitochondrial dehydrogenase activity using the yellow 3-(4,5-dimethyl-2-thiazolyl)- 2,5-diphenyl-2H-tetrazolium bromide (MTT, Sigma) as substrate.<sup>[42]</sup>

**Flow cytometry.** Cells collected from the peritoneal cavities were first washed with PBS and then re-suspended in FACS buffer (PBS containing 1 % FCS and 0.02 % NaN<sub>2</sub>) containing CD16/CD32 Fc $\gamma$ IIR blocking antibody (clone 93; eBioscience, Wembley, UK) for 30 min at 4 °C. Thereafter, cells were labelled for 60 min at 4 °C

with the following conjugated antibodies (all from BioLegend, London, UK): GR1 (1:300; clone RB6-8C5), F480 (1:300; clone BM8), B220 (1:200; clone RA3-6B2), CD115 (1:200; clone AFS98).<sup>[43]</sup> Flow cytometry was performed on BriCyte E6 flow cytometer (Mindray Bio-Medical Electronics, Nanshan, China) using MRFlow and FlowJo software operation.

***Enzyme-linked immunosorbent assay (ELISA).*** The levels of TNF- $\alpha$ , IL-6, IL-10 and MCP-1 in the peritoneal exudates at 24h were measured using commercially available enzyme-linked immunosorbent assay kit (ELISA kits, eBioscience Co., San Diego, CA, USA) according to the manufacturer instructions.<sup>[44]</sup>

#### **4.4.4. *IN VIVO* STUDY**

***Induction of peritonitis in mice.*** To examine the anti-inflammatory action of peptide **1** and **9**, mice were randomly divided into different groups: control group (Ctrl), model group (Zymosan), zymosan+peptides (1, 3 and 10 mg/kg) groups (peptide **1** and **9**), and zymosan+dexamethasone (3 mg/kg) group (Dex). Animals received the peptides or Dex intraperitoneally (i.p.) 30 min after i.p. injection of zymosan (500 mg/kg).<sup>[45]</sup> Peritonitis was induced by administering 500 mg/kg of zymosan dissolved in PBS and then boiled before the i.p. injection (0.5 mL) at selected time points (4 and 24 h).<sup>[46]</sup> Peritoneal exudates were collected and then cell number of lavage fluids was determined by TC10 automated cell counter (Bio-Rad, Milan, Italy) using disposable slides, TC10 trypan blue dye (0.4 % trypan blue dye w/v in 0.81 % sodium chloride and 0.06 % potassium phosphate dibasic solution) and a CCD camera to count cells based on the analyses of captured images. The remaining lavage fluids were centrifuged at 3000 rpm for 20 min at 4 °C and supernatants frozen at -80 °C for further ELISA analysis.<sup>[47]</sup>

**Statistical analysis.** The results obtained were expressed as the mean  $\pm$  SEM. Statistical analysis was performed by two-way ANOVA followed by Dunnett's posttest when comparing more than two groups. Statistical analysis was performed by using GraphPad Prism 7.0 software (San Diego, CA, USA).<sup>[48]</sup>

#### 4.5. REFERENCES

- [1] K.A. Brogden, J.M. Guthmiller, C.E. Taylor. Human polymicrobial infections. *Lancet*. 2005, 365, 253-255.
- [2] A.Y. Peleg, D.A. Hogan, E. Mylonakis. Medically important bacterial–fungal interactions. *Nat. Rev. Microbiol.* 2010, 8, 340–349.
- [3] E. Chryssanthou, U. Broberger, B. Petrini. *Malassezia pachydermatis* fungaemia in a neonatal intensive care unit. *Acta Paediatr.* 2001, 90, 323–327.
- [4] J. Bannoehr, L. Guardabassi. *Staphylococcus pseudintermedius* in the dog: taxonomy, diagnostics, ecology, epidemiology and pathogenicity. *Vet. Dermatol.* 2012, 23, 253–266.
- [5] A.A. Ferran, J. Liu, P.L. Toutain, A. Bousquet-Mélou. Comparison of the *in vitro* activity of five antimicrobial drugs against *Staphylococcus pseudintermedius* and *Staphylococcus aureus* biofilms. *Front. Microbiol.* 2016, 7:1187.
- [6] J. Guillot, R. Bond. *Malassezia* yeasts in veterinary dermatology: an updated overview. *Front. Cell. Infect. Microbiol.* 2020, 10:79.
- [7] I. Ghasemzadeh, S.H. Namazi. Review of bacterial and viral zoonotic infections transmitted by dogs. *J. Med. Life.* 2015, 8, 1–5.
- [8] A.M.P. Oliveira, J.S.P. Devesa, P.B. Hill. *In vitro* efficacy of a honey based gel against canine clinical isolates of *Staphylococcus pseudintermedius* and *Malassezia pachydermatis*. *Vet. Dermatol.* 2018, 29, 180-e65.
- [9] T. Holm, J. Bruchmann, A. Scheynius, U. Langel. Cell-penetrating peptides as antifungals towards *Malassezia sympodialis*. *Lett. Appl. Microbiol.* 2012, 54, 39–44.
- [10] N. Al-Sweih, S. Ahmad, L. Joseph, S. Khan, Z. Khan. *Malassezia pachydermatis* fungemia in a preterm neonate resistant to fluconazole and flucytosine. *Med. Mycol. Case Rep.* 2014, 5, 9–11.
- [11] M.L. Mangoni, A.C. Rinaldi, A.D. Giulio, G. Mignogna, A. Bozzi, D. Barra, M. Simmaco. Structure-function relationships of temporins, small antimicrobial peptides from amphibian skin. *Eur. J. Biochem.* 2000, 267, 1447–1454.
- [12] M.L. Mangoni. Temporins, anti-infective peptides with expanding properties. *Cell. Mol. Life Sci.* 2006, 63, 1060–1069.
- [13] M.L. Mangoni, Y. Shai. Temporins and their synergism against Gram-negative bacteria and in lipopolysaccharide detoxification. *Biochim. Biophys. Acta Biomembr.* 2009, 1788, 1610–1619.
- [14] P. Grieco, A. Carotenuto, L. Auriemma, M.R. Saviello, P. Campiglia, I. Gomez-Monterrey, L. Marcellini, V. Luca, D. Barra, E. Novellino, M.L. Mangoni. The effect

of d-amino acid substitution on the selectivity of temporin L towards target cells: identification of a potent anti-Candida peptide. *Biochim. Biophys. Acta Biomembr.* 2013, 1828, 652–660.

[15] F. Merlino, A. Carotenuto, B. Casciaro, F. Martora, M.R. Loffredo, A. Di Grazia, A.M. Yousif, D. Brancaccio, L. Palomba, E. Novellino, M. Galdiero, M.R. Iovene, M.L. Mangoni, P. Grieco. Glycine-replaced derivatives of [Pro<sup>3</sup>,DLeu<sup>9</sup>]TL, a temporin L analogue: evaluation of antimicrobial, cytotoxic and hemolytic activities. *Eur. J. Med. Chem.* 2017, 139: 750–761.

[16] M. Zaiou. Multifunctional antimicrobial peptides: therapeutic targets in several human diseases. *J. Mol. Med.* 2007, 85, 317–329.

[17] R. Capparelli, A. Romanelli, M. Iannaccone, N. Nocerino, R. Ripa, S. Pensato, C. Pedone, D. Iannelli. Synergistic antibacterial and anti-Inflammatory activity of Temporin A and modified Temporin B *in vivo*. *PLoS One.* 2009, 4:e7191.

[18] C.N. Serhan. Novel lipid mediators and resolution mechanisms in acute inflammation: to resolve or not? *Am. J. Pathol.* 2010, 177, 1576–1591.

[19] M.L. Mangoni, A. Carotenuto, L. Auriemma, M.R. Saviello, P. Campiglia, I. Gomez-Monterrey, S. Malfi, L. Marcellini, D. Barra, E. Novellino, P. Grieco. Structure-activity relationship, conformational and biological studies of temporin L analogues. *J. Med. Chem.* 2011, 54, 1298–1307.

[20] E. Buommino, A. Carotenuto, I. Antignano, R. Bellavita, B. Casciaro, M.R. Loffredo, F. Merlino, E. Novellino, M.L. Mangoni, F.P. Nocera, D. Brancaccio, P. Punzi, D. Roversi, R. Ingenito, E. Bianchi, P. Grieco. The Outcomes of decorated prolines in the discovery of antimicrobial peptides from Temporin-L. *Chem. Med. Chem.* 2019, 14, 1283–1290.

[21] S. Gottschalk, L.E. Thomsen. The Interaction of antimicrobial peptides with the membrane and intracellular targets of *Staphylococcus aureus* Investigated by ATP leakage, DNA-binding analysis, and the expression of a LexA-controlled gene, recA. *Methods Mol. Biol.* 2017, 1548, 297–305.

[22] R. Bellavita, A. Falanga, E. Buommino, F. Merlino, B. Casciaro, F. Cappiello, M.L. Mangoni, E. Novellino, M.R. Catania, R. Paolillo, P. Grieco, S. Galdiero. Novel temporin L antimicrobial peptides: promoting self-assembling by lipidic tags to tackle superbugs. *J. Enzyme Inhib. Med. Chem.* 2020, 35, 1751–1764.

[23] D. Brancaccio, E. Pizzo, V. Cafaro, E. Notomista, F. De Lise, A. Bosso, R. Gaglione, F. Merlino, E. Novellino, F. Ungaro, P. Grieco, M. Milanga, F. Quaglia, A. Miro, A. Carotenuto. Antimicrobial peptide Temporin-L complexed with anionic cyclodextrins results in a potent and safe agent against sessile bacteria. *Int. J. Pharm.* 2020, 584, 119437.

[24] E.J.U. Von Asmuth, J.G. Maessen, C.J. van der Linden, W.A. Buurman. Tumor necrosis factor alpha and interleukin 6 in zymosan-induced shock model. *Scand. J. Immunol.* 1991, 34, 197–206.

- [25] S. Cuzzocrea, A. Filippelli, B. Zingarelli, M. Falciani, A.P. Caputi, F. Rossi. Role of nitric oxide in a non-septic shock model induced by zymosan in the rat. *Shock*. 1997, 7, 351–358.
- [26] E.J.U. Von Asmuth, J.G. Maessen, C.J. van der Linden, W.A. Buurman. Tumor necrosis factor alpha and interleukin 6 in zymosan-induced shock model. *Scand. J. Immunol.* 1991, 34, 197–206.
- [27] M.J. Jansen, T. Hendriks, M.T.E. Vogels, J.W.M. van der Meer, R.J.A. Goris. Inflammatory cytokines in an experimental model for the multiple organ dysfunction syndrome. *Crit. Care Med.* 1996, 24, 1196–1204.
- [28] M.R. Mainous, P. Tso, R.D. Berg, E.A. Deitch. Studies of the route, magnitude, and time course of bacterial translocation in a model of systemic inflammation. *Arch. Surg.* 1991, 126, 33–37.
- [29] F. D'Acquisto, F. Maione, M. Pederzoli-Ribeil. From IL-15 to IL-33: the never-ending list of new players in inflammation. Is it time to forget the humble aspirin and move ahead? *Biochem. Pharmacol.* 2010, 79, 525–534.
- [30] S. Liu, J. Zhang, Q. Pang, S. Song, R. Miao, W. Chen, Y. Zhou, C. Liu. The protective role of curcumin in zymosan-induced multiple organ dysfunction syndrome in mice. *Shock*. 2016, 45, 209–219.
- [31] J. Xie, L. Yang, L. Tian, W. Li, L. Yang, L. Li. Macrophage migration inhibitor factor upregulates MCP-1 expression in an autocrine manner in hepatocytes during acute mouse liver injury. *Sci. Rep.* 2016, 6, 27665.
- [32] K.W. Moore, R. de Waal Malefyt, R.L. Coffman, A. O'Garra. Interleukin-10 and the interleukin-10 receptor. *Annu. Rev. Immunol.* 2001, 19, 683–765.
- [33] F. Merlino, S. Tomassi, A.M. Yousif, A. Messere, L. Marinelli, P. Grieco, E. Novellino, S. Cosconati, S. Di Maro, Boosting fmoc solid-phase peptide synthesis by ultrasonication. *Org. Lett.* 2019, 21, 6378–6382.
- [34] E. Buommino, F.P. Nocera, A. Parisi, A. Rizzo, G. Donnarumma, K. Mallardo, F. Fiorito, A. Baroni, L. De Martino. Correlation between genetic variability and virulence factors in clinical strains of *Malassezia pachydermatis* of animal origin. *New. Microbiol.* 2016, 39, 216–223.
- [35] A. Schumacher, T. Vranken, A. Malhotra, J. J. C. Arts, P. Habibovic. *In vitro* antimicrobial susceptibility testing methods: agar dilution to 3D tissue-engineered models. *Eur. J. Clin. Microbiol. Infect. Dis.* 2018, 37, 187–208.
- [36] C. Cafarchia, L.A. Figueredo, V. Favuzzi, M.R. Surico, V. Colao, R. Iatta, M.T. Montagna, D. Otranto. Assessment of the antifungal susceptibility of *Malassezia pachydermatis* in various media using a CLSI protocol. *Vet. Microbiol.* 2012, 159, 536–540.
- [37] O.O. Olajuyigbe, A.J. Afolayan. *In vitro* antibacterial and time-kill evaluation of the *Erythrina caffra* thunb. extract against bacteria associated with diarrhea. *Sci. World. J.* 2012, 738314.

- [38] S.K. Pillai, R.C. Moellering, G.M. Eliopoulo. Antimicrobial combinations. In *Antibiotics in Laboratory Medicine*, 5th ed; Lorian, V., Ed.; The Lippincott Williams & Wilkins Co.: Philadelphia, PA, USA, 2005; pp. 365–440.
- [39] F. Barra, E. Roschetto, A.A. Soriano, A. Vollaro, I. Postiglione, G.M. Pierantoni, G. Palumbo, M.R. Catania. Photodynamic and antibiotic therapy in combination to fight biofilms and resistant surface bacterial infections. *Int. J. Mol. Sci.* 2015, 16, 20417–20430.
- [40] S. Stepanović, D. Vuković, V. Hola, G. Di Bonaventura, I. Djukić, Ćirković, F. Ruzicka. Quantification of biofilm in microtiter plates: overview of testing conditions and practical recommendations for assessment of biofilm production by staphylococci. *Apmis.* 2007, 115, 891–899.
- [41] A. Vollaro, M.R. Catania, M.R. Iesce, R. Sferruzza, B. D’Abrosca, B. Donnarumma G, De Filippis A, Cermola F, DellaGreca M, Buommino E. Antimicrobial and anti-biofilm properties of novel synthetic lignan-like compounds. *New Microbiol.* 2019, 42, 21–28.
- [42] C. Irace, G. Misso, A. Capuozzo, M. Piccolo, C. Riccardi, A. Luchini, M. Caraglia, L. Paduano, D. Montesarchio, R. Santamaria. Antiproliferative effects of ruthenium based nucleolipidic nanoaggregates in human models of breast cancer in vitro: insights into their mode of action. *Sci. Rep.* 2017, 7, 45236.
- [43] F. Raucci, A.J. Iqbal, A. Saviano, P. Minosi, M. Piccolo, C. Irace, F. Caso, R. Scarpa, S. Pieretti, N. Mascolo, F. Maione. IL-17A neutralizing antibody regulates monosodium urate crystal-induced gouty inflammation. *Pharmacol. Res.* 2019, 147, 104351.
- [44] V. Baradaran Rahimi, H. Rakhshandeh, F. Raucci, B. Buono, R. Shirazinia, A. Samzadeh Kermani, F. Maione, N. Mascolo, V.R. Askari. Anti-inflammatory and anti-oxidant activity of portulaca oleracea extract on LPS-induced rat lung injury. *Molecules.* 2019, 24, 139.
- [45] B.E. Chatterjee, S. Yona, G. Rosignoli, R.E. Young, S. Nourshargh, R.J. Flower, M. Perretti. Annexin 1-deficient neutrophils exhibit enhanced transmigration *in vivo* and increased responsiveness *in vitro*. *J. Leukoc. Biol.* 2005, 78, 639–646.
- [46] S. Pace, A. Rossi, V. Krauth, F. Dehm, F. Troisi, R. Bilancia, C. Weinigel, S. Rummler, O. Werz, L. Sautebin, Sex differences in prostaglandin biosynthesis in neutrophils during acute inflammation. *Sci. Rep.* 2017, 7, 3759.
- [47] F. Maione, N.N. Paschalidis, A.J. Iqbal, T. Crompton, M. Perretti, F. D’Acquisto. Analysis of the inflammatory response in HY-TCR transgenic mice highlights the pathogenic potential of CD4- CD8- T cells. *Autoimmunity.* 2010, 43, 672–681.
- [47] M.J. Curtis, R.A. Bond, D. Spina, A. Ahluwalia, S.P.A. Alexander, M.A. Giembycz, A. Gilchrist, D. Hoyer, P.A. Insel, A.A. Izzo, A.J. Lawrence, D.J. MacEwan, L.D. Moon, S. Wonnacott, A.H. Weston, J.C. McGrath, Experimental



design and analysis and their reporting: new guidance for publication in BJP. *Br. J. Pharmacol.* 2015, 172, 3461–34.

# CHAPTER 5

## CONSTRAINING THE $\alpha$ -HELIX CONTENT BY CYCLIZATION STRATEGIES

**CONTRIBUTIONS:** Peptide synthesis; fluorescence assays (Laurdan and Thioflavin T assays); circular dichroism; protease stability assay.

## 5.1. MACROCYCLIZATION STRATEGIES

The intramolecular macrocyclization of peptides is a smart chemical strategy for tuning pharmacodynamic and pharmacokinetic properties of peptide-based molecules of potential therapeutic interest.<sup>[1,2]</sup> Among the most popular cyclizations, head-to-tail reactions and side-chain-to-side-chain tethering induced by lactam-, disulfide- and 1,4 or 1,5-triazolic- bridges,<sup>[3,4]</sup> produce limited conformational flexibility with respect to the original linear sequence, hence improving binding affinity and specificity to targets, as well as membrane interaction and cell-permeability.<sup>[5,6]</sup> Many cyclic peptides, especially of natural origin, are endowed with a wide range of biological activities, such as anticancer, antifungal, antiviral and anti-inflammatory, including antimicrobial one.<sup>[7,8]</sup> For instance, **romidepsin** (*i.e.* a 5-mer cyclic depsipeptide), Istodax®, is a potent anticancer drug used in T-cell lymphoma;<sup>[9]</sup> **micafungin** (*i.e.* a cyclic hexapeptide), Mycamine®, approved as an antifungal agent, is effective against *Candida* infections;<sup>[10]</sup> **alisporivir** (cyclic undecapeptide), a cyclophilin inhibitor used in the treatment of hepatitis C (HCV), has passed phase II trials as an antiviral drug.<sup>[11]</sup> Regarding the antibiotic drug discovery, macrocyclic peptide-based molecules are considered among the privileged scaffolds in antibiotic drug discovery,<sup>[12]</sup> but only a restricted number of them have been approved for therapy. Of both natural and synthetic origins, there are **daptomycin** as cyclic lipopeptide, and **vancomycin** together with derivatives **oritavancin** and **dalbavancin** as cyclic glycopeptides, which are all essentially used to treat infections caused by Gram-positive bacteria, including multidrug-resistant strains.<sup>[9]</sup> Others, albeit a few, are described as anti-Gram-negative bacteria, such as **colistin**, a polymyxin lipopeptide originating from genus *Paenibacillus* that was approved by Food and Drug Administration (FDA) and was characterized by a potent and specific activity against several Gram-negative bacteria, including *Pseudomonas aeruginosa* and *Acinetobacter baumannii*; and **murepavadin**, a synthetic cyclic  $\beta$ -hairpin peptidomimetic identified as *Pseudomonas*-specific antibiotic.<sup>[13,14]</sup>

Therefore, this emerging class of therapeutics along with a fancy chemical manipulation, could lead to novel therapeutic approaches and to the discovery of molecules useful in the fight against infectious diseases of microbial origins. To cope with this challenge, prodigious research interest is focused on natural product screening that has been for a long time the most productive source for discovering new antibiotics. In this light, temporins represent a valid alternative.<sup>[15,16]</sup> Temporin L (TL) is the leader of temporin family for its remarkable antimicrobial activity, but unfortunately possess a strong hemolytic activity correlated to its  $\alpha$ -helix structure that extends along its entire peptide sequence.<sup>[17]</sup> Indeed, in a previous SAR study performed on TL, simultaneous disruption of its  $\alpha$ -helix in *N*-terminus by an introduction of proline in position 3 and a stereoinversion of amino acids in C-terminus,<sup>[18]</sup> induced a dramatic reduction of hemolytic activity and antimicrobial activity, with the sole exception of the analogue [Pro<sup>3</sup>,DLeu<sup>9</sup>]TL. This compound preserved a good antimicrobial activity against Gram-positive and Gram-negative strains since the interruption of  $\alpha$ -helix provoked by D-Leu at position 9 did not compromise the antibacterial activity. Instead, the disruption of  $\alpha$ -helix in *N*-terminus by the Pro<sup>3</sup> incorporation conferred to [Pro<sup>3</sup>,DLeu<sup>9</sup>]TL analogue the non-toxicity towards human erythrocytes and keratinocytes.<sup>[18]</sup> Therefore, while  $\beta$ -turn structure induced by Pro<sup>3</sup> led to low hemolytic activity, the  $\alpha$ -helix structure in C-terminus seemed to be crucial for antimicrobial activity. In this respect, we envisaged an  $\alpha$ -helix stabilization at the C-terminus region of [Pro<sup>3</sup>,DLeu<sup>9</sup>]TL by means of an intramolecular macrocyclization strategy that may lead to novel derivatives potentially endowed with an increased antimicrobial spectrum and lower cytotoxicity.<sup>[19,20]</sup> One of the most prominent and straightforward crosslinking strategies for helix stabilization consists of a side-chain-to-side-chain tethering by incorporation of precursor amino acids in *i,i+4* positions to bridge one turn of the helix.<sup>[21]</sup> Particularly, we first reasoned upon the application of the lactam and 1,4-substituted [1,2,3]-triazole tethering, between diverse residues placed in *i,i+4*

positions, as these are known to be crucial for optimal helicity and synthetically advantageous (Figure 1).<sup>[5,22]</sup> A second series was then realized when positions 6 and 10 of linear [Pro<sup>3</sup>,DLeu<sup>9</sup>]TL, respectively, were identified as the best positions for replacement with amino acids carrying modified side chains suitable for cyclization (Bellavita *et al*, unpublished results). Thus, more crosslinking strategies, by hydrocarbon and linkers, were embraced to further evaluate the correlation between  $\alpha$ -helical content and biological activity. The entire library of compounds was analyzed by means of antimicrobial against Gram-positive and Gram-negative ATCC strains and the cytotoxicity activity of the most promising peptides was evaluated on keratinocytes. The percentage of  $\alpha$ -helical content of cyclic peptides **4**, **9**, **12**, **13** was calculated by CD studies in water and membrane mimicking environment (SDS and DPC micelles, liposomes). Additionally, the mechanism of action of the most promising cyclic peptide **4** was carried out by fluorescence assays Laurdan and Thioflavin T assays, and an improvement of its protease stability due to  $\alpha$ -helix constriction by lactam cross-link was assessed in the presence of human serum.

## **5.2. RESULTS AND DISCUSSIONS**

### **5.2.1. DESIGN OF STAPLED $\alpha$ -HELICAL PEPTIDES**

The design of our stapled  $\alpha$ -helical temporin derivatives was inspired by previous conformational NMR studies on [Pro<sup>3</sup>,DLeu<sup>9</sup>]TL performed both in SDS and in DPC micelles.<sup>[18]</sup> The linear precursor [Pro<sup>3</sup>,DLeu<sup>9</sup>]TL adopts an  $\alpha$ -helix structure along residues 5–8 in SDS and along the residues 5–10 in DPC micelles; while in both micelles has shown a  $\beta$ -turn centered on Pro<sup>3</sup>. In order to stabilize the  $\alpha$ -helix structure and to improve the antimicrobial activity, we designed side-chain lactam-bridged peptides (**2–6**) and side-chain triazole-bridged peptides (**7–11**) (Table 1), incorporating cyclizing amino acids in *i,i+4* positions starting from Trp<sup>4</sup> (Figure 1). Our choice to perform this SAR study using lactam cross-linker as  $\alpha$ -helix inducer

is supported by its capacity to confer to peptide the greatest  $\alpha$ -helical stabilization (100%), in contrast to triazole constraint that gives more conformational flexibility and less helical content (62%), as elsewhere reported.<sup>[23–25]</sup> In this study, the L/D-Glu (*i*) and L/D-Lys residues were incorporated in *i,i+4* positions to the synthesis of lactam bridge, while L/D-propargylglycine (L/D- Pra) and L/D-Lys(N<sub>3</sub>) residues were chosen to synthesize 1,4-triazolic bridged peptides. In addition, during the incorporation of cyclizing amino acids, positively charged Lys<sup>7</sup> and Arg<sup>11</sup> residues were not replaced for their essential role in bacterial membrane interaction.

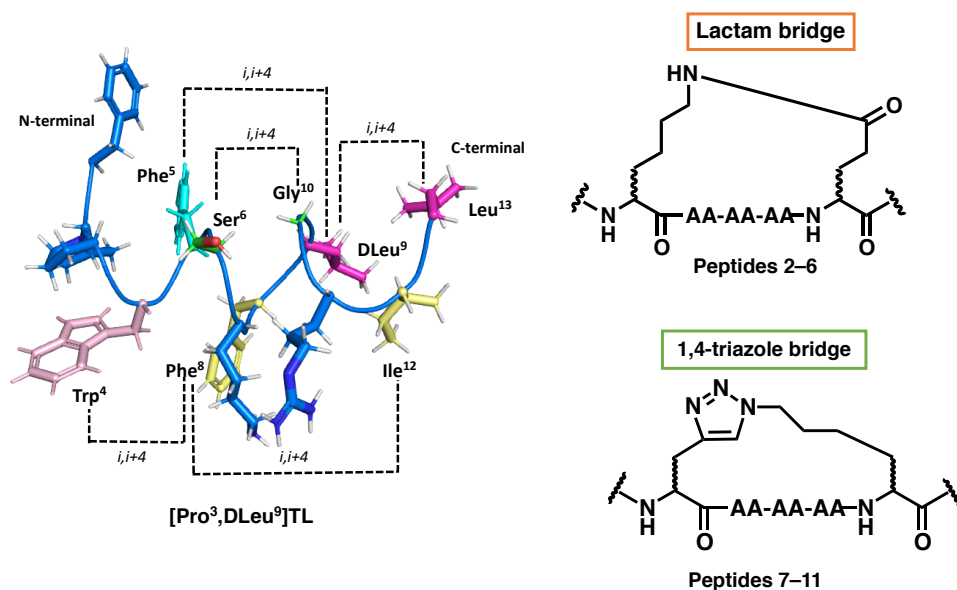


**Figure 1.** Design of  $\alpha$ -helical stapled peptides incorporating lactam bridge (peptides 2–6) and 1,4-triazolic bridge (peptides 7–11) in different *i,i+4* positions of linear precursor [Pro<sup>3</sup>,DLeu<sup>9</sup>]TL.

By the first screening of antimicrobial activity of cyclic peptides **2–11**, we identified the best staple *i,i+4* position corresponding to Ser<sup>6</sup> (*i*) and Gly<sup>10</sup> (*i+4*) in linear [Pro<sup>3</sup>,DLeu<sup>9</sup>]TL, to investigate  $\alpha$ -helical stabilization induced by further cross-links, such as hydrocarbon and disulfide bridges.

**Table 1.** Sequence of lactam-bridged (2–6) and 1,4-triazolic-bridged peptides (7–11). **PRA** and **Az** correspond to propargylglycine and lysine azido residues, respectively.

Peptides	Sequence
[Pro <sup>3</sup> , DLeu <sup>9</sup> ]TL(1)	F V P W F S K F I G R I L
2	F V P W F S K F <b>K G R I E</b>
3	F V P W F S K <b>K I G R E L</b>
4	F V P W F <b>K K F I E</b> R I L
5	F V P W <b>K S K F E</b> G R I L
6	F V P <b>K F S K E</b> I G R I L
7	F V P W F S K F <b>D P R A G R I A z</b>
8	F V P W F S K <b>P R A I G R A z L</b>
9	F V P W F <b>P R A K F I A z</b> R I L
10	F V P W <b>P R A S K F D A z</b> G R I L
11	F V P <b>P R A F S K A z</b> I G R I L

Specifically, the lactam bridge in peptide **4** was replaced with an all-hydrocarbon bridge introducing Fmoc-(*S*)-2-(4-pentenyl)alanine residues in positions 6 and 10, and after the elongation of the linear sequence the peptide was treated with the RCM catalyst to generate the hydrocarbon-bridged peptide **12**. In addition, we designed peptide **13** featured by a disulfide bridge between two cysteines placed at positions 6 and 10, by predicting a reduction of helical content since disulfide cross-link induces typically helicity when is placed at *i,i*+3 positions.

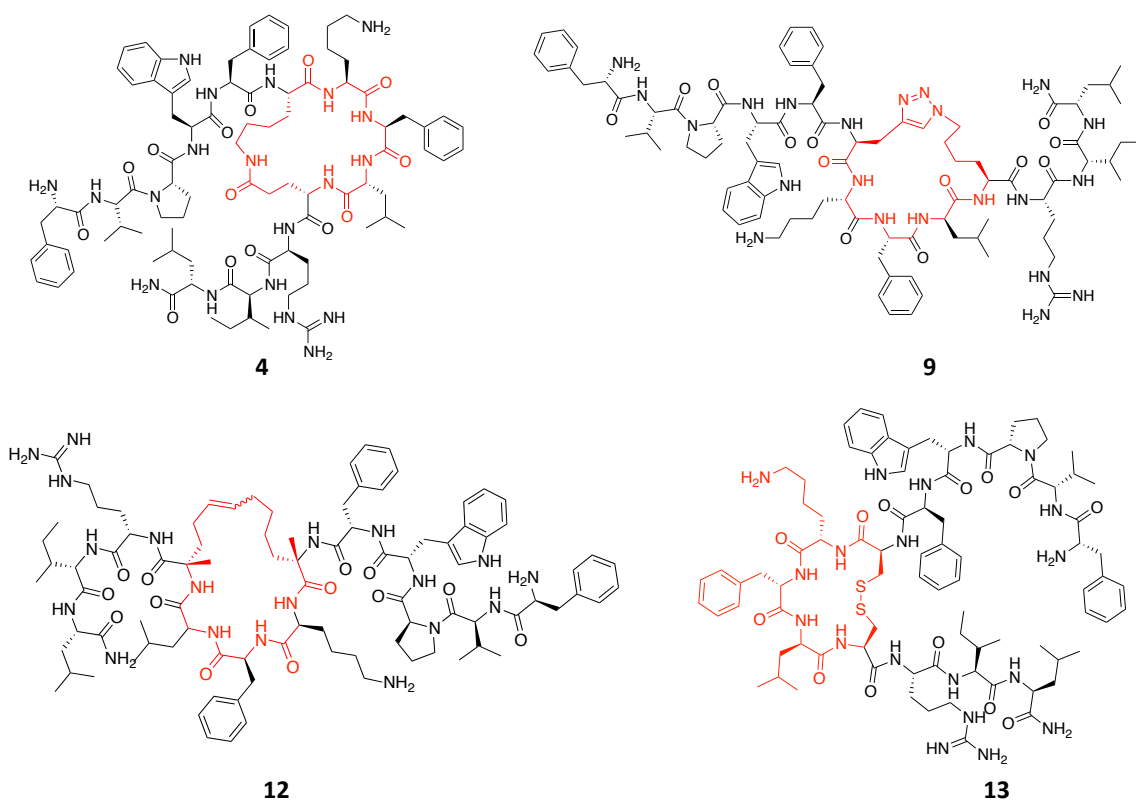


**Figure 2.** Structures of  $\alpha$ -helical stapled peptides **4,9,12** and **13** featured by a side-chain-to-side-chain tethering in positions 6 and 10.

### 5.2.2. HELICAL STABILIZATION VERSUS BIOLOGICAL ACTIVITY

**Antibacterial activity.** The antimicrobial activities of peptides **1-13** against a range of reference bacterial strains, including *S. aureus* ATCC 25923, *S. epidermidis* ATCC 12228, *Bac. megaterium* Bm11, *E. coli* ATCC 25922, *P. aeruginosa* ATCC 27853, and *Ac. baumannii* ATCC 19606, were assessed by the broth microdilution assay. The resulting minimal growth inhibitory concentration (MIC) values are reported in Tables 2. We evaluated the effects produced by the lactam and triazole bridges in different  $i,i+4$  positions along the peptide sequence of the reference linear peptide **1** (Table 1). As reported, peptides **2** and **3** displayed the same antimicrobial behavior, albeit poor, as they were not effective against the Gram-negative strains



(>100  $\mu\text{M}$ ), while both weakly worked on the Gram-positive strain of *Bac. megaterium* (50  $\mu\text{M}$ ). Peptide **4** resulted to be active with a strong efficacy towards *S. aureus* ATCC 25923 and *S. epidermidis* ATCC 12228 (MIC of 3.12  $\mu\text{M}$ ) and towards *Bac. megaterium* Bm11 with MIC value of 1.56  $\mu\text{M}$ . Differently, the activity of peptide **4** resulted to be 2-fold lower (MIC of 25  $\mu\text{M}$ ) than parent peptide **1** (MIC of 12.5  $\mu\text{M}$ ) against *E. coli* ATCC 25922 and has showed a substantial loss of activity towards *P. aeruginosa* ATCC 27853 (MIC of 100  $\mu\text{M}$ ). Interestingly, peptide **4** exhibited stronger activity than linear peptide **1** against Gram-negative strain of *Ac. baumannii* ATCC 19606 with a MIC value of 3.12  $\mu\text{M}$ . Peptides **5** and **6** were found to be poorly active both on Gram-positive and Gram-negative strains (MIC>100  $\mu\text{M}$ ). Among triazole-bridged peptides **7–11**, only peptide **9** displayed a strong activity towards *S. aureus* ATCC 25923 with MIC value of 3.12  $\mu\text{M}$  and *S. epidermidis* ATCC 12228 and *Bac. megaterium* Bm11 with MIC values of 1.56  $\mu\text{M}$ , while this peptide did not show any antimicrobial effect up to 100  $\mu\text{M}$  against *E. coli* ATCC 25922 and *P. aeruginosa* ATCC 27853 and has exhibited a weak activity on *Ac. baumannii* ATCC 19606 with a MIC value of 25  $\mu\text{M}$ . Regarding the triazole bridged peptides **7**, **10**, **11** have completely lost the activity both on Gram-negative (*E. coli* ATCC 25922 and *P. aeruginosa* ATCC 27853) and Gram-positive (*S. aureus* ATCC 25923 and *S. epidermidis* ATCC 12228) and displayed a weak activity against Gram-positive strain of *Bac. megaterium* Bm11 in comparison to peptide **1**. In contrast, triazole-bridged peptide **8** was able to counteract only the bacterial growth of *Bac. megaterium* at 3.12  $\mu\text{M}$  concentration, in fact, a dramatic reduction of activity was observed against Gram-negative strains (*E. coli* ATCC 25922 and *P. aeruginosa* ATCC 27853) and Gram-positive strains (*S. aureus* ATCC 25923 and *S. epidermidis* ATCC 12228) in comparison to parent peptide **1**.

**Table 2.** Antimicrobial activity of designed compounds **2–13**.

Peptides	MIC values ( $\mu\text{M}$ ) <sup>a</sup>					
	<i>E. coli</i> ATCC 25922	<i>P.</i> <i>aeruginosa</i> ATCC 27853	<i>Ac.</i> <i>baumannii</i> ATCC 19606	<i>S. aureus</i> ATCC 25923	<i>S.</i> <i>epidermidis</i> ATCC 12228	<i>Bac.</i> <i>megaterium</i> Bm11
<b>1</b>	12.5	50	6.25	6.25	6.25	1.56
<b>2</b>	>100	>100	>100	>100	>100	50
<b>3</b>	>100	>100	>100	>100	>100	50
<b>4</b>	25	100	3.12	3.12	3.12	1.56
<b>5</b>	>100	>100	>100	>100	>100	100
<b>6</b>	>100	>100	>100	>100	>100	>100
<b>7</b>	>100	>100	100	>100	>100	25
<b>8</b>	50.0	>100	25	100	50	3.12
<b>9</b>	>100	>100	25	3.12	1.56	1.56
<b>10</b>	>100	>100	>100	>100	>100	6.25
<b>11</b>	>100	>100	>100	>100	>100	12.5
<b>12</b>	>100	>100	>100	>100	>100	100
<b>13</b>	25	>100	25	100	6.25	1.56

This biological data highlighted that deleting aromatic amino acids such as phenylalanine and tryptophan for the incorporation of a lactam or triazole bridge induced a dramatic loss of activity since are residues implicated in membrane interactions. Instead, when Ser<sup>6</sup> and Gly<sup>10</sup> residues were substituted with appropriate cyclizing amino acids, an enhancement of antibacterial activity was observed because these residues probably are less involved in interactions and are placed on the face of helix oriented towards the solvent. In addition, an  $\alpha$ -helix constraint induced by a lactam (**4**) or triazole bridge (**9**) in these positions increased significantly the activity against Gram-positive strains, while it is unclear the correlation between secondary structure and antimicrobial activity against Gram-negative.

Once identified the positions 6 and 10 as the best to introduce a staple, we embraced hydrocarbon and disulfide bridges to evaluate further the correlation between  $\alpha$ -

helical content and biological activity. Surprisingly, peptide **12** featured by all-hydrocarbon bridge has dramatically lost the activity (MIC > 100  $\mu\text{M}$ ) both towards Gram-positive and Gram-negative strains. This result suggested that too hydrophobicity caused a loss of optimal hydrophilic/hydrophobic ratio of the peptide, influencing drastically the biological activity. Instead, peptide **13** featured by a disulfide bridge, preserved the same activity profile of linear parent peptide **1** towards *S. epidermidis* ATCC 12228 (MIC of 6.25  $\mu\text{M}$ ) and *Bac. megaterium* Bm11 (MIC of 1.56  $\mu\text{M}$ ), while was resulted to be inactive against *S. aureus* ATCC 25923 (MIC of 100  $\mu\text{M}$ ). In contrast, as reported in table 2, this peptide exhibited a weak activity towards *E. coli* ATCC 25922 and *Ac. baumannii* ATCC 19606 (MIC of 25  $\mu\text{M}$ ) and did not show the effect on *P. aeruginosa* ATCC 27853 (MIC of >100  $\mu\text{M}$ ).

**Cytotoxicity towards human keratinocytes.** The extent of cytotoxic effects of most promising antimicrobial peptides **4** and **9** were assessed on keratinocytes (HaCaT cells), as nucleated human cells sometimes interested by Gram-positive and Gram-negative colonization, and results are shown in Figure 3.

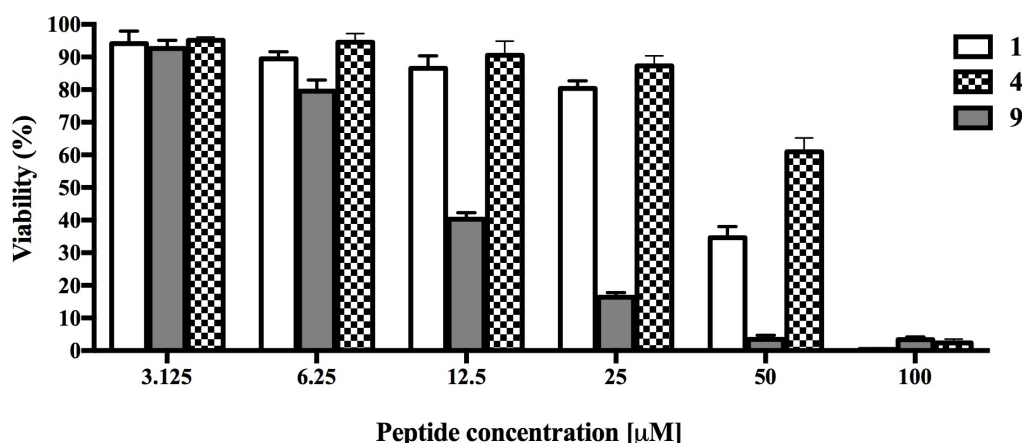


**Figure 3.** The viability of peptide-treated HaCaT cells evaluated by MTT assay at 24 h. All data are expressed as a percentage with respect to the untreated control cells and are the mean of three independent experiments  $\pm$  standard error of the mean (SEM).

In particular, the cytotoxicity was evaluated by the 3-(4,5-dimethylthiazol-2-yl)-2,5-diphenyltetrazolium bromide (MTT) assay and is expressed as the viability percentage of peptide-treated cells calculated on the basis of inhibition of MTT reduction to its insoluble formazan crystals by mitochondrial dehydrogenases compared to that of untreated control cells. As reported in Figure 3, after 24 h treatments the cell viability decreased in a concentration-dependent manner for all peptides. Among these, peptides **9** carrying a 1,4-substituted [1,2,3]-triazole showed the strongest cytotoxicity, causing a reduction in cell viability of about 40% at the 12.5  $\mu\text{M}$  concentration. Interestingly, peptide **4** endowed with a lactam bridge, showed a cytotoxic effect significantly decreased for all the concentrations tested. In fact, peptide **4** at the 25  $\mu\text{M}$  concentration showed cell viability of ~60% more when compared to triazole bridged peptide **9** (80% for peptide **4** versus 15% for peptide **9**), and the 60% of cell viability can be detected at 50  $\mu\text{M}$  concentration. Thus, compound **4** was selected as the peptide with an overall higher antibacterial activity and lower cytotoxicity up to a concentration of 50  $\mu\text{M}$  in comparison with the reference peptide **1** (about 60% versus 35% of **1** at 50  $\mu\text{M}$ ). Noteworthy, peptides **4** and **9** can be considered harmless at a concentration below 6.25  $\mu\text{M}$ , as their MIC values encountered against reference strains are resulted to be inferior.

### 5.2.3. MEASUREMENT OF HELICITY BY CIRCULAR DICHROISM

The secondary structure of the linear peptide (**1**) and its cyclic analogues (**4**, **9**, **12**, **13**) was explored by circular dichroism (CD). CD spectroscopy studies were performed in water, in sodium dodecyl sulfate (SDS), and in dodecylphosphocholine (DPC) micelles that mimic bacterial and mammalian membranes, respectively.<sup>[27]</sup> The secondary structure content was predicted based on the CD spectra from 200 to 260 nm using the online server for protein secondary structure analyses, DichroWeb.<sup>[28]</sup>

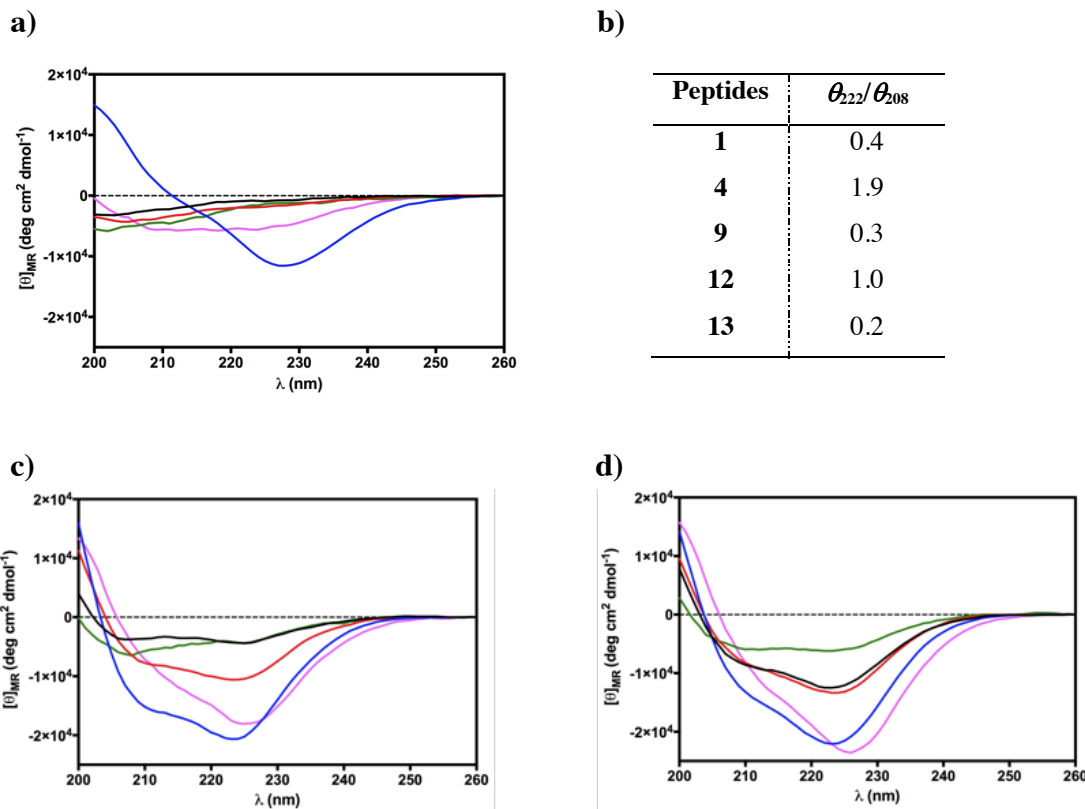


**Figure 4.** Panel A reports CD spectra of peptide **1** and its cyclic analogues **4**, **9**, **12** and **13** in water (**1**, black line; **4**, blue line; **9**, red line; **12**, magenta line; **13**, green line). Panel B reports the ratio of the ellipticities at 222 and 208 nm, which discriminates between monomeric and oligomeric states of helices for peptides **1**, **4**, **9**, **12** and **13**. Panels C and D report CD spectra of peptides **1**, **4**, **9**, **12** and **13** in SDS and in DPC micelles, respectively (**1**, black line; **4**, blue line; **9**, red line; **12**, magenta line; **13**, green line).

The algorithm CONTIN-LL was used to the values of  $\text{nrmsd} < 0.100$ ; instead, for the values of  $\text{nrmsd} > 0.100$  the algorithm CDSSTR was used.<sup>[28,29]</sup> CD spectra in water revealed the prevalence of disordered conformers for compounds **1**, **9**, **12**, **13** with a minimum close to 200 nm (Figure 4, panel a). As depicted in Figure 4, the Glu<sup>6</sup>-Lys<sup>10</sup> lactam crosslinked peptide **4** showed a strong  $\alpha$ -helicity in water with an intense minimum close to 222 nm and a positive maximum at 200 nm. Since the shape of CD spectra suggested the presence of  $\alpha$ -helix aggregates, we calculated the ratio of the ellipticities at 222 and 208 nm, which helps in discriminating between monomeric and oligomeric states of helices.<sup>[30]</sup> In fact, the ratio  $\theta_{222}/\theta_{208}$  calculated for peptide **4** was

greater than 1.0 (Figure 4, panel b), indicating an  $\alpha$ -helical conformation in its oligomeric state; instead other peptides were in a monomeric state as the ratio  $\theta_{222}/\theta_{208}$  is lower than 0.8.

**Table 3.** Secondary structure percentages of TL analogues.

Pept	Water				SDS solution				DPC solution			
	<i>h</i>	<i>b</i>	<i>t</i>	<i>r</i>	<i>h</i>	<i>b</i>	<i>t</i>	<i>r</i>	<i>h</i>	<i>b</i>	<i>t</i>	<i>r</i>
<b>1</b>	3	37	21	38	28	22	15	34	53	16	12	18
<b>4</b>	43	26	11	20	82	3	10	5	75	5	7	13
<b>9</b>	6	28	16	49	48	20	15	16	56	16	10	19
<b>12</b>	23	20	16	41	63	4	5	28	88	7	5	0
<b>13</b>	8	22	19	50	25	20	17	37	32	16	17	35

Instead, hydrocarbon-bridged peptide **12** was less helical and less structured in water, with weak ellipticity at 220 nm, no maximum at 190 nm, and a negative minimum at 200 nm. Relative to the helical percentage of the lactam-stapled peptide (**4**) of about 43%, peptides **12** had a reduced helicity of 23%, according to the DichroWeb prediction (Table 3). Regarding CD spectra in SDS micelles, all peptides showed two minima close to 208 and 222 nm indicating a high helical propensity, with the exception of disulfide bridged peptide **13** (Figure 4, panel c). CD spectra of peptide **13** and its linear precursors **1** showed a weak ellipticity at 208 nm and a helical percentage of 25% and 28%, respectively, according to the DichroWeb prediction (Table 3). This result revealed that the disulfide bridge did not induce a strong helicity in  $i,i+4$  positions since there is no difference in helical content with its linear precursor **1**. In presence of 20mM SDS, the Glu<sup>6</sup>-Lys<sup>10</sup> lactam crosslinked peptide **4** and hydrocarbon-stapled peptide **12** showed the highest content of  $\alpha$ -helix about of 82% and 63%, respectively, followed by 1,4-triazolic-bridged peptide **9** with an  $\alpha$ -helical content of 48% according to the DichroWeb prediction (Table 3). These results combined with antimicrobial activities of  $\alpha$ -helical stapled peptides **4** and **9** have suggested a high correlation between secondary structure and biological activity, as an increase of  $\alpha$ -helix stabilization has promoted an improvement of

antibacterial activity against Gram-positive strains, regardless of the percentage of  $\alpha$ -helical content. Instead, although hydrocarbon-bridged peptide **12** has a high helical content (63%) in SDS micelles, it was resulted to be inactive both on Gram-positive and Gram-negative strains due to its high hydrophobicity given by hydrocarbon cross-link and phenylalanine (Phe<sup>1</sup> and Phe<sup>5</sup>) zipper. Interestingly, there is not a clear relationship between  $\alpha$ -helix stabilization and the antibacterial activity on Gram-negative bacteria. In fact, triazole-bridged peptide **9** has completely lost the activity towards Gram-negative differently from lactam-bridged peptide **4** that showed a weak activity against *E. coli* ATCC 25922 but a strong activity against *Ac. baumannii* ATCC 19606. In this context, we investigated the changes in secondary structures in presence of liposomes mimicking Gram-positive and mimicking Gram-negative membranes. The higher helical content (47%) of lactam-bridged peptide **4** than triazole-peptide **9** (23%) in presence of LUVs mimicking Gram-negative suggested that the strongest  $\alpha$ -helix stabilization induced by lactam bridge allowed to conserve the activity against Gram-negative. Besides, peptides **1**, **4** and **9** displayed a similar helical content in LUVs mimicking Gram-positive. In addition, the value of the ratio between  $\theta_{222}/\theta_{208}$  is higher than 1 both in LUVs mimicking Gram-positive and LUVs mimicking Gram-negative, thus confirming  $\alpha$ -helical conformation in an oligomeric state for all peptides (Figure 5, panel a and b).

In DPC micelles peptides **4**, **9**, **12**, **13** displayed similar behavior. CD spectra of all peptides revealed two minima close to 208 and 222 nm, indicating helical propensity (Figure 4, panel d). CD spectra showed that disulfide-bridged peptide **13** was less helical in DPC with weak ellipticity at 220 nm and a percentage of helical content of about 32% according to the DichroWeb prediction. As reported in table 3, lactam-stapled peptide **4** and hydrocarbon-stapled peptide **12** displayed the highest content of  $\alpha$ -helix about 75% and 88%, respectively, followed by triazole-bridged peptide **9** with a helical content of 56%. These results showed that there is not a correlation between cytotoxicity and helical content, since lactam-stapled peptide **4** with the

highest helical content was resulted to be the least cytotoxic, even to a high concentration of 50  $\mu\text{M}$ .

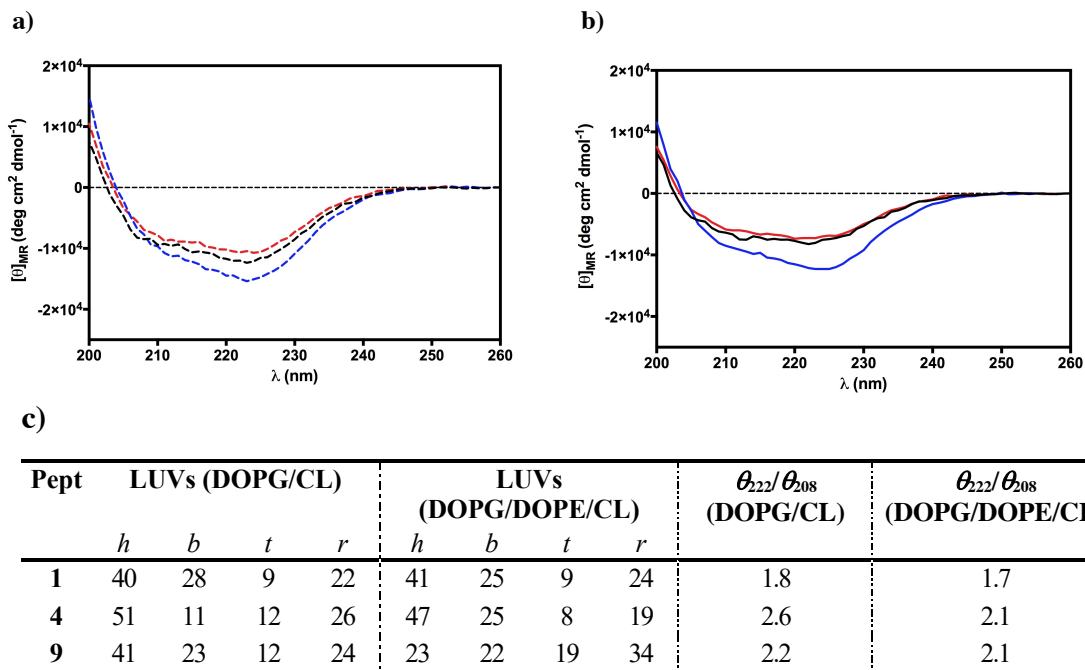


**Figure 5.** Panels A and B report CD spectra of peptides **1**, **4** and **9** in LUVs mimicking Gram-positive and Gram-negative membrane, respectively (**1**, black line; **4**, blue line; **9**, red line; **12**, magenta line; **13**, green line). Panel C reports the ratio of the ellipticities at 222 and 208 nm, which discriminates between monomeric and oligomeric states of helices for peptides **1**, **4** and **9**.

#### 5.2.4. MODE OF ACTION STUDIES

**Membrane fluidity.** The mechanism of action underlying the antimicrobial activity of lactam-bridged peptide **4** endowed with an overall higher antibacterial activity and lower cytotoxicity in comparison to **1** was then investigated.

First off, a membrane fluidity study was performed using Laurdan as a membrane probe. Laurdan has the capacity to insert into membranes and to distribute between liquid phases,<sup>[31]</sup> and has a spectral sensitivity to changes of phospholipid phase state.<sup>[32]</sup> The emission spectrum of Laurdan is at 490 nm when phospholipids are in a disordered phase and it shifts to 440 nm when lipids are in a more packed phase.



The Generalized Polarisation (GP) parameter was used to measure quantitatively the emission shift of the Laurdan probe.<sup>[32]</sup> The variation of fluidity membrane in presence of peptide was evaluated at 5 and 30  $\mu$ M.

**Table 4.** Membrane fluidity evaluation using the GP value.

<i>GP<sub>laurdan</sub></i>			
<b>Cmpd</b>	<b>DOPG/CL</b>	<b>DOPG/CL + cmpd<sup>a</sup></b>	<b>DOPG/CL+cmpd<sup>b</sup></b>
<b>1</b>	-0.32	-0.19	0.03
<b>4</b>	-0.32	-0.23	0.04
<i>GP<sub>laurdan</sub></i>			
<b>Cmpd</b>	<b>DOPG/DOPE/CL</b>	<b>DOPG/DOPE/CL + cmpd<sup>a</sup></b>	<b>DOPG/DOPE/CL + cmpd<sup>b</sup></b>
<b>1</b>	-0.14	-0.1	0.05
<b>4</b>	-0.14	-0.07	0.1

cmpd<sup>a</sup>: concentration is 5 $\mu$ M; cmpd<sup>b</sup>: concentration is 30 $\mu$ M

LUVs composed of DOPG/CL (58/42) mimicking Gram-positive membrane and DOPG/DOPE/CL (63/23/12) mimicking Gram-negative membrane were prepared. LUVs fluidity was evaluated before and after the addition of lactam-bridged peptide **4** and its linear precursor **1** at 25°C. Before the addition of peptides, LUVs emission mimicking both Gram-positive and Gram-negative membranes indicated the presence of a disordered phase with a maximum at 490 nm (Table 4). The membrane fluidity was not significantly changed in presence of cyclic peptide **4** and its precursor **1** at a concentration of 5  $\mu$ M; in fact, GP parameter indicated the presence of a disordered phase both for Gram-positive and Gram-negative liposomes (Table 4). Interestingly, a significant shift of the GP value towards more ordered membranes of both membranes mimicking Gram-positive and Gram-negative bacteria was observed at a concentration of 30  $\mu$ M of both peptides.

**Peptide aggregation.** The tendency of the peptide to form aggregates in the bacterial membrane was detected using Thioflavin T (ThT) as the fluorescent probe.<sup>[33]</sup> The lactam-stapled peptide (**4**) and the parent peptide **1** showed similar behavior in presence of LUVs mimicking Gram-positive (DOPG/CL, 58/42) and LUVs mimicking Gram-negative (DOPG/DOPE/CL, 63/23/12). We observed a dramatic increase of fluorescence as a function of concentration for both peptides, indicating a progressive phenomenon of aggregation in LUVs (Figure 6).

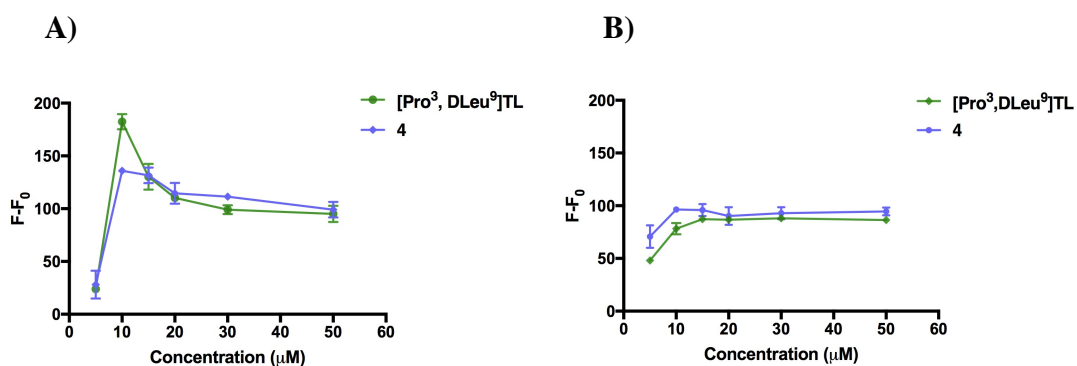


**Figure 6.** Peptide aggregation by monitoring ThT emission in presence of LUVs mimicking Gram-positive (**A**) and Gram-negative (**B**) membranes.  $F$  indicates the value of fluorescence intensity after peptide addition and  $F_0$  the initial fluorescence in the absence of peptide on the y-axis.

In particular, lactam-bridged peptides **4** and its linear precursor **1** produced a drastic increase of fluorescence at the concentration of 10  $\mu\text{M}$  in presence of LUVs mimicking Gram-positive, indicating that both peptides oligomerize significantly in liposomes (Figure 6, panel A). Remarkably, in liposomes mimicking Gram-negative membrane, we observed an intense increase of ThT fluorescence emission after the addition of both peptides at 5  $\mu\text{M}$  (Figure 6, panel B). These results suggested that both peptides have a notable tendency to oligomerize inside the bacterial membrane. Thus, by combining the membrane fluidity and oligomerization studies, we hypothesized a membrane-perturbing mechanism of lactam-bridged peptide **4** like its linear counterpart **1** as previously described,<sup>[18]</sup> consisting of the membrane interaction with a consequent aggregation inside the membrane and membrane disintegration via toroidal or barrel stave models.

### 5.2.5. LACTAMIZATION IMPROVES PROTEOLYTIC STABILITY

Despite several advantages in the use of peptides as drugs, their low proteolytic degradation remains a hard challenge. Macrocyclization strategies have been shown to increase peptide stability against proteolytic degradation,<sup>[35]</sup> in fact constrained peptides are not easily recognized by exo- and endopeptidase and result in more resistant towards proteolytic processing compared to their linear counterpart. In this context, we investigated the metabolic stability both of the lactam bridged peptide (**4**) and its linear precursor **1** (Figure 7). Peptides were incubated with 90% fresh human serum at  $37\pm 1$  °C within 12 hours. The percentage of the intact peptide was monitored by the peak area of the RP-HPLC performed on a Phenomenex Kinetex column (4.6 mm x 150 mm, 5  $\mu$ m, C18) chromatograms using a linear gradient from 10 to 90% MeCN (0.1% TFA) in water (0.1% TFA) over 20 min (flow rate of 1 mL/min, and absorbance detection at 220 nm). The data revealed that lactam-bridged peptide (**4**) had higher proteolytic stability than linear precursor; in fact, ~ 60% of the linear peptide was degraded within 45 min, whereas nearly about of 68% of lactam-stapled peptide (**4**) was intact after 2h of incubation (Figure 7). Interestingly, a percentage of about 50% of peptide **4** was detected after 6h of treatment with human serum. These results showed that lactamization could be an efficacious strategy to reduce protease susceptibility typical in AMPs.

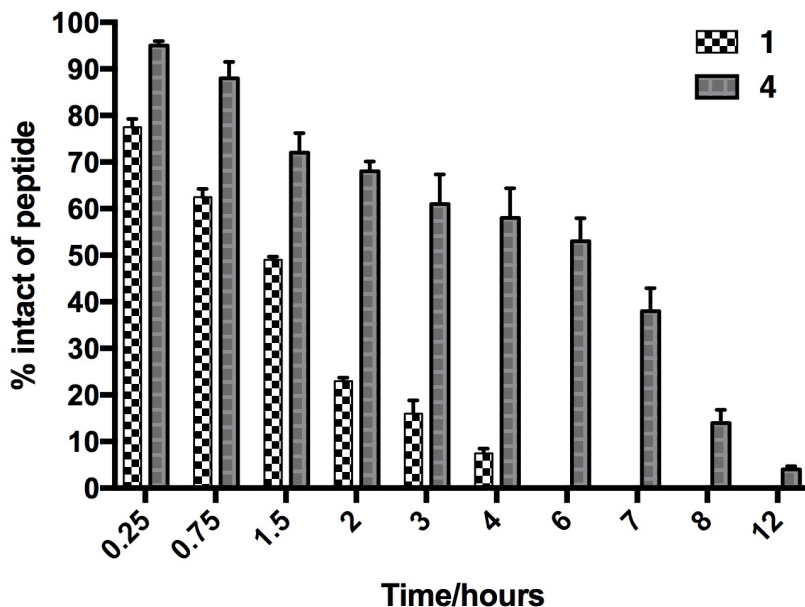


**Figure 7.** The percentage intact of lactam-stapled peptide (**4**) and its linear precursor (**1**) by an incubation with 90% human serum at  $37\pm 1$  °C at different times (0.25h, 0.75h, 1.5h, 2h, 3h, 6h, 7h, 8h and 12h).

### 5.3. CONCLUSIONS

In conclusions, by a constriction of  $\alpha$ -helix structure of [Pro<sup>3</sup>,DLeu<sup>9</sup>]TL analogue (**1**) using different side chain cross-links, including lactam-, 1,4-triazolic-, hydrocarbon- and disulfide bridges, we developed the first-in-class cyclic Temporin L antimicrobial analogue (**4**) with a good biological profile. This peptide (**4**) bearing lactam bridge between side chains of Lys<sup>6</sup> and Glu<sup>10</sup> showed the highest helical content both in aqueous solution and in SDS micelles and an improved antimicrobial activity against Gram-positive strains and *Ac. baumannii* ATCC 19606 (Gram-negative strain). Interestingly, peptide **4** did not show significant cytotoxicity on human keratinocytes even at a high concentration of 50  $\mu$ M and has high proteolytic stability within 6h. These results demonstrated a strong correlation between secondary structure and antimicrobial activity. Moreover, the fluorescence assays focused on antimicrobial mechanism showed that peptide **4** like its linear precursor

**1** interacts with the bacterial membrane, influencing the membrane stability and oligomerizing in LUVs mimicking Gram-positive and Gram-negative membranes. Finally, the data suggest that this lactam-bridged peptide **4** has the characteristics desired to be good candidate in the development of novel antimicrobial agents for topical applications.

#### 5.4. FUTURE PERSPECTIVE

The lactam-bridged peptide **4** represents our lead compound to perform chemical modifications to improve the antimicrobial activity against Gram-negative strains, considering that are more resistant and more difficult to tackle than Gram-positive strains. A synthetic strategy could be a replacement of lactam bridge with a positive charged bridge in order to increase peptide cationicity, as is typically considered the driving force for the interaction with bacterial membrane. In this context, we designed and synthesized guanidine-bridged peptide **14** bearing a guanidinium bridge in positions 6 and 10, which has a net positive charge of +4 in comparison to lactam-bridged peptide **4** featured by a net positive charge of +3. Preliminary antibacterial results on some Gram-positive and Gram-negative strains have shown an activity 4-fold stronger on *E. coli* ATCC 25922 (MIC of 6.25  $\mu\text{M}$ ) than lactam-bridged peptide **4** (MIC of 25  $\mu\text{M}$ ) and a slightly improved activity against *Ac. baumannii* ATCC 19606 (MIC of 1.56  $\mu\text{M}$ ) in comparison with peptide **4**. Additionally, the guanidine-bridged peptide **14** conserved a strong antimicrobial activity against *S. aureus* ATCC 25923 (MIC of 3.12  $\mu\text{M}$ ), *S. epidermidis* ATCC 12228 (MIC of 1.56  $\mu\text{M}$ ) and *Bac. megaterium* Bm11 (0.39  $\mu\text{M}$ ). These promising results suggested to investigate cytotoxicity of this peptide on human keratinocytes and to perform conformational studies by CD measurements to evaluate an  $\alpha$ -helix stabilization induced by a guanidinium cross-link.

## 5.5. EXPERIMENTAL SECTION

### 5.5.1. CHEMISTRY

**Materials.** All  $N^\alpha$ -Fmoc-protected amino acids were acquired from GL Biochem Ltd (Shanghai, China). The rink amide resin with a loading substitution of 0.72 mmol/g was purchased by Iris-Biotech GMBH. Anhydrous solvents [N,N-dimethylformamide (DMF), dichloromethane (DCM), 1,2-dichloroethane (DCE)] were obtained from Sigma-Aldrich/Merck. All useful reagents for the synthesis of cyclic peptides, such as 1,3-dimethylbarbituric acid, tetrakis(triphenylphosphine)palladium(0) [Pd(PPh<sub>3</sub>)<sub>4</sub>], ascorbic acid, copper (I) iodide, 2,4,6-collidine, 2,2,2-trifluoroethanol, were purchased from Sigma-Aldrich/Merck. Fmoc-Lys(Alloc)-OH, Fmoc-DLys(Alloc), Fmoc-Glu(OAll)-OH, Fmoc-DGlu(OAll)-OH, Fmoc-Pra-OH, Fmoc-L-Lys(N<sub>3</sub>)-OH, Fmoc, Lys(Mmt)-OH, N,N-diisopropylethylamine (DIEA), piperidine, and trifluoroacetic acid (TFA) were purchased from Iris-Biotech GMBH. (S)-Fmoc-2-(4'-pentenyl)alanine-OH was obtained by Okeanos Tech. Co.

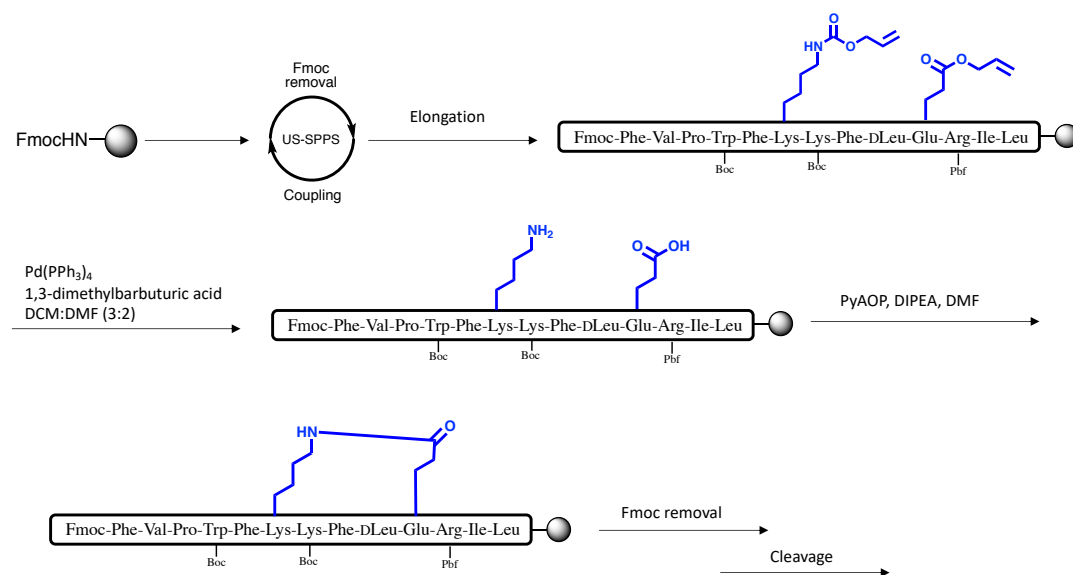
Phospholipids: 1,2-dioleoyl-sn-glycero-3-phosphoethanolamine (DOPE), 1,2-dioleoyl-sn-glycero-3-phospho-(1'-rac-glycerol) sodium salt (DOPG), and cardiolipin (CL) sodium salt (Heart, Bovine) were purchased from Avanti Polar Lipids (Birmingham, AL, USA), Phosphate-buffered saline (PBS) tablets were bought by Life Technologies Corporation. 8-aminonaphthalene-1,3,6-trisulfonic acid, disodium salt (ANTS) and p-xylene-bis-pyridinium bromide (DPX) were purchased from Molecular Probes. Thioflavin T, 6-dodecanoyl-N,N-dimethyl-2-naphthylamine (Laurdan), sodium dodecyl sulfate (SDS) and dodecylphosphocholine (DPC) were purchased by Sigma-Aldrich-Merck. Human serum from human male AB plasma, USA origin, sterile-filtered was obtained by Sigma-Aldrich-Merck.

**Construction of linear peptide sequences.** Prior cyclization, the peptide sequences were assembled stepwise relying on the ultrasound-assisted solid-phase peptide

synthesis (US-SPPS), performed in combination with the Fmoc-based protection strategy.<sup>[36]</sup> The elongation of linear sequence was carried out as previously described in Chapter 3.

***Side chain-to-side chain tethering by lactamization.*** The synthesis of side-chain to side-chain lactam bridged cyclic peptides (**2–7**) was performed on the resin by cyclization between the side-chain amino group of a lysine residue and the side-chain carboxyl group of a glutamic acid residue in *i, i+4* positions. Fmoc-Glu(OAll) and Fmoc-Lys(Alloc) were selected like lactam precursors. After linear assembly, the simultaneous deprotection of the allyl and alloc functional groups were carried out in orthogonal condition with respect to the Fmoc/*t*Bu.<sup>[37]</sup> The resin was treated with a solution of Pd(PPh<sub>3</sub>)<sub>4</sub> (0.15 equiv) and 1,3-dimethylbarbituric acid (3 equiv) in DCM/DMF (3:2 *v/v*) and gently shaken for 1 h under argon (Scheme 1). The resin was filtered, washed with DMF (3 × 2 mL) and DCM (3 × 2 mL) and dried. Then, the deprotection procedure was repeated for the second time as described above. After the washing with DCM (3 × 2 mL) and DMF (3 × 2 mL) and a solution of 0.5% of sodium *N,N*-diethyldithiocarbamate in DMF (2×30min), the complete removal was monitored by LC-MS analysis of the residue obtained from the cleavage of an aliquot of resin [5 mg treated with 1 mL of TFA/TIS/H<sub>2</sub>O (95:2.5:2.5, *v/v/v*)], and by Kaiser test, giving colorless beads for the presence of free primary ε-amine group in lysine side chain. The side chain to side chain cyclization on the resin was performed by using PyBop (2 equiv) and DIEA (4 equiv), which are known effective coupling reagents for the intramolecular amide bond formation and using DMF/DCM (1:1, *v/v*) as solvents, for 12h at room temperature (Scheme 1). After washing DMF (3 × 2 mL) and DCM (3 × 2 mL), this coupling was ascertained by LC-MS and by Kaiser test. Finally, the N-terminal Fmoc group was removed and the peptidyl-resin was washed three times with DCM and dried in vacuo. The peptides **2–7** were cleaved from the resin and simultaneously deprotected by treatment with a

cocktail of TFA/TIS/H<sub>2</sub>O (95:2.5:2.5, v/v/v) at rt for 3 h. Then, the resin was removed by filtration and crude peptides were precipitated and washed with chilled Et<sub>2</sub>O twice and were separated by centrifugation (2 × 15min, 6000 rcf). The supernatants were removed, the crude peptides were dried in vacuo and then were dissolved in 10% MeCN in H<sub>2</sub>O and purified by HPLC preparative.

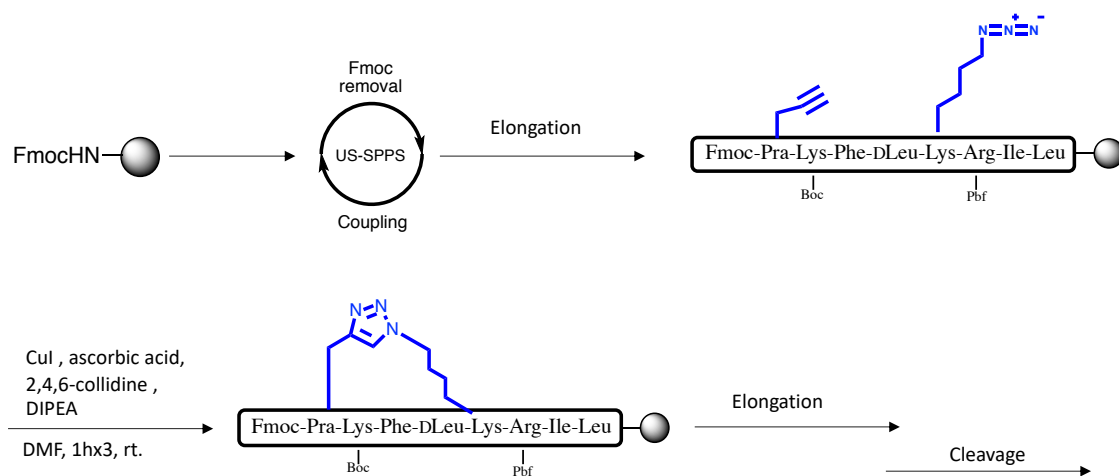


**Scheme 1.** Synthesis of lactam-bridged peptide 4.

**On resin “Click” construction of 1,4-triazolic-bridged peptides 7–11.** Copper (I)-catalysed azide-alkyne cycloaddition on solid phase (CuAAC-SP) was used to obtain the selective formation of 1,4-disubstituted [1,2,3]-triazole regioisomer. The side chain-to-side chain CuAAC-SP cyclization was performed between alkyne moiety in propargylalanine<sup>6</sup> side chain and azido moiety in lysine<sup>10</sup> side chain (Scheme 2). The linear peptide sequence (0.1 mmol) was assembled until Fmoc-Pra<sup>6</sup> following the US-SPPS procedure, CuAAC-SP was achieved using following protocol: copper iodide (1 equiv) as the catalyst and ascorbic acid (3 equiv) were dissolved in DMF (3 ml) and then 2,4,6-collidine (5 equiv) and DIEA (10 equiv) were added.<sup>[38]</sup> The solution was added to the resin placed in SPPS reactor and gently shaken for 1 h, at



rt. After the first cycle, the resin was washed with DCM and DMF and the CuAAC-SP procedure was repeated two more times as described above. The complete formation of 1,4-triazole bridge was monitored by retention time shifts by LC-MS analysis of a residue obtained from the cleavage of an aliquot of resin. After the complete conversion by CuAAC-SP, the synthesis was proceeded by US-SPPS protocol until Fmoc-Phe. Ultimately, the N-terminal Fmoc group was removed and the 1,4-disubstituted [1,2,3]-triazole peptide **15** was released from the resin and the protecting groups were removed using a cocktail of TFA/TIS/H<sub>2</sub>O (95:2.5:2.5 v/v/v) at rt for 3 h.

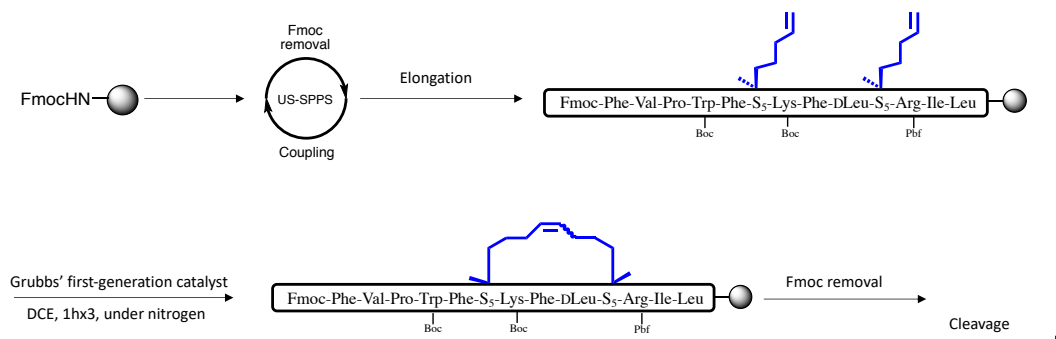


**Scheme 2.** Synthesis of 1,4-triazolic bridged-peptide **9**.

### ***Synthesis of hydrocarbon-bridged peptide 12 via Ring Closing Metathesis (RCM).***

During the construction of linear peptide sequence, Fmoc-S<sub>5</sub>-OH residues were incorporated in *i,i+4* positions for the formation of olefin bridge. The ring closing metathesis was carried on resin-bound on fully protected peptide. Once the peptide was assembled until Fmoc-Phe, the resin was washed with DCM and DCE.<sup>[39]</sup> The resin was treated with a fresh catalyst solution (3 mL) of a 6mM solution of Grubbs'

first-generation catalyst in DCE ( 4.94 mg×mL<sup>-1</sup>, 20 mol% relative to the resin substitution) (Scheme 3).



**Scheme 3.** Synthesis of hydrocarbon-bridged peptide **12**.

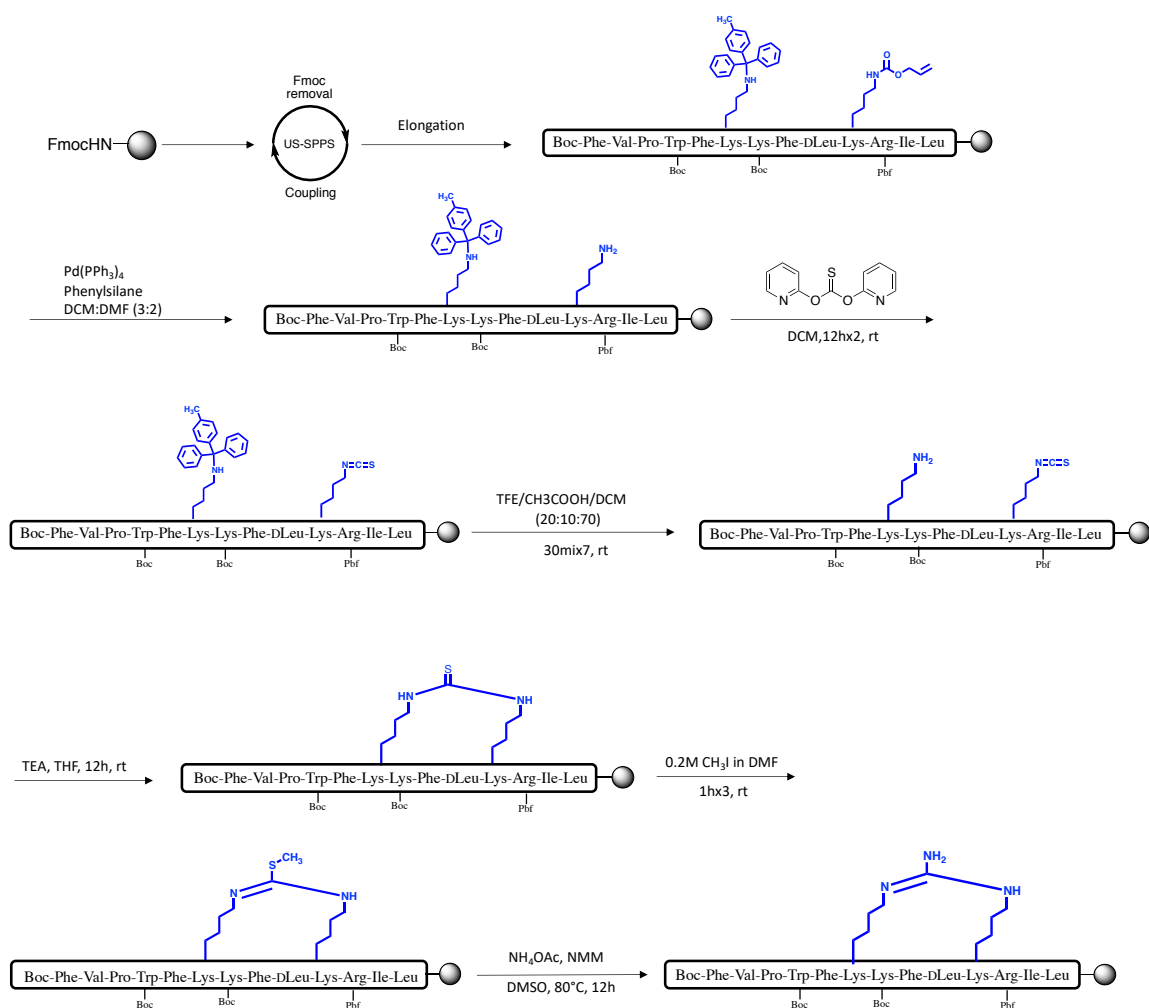
The resulting suspension was gently agitated under constant nitrogen flow for 2h. After the first round, the RCM reaction was repeated twice in the same condition. In the end of three cycles, the resin was washed with DCE (3 × 1min) and DCM (3 × 1min) and then dried under a stream of nitrogen. The conversion in olefin bridge was monitored by LC-MS and HPLC profile did not show two product peaks corresponding olefin isomers in a gradient of 30 minutes. Finally, the N-terminal Fmoc group was removed and the stapled peptide **12** was released from the resin by the treatment with a cocktail of TFA/TIS/H<sub>2</sub>O (95:2.5:2.5 v/v/v) at rt for 3 h.

**Disulfide stapling of peptide 13.** The synthesis of disulfide bridge between two cysteine residues in *i,i+4* positions was achieved by N-chlorosuccinimide (NCS) oxidation in solution.<sup>[40]</sup> After the synthesis and the fully cleavage of linear peptide sequence, the crude peptide with a purity > 90% was dissolved in H<sub>2</sub>O (C<sub>f</sub>=0.5mM) and a solution containing NCS (1 equiv) in H<sub>2</sub>O (5 ml) was added under stirring. The mixture was shaken for 15 minutes at room temperature and lyophilized. The

oxidation by NCS was monitored by LC-MS and subsequently the peptide **13** was purified by preparative HPLC.

**Synthesis of guanidine-bridged peptide 14.** Two orthogonally protected diaminoacyl residues, Fmoc-Lys(Alloc)-OH and Fmoc-Lys(Mmt)-OH, were selected and incorporated in linear peptide sequence by US-SPPS strategy. The elongation of linear peptide sequence was carried out using US-SPPS protocol and Boc-Phe was used as N-terminal amino acid because the guanidinylation step requires basic conditions deprotecting easily Fmoc group. After washing with DCM and DMF, alloc group in Lys<sup>10</sup> side chain was deprotected using a solution of Pd(PPh<sub>3</sub>)<sub>4</sub> (0.15 equiv) and phenylsilane (3 equiv) in DCM/DMF dry (3:2 v/v) and shaken gently the resin for 1h under argon (Scheme 4). Then, the resin was washed with DMF and DCM, and the deprotection procedure was repeated for the second time. The complete removal was monitored by LC-MS analysis of the residue obtained from the cleavage of an aliquot of resin (5 mg). The free amino group in Lys<sup>10</sup> side chain was converted to isothiocyanate by reaction with di-2-pyridylthionocarbonate (5 equiv) in DCM for 12h at room temperature.<sup>[41]</sup> The complete conversion was observed after two treatments and was monitored by LC-MS analysis. The Mmt group in Lys<sup>6</sup> side chain was removed by seven 30 min treatments with a cocktail of TFE/CH<sub>3</sub>COOH/DCM (20:10:70, v/v/v). The Mmt deprotection was monitored by LC-MS analysis, performing an acetylation test on free amino group by a treatment of a small aliquot of resin with a solution of Ac<sub>2</sub>O (2 equiv) and DIEA (4 equiv) in DMF (2×5min). After the complete Mmt deprotection, the thiourea bridge was carried out conditioning the resin in THF and adding TEA (10 equiv) for 12h at room temperature. S-methylation of thiourea was achieved treating the resin with a solution 0.2M of CH<sub>3</sub>I in DMF three times for 1h at rt. The conversion of S-Me-isothiourea bridge in guanidine bridge was performed by the treatment of the resin with a 2M solution of ammonium acetate (NH<sub>4</sub>OAc) in DMSO (3mL) and morpholine (1 equiv) was added, for 12h at 80°C. The complete

conversion was achieved after two treatment of 12h. Every step reactions were monitored by LC-MS. In the end, the peptide **14** was released from the resin and the protecting groups were removed using a cocktail of TFA/TIS/H<sub>2</sub>O (95:2.5:2.5 v/v/v) at rt for 3 h.



**Scheme 4.** Synthesis of guanidine-bridged peptide **14**.

**Peptide purification.** Purification of peptides **2–14** was performed by RP-HPLC (Shimadzu Preparative Liquid Chromatograph LC-8A) equipped with a preparative column (Phenomenex Kinetex C18 column, 5  $\mu\text{m}$ , 100  $\text{\AA}$ , 150 x 21.2 mm) using

linear gradients of MeCN (0.1% TFA) in water (0.1% TFA), from 10 to 90% over 30 min, with a flow rate of 10 mL/min and UV detection at 220 nm.

**Table 5.** Analytical data of peptides 2–14.

Peptides	R <sub>t</sub> (min)	MS Calcd	MS Found
2	11.6	1620.9	[M+2H] <sup>+/2</sup> =811.9
3	11.4	1586.9	[M+2H] <sup>+/2</sup> =794.5
4	13.9	1704.1	[M+2H] <sup>+/2</sup> =853.0
5	11.3	1587.9	[M+2H] <sup>+/2</sup> =794.9
6	14.7	1514.9	[M+2H] <sup>+/2</sup> =757.9
7	11.6	1630.9	[M+2H] <sup>+/2</sup> =816.5
8	11.3	1596.9	[M+2H] <sup>+/2</sup> =799.9
9	14.5	1714.1	[M+2H] <sup>+/2</sup> =858.0
10	13.2	1596.9	[M+2H] <sup>+/2</sup> =799.9
11	11.7	1523.9	[M+3H] <sup>+/3</sup> =508.3
12	14.9	1714.0	[M+2H] <sup>+/2</sup> =858.3
13	12.9	1669.1	[M+2H] <sup>+/2</sup> =835.3
14	13.2	1746.2	[M+3H] <sup>+/3</sup> =583.0

Final products were obtained by lyophilization of the appropriate fractions after removal of the MeCN by rotary evaporation. All peptides were characterized by RP-HPLC using linear gradients of MeCN (0.1% TFA) in water (0.1% TFA), from 10 to 90% over 20 min (Table 5). All compounds examined for biological activity were purified to >96%.

## 5.5.2. BIOLOGY

**Antimicrobial and cytotoxicity assays.** Minimal inhibitory concentrations (MIC) of all the peptides were determined in Mueller–Hinton medium by the broth microdilution assay as described in Chapter 2.<sup>[18]</sup>

The hemolytic assay and the colorimetric MTT assay were carried out following the procedures described in Chapter 2.<sup>[22]</sup>

**Proteolytic stability assays.** Human serum from human male AB plasma was acquired by Sigma-Aldrich-Merck. The proteolytic stability of linear peptide **1** and

lactam bridged analogue **4** was determined by employing the analytical RP-UHPLC was performed on a Shimadzu Nexera, equipped with a Phenomenex Kinetex column (C18, 4.6 mm x 150 mm, 5 mm) and H<sub>2</sub>O (0.1% TFA) and MeCN (0.1% TFA) as eluents. The procedure was in detail described in Chapter 3.

### **5.5.3. LAURDAN AND THIOFLAVIN T ASSAYS.**

Laurdan is extensively used as fluorescent probe in membrane fluidity study,<sup>[31]</sup> while the fluorescent dye Thioflavin T (ThT) is widely used to quantify peptide aggregation in presence of bacterial membranes.<sup>[32]</sup>

These assays for investigating the mechanism of action were performed according to the procedures described in Chapter 3.

### **5.5.4. CONFORMATIONAL ANALYSIS**

***Circular dichroism spectroscopy.*** CD spectra for peptides **4, 9, 12, 13** were recorded using quartz cells of 0.1 cm path length with a JASCO J-710 CD spectropolarimeter at 25°C. All spectra were measured in the 260-190 nm spectral range, 1 nm bandwidth, 4 accumulations and 100 nm/min scanning speed. Each peptide was dissolved in water to prepare a 1mM peptide stock solution. The CD spectra were performed in water, in SDS (20 mM) and in DPC (20 mM) using a peptide concentration of 50 μM. The secondary structure content of the peptides was predicted using On Line Circular Dichroism Analysis, DICHROWEB.<sup>[28]</sup> Input and output units, and the wavelength step were  $\theta$  (mdeg) and 1.0 nm, respectively. The algorithm used was CONTIN-LL and reference database was set-7.<sup>[29]</sup> When we have NRMSD > 0.100, we used the CDSSTR method.<sup>[30]</sup>

***Circular dichroism spectroscopy in SUVs.*** CD spectra using SUVs were recorded only for linear peptide **1**, cyclic peptides **4** and **9**. SUVs were prepared as reported: lipids (Gram-positive, DOPG/CL, 58/42 ratio in moles; Gram-negative

DOPG/DOPE/CL, 63/23/12 ratio in moles) were dissolved in chloroform and an identical volume of peptide solution dissolved in TFE was added. Then, the samples were vortexed and lyophilized overnight. CD spectra were recorded at a peptide concentration of 8  $\mu\text{M}$  and at a lipid final concentration of 100  $\mu\text{M}$ . For the measurement, the SUVs with peptide were rehydrated with phosphate buffer 5 mM, pH= 7.4 for 1h and sonicated for 30 min.<sup>[30]</sup> CD spectra were recorded at 25°C on a Jasco J-715 spectropolarimeter in a 1 cm quartz cell using 3 consecutive scans from 260 to 200 nm, 3 nm bandwidth, a time constant of 16s, and a scan rate of 10 nm/min.

## 5.6. REFERENCES

- [1] R. Jwad, D. Weissberger, L. Hunter. Strategies for fine-tuning the conformations of cyclic peptides. *Chem. Rev.* 2020, 120, 9743–9789.
- [2] K. Shinbara, W. Liu, R.H.P. van Neer, T. Katoh, H. Suga. Methodologies for backbone macrocyclic peptide synthesis compatible with screening technologies. *Front. Chem.* 2020, 8:447.
- [3] A.A. Vinogradov, Y. Yin, H. Suga. Macrocyclic peptides as drug candidates: recent progress and remaining challenges. *J. Am. Chem. Soc.* 2019, 141, 4167–4181.
- [4] Sim, S.; Kim, Y.; Kim, T.; Lim, S.; Lee, M. Directional Assembly of  $\alpha$ -Helical Peptides Induced by Cyclization. *J. Am. Chem. Soc.* 2012, 134, 20270-20272.
- [5] K.J. Skowron, T.E. Speltz, T.W. Moore. Recent structural advances in constrained helical peptides. *Med. Res. Rev.* 2019, 39, 749–770.
- [6] S. Kannan, P.G.A. Aronica, S. Ng, D.T. Gek Lian, Y. Frosi, S. Chee, J. Shimin, T.Y. Yuen, A. Sadruddin, H.Y.K. Kaan, A. Chandramohan, J.H. Wong, Y.S. Tan, Z.W. Chang, F.J. Ferrer-Gago, P. Arumugam, Y. Han, S. Chen, L. Rénia, C.J. Brown, C.W. Johannes, B. Henry, D.P. Lane, T.K. Sawyer, C.S. Verma, A.W. Partridge. Macrocyclization of an all-D linear  $\alpha$ -helical peptide imparts cellular permeability. *Chem. Sci.* 2020, 11, 5577–5591.
- [7] X. Jing, K. Jin. A gold mine for drug discovery: strategies to develop cyclic peptides into therapies. *Med. Res. Rev.* 2020, 40, 753–810.
- [8] D.S. Nielsen, N.E. Shepherd, W. Xu, A.J. Lucke, M.J. Stoermer, D.P. Fairlie. Orally absorbed cyclic peptides. *Chem. Rev.* 2017, 117, 8094–8128.
- [9] M.T. Lai, C.C. Yang, T.Y. Lin, F.J. Tsai, W.C. Chen. Depsipeptide (FK228) inhibits growth of human prostate cancer cells. *Urol. Oncol: Sem. Orig. Invest.* 2008, 26, 182–189.
- [10] F. Ikeda, S. Tanaka, H. Ohki, S. Matsumoto, K. Maki, M. Katashima, D. Barrett, D.; Y. Aoki. Role Of micafungin in the antifungal armamentarium. *Curr. Med. Chem.* 2007, 14, 1263–1275.

- [11] P. Gallay, K. Lin. Profile of alisporivir and its potential in the treatment of hepatitis C. *Drug Des. Dev. Ther.* 2013, 7, 105–115.
- [12] A. Luther, C. Bisang, D. Obrecht. Advances in macrocyclic peptide-based antibiotics. *Bioorg. Med. Chem.* 2018, 26, 2850–2858.
- [13] C.H. Chen, T.K. Lu. Development and challenges of antimicrobial peptides for therapeutic applications. *Antibiotics (Basel)*. 2020, 9: 24.
- [14] M.I. McLaughlin, W.A. van der Donk. The fellowship of the rings: macrocyclic antibiotic peptides reveal an anti-Gram-negative target. *Biochemistry*. 2020, 59, 343–345.
- [15] M.L. Mangoni, A.C. Rinaldi, A. Di Giulio, G. Mignogna, A. Bozzi, D. Barra, M. Simmaco. Structure function relationships of temporins, small antimicrobial peptides from amphibian skin. *Eur. J. Biochem.* 2000, 267, 1447–1454.
- [16] M.L. Mangoni, A. Carotenuto, L. Auriemma, M.R. Saviello, P. Campiglia, I. Gomez-Monterrey, S. Malfi, L. Marcellini, D. Barra, E. Novellino, P. Grieco. Structure-activity relationship, conformational and biological studies of Temporin L analogues. *J. Med. Chem.* 2011, 54, 1298–1307.
- [17] A. Carotenuto, S. Malfi, M.R. Saviello, P. Campiglia, I. Gomez-Monterrey, M.L. Mangoni, L. Marcellini, H. Gaddi, E. Novellino, P. Grieco. A different molecular mechanism underlying antimicrobial and hemolytic actions of temporins A and L. *J. Med. Chem.* 2008, 51, 2354–62.
- [18] P. Grieco, A. Carotenuto, L. Auriemma, M.R. Saviello, P. Campiglia, I. Gomez-Monterrey, L. Marcellini, V. Luca, D. Barra, E. Novellino, M.L. Mangoni. The effect of D-amino acid substitution on the selectivity of temporin L towards target cells: identification of a potent anti-candida peptide. *Biochim. Biophys. Acta.* 2013, 1828, 652–660.
- [19] M. Pelay-Gimeno, A. Glas, O. Koch, T.N. Grossmann. Structure-based design of inhibitors of protein–protein interactions: mimicking peptide binding epitopes. *Angew. Chem. Int. Ed. Engl.* 2015, 54, 8896–8927.
- [20] C.J. White, A.K. Yudin. Contemporary strategies for peptide macrocyclization. *Nat Chem.* 2011, 3, 509–524.
- [21] M.E. Jr. Houston, A.P. Campbell, B. Lix, C.M. Kay, B.D. Sykes, R.S. Hodges. Lactam bridge stabilization of  $\alpha$ -helices: the role of hydrophobicity in controlling dimeric versus monomeric- $\alpha$ -helices. *Biochemistry*. 1996, 35, 10041–10050.
- [22] F. Merlino, A. Carotenuto, B. Casciaro, F. Martora, M.R. Loffredo, A. Di Grazia, A.M. Yousif, D. Brancaccio, L. Palomba, E. Novellino, M. Galdiero, M.R. Iovene, M.L. Mangoni, P. Grieco. Glycine-replaced derivatives of [Pro<sup>3</sup>,DLeu<sup>9</sup>]TL, a temporin L analogue: evaluation of antimicrobial, cytotoxic and hemolytic activities. *Eur. J. Med. Chem.* 2017, 139, 750–761.
- [23] A.D. de Araujo, H.N. Hoang, W.M. Kok, F. Diness, P. Gupta, T.A. Hill, R.W. Driver, D.A. Price, S. Liras, D.P. Fairlie. Comparative  $\alpha$ -helicity of cyclic pentapeptides in water. *Angew. Chem. Int. Ed. Engl.* 2014, 53, 6965–6969.



- [24] J.W. Taylor. The synthesis and study of side-chain lactam-bridged peptides. *Biopolymers*. 2002, 66, 49–75.
- [25] Y. Tian, Y. Jiang, J. Li, D. Wang, H. Zhao, Z. Li. Effect of stapling architecture on physicochemical properties and cell permeability of stapled  $\alpha$ -helical peptides: a comparative study. *ChemBiochem*. 2017, 18, 2087–2093.
- [26] E. Buommino, A. Carotenuto, I. Antignano, R. Bellavita, B. Casciaro, M.R. Loffredo, F. Merlino, E. Novellino, M.L. Mangoni, F.P. Nocera, D. Brancaccio, P. Punzi, D. Roversi, R. Ingenito, E. Bianchi, P. Grieco, P. The outcomes of decorated prolines in the discovery of antimicrobial peptides from Temporin-L. *ChemMedChem*. 2019, 14, 1283–1290.
- [27] <http://dichroweb.cryst.bbk.ac.uk>.
- [28] L. Whitmore, B.A. Wallace. DICHROWEB, an online server for protein secondary structure analyses from circular dichroism spectroscopic data. *Nucleic Acids Res*. 2004, 32, 668–673.
- [29] N. Sreerama, R.W. Woody. Estimation of protein secondary structure from circular dichroism spectra: comparison of CONTIN, SELCON, and CDSSTR methods with an expanded reference set. *Anal. Biochem*. 2000, 287, 252–260.
- [30] S.Y. Lau, A.K. Taneja, R.S. Hodges. Synthesis of a model protein of defined secondary and quaternary structure. Effect of chain length on the stabilization and formation of two-stranded  $\alpha$ -helical coiled-coils. *J. Biol. Chem*. 1984;259, 13253–13261.
- [31] F.M. Harris, K.B. Best, J.D. Bell. Use of Laurdan fluorescence intensity and polarization to distinguish between changes in membrane fluidity and phospholipid order. *Biochim. Biophys. Acta*. 2002, 1565, 123–128.
- [32] T. Parasassi, G. De Stasio, G. Ravagnan, R.M. Rusch, E. Gratton. Quantitation of lipid phases in phospholipid vesicles by the generalized polarization of Laurdan fluorescence. *Biophys. J*. 1991, 60, 179–189.
- [33] C. Xue, T.Y. Lin, D. Chang, Z. Guo. Thioflavin T as an amyloid dye: fibril quantification, optimal concentration and effect on aggregation. *R. Soc. Open. Sci*. 2017, 4:160696.
- [34] N. Raheem, S.K. Straus. Mechanisms of action for antimicrobial peptides with antibacterial and antibiofilm functions. *Front. Microbiol*. 2019, 10:2866.
- [35] H. Li, Y. Hu, Q. Pu, T. He, Q. Zhang, W. Wu, X. Xia, J. Zhang. Novel stapling by lysine tethering provides stable and low hemolytic cationic antimicrobial peptides. *J. Med. Chem*. 2020, 63, 4081–4089.
- [36] F. Merlino, S. Tomassi, A.Y. Yousif, A. Messere, L. Marinelli, P. Grieco, E. Novellino, S. Cosconati, S. Di Maro. Boosting Fmoc solid-phase peptide synthesis by ultrasonication. *Org. Lett*. 2019, 21, 6378–6382.
- [37] F. Merlino, Y. Zhou, M. Cai, A. Carotenuto, A.M. Yousif, D. Brancaccio, S. Di Maro, S. Zappavigna, A. Limatola, E. Novellino, P. Grieco, V.J. Hruby. Development of macrocyclic peptidomimetics containing constrained  $\alpha,\alpha$ -

dialkylated amino acids with potent and selective activity at human melanocortin receptors. *J. Med. Chem.* 2018, 61, 4263–4269.

[38] V. Castro, H. Rodríguez, F. Albericio. CuAAC: An efficient click chemistry reaction on solid phase. *ACS Comb. Sci.* 2016, 18, 1, 1–14.

[39] Y.W. Kim, T.N. Grossmann, G.L. Verdine. Synthesis of all-hydrocarbon stapled  $\alpha$ -helical peptides by ring-closing olefin metathesis. *Nat. Protoc.* 2011, 6, 761–771.

[40] T.M. Postma, F. Albericio. N-Chlorosuccinimide, an efficient reagent for on-resin disulfide formation in solid-phase peptide synthesis. *Org. Lett.* 2013, 15, 3, 616–619.

[41] Y. Touati-Jallabe, E. Bojnik, B. Legrand, E. Mauchauffée, N.N. Chung, P.W. Schiller, S. Benyhe, M.C. Averlant-Petit, J. Martinez, J.F. Hernandez. Cyclic enkephalins with a diversely substituted guanidine bridge or a thiourea bridge: synthesis, biological and structural evaluations. *J. Med. Chem.* 2013, 56, 5964–5973.

## **PART II**

### *Anticancer Peptidomimetics*

*Project was supported by grant “Programma Star Linea 2, Mobilità Giovani Ricercatori”, University of Naples, Federico II.*

## ABSTRACT

Aberrant activation of signaling by the Wnt/ $\beta$ -catenin pathway is strongly implicated in the onset and progression of numerous types of cancer.  $\beta$ -Catenin serves as a central hub in Wnt signaling by engaging in crucial protein–protein interactions with both negative and positive effectors of the pathway. In cancer therapy, the most promising strategy to challenge the oncogenic Wnt signaling cascade consists in targeting and inhibiting directly oncoprotein  $\beta$ -catenin due to its overexpression with resultant overactivation of transcriptional machinery. In this light, our studies have been focused on the design and synthesis of stapled bicyclic peptidomimetics, as successful results related to inhibition of Wnt/ $\beta$ -catenin pathway have been recently achieved with the use of stapled peptides as PPI inhibitors. By combining hydrocarbon stapling and head-to-tail cyclization strategies, we synthesized a series of stapled bicyclics that differ in bridge length and double-bond position. Our results have highlighted a significant enhancement of binding activity towards  $\beta$ -catenin and potent inhibition of  $\beta$ -catenin/E-cadherin interaction only for the stapled bicyclic bearing an olefin bridge of 9-carbons length, thus suggesting a tight correlation between conformation and binding activity.

In addition, in order to promote a potent and selective inhibition of  $\beta$ -catenin, we probed a chemical ligation strategy to synthesize a bivalent inhibitor peptide. In our design, we chose a strain-promoted cycloaddition to tether two peptide inhibitors of  $\beta$ -catenin which bind two different binding sites. The two peptides were previously labeled with appropriate handles and then stitched together by a linker of optimized length. The resulting bivalent peptide showed a strong binding activity and a high affinity towards  $\beta$ -catenin.

# **CHAPTER 1**

## **INTRODUCTION**

## 1. 1. PROTEIN-PROTEIN INTERACTIONS

Protein-protein interactions (PPIs) constitute the backbone of signal transduction pathways and networks in physiological processes, including cell proliferation, cell division, transcription, translation and programmed cell death.<sup>[1,2]</sup> A large number of PPIs are involved in the various pathological states associated with the development of human diseases, such as neurodegeneration, cardiovascular disease, and cancer.<sup>[3]</sup> The acquisition of hallmark features of cancer (*e.g.* tumorigenesis, uncontrolled cell proliferation) is determined by a combination of genetic and epigenetic alterations, through inactivation or activation of signaling PPIs networks.<sup>[4]</sup> Targeting and modulating the “undruggable” PPIs represents a promising approach to switch-off the transmission of oncogenic signals.<sup>[5,6]</sup> The classic small molecule drug discovery approach is widely used for PPIs inhibition, however, small molecular scaffolds typically cover a smaller surface area (100–600 Å) than the expansive interfacial area (800-2000 Å) of PPIs.<sup>[7-9]</sup> Promising progress have also been achieved with designing peptides and antibodies as PPIs disruptors.<sup>[10,11]</sup> Despite they adapt better to PPIs interfaces because of their large molecular size, numerous challenges remain to be overcome due to their intrinsic biochemical properties.<sup>[12]</sup> For instance, antibodies have specific drawbacks such as high production costs, lack of oral bioavailability and poor cell penetration. While peptides, albeit poor proteolytic stability against circulating proteolytic enzymes and an intrinsic inability to penetrate cell membranes, exhibit significant advantages, including direct similarity to protein fragments, affordable synthesis and the possibility to incorporate a wide variety of functional groups.<sup>[14,15]</sup> Among the various peptides developed as PPI inhibitors, stapled peptides have attracted particular attention for their remarkable pharmacological performance, by owing their improved target affinity, increased cell penetration, and protection against proteolytic degradation. The all-hydrocarbon stapling technique developed by Verdine and co-workers in 2000,<sup>[16]</sup> confers a

significant increase of peptide helicity and reinforcement of the  $\alpha$ -helix conformation, which is typically engaged in PPI interfaces. Promising results have been achieved using this approach for the design of potent peptide inhibitors as potential therapeutics targeting extra/intracellular PPIs in cancer therapy. For instance, BID SAHBA and ALRN-6924 are stapled peptides targeting intracellular BCL-XL and MDM2/MDMX, respectively, and ALRN-6924 has actually already advanced to phase 2 clinical trials for treating solid tumors and lymphomas.<sup>[17,18]</sup> Nevertheless, stapled peptides still encounter huge challenges, since in some cases their poor proteolytic stability did not allow to produce a long-lived PPI inhibition *in vivo* application.<sup>[19]</sup>

## **1.2. WNT/ $\beta$ -CATENIN SIGNALING**

The Wnt/ $\beta$ -catenin signaling pathway plays important role in embryonic development and tissue homeostasis, as well as in several types of human cancer, such as colorectal cancer, breast cancer, melanoma, prostate cancer, and others.<sup>[21-23]</sup> As a central mediator of the signaling,  $\beta$ -catenin is implicated in different protein-protein interactions and controls the expression of several key genes that regulate the cell cycle and apoptosis. The transcriptional co-activator  $\beta$ -catenin is composed of 781 amino acids, has a central armadillo repeat domain (amino acids 140-664) with dynamic N- and C-terminal regions, and binds a several groups of proteins including pathway inhibitors (APC, Axin, ICAT) as well as transcription factors and other co-activators (TCF/Lef family, BCL9, CBP).<sup>[24]</sup> In the unstimulated cell,  $\beta$ -catenin is kept at low cytosolic levels being degraded by the multicomponent “destruction complex” (Figure 1), formed by the proteins Axin, adenomatous polyposis coli (APC) and the two serine-threonine kinases, glycogen synthase kinase 3 $\beta$  (GSK3 $\beta$ ) and casein kinase 1 $\alpha$  (CK1 $\alpha$ ).<sup>[25]</sup> These last two components are able to phosphorylate the serine and threonine residue in the N-terminal region of  $\beta$ -catenin, determining its ubiquitination by an E3 ubiquitin ligase complex, and finally its

proteasomal degradation. When the Wnt ligand is released, it binds the heterodimeric receptor complex of Frizzled (FZD) and low density lipoprotein receptor-related 5 or 6 (LRP5/6) on target cells (Figure 1), leading to the activation of kinases which induce phosphorylation of serine residues in the cytoplasmic tail of LRP5 and/or LRP6.<sup>[26,27]</sup> Whereas, the cytoplasmic part of FZD binds to Dishevelled (Dsh) that determines the interaction between the LRP5/6 and Axin, leading to an inhibition of the destruction complex and an accumulation of  $\beta$ -catenin in the cytosol. As a consequence,  $\beta$ -catenin translocates in the nucleus where interacts with the transcription factors TCF/Lef, leading to the release of transcriptional co-repressor Groucho from target genes and the recruitment of additional co-activators BCL9 and CBP.<sup>[28]</sup> The interaction  $\beta$ -catenin/TCF activates transcription of Wnt target genes, such as c-MYC and CyclinD1, leading to cell proliferation, differentiation, organogenesis, and tumorigenesis.

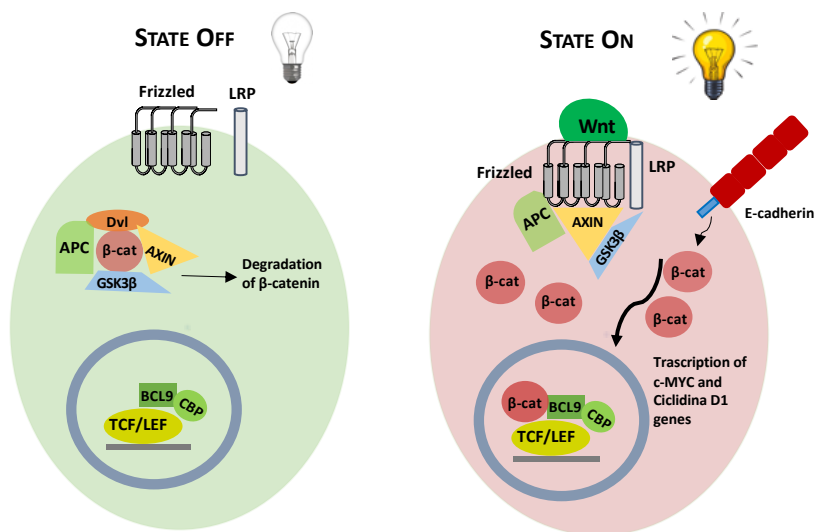


**Figure 1.** Overview of the canonical Wnt signaling pathway with its major components in the inactive (left) and active (right) states. In the inactive state  $\beta$ -catenin is degraded by the multicomponent destruction complex composed of Axin, APC, GSK3 $\beta$  and CK1 $\alpha$ . Instead, in an active state  $\beta$ -catenin translocates into nucleus and activates the transcription of Wnt target genes (c-MYC and Cyclin D1).



Consequently, oncogenic activation of Wnt/ $\beta$ -catenin pathway is triggered by high cytosolic levels of  $\beta$ -catenin for the inactivation of the destruction complex, caused by mutations in components of the pathway such as Axin and APC or by mutations at phosphorylation sites of  $\beta$ -catenin itself.<sup>[29,30]</sup> In addition,  $\beta$ -catenin is a structural component of cell-cell adherens junctions along with E-cadherin.<sup>[31]</sup> The extracellular region of E-cadherin extends on the outside surface and binds to cadherins present on adjacent cells; instead, the intracellular domain interacts with  $\beta$ -catenin in a complex with  $\alpha$ -catenin cytoskeleton, promoting cell-cell adhesion and stabilizing epithelial architecture.<sup>[32]</sup> In normal cells, E-cadherin triggers the epithelial-to-mesenchymal transition (EMT) involved in embryonic development. Instead, in carcinomas, a down-regulation of E-cadherin promotes invasion and metastasis caused by a loss of E-cadherin-mediated cell adhesion.<sup>[33]</sup> Consequently, this loss of cell adherens junctions induces a  $\beta$ -catenin release and its nuclear translocation, where interacts with the transcription machinery triggering an oncogenic transcription of Wnt target genes.<sup>[34]</sup>

### **1.3. DIRECT TARGETING OF $\beta$ -CATENIN**

Several strategies have been studied for inhibiting Wnt signaling by the use of cancer-specific molecules.<sup>[35]</sup> A strategy could consist of the activation of the destruction complex by the use of inhibitors of the Axin destabilizer tankyrase or of CK1 $\alpha$  activators,<sup>[36]</sup> to reduce the cytosolic levels of  $\beta$ -catenin and inhibiting its nuclear translocation. This strategy is ineffective in cells with a completely inactivated destruction complex or mutation in  $\beta$ -catenin, and in addition tankyrase and CK1 $\alpha$  are implicated in several cellular processes, increasing the risk of side-effects.<sup>[37,38]</sup> Another approach involves targeting of pathway components upstream. For instance, blocking the secretion of Wnt ligands through an administration of PORCN inhibitors (*e.g.* NCT02278133, ETC-1922159) that can lead to skeletal side effects including a loss of bone mass and strength;<sup>[38,39]</sup> or inhibiting the binding of

Wnt to FZD receptors by using monoclonal antibody directly binding to FZD receptors and disrupting the function of LRPs/FZDs (*e.g.* Vantictumab).<sup>[40]</sup> An alternative strategy aims at directly targeting and inhibiting directly the  $\beta$ -catenin, which is involved in various PPIs modulating a plethora of downstream biological processes.  $\beta$ -Catenin's armadillo has four different binding sites involving in the recognition of both activators such as TCF3/4, Lef1, BCL9 and inhibitors such as APC, ICAT and Axin, indicating that none of the binding sites is limited to a single interaction (Figure 2).<sup>[41,42]</sup> For instance, the binding sites 2 and 3 on the armadillo repeat are involved in the interaction of transcription factor TCF3/4 and the same binding site 2 is also implicated in the interaction with inhibitors Axin and APC. In addition, the four binding sites are implicated in the interaction with E-cadherin protein for the formation of cell-cell adherens junctions.<sup>[34,43]</sup>

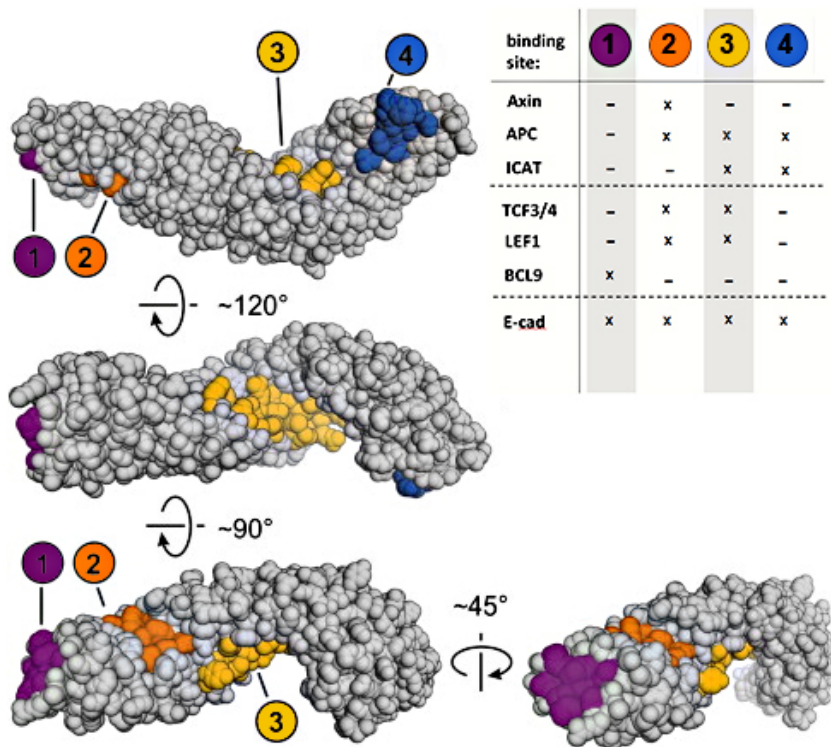


**Figure 2.** Crystal structure of  $\beta$ -catenin (PDB: 2Z6H) armadillo repeat and the four binding sites implicated in protein-protein interactions.<sup>[24]</sup>

The  $\beta$ -catenin/TCF4 interaction is the most studied among the several PPIs involving  $\beta$ -catenin, since an aberrant activation of this interaction is a necessary step in the genesis of many human cancers.<sup>[44]</sup> Inhibiting selectively  $\beta$ -catenin/TCF4 interaction downstream would reverse this effect and reduce reporter activity, without interfering with  $\beta$ -catenin/E-Cadherin and  $\beta$ -catenin/APC interactions.<sup>[44]</sup> Since the interface of TCF4/ $\beta$ -catenin is defined by the secondary structure  $\alpha$ -helix, promising results have been achieved with stapled peptide inhibitors, in particular with StAx-35 ( $K_D=13\text{nM}$ ) and StAx-35R ( $K_D=53\text{nM}$ ) peptides.<sup>[30]</sup> Both peptides displayed only moderate cellular uptake by colon cancer cells, while competing with TCF4 binding *in vitro* and suppressing the transcriptional Wnt activity. Moreover, promising results have been also observed by treatment with the stapled peptide SAH-BCL9<sub>B</sub>,<sup>[45]</sup> which is capable of competing with  $\beta$ -catenin/BCL9 dimerization *in vitro* and to suppress significantly angiogenesis and metastasis in colorectal carcinoma. Taken together, these successful results showed as stapled peptides may have the potential to serve as therapeutic agents to selectively inhibit oncogenic Wnt signaling.<sup>[46]</sup>

## 1.4. REFERENCES

- [1] Z. Li, A.A. Ivanov, R. Su, V. Gonzalez-Pecchi, Q. Qi, S. Liu, P. Webber, E. McMillan, L. Rusnak, C. Pham, X. Chen, X. Mo, B. Revennaugh, W. Zhou, A. Marcus, S. Harati, X. Chen, M.A. Johns, M.A. White, C. Moreno, L.A. Cooper, Y. Du, F.R. Khuri, H. Fu. The OncoPPI network of cancer-focused protein–protein interactions to inform biological insights and therapeutic strategies. *Nat. Commun.* 2017, 8:14356.
- [2] M. Pelay-Gimeno, A. Glas, O. Koch, T.N. Grossmann. Structure-based design of inhibitors of protein–protein interactions: mimicking peptide binding epitopes. *Angew. Chem. Int. Ed. Engl.* 2015, 54, 8896–8927.
- [3] G. Fischer, M. Rossmann, M. Hyvonen. Alternative modulation of protein–protein interactions by small molecules. *Curr. Opin. Biotechnol.* 2015, 35, 78–85.
- [4] B.T. Hennessy, D.L. Smith, P.T. Ram, Y. Lu, G.B. Mills. Exploiting the PI3K/AKT pathway for cancer drug discovery. *Nat. Rev. Drug Discov.* 2005, 4, 988–1004.

- [5] A.A. Ivanov, F.R. Khuri, H. Fu. Targeting protein–protein interactions as an anticancer strategy. *Trends. Pharmacol. Sci.* 2013, 34, 393–400.
- [6] L. Mabonga, A.P. Kappo. Protein-protein interaction modulators: advances, successes and remaining challenges. *Biophys. Rev.* 2019, 11, 559–581.
- [7] N. London, B. Raveh, O. Schueler-Furman. Druggable protein–protein interactions-- from hot spots to hot segments. *Curr. Opin. Chem. Biol.* 2013, 17, 952–959.
- [8] D. Reichmann, O. Rahat, M. Cohen, H. Neuvirth, S. Schreiber. The molecular architecture of protein–protein binding sites. *Curr. Opin. Struct. Biol.* 2007, 17, 67–76.
- [9] M.C. Smith, J.E. Gestwicki. Features of protein–protein interactions that translate into potent inhibitors: topology, surface area and affinity. *Expert. Rev. Mol. Med.* 2012, 14:e16.
- [10] A.A. Kaspar, J.M. Reichert. Future directions for peptide therapeutics development. *Drug Discov. Today.* 2013, 18, 807–817.
- [11] M.S. Kinch. An overview of FDA-approved biologics medicines. *Drug Discov. Today.* 2015, 20, 393–398.
- [12] H. Bruzzoni-Giovanelli, V. Alezra, N. Wolff, C.Z. Dong, P. Tuffery, A. Rebollo. Interfering peptides targeting protein–protein interactions: the next generation of drugs?. *Drug Discov. Today.* 2018, 23, 272–285.
- [13] J.L. Lau, M.K. Dunn MK. Therapeutic peptides: historical perspectives, current development trends, and future directions. *Bioorg. Med. Chem.* 2018;26:2700–2707.
- [14] H. Jubb, A.P. Higuero, A. Winter, T.L. Blundell. Structural biology and drug discovery for protein-protein interactions. *Trends Pharmacol. Sci.* 2012, 33, 241–248.
- [14] L. Nevola, E. Giralt. Modulating protein-protein interactions: the potential of peptides. *Chem. Commun. (Camb).* 2015, 51, 3302–3315.
- [15] M.R. Naylor, A.T. Bockus, M.J. Blanco, R.S. Lokey RS. Cyclic peptide natural products chart the frontier of oral bioavailability in the pursuit of undruggable targets. *Curr. Opin. Chem. Biol.* 2017, 38, 141–147.
- [16] G.L. Verdine, G.J. Hilinski. Stapled peptides for intracellular drug targets. *Methods Enzymol.* 2012, 503, 3–33.
- [17] L.D. Walensky, A.L. Kung, I. Escher, T.J. Malia, S. Barbuto, R.D. Wright, G. Wagner, G.L. Verdine, S.J. Korsmeyer. Activation of apoptosis *in vivo* by a hydrocarbon-stapled BH3 helix. *Science.* 2004, 305, 1466–1470.
- [18] Y.S. Chang, B. Graves, V. Guerlavais, C. Tovar, K. Packman, K.H. To, K.A. Olson, K. Kesavan, P. Gangurde, A. Mukherjee, T. Baker, K. Darlak, C. Elkin, Z. Filipovic, F.Z. Qureshi, H. Cai, P. Berry, E. Feyfant, X.E. Shi, J. Horstick, D.A. Annis, A.M. Manning, N. Fotouhi, H. Nash, L.T. Vassilev, T.K. Sawyer. Stapled  $\alpha$ -helical peptide drug development: a potent dual inhibitor of MDM2 and MDMX for p53-dependent cancer therapy. *Proc. Natl. Acad. Sci. U. S. A.* 2013, 110, 3445–3454.

- [19] A.C. Lai, C.M. Crews. Induced protein degradation: an emerging drug discovery paradigm. *Nat. Rev. Drug Discovery*. 2017, 16, 101–114.
- [20] B.T. MacDonald, K. Tamai, X. He. Wnt/ $\beta$ -catenin signaling: components, mechanisms, and diseases. *Dev. Cell*. 2009, 17, 9–26.
- [21] S. Yamamoto, O. Nishimura, K. Misaki, M. Nishita, Y. Minami, S. Yonemura, H. Tarui, H. Sasaki. Cthrc1 selectively activates the planar cell polarity pathway of Wnt signaling by stabilizing the Wnt-receptor complex. *Dev. Cell*. 2008, 15, 23–36.
- [22] M. Tada, M. Kai. Noncanonical Wnt/PCP signaling during vertebrate gastrulation. *Zebrafish*. 2009, 6, 29–40.
- [23] R.K. Miller, J.Y. Hong, W.A. Muñoz, P.D. McCrea.  $\beta$ -catenin versus the other armadillo catenins: assessing our current view of canonical Wnt signaling. *Prog. Mol. Biol. Transl. Sci.* 2013, 116, 387–407.
- [24] G. Hahne, T.N. Grossmann. Direct targeting of  $\beta$ -catenin: Inhibition of protein–protein interactions for the inactivation of Wnt signaling. *Bioorg. Med. Chem.* 2013, 21, 4020–4026.
- [25] H. Clevers, R. Nusse. Wnt/ $\beta$ -catenin signaling and disease. *Cell*. 2012, 149, 1192–205.
- [26] V.S. Spiegelman, T.J. Slaga, M. Pagano, T. Minamoto, Z.E. Ronai, S.Y. Fuchs. Wnt/ $\beta$ -catenin signaling induces the expression and activity of  $\beta$ TrCP ubiquitin ligase receptor. *Mol. Cell*. 2000, 5, 877–82.
- [27] A.D. Kohn, R.T. Moon. Wnt and calcium signaling:  $\beta$ -catenin-independent pathways. *Cell. Calcium*. 2005, 38, 439–446.
- [28] K.I. Takemaru, R.T. Moon. The transcriptional coactivator CBP interacts with  $\beta$ -catenin to activate gene expression. *J. Cell Biol.* 2000, 149, 249–254.
- [29] Y. Duchartre, Y.M. Kim, M. Kahn. The Wnt signaling pathway in cancer. *Crit. Rev. Oncol. Hematol.* 2016, 99, 141–149.
- [30] T.N. Grossmann, J.T. Yeh, B.R. Bowman, Q. Chu, R.E. Moellering, G.L. Verdine. Inhibition of oncogenic Wnt signaling through direct targeting of  $\beta$ -catenin. *Proc. Natl. Acad. Sci. U S A*. 2012, 109, 17942–17947.
- [31] M. Bienz.  $\beta$ -Catenin: A Pivot between Cell Adhesion and Wnt Signalling. *Curr Biol*. 2005 Jan 26;15(2):R64-7.
- [32] J. Heuberger, W. Birchmeier. Interplay of cadherin-mediated cell adhesion and canonical Wnt signaling. *Cold. Spring Harb. Perspect. Biol.* 2010, 2:a002915.
- [33] X. Tian, Z. Liu, B. Niu, J. Zhang, T.K. Tan, S.R. Lee, Y. Zhao, D.C. Harris, G. Zheng. E-Cadherin/ $\beta$ -Catenin Complex and the epithelial barrier. *J. Biomed. Biotechnol.* 2011, 2011:567305.
- [34] M. Kahn. Can we safely target the WNT pathway?. *Nat. Rev. Drug Discov.* 2014, 13, 513–532.
- [35] Y.S. Jung, J.I. Park. Wnt signaling in cancer: therapeutic targeting of Wnt signaling beyond  $\beta$ -catenin and the destruction complex. *Exp. Mol. Med.* 2020, 52, 183–191.

- [36] C.A. Thorne, A.J. Hanson, J. Schneider, E. Tahinci, D. Orton, C.S. Cselenyi, K.K. Jernigan, K.C. Meyers, B.I. Hang, A.G. Waterson, K. Kim, B. Melancon, V.P. Ghidu, G.A. Sulikowski, B. LaFleur, A. Salic, L.A. Lee, D.M. Miller, E. Lee. Small-molecule inhibition of Wnt signaling through activation of casein kinase 1alpha. *Nat. Chem. Biol.* 2010, 6, 829.
- [37] C.H. Park, J.Y. Chang, E.R. Hahm, S. Park, H.K. Kim, C.H. Yang. Quercetin, a potent inhibitor against beta-catenin/Tcf signaling in SW480 colon cancer cells. *Biochem. Biophys. Res. Commun.* 2005, 328, 227.
- [38] X. Wang, J. Moon, M.E. Dodge, X. Pan, L. Zhang, J.M. Hanson, R. Tuladhar, Z. Ma, H. Shi, N.S. Williams, J.F. Amatruda, T.J. Carroll, L. Lum, C. Chen C. The development of highly potent inhibitors for porcupine. *J. Med Chem.* 2013, 56, 2700–2704.
- [39] B. Madan, M.J. McDonald, G.E. Foxa, C.R. Diegel, B.O. Williams, D.M. Virshup. Bone loss from Wnt inhibition mitigated by concurrent alendronate therapy. *Bone Res.* 2018, 6, 17.
- [40] M.M. Fischer, B. Cancilla, V.P. Yeung, F. Cattaruzza, C. Chartier, C.L. Murriel, J. Cain, R. Tam, C.Y. Cheng, J.W. Evans, G. O'Young, X. Song, J. Lewicki, A.M. Kapoun, A. Gurney, W.C. Yen, T. Hoey T. WNT antagonists exhibit unique combinatorial antitumor activity with taxanes by potentiating mitotic cell death. *Sci. Adv.* 2017, 3, e1700090.
- [41] J.P. von Kries. G. Winbeck, C. Asbrand, T. Schwarz-Romond, N. Sochnikova, A. Dell'Oro, J. Behrens, W. Birchmeier W. Hot spots in beta-catenin for interactions with LEF-1, conductin and APC. *Nature Struct. Biol.* 2000, 7, 800–807.
- [42] J. Hulsken, W. Birchmeier, J.J. Behrens. E-cadherin and APC compete for the interaction with beta-catenin and the cytoskeleton. *Cell. Biol.* 1994, 127, 2061–2069.
- [43] B. Rubinfeld, B. Souza, I. Albert, S. Munemitsu, P. Polakis. The APC protein and E-cadherin form similar but independent complexes with alpha-catenin, beta-catenin, and plakoglobin. *J. Biol. Chem.* 1995, 270, 5549–5555.
- [44] F. Poy, M. Lepourcelet, R.A. Shivdasani, M.J. Eck. Structure of a human Tcf4– $\beta$ -catenin complex. *Nat. Struct. Biol.* 2001, 8, 1053–1057.
- [45] K. Takada, D. Zhu, G.H. Bird, K. Sukhdeo, J.J. Zhao, M. Mani, M. Lemieux, D.E. Carrasco, J. Ryan, D. Horst, M. Fulciniti, N.C. Munshi, W. Xu, A.L. Kung, R.A. Shivdasani, L.D. Walensky, D.R. Carrasco. *Sci. Transl. Med.* 2012, 4, 148ra117.
- [46] A.M. Ali, J. Atmaj, N. Van Oosterwijk, M.R. Groves, A. Dömling. Stapled peptides inhibitors: a new window for target drug discovery. *Comput. Struct. Biotechnol. J.* 2019, 17, 263–281.

## **CHAPTER 2**

# **BICYCLIC STAPLED PEPTIDES INHIBITORS OF $\beta$ -CATENIN**

**CONTRIBUTIONS:** Peptide synthesis; peptide characterization via fluorescence polarization.

## 2.1. TARGETING $\beta$ -CATENIN/E-CADHERIN INTERACTION

Cell-cell adherens junctions are coordinated by the  $\beta$ -catenin/E-cadherin interaction.<sup>[1,2]</sup> In the formation of adherens junctions, the intracellular region of E-cadherin is also implicated in the binding to the protein plakoglobin, which is a  $\beta$ -catenin homolog involved in the assembly of desmosomes.<sup>[3]</sup> The sequences of the arm domains of these two proteins are 79% identical, whereas the N- and C-terminal tails display lower homology of 45 and 27%, respectively (Figure 1, panel A).<sup>[4,5]</sup> The crystal structure of plakoglobin/E-cadherin complex shows that E-cadherin forms the same interactions as those established with residues of the  $\beta$ -catenin's armadillo. As results of a detailed study of the crystal structure of Plakoglobin/E-cadherin, a series of truncations was performed on the E-cadherin sequence both in N- and C-terminus (Wendt *et al.*, unpublished data), identifying the bioactive fragment in the groove between arm repeats 6–9, which adopts an antiparallel  $\beta$ -sheet structure and involves E-Cadherin residues 628–633 and 674–679 (Figure 1, panel B). The C-terminal strand (674–679) of the  $\beta$ -sheet buried between H3 of arm repeat 6–8 is implicated in interactions with  $\beta$ -catenin, while the N-terminal strand is less involved in interactions since one face of the strand is oriented towards the solvents.<sup>[6,7]</sup> Inducing a  $\beta$ -turn constriction by the incorporation of the turn-inducing D-Proline-L-Proline template and a head-to-tail lactamization between N- and C-terminal  $\beta$ -alanine residues,<sup>[8]</sup> a potent macrocyclic  $\beta$ -hairpin, referred to as  **$\beta$ -Ecad** (Figure 1, panel C), was identified (Wendt *et al.*, unpublished).  **$\beta$ -Ecad** exhibits a potent activity of IC<sub>50</sub> 3.7±0.4  $\mu$ M in  $\beta$ -catenin/E-Cadherin competition interaction and binds to  $\beta$ -catenin with high affinity ( $K_D$ = 0.17±0.01  $\mu$ M). In order to improve the binding affinity and selectivity of  **$\beta$ -Ecad**, Wendt and co-workers have chosen to synthesize a library of bicyclic peptidomimetics since are generally featured by an elevated conformational rigidity,<sup>[9]</sup> more protease stability, and high membrane permeability to inhibit the “undruggable” PPIs.<sup>[10–12]</sup>



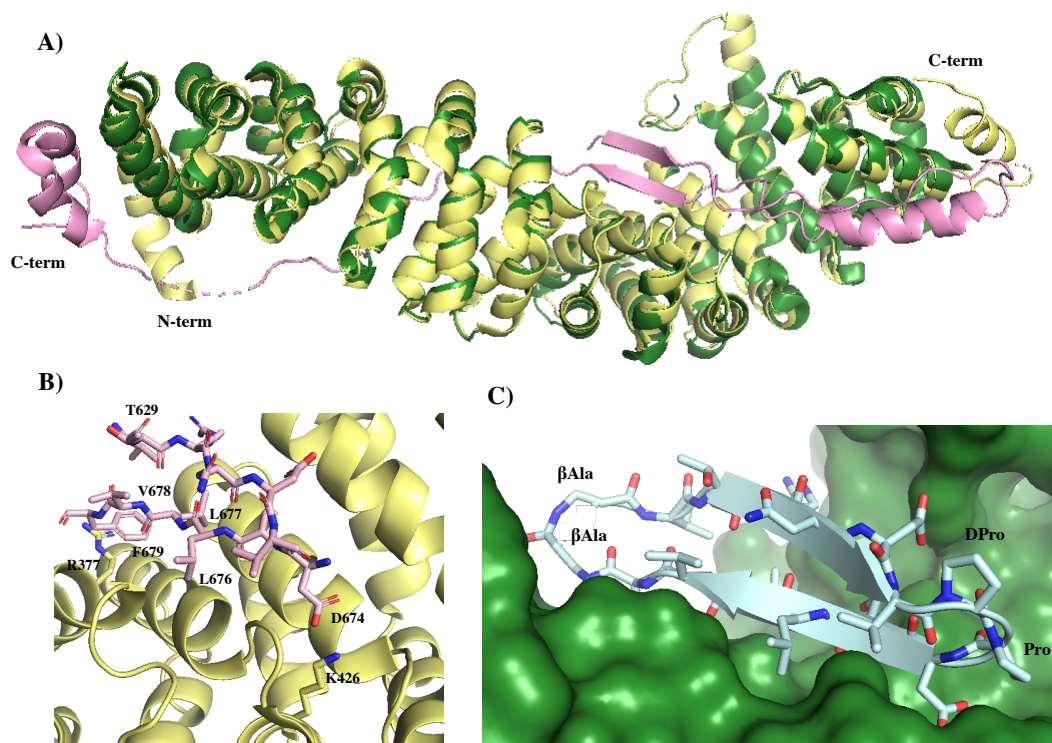


**Figure 1.** (A) Superposition of  $\beta$ -Catenin (green, PDB ID 1JDH) and Plakoglobin bound to E-Cadherin (E-Cadherin: pink, Plakoglobin: yellow, PDB ID 3IQF). (B) Interactions of hot-spot residues (side-chains shown as sticks) in the C-terminal  $\beta$ -strand of the bioactive fragment (pink) and Plakoglobin (yellow). (C) The crystal structure of  $\beta$ -Ecad/ $\beta$ -catenin complex (Wendt et al., unpublished data).

Based on the monocyclic peptide  **$\beta$ -Ecad** has three cross-strand pairs in the core of its  $\beta$ -harpin, two H-bonded (HB; T629-V678, N631-L676) and one non-H-bonded (NHB; D632-S675) were selected to introduce a further conformational restriction by applying the approach of cysteine stapling (Figure 2). These cross-strand pairs T629-V678, N631-L676, D632-S675 were selected for cysteine exchange, yielding the monocyclic peptides EC-*x*, EC-*y*, EC-*z*, respectively.

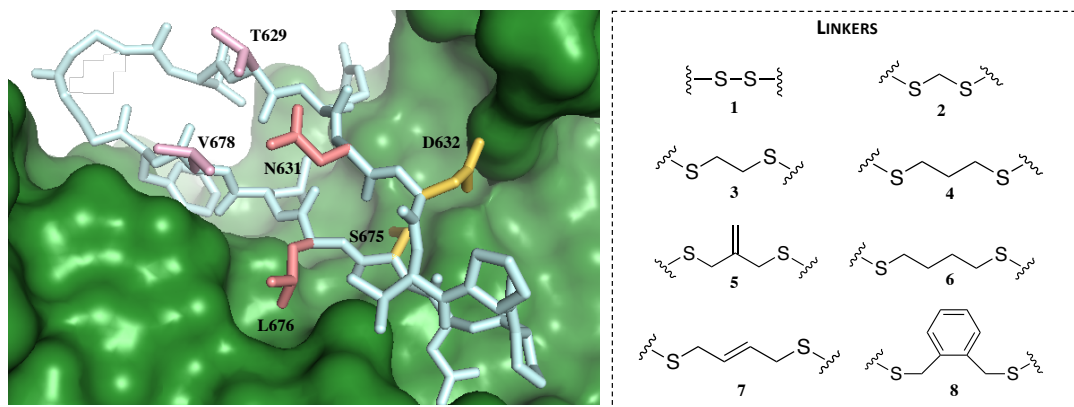


**Figure 2.** Crystal structure of  $\beta$ -Ecad and its cross-strand positions are showed in different colors (on the left). The different linkers used for cysteine stapling in a previous study (on the right) (Wendt *et al.*, unpublished data).

A library of cysteine bridged bicyclic peptidomimetics was synthesized using monocyclic peptides with two cysteines which were reacted with a set of commercially available thiol-reactive *bis*-electrophiles in order to evaluate the effect of an additional stabilization of  $\beta$ -hairpin induced by diverse linkers on the activity (Figure 2) (Wendt *et al.*, unpublished data). In the  $\beta$ -catenin/E-Cadherin competition, the highest activity was observed for *trans*-but-2-ene-bridged bicyclic **EC-x<sub>8</sub>** and the *o*-xylene bridged bicyclics **EC-y<sub>7</sub>** and **EC-z<sub>7</sub>**. Starting from this promising binding results of bicycles, we designed and synthesized a small library of hydrocarbon stapled bicyclic peptidomimetics characterized by an olefin bridge (**St-1–St-6**), investigating the effect of the length of the olefin bridge and the position of the staple on binding activity by competition fluorescence assay.

## 2.2. RESULTS AND DISCUSSIONS

### 2.2.1. DESIGN OF STAPLED BICYCLICS

The preliminary binding results of bicyclic cysteine-bridged peptides represented our starting point to design a small library of stapled bicyclic peptidomimetics. By applying the cysteine stapling using different linkers, the best binding activity in  $\beta$ -catenin/E-Cadherin competition interaction was achieved by the introduction of the

*o*-xylene bridge in EC-*y* and EC-*z* and *trans*-but-2-ene (**7**) linker in EC-*x*, yielding bicyclic EC-*x*<sub>8</sub>, EC-*y*<sub>7</sub> and EC-*z*<sub>7</sub>. Remarkably, the *trans*-but-2-ene-bridged bicyclic EC-*x*<sub>8</sub> showed a binding activity of IC<sub>50</sub> 2.2±0.3 μM, while the *o*-xylene bridged bicyclics EC-*y*<sub>7</sub> and EC-*z*<sub>7</sub> displayed an activity of IC<sub>50</sub> 3.7±0.8 μM and IC<sub>50</sub> 5.7±0.6 μM, respectively (Table 1). Their activity is very similar to that of reference peptide β-Ecad.

**Table 1.** Sequence of the most active peptides and their binding affinity (IC<sub>50</sub>) in β-catenin/E-Cadherin competition. The structure of linker is represented in Figure 2. β corresponds to β-Alanine residues involving in head-to-tail lactamization.

Peptide	Sequence	Linker	IC <sub>50</sub> (μM)
β-Ecad	[β V T <sup>629</sup> R N <sup>631</sup> D <sup>632</sup> V p P D S <sup>675</sup> L <sup>767</sup> L V <sup>678</sup> F β]	-	3.7±0.4
EC- <i>x</i>	[β V C R N D V p P D S L L C F β]	-	~100
EC- <i>y</i>	[β V T R C D V p P D S C L V F β]	-	11±0.5
EC- <i>z</i>	[β V T R N C V p P D C L L V F β]	-	>200
EC- <i>x</i> <sub>8</sub>	[β V C R N D V p P D S L L C F β]	<b>7</b>	2.2±0.3
EC- <i>y</i> <sub>7</sub>	[β V T R C D V p P D S C L V F β]	<b>8</b>	5.7±0.6
EC- <i>z</i> <sub>7</sub>	[β V T R N C V p P D C L L V F β]	<b>8</b>	3.7±0.8

The improved activity of EC-*x*<sub>8</sub> compared to monocyclic EC-*x* was probably correlated to an additional interaction between the carbon-carbon double bond of linker along the bridge and β-catenin, suggesting that it could represent a “sweet spot” that contributes strongly to β-catenin binding. In this context, we designed a small library of bicyclic peptidomimetics featured by an hydrocarbon staple in order to enhance binding affinity, target specificity and cell permeability.<sup>[13–16]</sup> In this study, the pair of cysteine residues in monocyclics EC-*x*, EC-*y*, EC-*z* was replaced by an olefinic (*S*)-*N*-Fmoc-2-(4'-pentenyl) glycine (Fmoc-S<sub>5</sub><sup>\*</sup>-OH) residue for forming the olefin bridge of 8-carbons length in bicycles **St-1**, **St-5** and **St-6** (Table 1). Considering the promising result obtained by the introduction of *trans*-but-2-ene linker in monocyclic EC-*x*, we selected this cross-strand pairs T629-V678 to build

olefin bridges of different length, evaluating the correlation between peptide conformation and binding affinity. Fmoc-S<sub>5</sub><sup>\*</sup>-OH and (S)-N-Fmoc-2-(5'-hexenyl)glycine (Fmoc-S<sub>6</sub><sup>\*</sup>-OH) residues were used, in diverse combinations, to achieve stapled bicycles **St-2** and **St-3** characterized by an olefin linker of 9-carbons and **St-4** featuring by a olefin linker of 10-carbons (Figure 3).

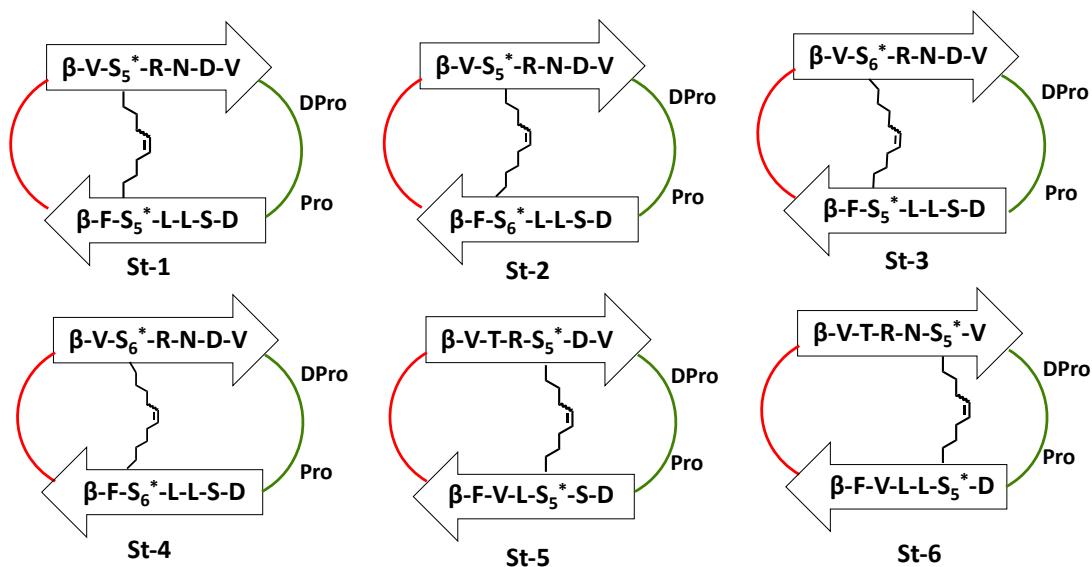


**Figure 3.** Structures of stapled bicyclics **St-1-6**.  $\beta$  corresponds to  $\beta$ -Alanine residues involving in head-to-tail lactamization.

### 2.2.2. ST-3 BINDS $\beta$ -CATENIN

The inhibitory activity of the stapled bicycles **St-1-6** was investigated in a competition fluorescence polarization assay (Figure 4). The reference monocyclic  $\beta$ -Ecad and the long linear sequence E-Cadherin corresponding to V<sup>782</sup>-F<sup>833</sup> residues (Long E-Cad) were used as controls. The stapled bicycles were titrated with the protein  $\beta$ -catenin and the tracer ligand (FITC-labeled Long E-Cad). The highest concentration of competitors was 30  $\mu$ M. The bicycles **St-1-St-4** were obtained from a stapling between olefin amino acids incorporated in cross strand pair corresponding

to T629-V678 residues in monocyclic  **$\beta$ -Ecad**. The bicyclic **St-1**, featured by an 8-carbons linker formed between two  $S_5^*$  residues, displayed a reduced binding affinity with an  $IC_{50}$  of 30  $\mu$ M compared to reference monocyclic  **$\beta$ -Ecad**.

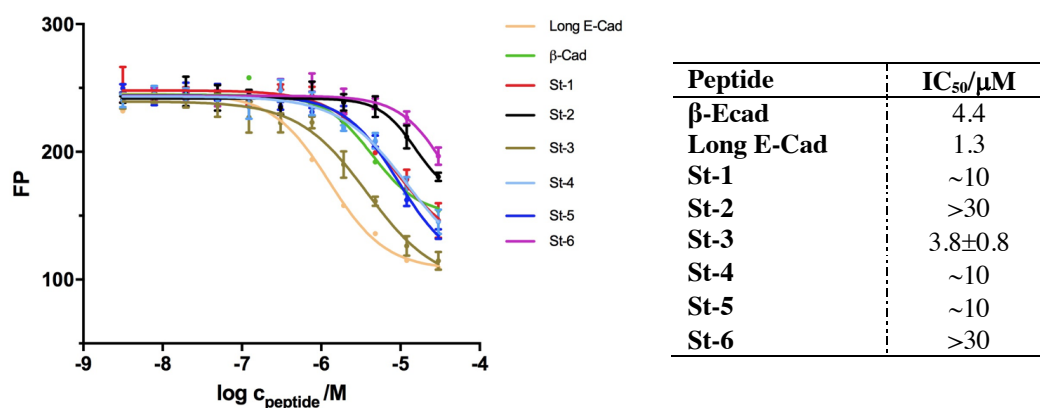


**Figure 4.** The binding activities of stapled bicyclics **St-1–St-6** in  $\beta$ -catenin/Long-E-Cadherin competition. In the table,  $IC_{50}$  values were determined in competition FP binding assays. A right-shift of the competition curve of two orders of magnitude compared to  **$\beta$ -Ecad** ( $IC_{50}$  4.4  $\mu$ M) was observed. No lower plateau was reached in the titration in the assay.

Regarding bicycles **St-2** and **St-3** showed a significant difference in binding activity. In particular, **St-2** exhibited a very weak activity with  $IC_{50}$  value exceeding 30  $\mu$ M, while **St-3** showed an 8-fold stronger competition binding ( $IC_{50}$  of  $3.8 \pm 0.8$   $\mu$ M) than **St-2**. Both peptides have a 9-carbons linker formed by a staple linkage between  $S_5^*$  and  $S_6^*$ , but the exchange of olefinic amino acids position has caused a notable reduction in binding affinity (Figure 4). Instead, a longer linker of 10-carbons formed by  $S_6^*$  and  $S_6^*$  amino acids in bicyclic **St-4** caused a slight reduction of binding activity ( $IC_{50} \sim 10$   $\mu$ M) compared to monocyclic  $\beta$ -Ecad. Regarding bicyclic **St-5**, in which two  $S_5^*$  residues were incorporated in the cross strand pair N631-L676 of monocyclic  **$\beta$ -Ecad**, displayed a 2-fold lower ( $IC_{50}$  of  $\sim 10$   $\mu$ M) binding activity than **St-3**. In addition, bicyclic **St-6**, in which two  $S_5^*$  residues were incorporated in the

cross strand pair D632-S67, has lost drastically the binding affinity on  $\beta$ -catenin with  $IC_{50}$  value exceeding 30  $\mu$ M.

## 2.3. CONCLUSIONS & FURTHER PERSPECTIVES

In conclusion, we designed and synthesized a small library of stapled bicycles **St-1–St-6**, yielding the most promising stapled bicycles **St-3** featured by a 9-carbons linker. In particular, **St-3** displayed a high affinity towards  $\beta$ -catenin with  $IC_{50}$  of  $3.8\pm 0.8$   $\mu$ M, fully restored binding activity to levels of monocyclic  **$\beta$ -Ecad** ( $IC_{50}\sim 4$ ). Considering these promising results, potential use of **St-3** as a potential anticancer agent will be explored. Firstly, considering that E-cadherin and transcriptional factor TCF4 share the same binding on  $\beta$ -catenin, the competition binding assay will be performed with TCF4 to evaluate the capability of stapled bicyclic **St-3** to interfere with  $\beta$ -catenin/TCF4 interaction and reduce the expression of Wnt target genes. On the other hand, the ability of **St-3** to cross the membrane cell and to inhibit the  $\beta$ -catenin/TCF4 interaction into the nucleus will be evaluated by the cell permeability and reporter gene assays using different cancer cell lines. Finally, the double bond isomers **St-3** will be investigated by NMR spectroscopy.

## 2.4. EXPERIMENTAL SECTIONS

### 2.4.1. CHEMISTRY

**Materials.**  $N^\alpha$ -Fmoc-protected amino acids and 2-chlorotrityl chloride resin were purchased from Iris Biotech. (*S*)-*N*-Fmoc-2-(4'-pentenyl)glycine (Fmoc- $S_5^*$ -OH) and (*S*)-*N*-Fmoc-2-(5'-hexenyl)glycine (Fmoc- $S_6^*$ -OH) were purchased by Okeanos Okeanos Technology Co. Coupling reagents, Oxyma (ethyl cyano (hydroxyimino) acetate) and COMU (1-Cyano-2-ethoxy-2-oxoethylideneaminoxy)dimethylamino-morpholino-carbenium hexafluorophosphate, *N,N*-Diisopropylethylamine (DIEA), piperidine, trifluoroacetic acid (TFA) and 1,2-dichloroethane (DCE) were purchased

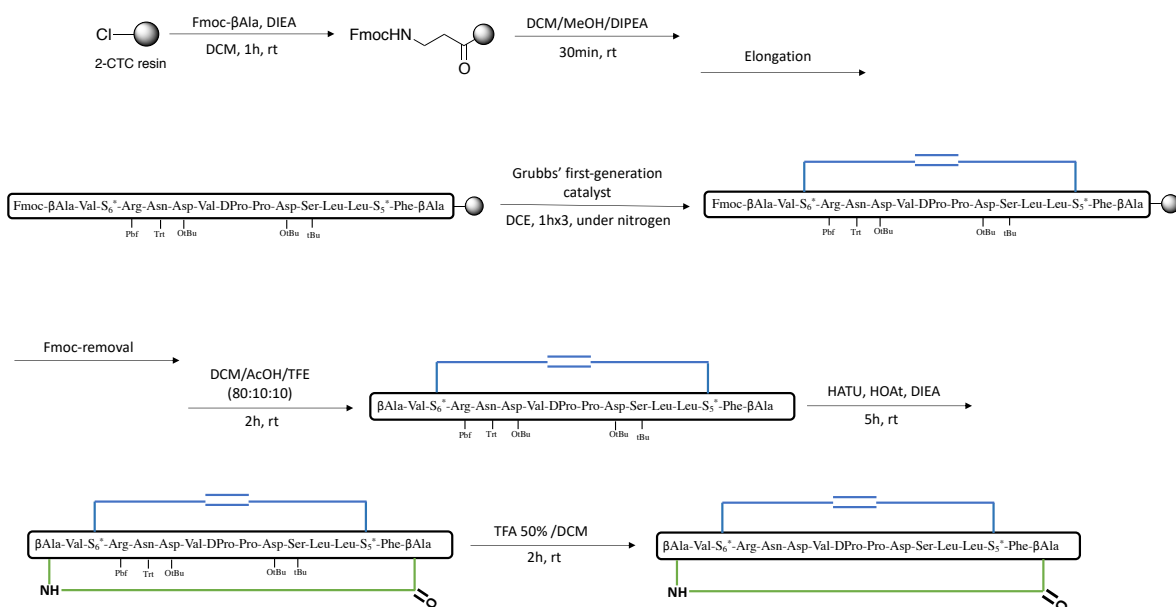
from Sigma–Aldrich. HATU (1-[Bis(dimethylamino)methylene]-1H-1,2,3-triazolo[4,5-b]pyridinium 3-oxid hexafluorophosphate and HOAt (3H-[1,2,3]-Triazolo[4,5-b]pyridin-3-ol) were purchased from NovaBiochem. Grubbs' first-generation catalyst for ring closing metathesis was obtained from Fluorochem. All chemicals were reagent grade acquired from commercial sources and used without further purification.

**Linear peptide synthesis.** Linear peptides were synthesized in a stepwise manner using the conventional solid-phase peptide synthesis (SPPS), as Fmoc/*t*Bu strategy. 2-Chlorotrityl chloride resin (1.60 mmol/g as loading substitution, 2 equiv relative to the mmol of first amino acid) was used as solid support. The resin, previously swollen for 30 min in DCM, was reacted with the corresponding first amino acid,  $N^{\alpha}$ -Fmoc- $\beta$ -alanine (2.5 equiv), along with DIPEA (8 equiv relative to mmol of first amino acid) in anhydrous DCM, and the resulting reaction mixture was stirred on an automated shaker for 1 h (Scheme 1). The resin was washed with DMF ( $\times 3$ ) and DCM ( $\times 3$ ), then, to endcap any remaining unreacted 2-chlorotrityl chloride groups, and was treated with a mixture of DCM/MeOH/DIPEA (80:15:5, *v/v/v*) and stirred on an automated shaker for 30 min. After initial functionalization step, linear peptides were assembled by repeated cycles of Fmoc deprotection and coupling step reactions. The  $N^{\alpha}$ -Fmoc protecting group was removed by the treatment with a solution of 20% piperidine in DMF for 5 min. Subsequently the reaction solution was discarded and the Fmoc deprotection was repeated. The coupling reactions were carried out adding a solution of Fmoc-amino acid (3 equiv), COMU (3 equiv), Oxyma (3 equiv) and DIPEA (6 equiv) in DMF to the resin, and the resulting suspension was gently shaken for 25 min. Then, the reaction solution was flushed away, and the coupling repeated for additional 25 min. Then, the linear resin-bound intermediate was elongated by repeating cycles of coupling and deprotection step reactions. After each coupling and Fmoc-deprotection reaction the resin was washed

with DMF and DCM. The correct assembly of linear sequence was ascertained by LC-MS analysis of a residue obtained from the cleavage of an aliquot of resin [5mg treated with 1ml of TFA/TIS/H<sub>2</sub>O (95:2.5:2.5, v/v/v) for 1 h].

**Stapled bicyclic synthesis.** During the construction of linear peptide sequence, the olefinic amino acids Fmoc-S<sub>5</sub>\*OH or Fmoc-S<sub>6</sub>\*-OH were incorporated for the formation of olefin bridge. The ring closing metathesis was carried on resin-bound and fully protected peptides. After the linear assembly until Fmoc-βAla, the resin was washed with DCM and DCE.<sup>[17]</sup> The resin was treated with a fresh catalyst solution of a 6 mM solution of Grubbs' first-generation catalyst in DCE (4.94 mg×mL<sup>-1</sup>, 20 mol% relative to the resin substitution). The resulting suspension was gently agitated with constant nitrogen flow for 1h (Scheme 1). After the first round, the RCM reaction was repeated two times in the same condition. Subsequently, the resin was washed with DCE and DCM and then dried. The conversion in olefin bridge was monitored by LC-MS and HPLC chromatogram for each peptide showed two product peaks corresponding olefin isomers using a linear gradient of MeCN (0.1% TFA) in water (0.1% TFA) from 5 to 95% over 30 min. Upon the achievement of the stapled peptide, the head-to-tail cyclization was performed in solution. The partial cleavage of the protected stapled peptide from the resin was affected with a cocktail of CH<sub>3</sub>COOH/2,2,2-trifluoroethanol/DCM (80:10:10, v/v/v) for 2 h, to generate free *N*-terminal amino and *C*-terminal carboxylic groups. The resin was removed by filtration and washed with DCM. The filtrate was collected, the solvent was removed under reduced pressure forming an azeotropic mixture with *n*-hexane to remove acetic acid.





**Scheme 1.** Synthesis of stapled bicyclic **St-3**.

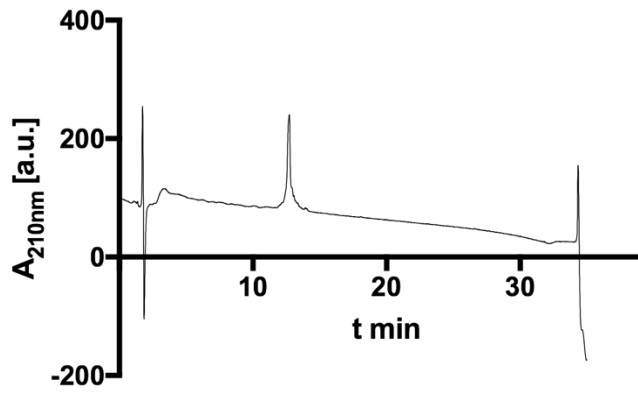
Then, residual was dissolved in H<sub>2</sub>O/MeCN (1:1, v/v) and lyophilized. The selective head-to-tail intra-molecular cyclization was performed dissolving the crude peptide in DCM/DMF (9:1, v/v, C<sub>f</sub> = 0.5 mM) and DIPEA (2.4 equiv) was added, then under continuous agitation, after 15 min, HATU (1.2 equiv) and HOAt (1.2 equiv), were added.<sup>[18]</sup> The resulting reaction mixture was stirred for 5 h. The reaction was quenched with saturated aq. NH<sub>4</sub>Cl. The organic phase was washed with saturated NH<sub>4</sub>Cl solution (3×), saturated NaCl solution (3×) and dried over Na<sub>2</sub>SO<sub>4</sub>. The solvent was removed under reduced pressure and the side-chain protection groups was removed by using a 50% TFA solution in DCM for 2 h at room temperature. Then, TFA was evaporated and crude peptide was washed in cold diethyl ether and precipitated peptides were separated by centrifugation (15 min, 4 °C, 4000 rcf). The supernatant was removed, and crude peptide was dissolved in MeCN/H<sub>2</sub>O (1/1, v/v) and purified by preparative HPLC.

**Purification and Characterization.** Peptide purification was performed using reversed-phase HPLC (HPLC: Agilent 1100, Column: Macherey-Nagel Nucleodur C18, 10 × 125 mm, 110 Å, 5 μm) with solvent A (H<sub>2</sub>O + 0.1% TFA) and solvent B (MeCN + 0.1% TFA). A gradient elution was used from 20 to 60% of solvent B over 40 min and a flow rate of 6 mL min<sup>-1</sup>. Subsequently peptides were characterized using a reverse-phase HPLC coupled to ESI-MS (Agilent 1260 + quadrupole 6120, Column: Agilent Zorbax C18, 4.6 × 150 mm, 5 μm) with solvent A (H<sub>2</sub>O + 0.1 % TFA) and solvent B (MeCN + 0.1 % TFA) (Table 2). After the purification by preparative HPLC, the pure profile of bicyclics showed a single geometric isomer, with the exception of **St-2**, **St-3** and **St-6** that resulted in a mixture of *cis* and *trans* isomers in different ratio (Figure 5).

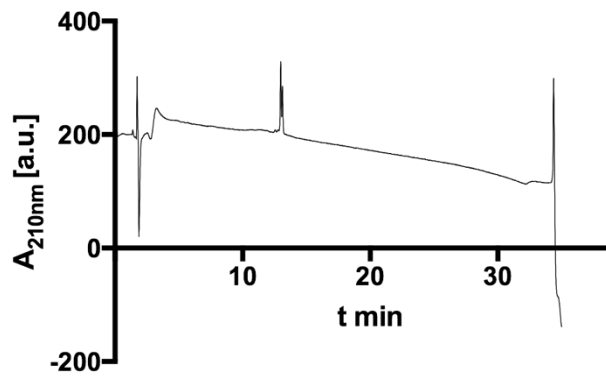
**Table 2.** Analytical data of stapled bicycles **St-1–St-2**.

<b>Cmpd#</b>	<b>R<sub>t</sub>(min)</b>	<b>MW calcd</b>	<b>MW found</b>
<b>St-1</b>	12.8	1717.9	[M+2H/2] <sup>+</sup> = 859.9
<b>St-2*</b>	13.0/13.1	1730.9	[M+2H/2] <sup>+</sup> = 866.6
<b>St-3*</b>	18.0/18.1	1730.9	[M+2H/2] <sup>+</sup> = 866.6
<b>St-4</b>	18.3	1744.9	[M+2H/2] <sup>+</sup> = 873.7
<b>St-5</b>	17.8	1690.9	[M+2H/2] <sup>+</sup> = 846.2
<b>St-6*</b>	12.3/14.1	1714.9	[M+2H/2] <sup>+</sup> =858.7

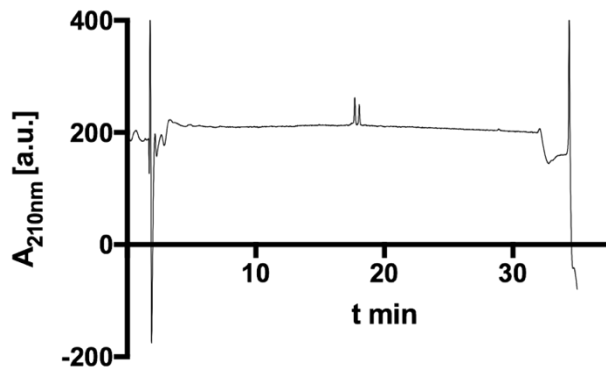
\*HPLC profile showed the mixture of *cis* and *trans* isomers.



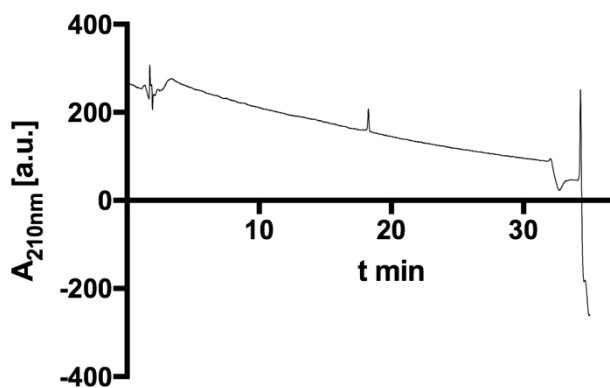
**St-1**



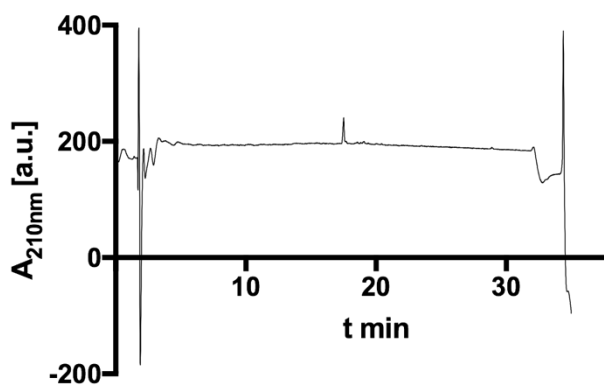
**St-2**



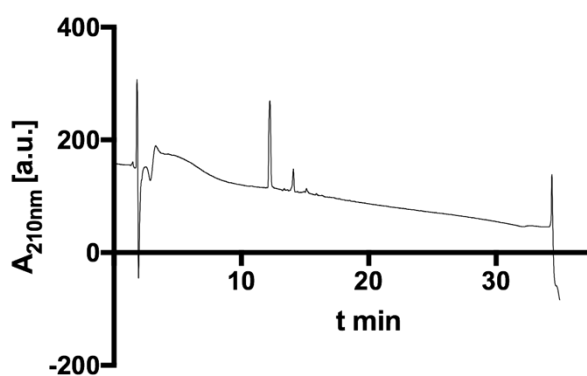
**St-3**



**St-4**



**St-5**



**St-6**

**Figure 5.** The HPLC chromatograms of stapled bicycles. Chromatograms referred to **St-2**, **St-3** and **St-6** show the mixture of geometric isomers.

## 2.4.2. BINDING ASSAY

**Competition fluorescence polarization assay.** In a 384-well plate non-labelled peptide competitor was titrated in FP-buffer (20 mM TRIS pH 8.0, 150 mM NaCl, 10% glycerol, 5mM  $\beta$ -mercaptoethanol, 0.01% Tween-20). In a separate vessel, a solution of 1  $\mu$ M  $\beta$ -catenin<sub>1-781</sub> and 40 nM FITC-labelled Long E-Cadherin peptide was prepared in FP buffer and incubated on ice for 30 min. Subsequently the protein-peptide complex was added to the titration series of peptide competitor with a final concentration of 10 nM Long E-Cad peptide, 250 nM  $\beta$ -catenin<sub>1-781</sub> and  $3 \times 10^{-5}$  M to  $2.01 \times 10^{-10}$  M peptide competitor. After an incubation time of 1 h at room temperature, the fluorescence polarization (FP) values were measured at room temperature (Tecan Spark 20M,  $\lambda_{\text{Ex}} = 470$  nm;  $\lambda_{\text{Em}} = 525$  nm). Measurements were conducted in triplicates. Data points were fitted using a non-linear regression fit in Graphpad's Prism 5.0.

## 2.5. REFERENCES

- [1] M. Conacci-Sorrell, J. Zhurinsky, A. Ben-Ze'ev. The cadherin-catenin adhesion system in signaling and cancer. *J. Clin. Invest.* 2002, 109, 987–991.
- [2] J. Heuberger, W. Birchmeier. Interplay of cadherin-mediated cell adhesion and canonical Wnt signaling. *Cold. Spring. Harb. Perspect. Biol.* 2010, 2:a002915.
- [3] M. Bienz, H. Clevers. Linking colorectal cancer to Wnt signaling. *Cell.* 2000, 103, 311–320.
- [4] Z. Aktary, M. Pasdar. Plakoglobin: role in tumorigenesis and metastasis. *Int. J. Cell. Biol.* 2012, 2012:189521.
- [5] H.J. Choi, J.C. Gross, S. Pokutta, W.I. Weis. Interactions of plakoglobin and beta-catenin with desmosomal cadherins: basis of selective exclusion of alpha- and beta-catenin from desmosomes. *J. Biol. Chem.* 2009, 284: 31776-88.
- [6] D.M. Krüger, H. Gohlke. DrugScorePPI webserver: fast and accurate in silico alanine scanning for scoring protein-protein interactions. *Nucleic. Acids Res.* 2010, 38(Web Server issue):W480-6.
- [7] Keith Laidig and Darwin Alonso. Interface alanine scanning tool robeta server.
- [8] R. Fasan, R.L. Dias, K. Moehle, O. Zerbe, J.W. Vrijbloed, D. Obrecht, J.A. Robinson. Using a beta-hairpin to mimic an alpha-helix: cyclic peptidomimetic inhibitors of the p53–HDM2 protein–protein interaction. *Angew. Chem. Int. Ed. Engl.* 2004, 43, 2109–2112.

- [9] S. Ahangarzadeh, M.M. Kanafi, S. Hosseinzadeh, A. Mokhtarzadeh, M. Barati, J. Ranjbari, L. Tayebi. Bicyclic peptides: types, synthesis and applications. *Drug. Discov. Today*. 2019, 24, 1311–1319.
- [10] C.A. Rhodes CA, D. Pei. Bicyclic peptides as next-generation therapeutics. *Chemistry*. 2017, 23, 12690–12703.
- [11] L.D. Walensky, G.H. Bird. Hydrocarbon-stapled peptides: principles, practice, and progress. *J. Med. Chem.* 2014, 57, 6275–6288.
- [12] G.L. Verdine, G.J. Hilinski. Stapled peptides for intracellular drug targets. *Methods Enzymol.* 2012, 503, 3–33.
- [13] A.M. Ali, J. Atmaj, N. Van Oosterwijk, M.R. Groves, A. Dömling. Stapled peptides inhibitors: a new window for target drug discovery. *Comput. Struct. Biotechnol. J.* 2019, 17, 263–281.
- [14] D. Sindhikara, M. Wagner, P. Gkeka, S. Güssregen, G. Tiwari, G. Hessler, E. Yapici, Z. Li, A. Evers. Automated design of macrocycles for therapeutic applications: from small molecules to peptides and proteins. *J. Med. Chem.* 2020, 63, 12100–12115.
- [15] Y.S. Tan, D.P. Lane, C.S. Verma. Stapled peptide design: principles and roles of computation. *Drug. Discov. Today*. 2016, 21, 1642–1653.
- [16] L. Dietrich, B. Rathmer, K. Ewan, T. Bange, S. Heinrichs, T.C. Dale, D. Schade, T.N. Grossmann. Cell permeable stapled peptide inhibitor of Wnt signalling that targets  $\beta$ -Catenin protein-protein interactions. *Cell. Chem. Biol.* 2017, 24, 958–968.
- [17] Y.W. Kim, T.N. Grossmann, G.L. Verdine. Synthesis of all-hydrocarbon stapled  $\alpha$ -helical peptides by ring-closing olefin metathesis. *Nat. Protoc.* 2011, 6, 761–771.
- [18] A.M. Yousif, V. Ingangi, F. Merlino, D. Brancaccio, M. Minopoli, R. Bellavita, E. Novellino, M.V. Carriero, A. Carotenuto, P. Grieco. Urokinase receptor derived peptides as potent inhibitors of the formyl peptide receptor type 1-triggered cell migration. *Eur. J. Med. Chem.* 2018, 143, 348–360.

## **CHAPTER 3**

# **BIVALENT PEPTIDE INHIBITORS OF $\beta$ - CATENIN AND TCF INTERACTION**

**CONTRIBUTIONS:** Peptide design and synthesis; biophysical characterization

### 3.1. BIOORTHOGONAL REACTIONS

Templated chemistry includes bioorthogonal reactions used to assemble molecules together in living systems.<sup>[1]</sup> In a biological system, a bioorthogonal reaction between molecules functionalized by reactive handles must be fast and selective under physiological conditions and may not interfere with other biological processes.<sup>[2]</sup> This strategy is widely implicated in chemical biology for the formation of bioactive compounds by direct *in situ* synthesis of drugs or through triggered drug release.<sup>[3]</sup> A large number of bioorthogonal reactions such as Staudinger ligation, click reaction, triazine ligation and photo-click reaction have been applied in bio-labeling.<sup>[4]</sup> The copper-catalyzed azide-alkyne cycloadditions (CuAAC) and the strain-promoted click reaction (SPAAC), are highly selective and are the most widely applied to stitch together molecules at their site of action.<sup>[5]</sup> The synthesis of bioconjugates can be facilitated by labeling the peptide or biomacromolecules with an azide and an alkyne probes, respectively. The CuAAC reaction requires the use of millimolar concentrations of copper(I) as the catalyst, which may cause oxidation of cysteine, methionine, and histidine residues and in addition, its toxicity does not make the application of CuAAC feasible in living cells.<sup>[6]</sup> This challenge was overcome by the alternative synthetic route SPAAC developed by Bertozzi and co-workers, in which the linear alkyne moiety was replaced by a strained cyclooctyne ring.<sup>[7]</sup> The high degree of ring strain confers a high reactivity making the use of copper obsolete, in fact, the cyclooctyne ring is able to react spontaneously with azide under the physiological environment, without the need of a catalyst.<sup>[8,9]</sup> For the bioorthogonal reactions to work in living systems, the rate of product formation should be fast (within hours) at low concentrations. Remarkably, in some cases it has been reported that protein target can accelerate bioorthogonal reactions acting as a template, leading to the *in situ* formation of its inhibitors.<sup>[10,11]</sup> This could represent an enormous benefit to perform bioconjugations using low concentrations of bioactive compounds in living cells, preventing their accumulation and resulting



toxicity when are used at high concentrations.<sup>[12]</sup> Several examples of reactions catalyzed by macromolecules acting as templates have been reported in the literature, such as the self-replication of nucleic acids and peptides and the generation of DNA-encoded libraries.<sup>[13-15]</sup> In this context, our goal was to design a protein-templated reaction mediated by  $\beta$ -catenin as the catalyst in a bioorthogonal reaction between two inhibitors that bind different binding sites close to each other. The stapled peptide **StAx-35R** and monocyclic peptide  **$\beta$ -Ecad** were chosen as inhibitors derived from catenin binding domains of Axin and E-cadherin, respectively.<sup>[16,17]</sup> Firstly, SPAAC reaction was selected as a ligation reaction to stitch together **StAx-35R** peptide labeled by azide handle in C-terminal and  **$\beta$ -Ecad**, which was subjected by chemical modifications to introduce the cyclooctyne probe. Our first objective was to synthesize the bivalent inhibitor **St-Cad** by SPAAC reaction and to investigate its inhibitory activity by FP competition assay and its affinity by direct FP assay using a fluorescence label. Before evaluating the ability of  $\beta$ -catenin to act as the template in this SPAAC reaction leading to the *in situ* formation of bivalent inhibitor **St-Cad**, we studied the kinetics of this reaction both in aqueous solution and in buffer without protein. The reaction was monitored by LC-MS system, calculating the product yields by integrating the peak areas and UV-Vis spectroscopy following the absorption of DBCO moiety.

## 3.2. RESULTS AND DISCUSSIONS

### 3.2.1. Design

Targeting and inhibiting the oncoprotein  $\beta$ -catenin is considered a promising strategy for cancer therapy due to its overexpression with resultant overactivation of transcriptional machinery. Our first objective was to design and synthesize a bivalent inhibitor of two different binding sites on  $\beta$ -catenin, increasing the potency and selectivity of inhibition. We selected the stapled peptide **StAx-35R** and monocyclic

peptide  **$\beta$ -Ecad** to perform our study. **StAx-35R** is a potent inhibitor ( $K_D= 53$  nM) that binds the same binding site of TCF4 on  $\beta$ -catenin (Figure 1, panel A) and promotes a strong inhibition of  $\beta$ -catenin/TCF4 interaction *in vitro*.<sup>[17]</sup> On the other hand, monocyclic peptide  **$\beta$ -Ecad** derived from a detailed study of the crystal structure of Plakoglobin/E-cadherin, binds the binding site of E-cadherin (Figure 1, panel A). It exhibits a potent activity with an  $IC_{50}$  value of  $3.7\pm 0.4$   $\mu$ M in  $\beta$ -catenin/E-Cadherin competition and a high affinity towards  $\beta$ -catenin ( $K_D= 0.17\pm 0.01$   $\mu$ M) (Wendt *et al.*, unpublished data).

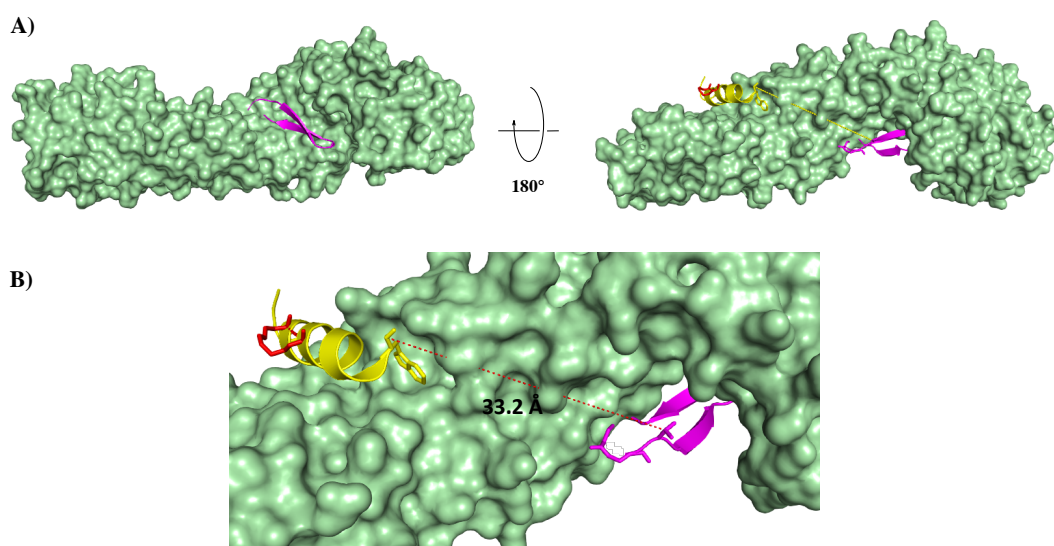


**Figure 1.** (A) Superimposed structures of  $\beta$ -catenin with **StAx-35R** (yellow, PDB ID 4DJS) and  **$\beta$ -Ecad** (unpublished data). (B) Detailed view of distance between the binding sites of **StAx-35R** and  **$\beta$ -Ecad** on  $\beta$ -catenin.

A library of  **$\beta$ -Ecad**-derived monocyclic peptides (**1–6**) was designed by replacing two  $\beta$ Ala residues in  **$\beta$ -Ecad** with the residue L/D-Lysine and an acidic spacer such as Gly, PEG2, or  $\beta$ Ala (Table 1). Both residues are involved in a head-to-tail cyclization. The L/D-Lys side chain is essential for the incorporation of dibenzocyclooctyne (DBCO) handle to perform subsequently the SPAAC reaction. The binding activity of all monocyclic peptides was measured by fluorescence

polarization (FP) competition assay and the most promising peptide was labeled with a DBCO probe to react with **StAx-N<sub>3</sub>** peptide in a SPAAC. The azide handle was introduced in **StAx-35R** peptide using an azido lysine linked to a PEG4 spacer at the C-terminus.

**Table 1.** Sequences of cyclic peptides **1–6**.

Peptide	Sequence
<b>β-Ecad</b>	[ <b>β V T<sup>629</sup> R N<sup>631</sup> D<sup>632</sup> V p P D S<sup>675</sup> L<sup>767</sup> L V<sup>678</sup> F β</b> ]
<b>1</b>	[ <b>K V T R N D V p P D S L L V F β</b> ]
<b>2</b>	[ <b>k V T R N D V p P D S L L V F β</b> ]
<b>3</b>	[ <b>K V T R N D V p P D S L L V F G</b> ]
<b>4</b>	[ <b>k V T R N D V p P D S L L V F G</b> ]
<b>5</b>	[ <b>K V T R N D V p P D S L L V F PEG2</b> ]
<b>6</b>	[ <b>k V T R N D V p P D S L L V F PEG2</b> ]

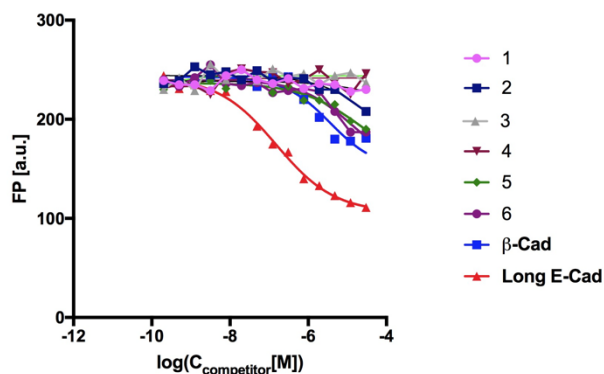
For the design of the bivalent inhibitor with a stable triazole linker, an approximate distance of 33.2 Å was detected between the two binding sites based on a crystal structures study (Figure 1, panel B). In fact, in order to keep this distance to inhibit simultaneously both binding sites, two inhibitors were tethered through a linker of 41-atoms length, yielding the bivalent inhibitor **St-Cad**.

### 3.2.2. LIMA BINDS β-CATENIN

The activity of the cyclic peptides **1–6** was investigated in competition fluorescence polarization assay in a single measurement (Figure 2, panel A). The reference **β-Ecad** and the long linear sequence E-Cadherin corresponding to V<sup>782</sup>–F<sup>833</sup> residues (Long E-Cad) were used as controls. Peptides **1–6** were titrated with β-Catenin and tracer ligand (FITC-labeled Long E-Cad). The highest concentration of competitors was 30 μM. The monocyclic peptides **1–4** exhibited a weak binding with an IC<sub>50</sub> >20 μM compared to reference monocyclic **β-Ecad**. Only peptide **5** (also called **Lima**) preserved a good activity with an IC<sub>50</sub> ~10 μM, while peptide **6** showed a

reduced activity with a value of  $IC_{50}$  of  $\sim 15 \mu\text{M}$ . The dramatic reduction of activity of peptides **1–4** is probably caused by the slight reduction of the ring size in comparison to reference monocyclic  $\beta\text{-Ecad}$ . In particular, peptides **1–4** have a ring of 49 (**1** and **2**) and 48 (**3** and **4**) members in comparison to monocyclic  $\beta\text{-Ecad}$  featured by a ring of 50 members. Likely, the reduction of ring size confers a higher rigidity to peptides **1–4**, influencing their interaction with the binding site on  $\beta\text{-Catenin}$ . Conversely, peptides **5** and **6** are macrocycles of 54 members which showed a similar  $IC_{50}$  regardless of conformational change induced by the configuration of a lysine residue (L-Lys in **Lima**, D-Lys in **6**).

**A)**



Peptide	$IC_{50}/\mu\text{M}$
<b>1</b>	>30
<b>2</b>	>30
<b>3</b>	>30
<b>4</b>	>30
<b>5 (Lima)</b>	$\sim 10$
<b>6</b>	$\sim 15$
$\beta\text{-Ecad}$	5
<b>Long E-Cad</b>	0.96

**B)**

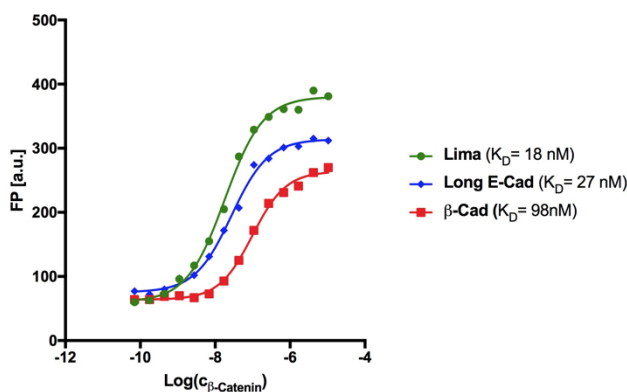


**Figure 2.** (A) . The binding activities of peptides **1–6** in  $\beta\text{-catenin/Long-E-Cadherin}$  competition in a single measurement.  $IC_{50}$  values were determined in competition FP binding assays. (B) The binding of fluorescein-labeled **Lima** to  $\beta\text{-Catenin}$  was confirmed in a direct binding FP assay. Binding curves obtained in titration of fluorescein-labeled **Lima**, FITC-labeled **Long E-Cadh** and FITC-labeled  $\beta\text{-Ecad}$  peptides with  $7.05 \times 10^{-11}\text{M}$ – $1.05 \times 10^{-5}\text{M}$   $\beta\text{-catenin}$ .  $C_{\text{peptide}}=10\text{nM}$ . The  $K_D$  values derived from the titration.

Therefore, the competition results were impressive, hence **Lima** peptide with an  $IC_{50} \sim 10 \mu\text{M}$  was chosen to be labeled to determine its affinity for  $\beta$ -Catenin by a fluorescence polarization binding assay (Figure 2, panel B). For the assay, the fluorescein was introduced on  $\epsilon$ -amino group in the lysine side chain of **Lima** peptide. Fluorescein isothiocyanate-labeled **Long E-Cadh** and fluorescein-labeled  **$\beta$ -Ecad** were used as controls of known  $K_D$ . **Lima** has shown a high affinity towards  $\beta$ -catenin with  $K_D$  of 18 nM. The interaction between **Lima** and  $\beta$ -catenin, previously observed in a competition setup, was confirmed in the direct binding assay, thus validating the possibility to functionalize **Lima** peptide with dibenzocyclooctyne probe for the synthesis of bivalent peptide inhibitor.

### 3.2.3. SYNTHESIS OF CLICK HANDLE-CONTAINING PEPTIDES

The synthesis of bivalent inhibitor requires peptide probes equipped with appropriate click handles (Table 2). **Lima** was equipped with dibenzocyclooctyne handle on lysine side chain, achieving **Lima-DBCO** peptide. The DBCO handle was introduced on  $\epsilon$ -amino group in lysine side chain using DBCO-NHS ester. In general, the DBCO handle is labile under strong acidic condition, in fact can be just introduced after cleaving the peptide from the resin.<sup>[18]</sup> In particular, the pure peptide **Lima** was dissolved in phosphate buffer (50 mM, pH =8.5) for a final concentration of 1 mM. DBCO-NHS ester (6 equiv) dissolved in DMSO was added along with DIPEA (6 equiv) under stirring. The reaction was stirred overnight and then quenched by adding 1% (v/v) aqueous TFA.

Instead, stapled **StAx-N<sub>3</sub>** was equipped with an azide handle C-terminally. Azide is highly stable in acidic and alkaline conditions, in fact it can be incorporated during the synthesis on solid support.<sup>[18]</sup> The Rink amide resin was pre-loaded with Fmoc-Lys(Mmt)-OH, useful for the introduction of azide probe. The linear sequence was assembled until Fmoc-Arg(Pbf) by standard solid-phase peptide synthesis (SPPS). First, the synthesis of olefin bridge was performed on the resin by RCM reaction and

then the N-terminal amino group was acetylated. For the introduction of azide probe, Mmt group on lysine side chain in C-terminus was selectively removed using a mixture of AcOH/TFE/DCM (10:10:80, v/v) and Fmoc-NH(PEG4)-OH was added by the coupling protocol. Then, the Fmoc group was removed and Fmoc-Lys(N<sub>3</sub>)-OH was added for the incorporation of azide handle in **StAx-N<sub>3</sub>** peptide. Last, the N-terminal Fmoc group of azido lysine was removed and then acetylated.

**Table 2.** Sequence of click handle-containing peptides.

Peptide	Sequence
<b>DBCO-Lima</b>	[K (DBCO) V T R N D V p P D S L L V F PEG2]
<b>StAx-35R</b>	Ac-R R W P R S <sub>5</sub> I L D S <sub>5</sub> H V R R V W R K [PEG4-Lys(N <sub>3</sub> )-Ac]-NH <sub>2</sub>
<b>Fam-StAx-N<sub>3</sub></b>	Fam-PEG2-R R W P R S <sub>5</sub> I L D S <sub>5</sub> H V R R V W R K [PEG4-Lys(N <sub>3</sub> )-Ac]-NH <sub>2</sub>

### 3.2.4. BIVALENT INHIBITOR OF $\beta$ -CATENIN

**Synthesis of bivalent inhibitor.** The strain-promoted click reaction (SPAAC) was chosen as a ligation reaction to stitch **Lima** and **Stax** peptides, resulting in the ligation product **St-Cad**. First, a **Lima-DBCO** peptide stock solution in DMSO was prepared due to its poor solubility in both water and buffer. **Lima-DBCO** was combined with an excess of **Stax-N<sub>3</sub>** (1.2 equiv) in H<sub>2</sub>O for a final concentration of 1 mM. The reaction was incubated with gentle shaking at room temperature for 5 h, yielding ligated triazole product **St-Cad** (Figure 3). Subsequently, the reaction was diluted with H<sub>2</sub>O and purified by preparative HPLC using C18 column and a gradient elution from 20 to 40% of MeCN (0.1%TFA) in water (0.1%TFA) over 40 min, at a flow rate of 6 mL min<sup>-1</sup>. The same synthetic strategy was used for the formation of **Fam-St-Cad** combining **Lima-DBCO** and **Fam-Stax-N<sub>3</sub>**.

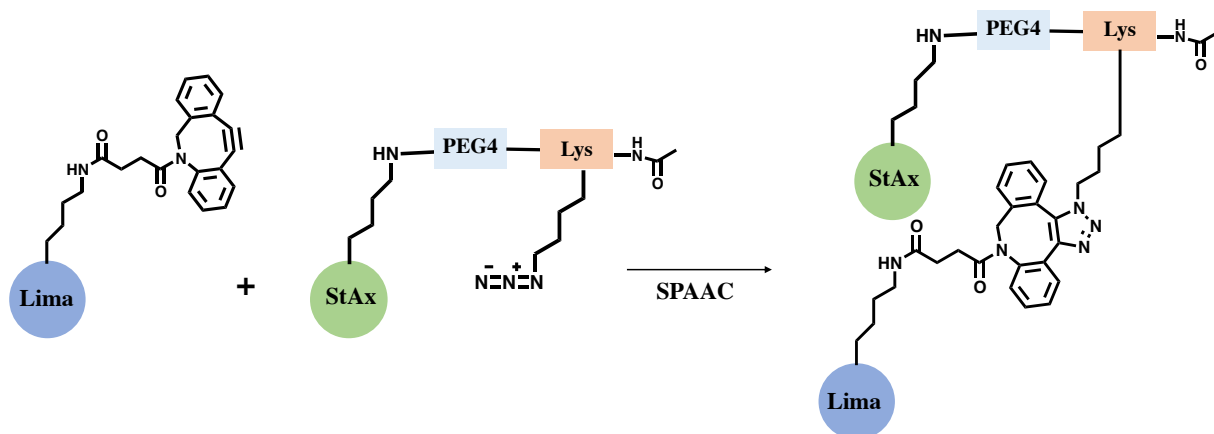


**Figure 3.** Synthesis of bivalent inhibitor **St-Cad** by SPAAC.

**Competition FP binding assay.** The activity of bivalent inhibitor **St-Cad** and **StAx-N<sub>3</sub>** was investigated in a competition fluorescence polarization assay (Figure 3). The measurement of **Lima+DBCO** could not be performed due to its high instability in DMSO detected by LC-MS analysis. We used Fitc-TCF4 (Fitc-PEG2DELISFKDEGEQEβBERDLADVKSSLVN) as a tracer ligand since this ligand binds both the binding site of **StAx** and that of **Lima** on β-Catenin. The peptides were titrated and Fitc-TCF4 and β-catenin kept at a constant concentration. The highest competitor concentration was  $3.75 \times 10^{-6}$  M. The binding was detected by decreasing fluorescence polarization upon displacement of Fitc-TCF4 from the binding sites. **StAx**, **Long E-Cad**, **β-Ecad** and **Lima** peptides were used as controls. The bivalent peptide **St-Cad** showed potent binding activity with an  $IC_{50}$  of  $0.6 \pm 0.1$  μM compared to its precursors **StAx-N<sub>3</sub>** and **Lima**. Interestingly, **St-Cad** was 7- and 4-fold more potent than **Long E-Cad** and **StAx-N<sub>3</sub>**, respectively. **StAx-N<sub>3</sub>** showed a weak binding activity with  $IC_{50}$  value exceeding 5 μM in comparison to **StAx-35R** ( $IC_{50} \sim 3 \mu M$ ), suggesting that azide handle affected the binding activity. Instead, β-

**Ecad** and **Lima** showed binding activity with  $IC_{50}$  value exceeding  $5 \mu\text{M}$  in this range of concentrations.

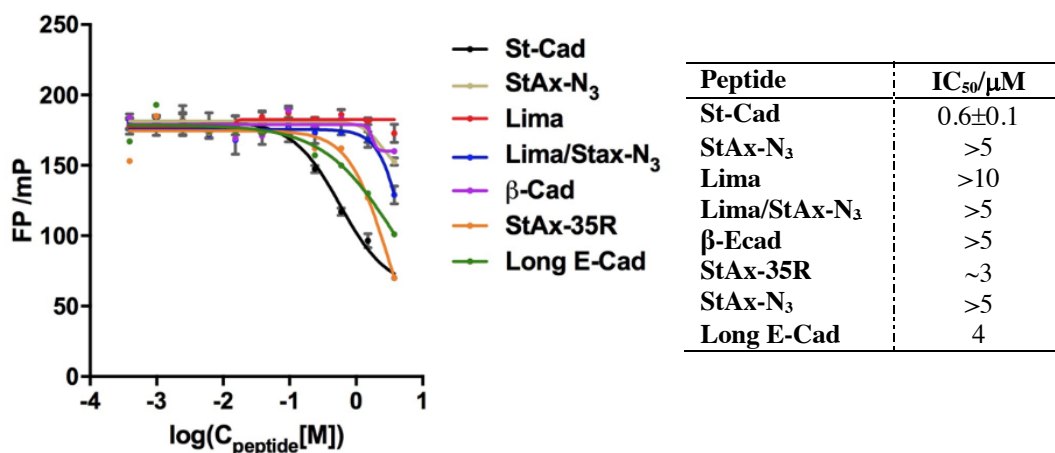


**Figure 4.** Competition binding FP assay in triplicate measurements to validate the activity of bivalent inhibitor **St-Cad**. Error bars represent standard error of the mean from three titrations.  $IC_{50}$  values are summarized in the adjacent table. Errors represent standard errors from three titrations. No lower plateau was reached in the titration.

Interestingly, an enhancement of potency was only observed when the two components **StAx-N<sub>3</sub>** and **DBCO-Lima** were covalently tethered together to yield the bivalent inhibitor **St-Cad**. In fact, an improved binding activity has not been observed when **StAx-N<sub>3</sub>** and **Lima** (1:1) were mixed (Figure 4) in presence of protein ( $IC_{50} > 5 \mu\text{M}$ ).

**Direct FP binding assay.** The dissociation constant ( $K_D$ ) value of **Fam-St-Cad** was calculated by direct fluorescence polarization binding assay (Figure 5). Fluorescein isothiocyanate-labeled **TCF4**, fluorescein-labeled  **$\beta$ -Ecad**, **Fitc-StAx** and **Fam-Lima** were used as controls of known  $K_D$ . **Fam-St-Cad** has shown a potent affinity for  $\beta$ -catenin with  $K_D < 2.5 \text{nM}$ , bringing the assay to its lower detection limits.



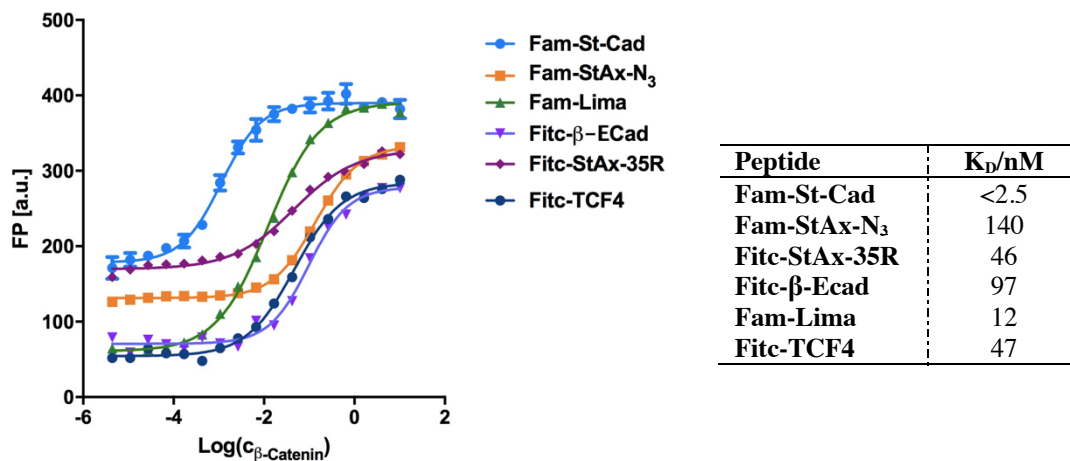


**Figure 5.** The binding of Fam-labeled **St-Cad** to  $\beta$ -Catenin was confirmed in the direct binding FP assay. Error bars represent standard errors of the mean from triplicate titrations. Table on the upper right summarizes  $K_D$  values derived from the titration. Errors are standard errors from three titrations.

### 3.2.5. PRELIMINARY KINETICS STUDIES

Before investigating the ability of  $\beta$ -catenin to catalyze the SPAAC between its inhibitors **StAx-N<sub>3</sub>** and **DBCO-Lima** with resultant formation of ligation product in situ, we performed kinetic studies in absence of protein. At first, the reactivity of click handle-containing peptide **DBCO-Lima** was assessed in water at varying concentrations. The reaction was performed both using high (300  $\mu$ M) and low concentrations (30  $\mu$ M and 10  $\mu$ M) of limiting reagent **DBCO-Lima** in presence of an excess of **Stax-N<sub>3</sub>** (1.2 equiv). The reaction was monitored by LC-MS at different time intervals (15 min, 1 h and 3 h) using a linear gradient from 5% to 95% MeCN in H<sub>2</sub>O over 10 min. Before the injection the reaction was quenched by adding TFA (1% v/v) and then product yields were determined by calculating the peak areas of click product at the wavelength of 210 nm. The formation of 50% click product was detected after 3 h at 300  $\mu$ M, 30  $\mu$ M and 10  $\mu$ M of **DBCO-Lima** using water as solvent (Figure 6). In order to find the optimal conditions to perform a kinetic study of the reaction between **DBCO-Lima** and **Stax-N<sub>3</sub>** in presence of  $\beta$ -catenin, the reactivity of click handle-containing peptides was also evaluated in TRIS buffer (150

mM NaCl, 50 mM TRIS-HCl, 0.5% glycerol, pH =8.10) at low concentrations. In fact, in biological systems, the reactive compounds are mostly used at low concentrations in contrast to a classic chemical synthesis where high concentrations ensure the product formation.

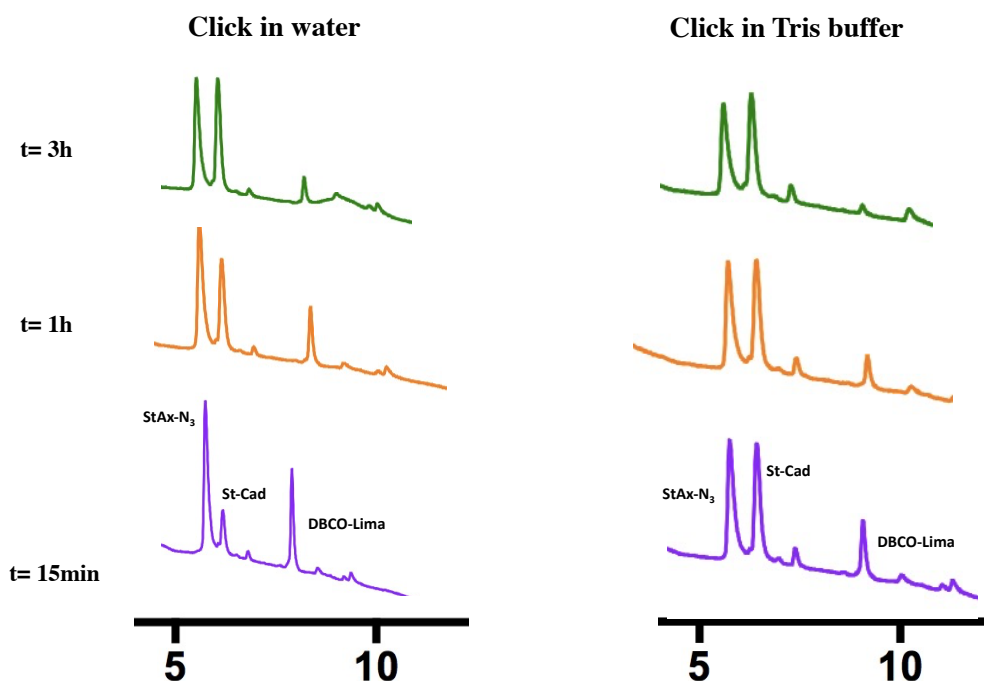


**Figure 6.** HPLC chromatograms at 15 min, 1 h and 3 h at a concentration of 10  $\mu\text{M}$  in water and in Tris buffer.

In this study, a restricted low concentrations range (10  $\mu\text{M}$  and 3  $\mu\text{M}$ ) of **DBCO-Lima** was considered, since the poor sensitivity of the used LC-MS system did not allow detecting the product formation below concentrations of 3  $\mu\text{M}$ . The aliquots of the reaction solutions were taken at known time intervals (15 min, 1 h and 3 h) and quenched adding TFA (1% v/v). The collected data at a concentration of 10  $\mu\text{M}$  showed the higher reactivity of dibenzocyclooctyne in basic condition than the aqueous solution. In fact, the reaction is very fast in Tris buffer, revealing the product formation of 50% after 15 min (Figure 6). Regarding, the kinetics reaction at the

lowest concentration of 3  $\mu\text{M}$  was studied using LC-MS system and UV-Vis spectroscopy. The reaction was monitored at the wavelength of 280 nm by LC-MS system. The ligation product formation was about 68% after 1 h, while after 3 h the limiting reagent **DBCO-Lima** was completely consumed and the total product conversion (100%) was detected (Figure 7).

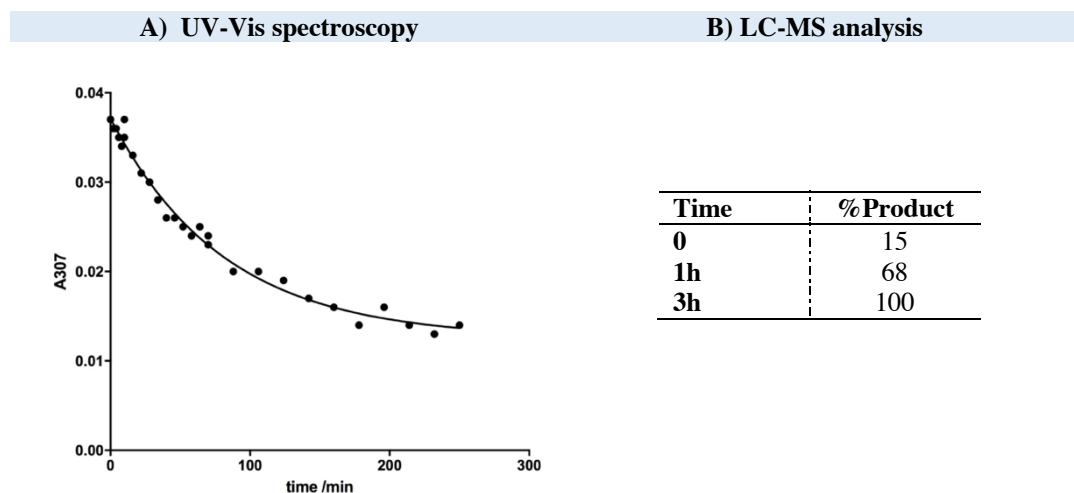


**Figure 7.** (A) The one phase decay curve obtained by monitoring the absorption of DBCO moiety at 307 nm within 6 h. (B) In the table the percentage of product formation was obtained integrating the peak areas at 280nm by LC-MS analysis.

Given that the LC-MS system does not have a high sensitivity and precision in detecting low concentrations, the kinetics study at the concentration of 3  $\mu\text{M}$  was also performed by UV-Vis spectroscopy following absorption of DBCO moiety at the wavelength of 307 nm within 6 h (Figure 7). The results showed that the reaction exhibits a fast rate also at low concentrations, revealing 50% of product formation after 56 min and the complete product formation was detected after 3 h, observing a reduction of the absorption of DBCO moiety.

These preliminary kinetics studies showed the high reactivity of DBCO handle, suggesting the necessity to optimize the reaction conditions before performing this peptide ligation in presence of  $\beta$ -catenin as the template. An alternative could be replace the dibenzocyclooctyne (DBCO) moiety with a functional handle featured

by a slow reactivity, for instance using less strained cyclooctynes as 3-alkoxycyclooctyne derivatives or the linear alkyne.<sup>[7]</sup> A further strategy may consist of changing the SPAAC with other bioorthogonal reactions featured by a lower kinetic, such as ligation reactions through aldehydes and ketones handles or Staudinger ligation.<sup>[19,20]</sup>

### 3.3. CONCLUSIONS

In conclusion, we designed and synthesized the first bivalent inhibitor **St-Cad** of  $\beta$ -catenin by applying the SPAAC reaction as a bioorthogonal reaction. **St-Cad** has shown potent binding activity with  $IC_{50}$  of  $0.6 \pm 0.1 \mu\text{M}$  in  $\beta$ -catenin/TCF4 competition and a high affinity towards  $\beta$ -catenin with a  $K_D < 2 \text{ nM}$ . Preliminary kinetics studies of this SPAAC reaction performed in water and in Tris buffer and at varying concentrations of limiting reagent **DBCO-Lima**. The results showed that the reaction was very fast even at the lowest concentration ( $3 \mu\text{M}$ ) of limiting reagent **DBCO-Lima** used in this study. In particular, LC-MS analysis and UV-Vis spectroscopy revealed 50% of product formation in 1h and the complete product formation was detected after 3 h. Before investigating the ability of  $\beta$ -catenin to act as a catalyst in this reaction in a living system, these data suggested the necessity to optimize the reaction conditions exchanging DBCO handle with functional probes featured by a slow reactivity or changing the ligation reaction.

### 3.4. EXPERIMENTAL SECTION

#### 3.4.1 CHEMISTRY

**Materials.** All  $N^\alpha$ -Fmoc-protected amino acids and 2-chlorotriyl chloride resin were purchased from Iris Biotech. (S)- $N$ -Fmoc-2-(4'-pentenyl)alanine (Fmoc-S<sub>5</sub>-OH) was purchased by Okeanos Okeanos Technology Co. Coupling reagents, COMU (1-

Cyano-2-ethoxy-2-oxoethylidenaminoxy)dimethylamino-morpholino-carbenium hexafluorophosphate and Oxyma (ethyl cyano (hydroxyimino) acetate), N,N-diisopropylethylamine (DIEA), 5-Carboxyfluorescein (5-FAM), dibenzocyclooctyne-N-hydroxysuccinimidyl ester (DBCO-NHS), 1,2-dichloroethane (DCE) were purchased from Sigma–Aldrich. 5/6-carboxyfluorescein succinimidyl ester (NHS-fluorescein) was purchased by Thermo Scientific.

HATU (1-[bis(dimethylamino)methylene]-1H-1,2,3-triazolo[4,5-b]pyridinium 3-oxid hexafluorophosphate and were purchased from NovaBiochem. Fmoc-NH(PEG2)-OH, Fmoc-Lys(N<sub>3</sub>)-OH, Fmoc-Lys(Mmt)-OH, piperidine and trifluoroacetic acid were purchased from Iris Biotech. Grubbs' first-generation catalyst for ring closing metathesis was obtained from Fluorochem. All were reagent grade acquired from commercial sources and used without further purification.

***Synthesis of head-to-tail cyclic peptides.*** The linear peptides were synthesized in a stepwise manner using standard solid-phase peptide synthesis (SPPS), Fmoc/tBu strategy. The 2-chlorotrityl chloride resin (1.60 mmol/g as loading substitution, 2 equiv relative to the mmol of first amino acid) was used as solid support. The resin, previously swollen for 30 min in DCM, was reacted with the corresponding first amino acid, N<sup>α</sup>-Fmoc-protected (2.5 equiv) and DIPEA (8 equiv relative to mmol of first amino acid) in anhydrous DCM, and the resulting reaction mixture was stirred on an automated shaker for 1 h. To endcap any remaining unreacted 2-chlorotrityl chloride groups, the resin was washed with DMF and DCM and then treated with a mixture of DCM/MeOH/DIPEA (80:15:5, v/v/v) and stirred on automated shaker for 30 min. The linear peptides were assembled by repeated cycles of Fmoc deprotection and coupling step reactions. The N<sup>α</sup>-Fmoc deprotection was carried out treating the resin with a solution of 20% piperidine in DMF (2×5min). The coupling reactions were performed using Fmoc-amino acid (3 equiv), COMU (3 equiv), Oxyma (3 equiv) and DIPEA (6 equiv) in DMF and the resulting suspension was gently shaken for 25 min. Then, the reaction solution was discarded, and the coupling repeated for

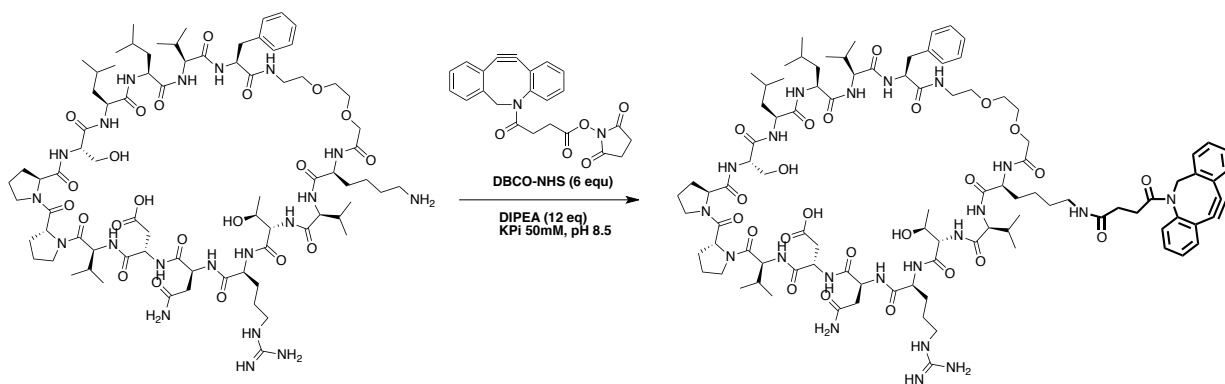
a second time for 25 min. After each coupling and Fmoc-deprotection reaction the resin was washed with DMF ( $\times 3$ ) and DCM ( $\times 3$ ). The linear resin-bound intermediate was elongated by repeated cycles of coupling and deprotection step reactions. The correct assembly of linear sequence was ascertained by LC-MS analysis of a residue obtained from the cleavage of an aliquot of resin [5mg treated with 1mL of TFA/TIS/H<sub>2</sub>O (95:2.5:2.5, v/v/v) for 1 h].

Peptides were released from the resin by a mixture of DCM/AcOH/TFE (80:10:10 v/v/v) for 2 h, keeping intact all the side chains protecting groups. The resin was removed by filtration and linear crude peptides were recovered by precipitation with DCM/n-hexane mixture. Then, residuals were dissolved in H<sub>2</sub>O/MeCN (1:1, v/v) and lyophilized. With protecting groups still tethered on functionalized side chains, the selective intra-molecular head-to-tail cyclization was thereby performed. The linear crude peptide was dissolved in DCM/DMF (9:1, C<sub>f</sub> = 0.5 mM) and DIPEA (2.4 equiv) was added, then under continuous agitation, after 15 min, HATU (1.2 equiv) and HOAt (1.2 equiv), were added.<sup>[21]</sup> The resulting reaction mixture was stirred for 5h. The reaction was quenched with saturated aq. NH<sub>4</sub>Cl. The organic phase was washed with saturated NH<sub>4</sub>Cl solution (3 $\times$ ), saturated NaCl solution (3 $\times$ ) and dried over Na<sub>2</sub>SO<sub>4</sub>. Finally, sidechain protecting groups were removed by using a 50% TFA solution in DCM for 2 h at room temperature. All peptides were purified by HPLC, using C18 column and a linear gradient from 20 to 40% MeCN in H<sub>2</sub>O over 40 min. All peptides were characterized using a reverse-phase HPLC equipped with ESI-MS (Agilent 1260 + quadrupole 6120, Column: Agilent Zorbax C18, 4.6  $\times$  150 mm, 5  $\mu$ m), by eluting solvent A (H<sub>2</sub>O + 0.1 % TFA) and solvent B (MeCN + 0.1 % TFA) (Table 3).

**Table 3.** Analytical data of head-to-tail cyclic peptides **1–6**.

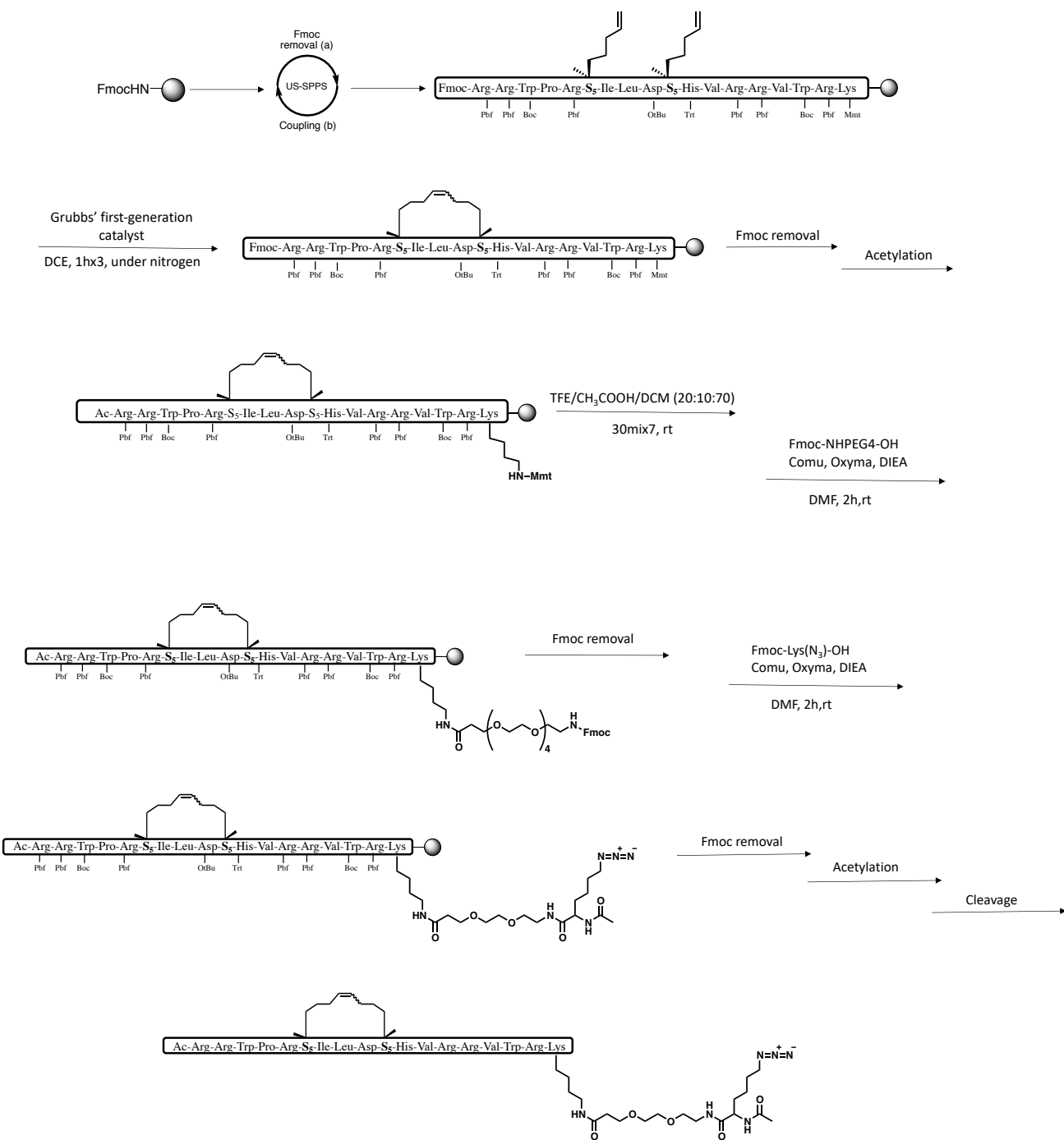
Cmpd#	R <sub>t</sub> (min)	MW calcd	MW found
<b>1</b>	18.1	1752	[M+2H/2] <sup>+</sup> =877.2
<b>2</b>	17.8	1752	[M+2H/2] <sup>+</sup> =877.1
<b>3</b>	18.6	1738	[M+2H/2] <sup>+</sup> =870.1
<b>4</b>	19.1	1738	[M+2H/2] <sup>+</sup> =870.1
<b>5 (Lima)</b>	17.0	1827	[M+2H/2] <sup>+</sup> =914.2
<b>6</b>	16.9	1827	[M+2H/2] <sup>+</sup> =914.2

**Incorporation of dibenzocyclooctyne-acid probe in Lima peptide.** The functionalization of **Lima** peptide with dibenzocyclooctyne (DBCO) handle was performed in solution on ε-amino group in lysine side chain using DBCO-NHS ester (Scheme 1). The DBCO is completely instable under strong acidic condition and cannot be introduced during SPPS. The pure **Lima** peptide was dissolved in potassium phosphate buffer (50 mM, pH 8.5) for a final concentration of 1 mM. DBCO-NHS (6 equiv) was first dissolved in DMSO and then added along with DIEA (12 equiv).<sup>[18,22]</sup> The reaction was incubated overnight. Subsequently the reaction was quenched by adding 1% (v/v) aqueous TFA, diluted with H<sub>2</sub>O/MeCN (1:1) and purified by preparative HPLC using C18 column and a linear gradient from 20 to 60% MeCN in H<sub>2</sub>O over 40 min.

**Scheme 1.** Labeling of **Lima** peptide using DBCO-NHS (6 eq) in presence of DIPEA (12 eq) in potassium phosphate buffer pH 8.5.

***Incorporation of azide probe in StAx-N<sub>3</sub>.*** StAx peptide has been functionalized with azide group using a Lys(N<sub>3</sub>) residue C-terminally. The synthesis was achieved on solid phase using the Rink amide-ChemMatrix as solid support. Fmoc-Lys(Mmt) was used as first amino acid for the following functionalization with N<sub>3</sub> group (Scheme 2). The sequence was assembled by repeated cycles of Fmoc deprotection and coupling step reactions until Fmoc-Arg(Pbf)-OH as described above. The ring-closing methathesis was performed treating the resin with a fresh catalyst solution of a 6 mM solution of Grubbs' first-generation catalyst in DCE (4.94 mg mL, 20 mol% relative to the resin substitution). The resulting suspension was gently agitated with a constant flow of nitrogen for 1 h. After the first round, the RCM reaction was repeated twice in the same condition. In the end of three cycles, the resin was washed with DCE (3 × 1 min) and DCM (3 × 1 min) and then dried under a stream of nitrogen. The conversion in olefin bridge was monitored by LC-MS analysis. Then, N-terminal Fmoc group was removed and the acetylation in N-terminus was achieved treating the resin with a solution of Ac<sub>2</sub>O/DIPEA/DMF (1/1/8, v/v/v), 2×10min. For the functionalization with azido lysine, the Mmt group in lysine side chain was removed adding to the resin a mixture of AcOH:TFE:DCM (10:20:70, v/v/v) for 30 min. The deprotection was repeated three times. Then, the Fmoc-NH(PEG4)-OH and Fmoc-Lys(N<sub>3</sub>)-OH were added by cycles of Fmoc deprotection and coupling step reactions. At the end, N-terminal Fmoc group of azido lysine was removed, and the acetylation was performed by adding Ac<sub>2</sub>O/DIPEA/DMF (1/1/8, v/v/v) for 10 min. After 10 min the reaction solution was discarded, and the acetylation repeated.





**Scheme 2.** The synthesis of StAx-N<sub>3</sub>.

**Fluorescent labeling.** Fluorescently labeled peptides were synthesized for the fluorescence polarization binding assay. **Lima** peptide was labeled with fluorescein on  $\epsilon$ -amino group (lysine side chain). The pure peptide was dissolved in DMF for to final concentration of 100  $\mu$ M and 150  $\mu$ M of a N-hydroxysuccinimide (NHS)-Fluorescein fresh stock solution in DMSO and 4% DIPEA (*v/v*) were added under agitation. The reaction, protected from light, was stirred for 3h and then the peptide was precipitated by adding cold diethyl ether and by centrifugation at 4000 rcf, 4°C, for 1h. The supernatant was discarded, and the peptide was dissolved in H<sub>2</sub>O/MeCN (1:1, *v/v*) and purified by HPLC preparative.

Instead, StAx-N<sub>3</sub> was labeled N-terminally on resin after the ring-closing metathesis reaction. First, N-terminal Fmoc group was removed using a solution of 20% piperidine in DMF (2×5min) and Fmoc-NH(PEG2)-OH linker was N-terminally attached using the amino acid coupling protocol described above. Then, the Fmoc protecting group was removed and 5-carboxyfluorescein (3 equiv) was added using COMU (3 equiv), Oxyma (3 equiv), DIEA (6 equiv) in DMF for 2h, at rt. The fluorescein labeling was ascertained by LC-MS analysis and then the synthesis was proceeded for the incorporation of azide motif. Specifically, the Mmt group in lysine side chain at the C-terminus was removed by AcOH:TFE:DCM (10:20:70, *v/v/v*), 3 × 30 min at rt, and the addition of Fmoc-NH(PEG4)-OH and Fmoc-Lys(N<sub>3</sub>)-OH was performed by cycles of Fmoc deprotection and coupling step reactions. At the end, the N-terminal Fmoc group of azido lysine was removed and an acetylation was performed by adding Ac<sub>2</sub>O/DIPEA/DMF (1/1/8, *v/v/v*), 2× 10 min, at rt. During acetylation an esterification of hydroxy groups of fluorescein was observed and their hydrolysis was performed treating the resin with a solution of 20% piperidine in DMF (3×5min).

**Peptide cleavage.** Peptides were released from solid support and the protecting groups were removed, simultaneously, treating the resin with a cocktail cleavage consisting in TFA/TIS/H<sub>2</sub>O (95/2.5/2.5, v/v/v) at rt for 3 h. The residuals were washed in cold diethyl ether and precipitated peptides were separated by centrifugation (15 min, 4 °C, 4000 rcf). The supernatant was removed and crude peptides were dissolved in MeCN/H<sub>2</sub>O (1/1, v/v) and purified by preparative HPLC.

**Purification and Characterization.** Peptide purification was performed using reversed-phase HPLC (HPLC: Agilent 1100, Column: Macherey-Nagel Nucleodur C18, 10 × 125 mm, 110 Å, 5 μm) with solvent A (H<sub>2</sub>O + 0.1 % TFA) and solvent B (MeCN + 0.1 % TFA). For separation a gradient elution was used with 20 % to 60 % of solvent B over 40 min and a flow rate of 6 mL min<sup>-1</sup>. Pure fractions were combined and lyophilized. Subsequently peptides were characterized using a reverse-phase HPLC coupled to ESI-MS (Agilent 1260 + quadrupole 6120, Column: Agilent Zorbax C18, 4.6 × 150 mm, 5 μm) with solvent A (H<sub>2</sub>O + 0.1 % TFA) and solvent B (MeCN + 0.1 % TFA).

**Table 4.** Analytical data of click handle containing peptides and bivalent inhibitor.

<b>Cmpd#</b>	<b>R<sub>t</sub>(min)</b>	<b>MW calcd</b>	<b>MW found</b>
<b>StAx-N<sub>3</sub></b>	16.7	2962.7	[M+3H/3] <sup>+</sup> =989.0
<b>Fam-StAx-N<sub>3</sub></b>	14.1	3423.9	[M+4H/4] <sup>+</sup> =857.4
<b>DBCO-Lima</b>	22.3	2116.1	[M+H/2] <sup>+</sup> =1057.7
<b>Fam-Lima</b>	21.1	2184.1	[M+2H/2] <sup>+</sup> =1093.2
<b>St-Cad</b>	13.7	5075.8	[M+4H/4] <sup>+</sup> =1270.9
<b>Fam-St-Cad</b>	16.9	5536.9	[M+4H/4] <sup>+</sup> =1386

### 3.4.2. BINDING ASSAY

**Competition fluorescence polarization assay.** In a 384-well plate non-labelled peptide competitor was titrated in FP-buffer (20 mM TRIS pH 8.0, 150 mM NaCl, 10% glycerol, 5mM β-mercaptoethanol, 0.01% Tween-20). For the binding activity of bivalent peptide **St-Cad**, in a separate vessel, a solution of 1 μM β-catenin<sub>1-781</sub> and

40 nM FITC-labelled TCF-4 peptide was prepared in FP buffer and incubated on ice for 30 min. Subsequently the protein-peptide complex was added to the titration series of peptide competitor with a final concentration of 10 nM TCF-4 peptide, 250 nM  $\beta$ -catenin<sub>1-781</sub> and  $2.52 \times 10^{-5}$  to  $3.75 \times 10^{-6}$  M peptide competitor. Instead, for the binding of peptides **1–6** a solution of 1  $\mu$ M  $\beta$ -catenin<sub>1-781</sub> and 40 nM FITC-labelled Long E-Cadherin peptide was prepared in FP buffer and incubated on ice for 30 min. Subsequently the protein-peptide complex was added to the titration series of peptide competitor with a final concentration of 10 nM Long-E-Cad peptide, 250 nM  $\beta$ -catenin<sub>1-781</sub> and  $3 \times 10^{-5}$  M to  $1.26 \times 10^{-9}$  M peptide competitor. In both cases, after an incubation time of 1 h at room temperature, the fluorescence polarization (FP) values were measured at room temperature (Tecan Spark 20M,  $\lambda_{\text{Ex}} = 470$  nm;  $\lambda_{\text{Em}} = 525$  nm). Measurements were conducted in triplicates. Data points were fitted using a non-linear regression fit in Graphpad's Prism 5.0.

**Direct fluorescence polarization assay.**  $\beta$ -Catenin<sub>1-781</sub> was serially diluted in FP buffer (20 mM TRIS pH 8.0, 150 mM NaCl, 10% glycerol, 5mM  $\beta$ -mercaptoethanol, 0.01% Tween-20) on a 384-well plate. Fluorescently-labelled peptides (100  $\mu$ M DMSO stock solutions) were diluted in FP-buffer to 40 nM and subsequently added to the dilution series of  $\beta$ -catenin<sub>1-781</sub> to a final concentration of 5 nM peptide and  $1.02 \times 10^7 \mu\text{M}$ -  $4.38 \mu\text{M}$   $\beta$ -catenin (used for the measurement of  $K_D$  of bivalent peptide **St-Cad**) and  $7.05 \times 10^{-11}$  M- $1.05 \times 10^{-5}$  M  $\beta$ -catenin (used for the measurement of  $K_D$  of **Lima** peptide). After incubation for 1 h on ice, FP values were measured at room temperature (Tecan Spark 20M,  $\lambda_{\text{Ex}} = 470$  nm;  $\lambda_{\text{Em}} = 525$  nm). For data analysis FP-values were fitted using a non-linear regression in Graphpad's Prism 5.0.

### 3.5. REFERENCES

- [1] N.K. Devaraj. The future of bioorthogonal chemistry. *ACS Cent. Sci.* 2018, 4, 952–959.
- [2] M. Zheng, L. Zheng, P. Zhang, J. Li, Y. Zhang. Development of bioorthogonal reactions and their applications in bioconjugation. *Molecules.* 2015, 20, 3190–3205.
- [3] C.P. Ramil, Q. Lin. Bioorthogonal chemistry: strategies and recent developments. *Chem. Commun.* 2013, 49, 11007–11022.
- [4] M.F. Debets, J.C. van Hest, F.P. Rutjes. Bioorthogonal labelling of biomolecules: New functional handles and ligation methods. *Org. Biomol. Chem.* 2013, 11, 6439–6455.
- [5] D. Antonow. Fragment-based approaches and the prospect of fragmented prodrugs. *Drug Discov. Today.* 2010, 15, 801–803.
- [6] V. Hong, S.I. Presolski, C. Ma, M.G. Finn. Analysis and optimization of copper-catalyzed azide-alkyne cycloaddition for bioconjugation. *Angew. Chem. Int. Ed.* 2009, 48, 9879–9883.
- [7] N.J. Agard, J.A. Prescher, C.R. Bertozzi. A strain-promoted [3 + 2] azide-alkyne cycloaddition for covalent modification of biomolecules in living systems. *J. Am. Chem. Soc.* 2004, 126, 15046–15047.
- [8] M.F. Debets, S.S. van Berkel, J. Dommerholt, A.T. Dirks, F.P. Rutjes, F.L. van Delft. Bioconjugation with strained alkenes and alkynes. *Acc. Chem. Res.* 2011, 44, 805–815.
- [9] E.M. Sletten, C.R. Bertozzi. Bioorthogonal chemistry: fishing for selectivity in a sea of functionality. *Angew. Chem. Int. Ed. Engl.* 2009, 48, 6974–6998.
- [10] N.K. Devaraj, R. Weissleder. Biomedical applications of tetrazine cycloadditions. *Acc. Chem. Res.* 2011, 44, 816–827.
- [11] X. Ning, J. Guo, M.A. Wolfert, G.J. Boons. Visualizing metabolically labeled glycoconjugates of living cells by copper-free and fast Huisgen cycloadditions. *Angew. Chem. Int. Ed.* 2008, 47, 2253–2255.
- [12] N. Brauckhoff, G. Hahne, J.T. Yeh, T.N. Grossmann. Protein-templated peptide ligation. *Angew. Chem. Int. Ed. Engl.* 2014, 53, 4337–4340.
- [13] P. Thirumurugan, D. Matosiuk, K. Jozwiak. Click chemistry for drug development and diverse chemical-biology applications. *Chem. Rev.* 2013, 113, 4905–4979.
- [14] W.S. Zielinski, L.E. Orgel. Autocatalytic synthesis of a tetranucleotide analogue. *Nature.* 1987, 327, 346–347.
- [15] D.H. Lee, J.R. Granja, J.A. Martinez, K. Severin, M.R. Ghadiri. A self-replicating peptide. *Nature.* 1996, 382, 525–528.
- [16] R.E. Kleiner, C.E. Dumelin, D.R. Liu. Small-molecule discovery from DNA-encoded chemical libraries. *Chem. Soc. Rev.* 2011, 40, 5707–5717.
- [17] T.N. Grossmann, J.T.H. Yeh, B.R. Bowman, Q. Chu, R.E. Moellering, G.L. Verdine. Inhibition of oncogenic Wnt signaling through direct targeting of  $\beta$ -catenin. *Proc. Natl. Acad. Sci. U.S.A.* 2012, 109, 17942.

- [18] M.D. Witte, C.S. Theile, T. Wu, C.P. Guimaraes, A.E. Blom, H.L. Ploegh. Production of unnaturally linked chimeric proteins using a combination of sortase-catalyzed transpeptidation and click chemistry. *Nat. Protoc.* 2013, 8, 1808–1819.
- [19] The Staudinger Ligation. C. Bednarek, I. Wehl, N. Jung, U. Schepers, S. Bräse. *Chem. Rev.* 2020, 120, 4301–4354.
- [20] C. Mamat, M. Gott, J. Steinbach. Recent progress using the Staudinger ligation for radiolabeling applications. *J. Labelled Comp. Radiopharm.* 2018, 61, 165–178.
- [21] A.M. Yousif, V. Ingangi, F. Merlino, D. Brancaccio, M. Minopoli, R. Bellavita, E. Novellino, M.V. Carriero, A. Carotenuto, P. Grieco. Urokinase receptor derived peptides as potent inhibitors of the formyl peptide receptor type 1-triggered cell migration. *Eur. J. Med. Chem.* 2018, 143, 348–360.
- [22] J. Wiener, D. Kokotek, S. Rosowski, H. Lickert, M. Meier. Preparation of single- and double-oligonucleotide antibody conjugates and their application for protein analytics. *Sci Rep.* 2020, 10:1457.